Impact of nicotinamide riboside, a precursor of NAD^+ on cardiac remodeling after myocardial infarction in rat

Selma Lopez-Vaquera

université
PARIS-SACLAY

Impact of nicotinamide riboside, a precursor of NAD^+ on cardiac remodeling after myocardial infarction in rat

L'impact du nicotinamide riboside, précurseur du NAD^+, sur le remodelage cardiaque après infarctus du myocarde chez le rat

Thèse de doctorat de l'université Paris-Saclay

École doctorale n° 569 : Innovation thérapeutique : du fondamental à l'appliqué (ITFA)
Spécialité de doctorat : Physiologie, physiopathologie
Graduate School : Santé et médicaments. Référent : Faculté de pharmacie

Thèse préparée dans l'unité de recheche **UMR-S 1180 (Université Paris-Saclay, Inserm)**, sous la direction de **Mathias MERICSKAY**, directeur de recherche à l'Inserm, Université Paris-Saclay

Thèse soutenue à Paris-Saclay, le 20 décembre 2021, par

Selma LÓPEZ-VAQUERA

Composition du Jury

Christian POÜS Professeur, Université Paris-Saclay	Président
Elise BELAÏDI Maîtresse de Conférence, HDR, Université de Grenoble Alpes	Rapporteure & Examinatrice
Paul MÜLDER Directeur de Recherche INSERM, Université de Rouen Normandie	Rapporteur & Examinateur
Catherine VERGELY-VANDRIESSE Professeure, Université Bourgogne Franche-Comté	Examinatrice
Mathias MERICSKAY Directeur de Recherche INSERM, Université Paris-Saclay	Directeur de thèse

THÈSE DE DOCTORAT
NNT : 2021UPASQ056

université PARIS-SACLAY

ÉCOLE DOCTORALE
Innovation thérapeutique
du fondamental à l'appliqué
(ITFA)

Titre : L'impact du nicotinamide riboside, précurseur du NAD^+, sur le remodelage cardiaque après infarctus du myocarde chez le rat

Mots clés : biologie cardiovasculaire, métabolisme énergétique, nutrition, remodelage cardiaque

Résumé : L'insuffisance cardiaque (IC) est l'une des diverses complications causées par l'infarctus du myocarde (IM) et sa prévalence est en hausse depuis quelques décennies. Il est toujours nécessaire de trouver de meilleures thérapies pour améliorer la qualité de vie des patients souffrant d'IC. Le riboside de nicotinamide (NR) est un précurseur du nicotinamide adénine dinucléotide (NAD^+), une molécule impliquée dans le métabolisme énergétique et qui est diminuée en cas d'IC.

Le NR a été testé dans plusieurs essais cliniques et s'est avéré efficace pour traiter plusieurs maladies. Nous avons voulu tester l'effet du NR par voie orale pendant 16 semaines après IM chez le rat.

Le NR a contrecarré la détérioration de la fonction cardiaque, prolongeant ainsi la durée de vie des animaux traités après IM. Nous concluons que le NR peut activer des voies métaboliques liées à la cardioprotection.

Title: Impact of nicotinamide riboside, a precursor of NAD+ on cardiac remodeling after myocardial infarction in rat

Keywords: cardiovascular biology, energy metabolism, nutrition, cardiac remodeling

Abstract: Myocardial infarction (MI) is characterized by cardiac tissue death due to a lack of blood delivery to the heart. Heart failure (HF) is one of the many complications caused by MI and its prevalence has been rising for the past decades. There is still a need to develop better therapies to improve HF patients' quality of life. One aspect that novel HF treatments should tackle is the disruption of energetic metabolism. Nicotinamide riboside (NR), is a precursor for nicotinamide adenine dinucleotide (NAD^+), a major molecule involved in energetic metabolism that is severely decreased upon HF.

NR has been tested in several clinical tests and has been proven to be effective to treat several diseases. We aimed to test the effect of oral NR for 16 weeks in a rat model of MI.

NR counteracted the deterioration of cardiac function, therefore extending the life span of treated rats that underwent MI.

We conclude that NR can activate metabolic pathways that are linked to cardioprotection.

Acknowledgments

First and foremost, I would like to thank the members of the jury: ***Christian Poüs***, ***Elise Belaïdi***, ***Paulus Mülder*** and, ***Catherine Vergely***. Thank you for accepting to evaluate my work, even in the current complicated circumstances. I appreciate the time dedicated to the review of the manuscript and the observations that allowed me to improve it.

I would like to thank the **U-MRS 1180** *labo* (Signalling and Cardiovascular Pathophysiology). I am grateful for this life-changing opportunity. It was a true privilege to carry out my work there, as I learned and developed my skills in such an enriching scientific environment. ***Ana Maria Gomez*** and ***Rodolphe Fischmeister***, directors of the U-1180 (2018-2021), thank you for welcoming me into your scientific home.

I sincerely thank **Consejo Nacional de Ciencia y Tecnología** (CONACYT) and the state of Nuevo León, Mexico for providing me a scholarship to pursue my Ph.D. degree.

Mathias Mericskay, my supervisor, I thank you for guiding me throughout these (almost) four years. Your knowledge and passion for science are inspiring. Above all, I truly appreciate the effort, patience, and empathy you demonstrated throughout my Ph.D. training.

A huge thank you all the members of Team 1: ***Anne Garnier***, ***Vladimir Veksler***, ***Jérôme Picquereau***, ***Renée Ventura-Clapier***, ***Iman Momken***, ***Mélanie Gressette***, and ***Ahmed Karoui***. I will forever treasure the priceless and vast scientific knowledge shared with me. Also, I am thankful for the helping hand I was offered many times as a clueless foreigner in France. Special thanks to Jérôme, Mélanie,

and Ahmed for the excellent work you carried out for this project and for teaching me the mitochondrial respiration assay.

I sincerely thank our collaborators for this project: ***Valérie Domergue*** and ***Florence Lefebvre***. Thank you for the great work you carried out with the MI model and for your priceless help with the samples collection. Thanks to ***Antoine Pilon*** for carrying out the cTnI quantification. Thanks to ***Susana Gomez***, for initiating me with echocardiography and the number of times you offered me guidance of all sorts. For being there during difficult times (sorry for the non-stop whining). Thanks to ***François Fenaille*** and ***Florence Castelli*** for performing the LC-MS assays. Thanks to ***Julie Hussin***, ***Pamela Mehanna***, **Jean-Christophe Grenier**, **Bénedicte Tremblay** and ***Matthieu Ruiz*** for the metabolomics analysis.

Thanks to ***Claudine Délomenie*** for your guidance with qPCR. Thanks to ***Bertrand Crozatier*** for sharing your expertise with echocardiography interpretation. Thanks to the Néonat crew (2018-2020) specially to ***Carole***, ***Anne-Sophie***, ***Robin***, ***Dawei***, ***Kaouter***, ***Délphine*** and ***Riu***. For sharing your neonatal cardiomyocyte isolation skills and expertise. Great teamwork!

Thank you ***Gladys Renée-Corail,*** for your kind assistance with administrative paperwork. Thank you so much, **Sophie**, your precious work made our Ph.D. lives so much easier.

A million thanks to ***Lucile***, **Anissa**, ***Robin***, ***Kaveen*** and ***Kévin***. I will be forever thankful for your help and good company. Best of luck to you!

Muchas gracias ***Arpit***, for the time we spent together and for being yourself. I will never forget our international delicious snacks and meals, and our super long

walks *all over* Île de France. I'm so grateful for the friendship that blossomed, after all. Thank you for being there for me!

Thanks to ***Madame et Monsieur Paul***. For showing me that the best french dishes are homemade. But most of all, for your patience and consideration during my stay at your home.

I dedicate this work **to my dear family**. I cannot find enough words to express how important you are to me. Thank you for keeping me grounded and reminding me of the things that matter the most in life. I'm immensely lucky to have you!

Contents

Table of Figures

Résumé

L'infarctus aigu du myocarde (IM) se définit comme la mort des cellules myocardiques causée par une ischémie prolongée. Bien que la mortalité liée à l'IM ait diminué au cours des dernières décennies, la prévalence de l'insuffisance cardiaque (IC) n'a cessé d'augmenter.

Une étape importante de l'évolution de l'IC est le remodelage du ventricule gauche (RVG), défini comme des changements structurels dans le ventricule gauche (VG) qui sont finalement liés au développement de l'IC. L'altération de l'homéostasie mitochondriale et le remodelage métabolique représentent également des processus physiopathologiques essentiels dans la progression du RVG. Malgré les progrès actuels des traitements de l'IC, ce syndrome se distingue par un mauvais pronostic, car les stratégies thérapeutiques ne s'attaquent pas à la perturbation de la bioénergétique du cœur.

Le NAD^+, molécule centrale du métabolisme, est classiquement connu comme un coenzyme impliqué dans les réactions redox du métabolisme énergétique et, est également un substrat pour des enzymes qui participent à des processus cruciaux dans le développement des pathologies cardiovasculaires, comme les polys (ADP-ribose) polymérases (PARP), les Sirtuines, et le CD38. Des études ont montré l'implication de la perturbation du métabolisme du NAD^+ dans des modèles d'IC et des échantillons humains. Dans le cœur sain, le principal substrat pour la synthèse du NAD^+ est le nicotinamide (NAM), par l'intermédiaire des enzymes nicotinamide phosphoribosyltransférase (NAMPT), l'enzyme limitant la vitesse de la voie de récupération du NAD^+. Le nicotinamide riboside (NR) est un autre précurseur du NAD^+, et est très prometteur pour restaurer le métabolisme cardiaque altéré. Le NR est le substrat de l'enzyme Nicotinamide Riboside-Kinase 2 (NMRK2), qui a besoin de moins d'énergie (ATP) pour synthétiser le NAD^+. Dans

le contexte de l'IC, il a été observé que l'expression de NMRK2 est fortement régulée à la hausse alors que NAMPT est régulée à la baisse, ce qui suggère que la voie NMRK2 pourrait jouer un rôle clé dans la synthèse du NAD^+ pendant la RVG dans un contexte de stress énergétique.

Nous avons donc, émis l'hypothèse que la stimulation de la voie NMRK2 serait bénéfique dans le contexte du RVG. Notre objectif principal était d'évaluer l'effet d'une supplémentation alimentaire avec NR, dans un modèle de rat d'IM pendant 16 semaines. À cet effet, nous avons étudié la fonction cardiaque systolique et diastolique, évalué la fonction mitochondriale et déterminé les niveaux de marqueurs du stress cardiaque et de signalisation énergétique. De plus, nous avons évalué l'impact de l'IM et du régime NR sur l'expression des enzymes de la voie de récupération du NAD^+, NAMPT et NMRK2. Grâce à la métabolomique LC-MS, nous avons identifié les métabolites et les voies qui sont modifiés pendant la RVG et le NR.

Nos résultats montrent que l'administration orale de NR pendant 16 semaines après un infarctus a permis d'améliorer la survie et de ralentir la progression de le RVG. Le NR n'a pas protégé contre la chute des capacités oxydatives mitochondriales maximales. Inversement, la NR a stimulé l'expression des enzymes impliquées dans le métabolisme du NAD^+.
Le NR a eu un impact important sur le métabolisme du VG, comme en témoigne la modulation du métabolisme des voies impliquées dans l'évolution de l'IC ont été modifiées par le NR, telles que le métabolisme du glutathion, la voie du pentose phosphate. En conclusion, nos données démontrent que la stimulation de la voie NMRK2 était suffisante pour contrecarrer l'évolution défavorable de la RVG. Les processus qui sous-tendent cet effet doivent encore être élucidés, car nos résultats mettent en évidence l'activation de plusieurs voies qui ont été précédemment associées à la cardioprotection.

Abstract

Acute myocardial infarction (MI) is the most severe subtype of ischemic heart disease and is defined as myocardial cell death caused by prolonged ischemia. Even though mortality linked to MI has been declining for the last decades, the prevalence of heart failure (HF) has been increasing steadily.

A milestone in HF post-MI evolution is adverse left ventricular (LV) remodeling (LVR), defined as structural changes in the LV, ultimately linked with developing HF. The alteration of mitochondrial homeostasis and metabolic remodeling also represent essential pathophysiological processes in adverse LVR progression. Regardless of current advances in HF treatments, this syndrome is distinguished by a poor prognosis, as therapeutic strategies do not address the perturbation of the heart's bioenergetics.

NAD^+, a central molecule to metabolism is classicly known as a coenzyme involved in redox reactions of energy metabolism and, is also a substrate for enzymes that participate in crucial processes in the development of cardiovascular pathologies, such as poly (ADP-ribose) polymerases (PARPs), Sirtuins, and CD38. Studies have shown the implication of NAD metabolism disruption in HF models and human samples. In the healthy heart, the main substrate for NAD^+ synthesis is nicotinamide (NAM), through the enzymes nicotinamide phosphoribosyltransferase (NAMPT), the rate-limiting enzyme of NAD^+ salvage pathway. Nicotinamide riboside (NR) is another precursor for NAD^+ and holds great promise for restoring altered cardiac metabolism. Notably, NR is the substrate of the enzyme Nicotinamide Riboside-Kinase 2 (NMRK2), which necessitates less energy (ATP) to synthesize NAD^+. In the context of HF, it has been observed that the expression of NMRK2 is strongly upregulated whereas NAMPT is downregulated, suggesting

that the NMRK2 pathway might have a key role in NAD^+ synthesis during LVR in the context of energy stress.

Thus, we hypothesized that stimulating the NMRK2 pathway would be beneficial in the context of LVR post-MI. Our primary aim was to evaluate the effect of dietary supplementation with the NAD^+ precursor, NR, in a rat model of MI for 16 weeks. To achieve our objective, we studied cardiac systolic and diastolic function, evaluated mitochondrial function, and determined levels of cardiac stress and energy signaling markers. Moreover, we assessed the impact of both, MI and NR diet, on the expression of the NAD salvage pathway enzymes, NAMPT and NMRK2. Additionally, through LC/MS metabolomics, we identified metabolites and pathways that are modified during LVR and NR.

Our results show that oral administration of NR for 16 weeks after MI was efficient to improve survival and counteract the progression of LVR. NR did not protect against the drop in maximal mitochondrial oxidative capacities. Conversely, NR boosted the expression of enzymes involved in NAD^+ metabolism.
NR had an important impact on the LV metabolome, evidenced by the modulation of pathways implicated in HF evolution, such as glutathione metabolism and the pentose phosphate pathway. In conclusion, our data demonstrate that stimulating the NMRK2 pathway was enough to counteract adverse LVR-post MI. The mechanistic processes underlying this effect have yet to be unraveled, as our results evidence the activation of several pathways that have been previously linked with cardioprotection.

Abbreviations

Δψm: Membrane potential

ACC: Acetyl Coenzyme A Carboxylase

Acetyl-CoA: Acetyl Coenzyme A

ACMS: 2-amino-3-carboxymuconate Semialdehyde

ADP: Adenosine Diphosphate

ADPR: ADP–Ribose

AMI: Acute Myocardial Infarction

AMP: Adenosine Monophosphate

AMPK: Adenosine monophosphate-activated Protein Kinase

ATP: Adenosine Triphosphate

BCAA: Branched Chained Amino Acids

BNP: Brain Natriuretic Peptide

C I-V: Mitochondrial complexes I-V

Ca^{2+}: Calcium ion

cADPR: Cyclic ADP–Ribose

CD38: Cyclic ADP-Ribose Cyclases 38

cDNA: Complementary Deoxyribonucleic Acid

CK: Creatine Kinase

CKM: Creatine Kinase, M-type

CO_2: Carbon dioxide

CoA: Coenzyme A

COL1A1: Collagen Type I Alpha 1 Chain

CPT: Carnitine Palmitoyltransferase

cTnI: Cardiac Troponin I

CVD: Cardiovascular Disease(s)

DCM: Dilated Cardiomyopathy

EF: Ejection Fraction

ETC: Electron Transport Chain

FA: Fatty Acids

FAD: Flavin Adenine Dinucleotide

$FADH_2$: Flavin Adenine Dinucleotide, hydroquinone form

FAO: Fatty Acid Oxidation

FFA: Free Fatty Acids

FOXO: Forkhead transcription factors

G6-P: Glucose 6-Phosphate

GLUT: Glucose Transporters

GSH: Glutathione, reduced

GSSG: Glutathione, oxidized

HF: Heart Failure

HPRT: Hypoxanthine Phosphoribosyltransferase

IDO: Indoleamine 2,3-dioxygenase

IHD: Ischemic Heart Disease

I/R: Ischemia/Reperfusion

K^+: Potassium ion

KO: Knockout

LAD: Left Anterior Descending

LCFA: Long Chain Fatty Acids

LC/MS: Liquid Chromatography-Mass Spectrometry

LDH: Lactate Dehydrogenase

LV: Left Ventricle

LVR: Left Ventricle Remodeling

M-A: Malate-aspartate

MCP: Mitochondrial Pyruvate Carrier

MI: Myocardial Infarction

mRNA: Messenger Ribonucleic Acid

Na^+: Sodium

NA: Nicotinic Acid

NAAD: Nicotinic Acid Adenine Dinucleotide

NAD: Nicotinamide Adenine Dinucleotide, oxidized

NADH: Nicotinamide Adenine Dinucleotide, reduced

NADP: Nicotinamide Adenine Dinucleotide Phosphate, oxidized

NADPH: Nicotinamide Adenine Dinucleotide Phosphate, reduced

NADS: Nicotinamide Adenine Dinucleotide Synthase

NAM: Nicotinamide

NAMPT: Nicotinamide Phosphoribosyltransferase

NAPRT: Nicotinic Acid Phosphoribosyltransferase

NMN: Nicotinamide Mononucleotide

NMNAT: Nicotinamide Mononucleotide Adenylyltransferase

NMRK: Nicotinamide Riboside Kinase

NR: Nicotinamide Riboside

NRF: Nuclear Respiratory Factor

NSTEMI: Non-ST segment Elevation Myocardial Infarction

O_2: Oxygen

OXPHOS: Oxidative Phosphorylation

PARP: Poly-ADP-ribose Polymerases

PCI: Percutaneous Coronary Intervention

PCr: Phosphocreatine

PDC: Pyruvate Dehydrogenase Complex

PDH: Pyruvate Dehydrogenase

PDK: Pyruvate Dehydrogenase Kinases

PDP: Pyruvate Dehydrogenase Phosphatase

PGC-1α: Peroxisome Proliferator-Activated Receptor Gamma Coactivator 1-alpha

PPAR: Peroxisome Proliferator-Activated Receptors

PPi: Inorganic Pyrophosphate

PPP: Pentose Phosphate Pathway

PRPP: Phosphoribosyl Pyrophosphate

QPRT: Quinolinate Phosphoribosyltransferase

ROS: Reactive Oxygen Species

SERCA: Sarcoplasmic Reticulum Ca^{2+}-atpase

SERCA2A: Sarcoplasmic/ Endoplasmic Reticulum Ca^{2+} ATPase 2a

SGLTs: Sodium-coupled active transporters or symporters

SIRT: Sirtuins

SRF: Serum Response Factor

STEMI: ST-segment elevation myocardial infarction

TAG: Triacylglycerol

TCA: Tricarboxylic Acid Cycle

TDO: Tryptophan 2,3-dioxygenase

TRP: L-Tryptophan

1 INTRODUCTION

1.1 THE CARDIOVASCULAR SYSTEM

The cardiovascular system is the transport system of the body, its main function is to supply oxygen (O_2) and nutrients to tissues and remove carbon dioxide (CO_2) and wastes from these tissues. It constitutes an interconnected circular system with several individual components that interact with each other. The cardiovascular system has three main components: the heart, the blood vessels, and the blood.

1.1.1 Structure and Anatomical Function of the Heart

The heart is a hollow, muscular organ that lies in the center of the thoracic cavity, known as the mediastinum. It consists of four chambers, which pump the blood, and of two valves at the opening of each chamber, which help maintain the blood flow in the right direction. It is suspended by its attachments to the great blood vessels within a thin fibrous sac called the pericardium. The heart is the main propeller of blood circulation all over the body. Through periodic and controlled stimulation of its muscles, it contracts and delivers the necessary blood output and pressure throughout the organism (Katz, 2010). The four chambers that comprise the heart are arranged in two similar pairs of pumps: the *right heart*, which pumps blood through the lungs, and the *left heart* that pumps blood through the systemic circulation to provide blood flow to the other organs and tissues. In turn, each of these two *hearts* is a two-chamber pump composed of an atrium (upper chamber) and a ventricle (lower chamber). The right and left hearts are separated by a wall called a septum. The atria are thin-walled structures located at the top, which act primarily as entryways for the blood. The ventricles are larger, thicker-walled chambers that receive the blood from the atria to propel the blood

through the pulmonary or systemic circulation (Mohrman & Heller, 2018). The heart is contained within a noncompliant fibrous sac called pericardium whose inner surface is continuous with the epicardium. The wall of the heart is composed of three distinct layers: the epicardium, the myocardium, and the endocardium. The epicardium is the outermost layer of the heart. It is constituted of the mesothelium that covers and protects the inner layers and is continuous with the pericardium. The myocardium is the thickest layer which is in the middle of the heart wall. It is composed mainly of cardiac muscle cells and is built upon collagen fibers, blood vessels, and nerve fibers. The muscular walls of the ventricles are made up of overlapping fiber bundles that follow spiral paths. The contraction of the myocardium pumps blood through the heart and into the major arteries. The endocardium is the innermost layer of the heart wall, it lines the chambers where the blood circulates and covers the heart valves. It is connected to the myocardium with a layer of connective tissue and is made of endothelium, which contributes to the regulation of muscle contraction within the myocardium (Katz, 2010).

1.1.2 Circulation Through the Heart

There are two distinct yet linked circuits in the circulation, the pulmonary and the systemic circulation (Figure 1). The pulmonary circulation transports blood to and from the lungs, where it recovers O_2 and delivers CO_2 for exhalation. On the other hand, the systemic circulation transports oxygenated blood to all the tissues and returns deoxygenated blood and CO_2 to the heart to be sent back to the pulmonary circulation. The atria and ventricles are separated by the atrioventricular valves: on the right, the tricuspid valve separates the right atrium from the right ventricle, and on the left, the mitral valve that separates the left atrium from the left ventricle (LV). Blood flows passively through all organs because the arterial pressure is kept higher than venous pressure by the pumping action of the heart.

The right ventricle sends deoxygenated blood from which is pumped through the pulmonic valve into the pulmonary circulation via the pulmonary arteries. The vessels branch out several times before reaching the pulmonary capillaries. Within the pulmonary capillaries, the blood is exposed to O_2-rich air, and gas exchange takes place: CO_2 exits, and O_2 enters. Oxygenated blood returning from the pulmonary capillaries travels across a series of vessels that merge to form the pulmonary veins. Then, the pulmonary veins carry the blood into the left atrium and pass through the mitral valve into the LV. From there, the blood is pumped through the aortic valve into the aorta, afterward the aorta branches into smaller arteries, which eventually branch into arterioles. Finally, arterioles divide into systemic capillaries, where exchange with tissue fluid and cells takes place. O_2 and nutrients exit the systemic capillaries to be consumed by the cells in their metabolic processes, and CO_2 and waste products will enter the blood. The capillaries will merge to form venules, then join to form veins, eventually flowing into the two major systemic veins, the superior vena cava, and the inferior vena cava. The venae cavae leads the circulation back into the right heart (Betts et al., 2013; Hall, 2015; Mohrman & Heller, 2018).

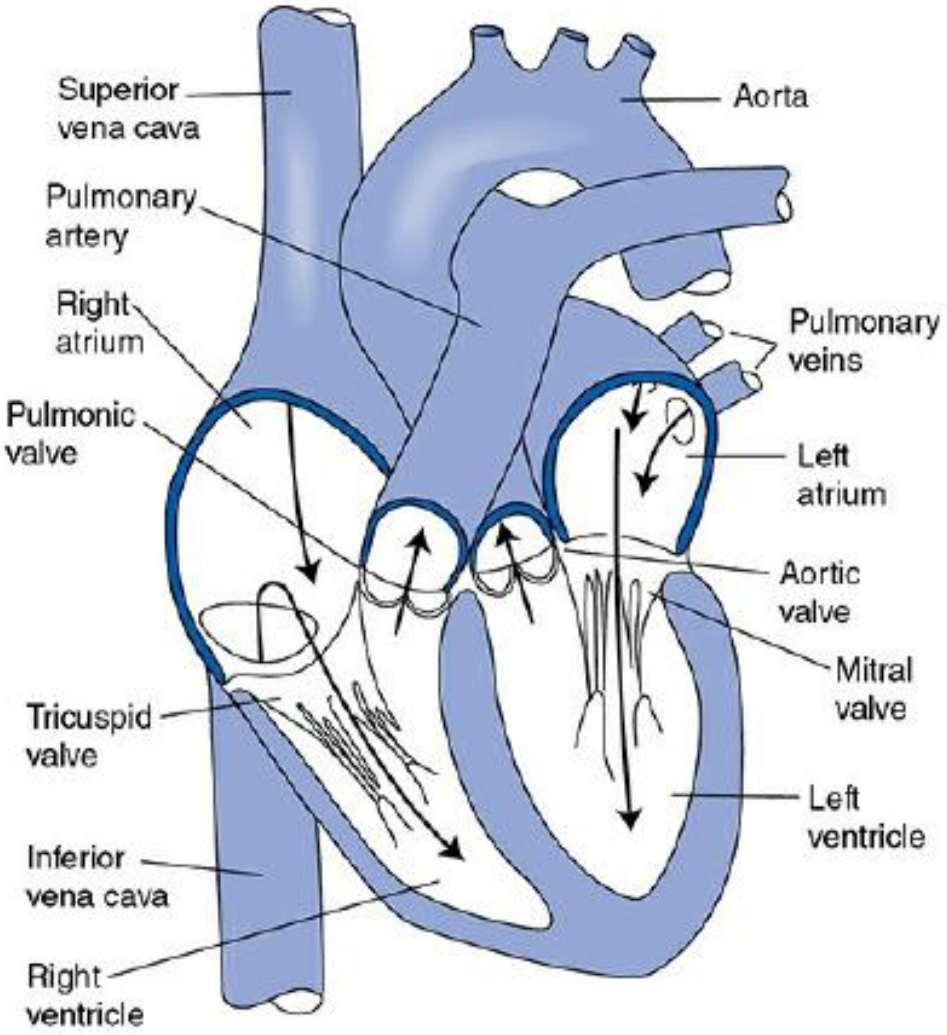

Figure 1. Anatomy of the heart

(Mohrman & Heller, 2018).

1.1.3 The Cardiac Cycle

The cardiac cycle consists of a period of relaxation called diastole, in which the heart is filled up with blood, followed by a period of contraction called systole. All these events occur from the beginning of one heartbeat to the beginning of the next one. During diastole, normal filling of the ventricles increases the volume of each ventricle, this volume is called end-diastolic volume. During systole, the volume decreases as the ventricles empty, this is called stroke volume output. The volume that remains in each ventricle is called the end-systolic volume. The fraction of the end-diastolic volume that is ejected is called the ejection fraction (EF) and is usually about 60% (Hall, 2015).

1.1.4 The Coronary Circulation

The blood supply of the heart is carried through the muscle layers that form the heart wall via the coronary arteries. The coronary arteries tend to be end arteries, meaning that each branch follows its course to some area of the heart muscle with few connections to other branches nearby. The major coronary arteries are the left main coronary artery, right coronary artery, left anterior descending (LAD), circumflex, and posterior descending artery (Figure 3). Two coronary arteries are leading out of the aorta, the right coronary artery and left main coronary artery. In its turn, the left main coronary artery divides into two principal branches: The LAD branch comes down the front of the heart between the two ventricles and the circumflex branch that coils around the left side and back of the heart. The right coronary artery divides into many branches that course through the right chambers of the heart as well as through a large part of the LV. The posterior descending artery is a continuation of either the right coronary artery or the circumflex (Katz, 2010; Phibbs, 2007).

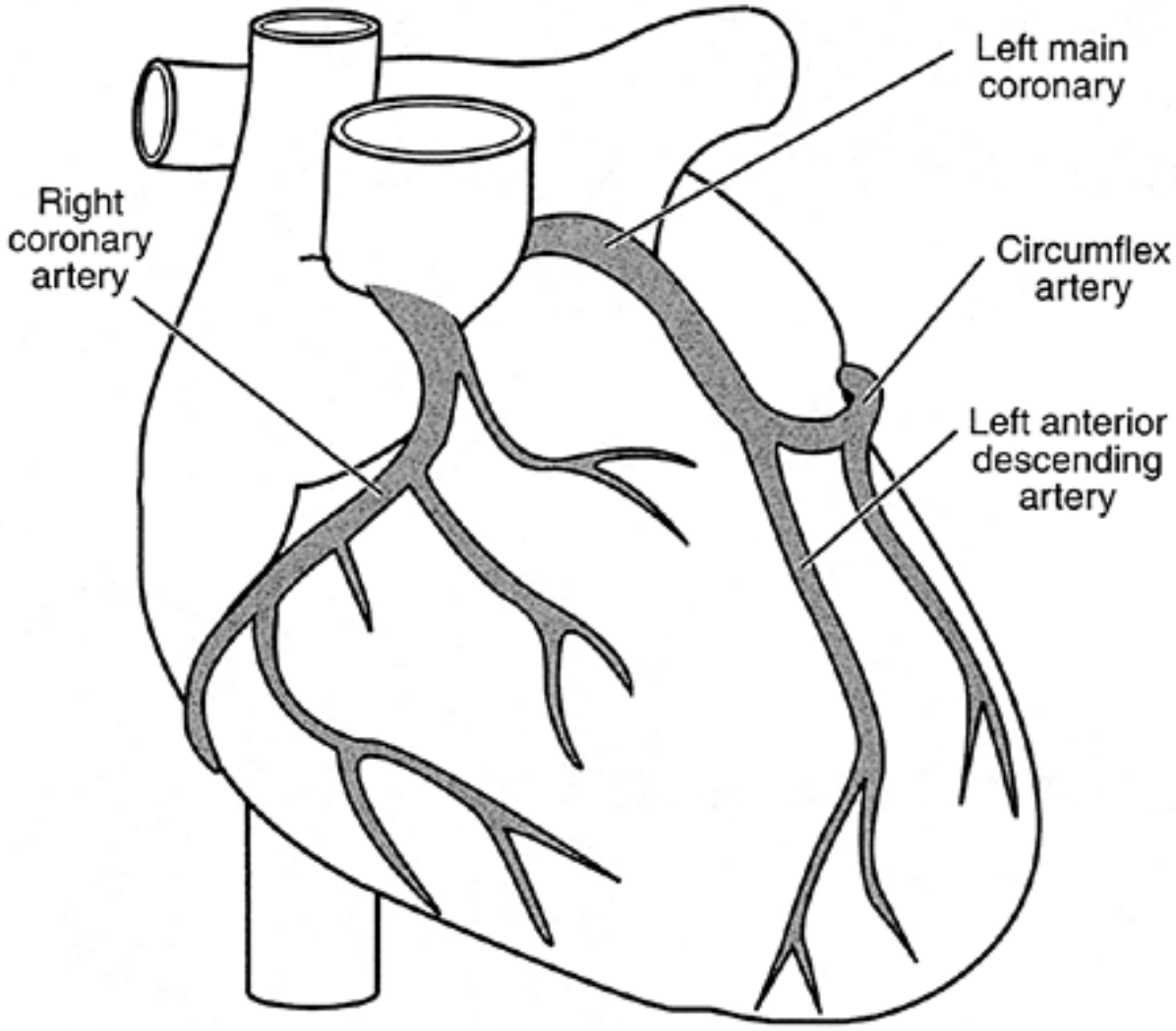

Figure 2. The coronary circulation

(Phibbs, 2007).

1.2 CARDIOVASCULAR DISEASES

1.2.1 Definition and epidemiology of Cardiovascular Disease

The term cardiovascular disease (CVD) refers to a wide range of diseases of the heart, vascular disease of the brain, and diseases of the blood vessels, namely:

1. Ischemic heart disease (IHD): Also referred to as coronary artery disease or coronary heart disease. Results from decreased myocardial perfusion that causes angina, myocardial infarction (MI), and/or heart failure (HF). It accounts for one-third to one-half of the cases of CVD.
2. Cerebrovascular disease: Diseases of the blood vessels supplying the brain. This term includes stroke and transient ischemic attack.
3. Peripheral artery disease: Diseases of the blood vessels supplying the limbs.
4. Rheumatic heart disease: Damage to the heart muscle and heart valves from rheumatic fever.
5. Aortic atherosclerosis: Including thoracic and abdominal aneurysms.
6. Congenital heart disease: Malformations of heart structure existing at birth (Olvera Lopez et al., 2020; World Health Organization, 2017).

CVD has become the leading cause of death worldwide over the last decade, causing near one-third of deaths worldwide (Mozaffarian et al., 2015). In 2019, it caused around 18.6 million deaths and led to 393 million disability-adjusted life-years (DALYs). This accounted for 32.84% of total deaths and 15.52% of DALYs lost during that year *(The Global Burden of Disease:* 2019 *Update)*. Strikingly, the acceleration of the increase in CVD now also affects low and middle-income countries, not only high-income countries (Zipes & Libby, 2018). The shift to sedentary lifestyles, consumption of high-calorie diets, saturated fats, and refined sugars are linked to the development of atherosclerosis and other metabolic dis-

turbances like metabolic syndrome, diabetes, and hypertension which are comorbidities of CVD (Olvera Lopez et al., 2020). Moreover, the Framingham Heart Study demonstrated that the lifetime risk of CVD is higher among individuals with both obesity and diabetes, with the lifetime risk of CVD approaching nearly 80% in obese women and nearly 90% in obese men (Fox et al., 2008). Although CVD may result from different etiologies such as emboli and rheumatic fever, the development of atherosclerosis is the common denominator in its pathophysiology.

1.2.2 Ischemic Heart Disease

Among CVD, IHD is also referred to as coronary artery disease, and atherosclerotic cardiovascular disease ranks as the most prevalent CVD. The incidence of IHD is expected to continue increasing due to the rise of the prevalence of obesity diabetes, metabolic syndrome, and global population aging. A recent study estimated that IHD affects around 126 million individuals, which accounts for 1.72% of the current global population. Moreover, 9 million deaths were caused by IHD, globally (Khan et al., 2020). IHD is the effect of multiple etiological risk factors and coexists with other diseases. It is widely known that detrimental modern lifestyle habits play a key role in its development, such as sedentarism, smoking, and the westernized diet rich in saturated fats and sugar and lacking in fruits and vegetables. Moreover, hypertension, hyperlipidemia, insulin resistance, obesity, and diabetes are also major risk factors (Calvert, 2014).

1.2.3 Acute Myocardial Infarction

1.2.3.1 Definition and Characteristics of Myocardial Infarction

Acute myocardial infarction (AMI) is the most severe subtype of IHD and is defined pathologically as myocardial cell death caused by prolonged ischemia. The term AMI is used to describe an acute myocardial injury in the presence of suspected acute myocardial ischemia. The onset of myocardial ischemia is the first

step in the development of myocardial infarction (MI) and is the consequence of imbalanced O_2 and nutrient supply and demand (Thygesen et al., 2019)**.** The disorder is diagnosed and assessed by clinical evaluation, electrocardiogram, biochemical tests, imaging, and pathological evaluation. The characteristic symptoms are typical ischemic-type chest discomfort, dyspnea, nausea, weakness, or a combination of these (Anderson & Morrow, 2017). For the sake of immediate treatment strategies, it is a standard practice to designate MI in patients with chest discomfort or other ischemic symptoms and that also present ST-segment elevations in 2 contiguous leads or new bundle branch blocks with ischemic repolarization patterns as an ST-elevation (STEMI). In contrast, patients without ST-segment elevation are usually designated non-ST-elevation MI (NSTEMI) (Thygesen et al., 2018). The STEMI and NSTEMI have in common the release of specific myocardial necrosis markers which define them clinically AMI and differentiate them from unstable angina, an acute coronary syndrome that cannot be classified as MI. Moreover, STEMI and NSTEMI can be considered as two separate pathophysiological entities as STEMI is a transmural event and NSTEMI is a sub-endocardial one (Di Stefano et al., 2009).

Furthermore, MI can also be classified into other diverse types based on pathological, clinical, and prognostic differences, alongside different treatment schemes (Table 1)**.** According to the Fourth Universal Definition of Myocardial Infarction to establish a diagnosis of acute myocardial infarction, types 1, 2, and 3, there must be a fluctuation in cardiac troponin levels, with at least one value above the 99th percentile upper reference limit and at least one of the following criteria must be met:

1. Myocardial ischemia symptoms: ischemic-type chest discomfort, dyspnea, nausea, weakness.
2. New ischemic electrocardiographic changes.
3. Development of pathological Q waves.

4. Imaging evidence of new loss of viable myocardium or new regional wall motion abnormality in a pattern consistent with an ischemic etiology.
5. Identification of a coronary thrombus by angiography or autopsy (not for type 2 or 3) (Thygesen et al., 2018).

Classification of MI	Clinical and diagnostic criteria
Type 1	Spontaneous MI is related to ischemia due to a primary coronary event such as plaque erosion and/or rupture, fissuring, or dissection.
Type 2	MI secondary to ischemia due to either increased oxygen demand or decreased supply, e.g., coronary artery spasm, coronary embolism, anemia, arrhythmias, hypertension, or hypotension.
Type 3	Sudden unexpected cardiac death, including cardiac arrest, often with symptoms suggestive of MI accompanied by new ST elevation, or new left bundle branch block, or evidence of fresh thrombus in a coronary artery by angiography and/or at autopsy, but death occurring before blood samples could be obtained, or at a time before the appearance of cardiac biomarkers in the blood.
Type 4a	MI associated with percutaneous coronary intervention (PCI). Elevation of cardiac troponin (cTn) values >5 times the 99th percentile upper reference limit (URL) in patients with normal baseline values. In patients with elevated pre-procedure cTn in whom the cTn level is stable (<=20% variation) or falling, the post-procedure cTn must increase by >20%.
Type 4b	MI associated with stent/scaffold thrombosis associated with PCI as documented by angiography or at autopsy using the same criteria utilized for type 1 MI.
Type 5	MI associated with coronary artery bypass grafting. It is suggested that a cTn value >10 times the 99th percentile URL is applied as the cut-off point during the first 48 hours following the procedure, occurring from a normal baseline cTn value.

Table 1. Clinical classification of MI

(Thygesen et al., 2007, 2018).

Cardiac troponins are considered as the preferred biomarkers for myocardial injury detection due to their specificity to myocardial tissue and their high sensitivity, by reflecting even microscopic zones of myocardial necrosis. Cardiac troponin T and cardiac troponin I (cTnI) are cardiac regulatory proteins that control the calcium-mediated interaction between actin and myosin. Both are expressed al-

most exclusively in the heart. cTnI has not been identified outside the myocardium. These proteins are detected through monoclonal antibodies in routine clinical use. The quantification of serum cTnI is superior in terms of sensitivity and specificity to cardiac muscle enzyme measurements in the assessment of cardiac muscle injury. Serum cTnI values are indicative of myocardial damage ranging from 0.1 to 2 mg/liter (Antman et al., 2000; Sharma et al., 2004; Thygesen et al., 2019).

During the 1970s it was established that thrombosis is the cause of nearly all AMI. Atherosclerosis with successive inflammation is the most common and most important cause of thrombosis, being the key feature of endothelial dysfunction. However, the causes of MI are not restricted to atherosclerosis. Among its causes, there are other several diverse etiologies, namely coronary Kawasaki's syndrome, trauma to coronary arteries, spontaneous coronary dissection, coronary mural thickening with a metabolic disease, or intimal proliferation (Fabry's disease), luminal spasm, coronary embolization, congenital coronary anomalies, supply-demand mismatch (Saleh & Ambrose, 2018).

1.2.3.2 Epidemiology of Myocardial Infarction

AMI is a frequent cardiac emergency that still represents a high risk for morbidity and mortality, although its management has improved considerably over the past decades (Anderson & Morrow, 2017). Mortality attributable to AMI has been declining for 40 years thanks to critical improvements in prevention strategies and treatment. Case-fatality rates for AMI decreased substantially between 2005 and 2015 as a result of better access to acute care for heart attack, timely transportation of patients, evidence-based medical interventions, and specialized health facilities such as percutaneous catheter intervention-capable centers (OECD, 2017). Regardless of the advances to tackle MI, this disease affects more than 7 million people around the world every year. It is the cause of 2.4 million deaths in the

United States, more than 4 million deaths in Europe and northern Asia, and more than a third of deaths in developed countries per year (Reed et al., 2017). According to the INTERHEART global case-control study, that included subjects from 52 countries; including high, middle, and low-income countries; 9 modifiable risks factors accounted for 90% of the risk of having a first MI: abnormal lipids, smoking, hypertension, diabetes, abdominal obesity, psychosocial factors, alcohol, reduced consumptions of fruits and vegetables, and lack of regular physical activity account for most of the risk of MI worldwide in both sexes and at all ages in all regions (Yusuf et al., 2004).

1.2.3.3 Pathophysiology and Treatment Myocardial Infarction

The onset of myocardial ischemia is triggered by an imbalance between O_2 and nutrients supply and demand and initiates the development of myocardial infarction. The deprivation of O_2 and nutrient supply results in a series of abrupt biochemical and metabolic myocardial perturbations. First, the absence of O_2 stops oxidative phosphorylation (OXPHOS), leading to mitochondrial membrane depolarization, adenosine triphosphate (ATP) depletion, and inhibition of myocardial contractile function. Second, ATP hydrolysis and depletion take place along with mitochondrial inorganic phosphate production. Third, there is an accumulation of lactate and a reduction of intracellular pH due to the switch of cellular metabolism to anaerobic glycolysis caused by the lack of O_2. Finally, these changes contribute to intracellular calcium overload (Calvert, 2014). Diminished glycogen, relaxed myofibrils, and sarcolemmal disruption are the first ultrastructural changes observed as early as 10 to 15 minutes after the onset of ischemia. Moreover, mitochondrial alterations start 10 minutes after coronary occlusion and are progressive (Thygesen et al., 2019). The earliest change observed in the progression of AMI is pallor of the myocardium, which appears 12 hours after the onset of irreversible ischemia. In small infarctions, recovery may be completed as early as 4 to

6 weeks or may take as long as 2 to 3 months when the area of infarction is larger. Healed infarcts appear white from scarring and the ventricular wall may be thinned (Burke & Virmani, 2007). The timely implementation of reperfusion therapy reduces the injury and salvages the myocardium after ischemia. This allows the restoration of O_2 levels and metabolic substrates, removing ischemic metabolites. After the first observations that reperfusion rescues ischemic myocardium from infarction but leaves salvageable myocardium up to 2 to 3 hours ischemia (Reimer & Jennings, 1979), there have been major improvements in pharmacotherapy, procedural techniques, and stent technology in the treatment of AMI. The routine use of antiplatelet agents such as clopidogrel, prasugrel, in addition to aspirin, reduces morbidity and mortality. Percutaneous coronary intervention (PCI) is the primary treatment for patients with STEMI. Drug-eluting coronary stents are safe and beneficial with a primary coronary intervention.

The infarct size, which is the result both from ischemia and reperfusion injury, is a determining factor in the prognosis of AMI. When PCI is not available, fibrinolytic therapy is an alternative. It decreases morbidity when it is carefully administered within 12 hours of symptoms onset (Rentrop & Feit, 2015). However, it is well known that reperfusion also induces further cardiomyocyte death. This phenomenon is known as reperfusion injury (RI). The lack of O_2 during ischemia causes a switch to anaerobic glycolysis followed by a build-up of lactate and a decrease in intracellular pH. The depletion of ATP and acidosis leads to cytosolic sodium (Na^+) accumulation through the Na^+/H^+ exchange, then the excess Na+ is extruded, in exchange for calcium (Ca^{2+}), through the reverse action of the plasma membrane Na^+/Ca^{2+}, Na^+/Ca^{2+} exchanger. The Ca^{2+} uptake by the sarcoplasmic reticulum Ca^{2+}-ATPase (SERCA) is prevented due to the drop in ATP, which leads to an excess of cytosolic Ca^{2+} (Figure 4).

Moreover, metabolic end-products such as hypoxanthine, xanthine, and succinate are accumulated. Upon reperfusion and re-oxygenation of the cell, the electron transport chain (ETC) is re-activated and restored which normalizes intracellular

pH and mitochondrial membrane potential (Δψm) and results in a large entry of Ca^{2+} into the mitochondrion. Reperfusion boosts reactive oxygen species (ROS) production through Complex I and the opening of the mitochondrial permeability transition pore is induced resulting in a drop of $\Delta\psi_m$, cytochrome *c* release, and subsequent activation of necrotic and apoptotic signaling cascades, and finally to cardiomyocyte death (Pell et al., 2016). Reperfusion injury may account for up to 50% of the final size of MI. There is evidence to suggest that cells die during the reperfusion period. Interventions applied solely at the onset of myocardial reperfusion reduce infarct size by 40–50%, suggesting that reperfusion injury can be targeted for therapeutic interventions (Calvert, 2014).

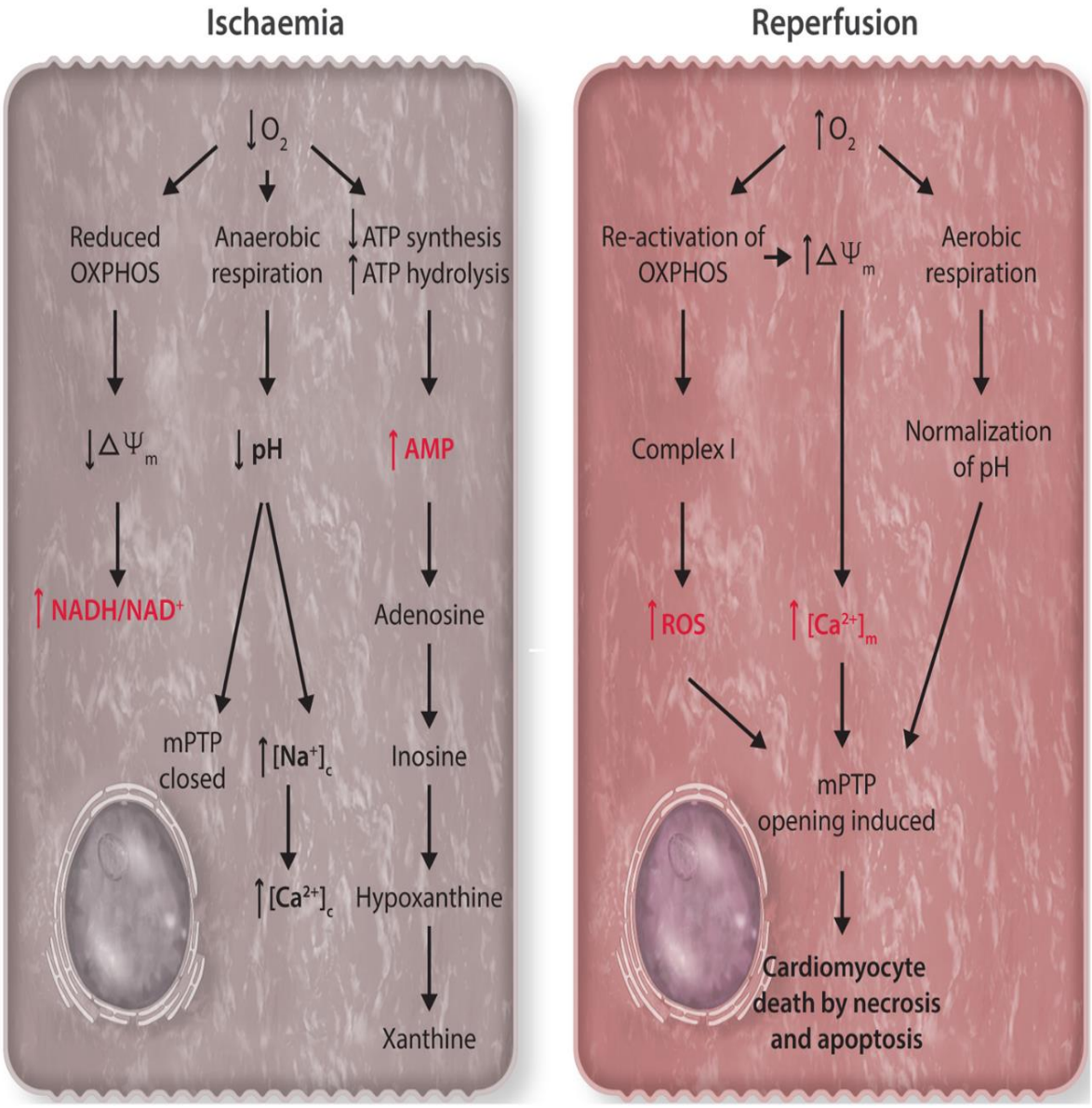

Figure 3. Illustration of the key components of I/R injury

(Pell et al., 2016).

Management of Acute Myocardial Infarction

In western countries, the management of AMI has greatly improved over the last decades. Consequently, the incidence and prevalence of post-MI HF continue to increase as more patients survive and live longer after a MI event. It has been shown that infarct size, within 1 month after primary PCI, is strongly associated with mortality and hospitalization for heart failure (HF) within 1 year (Stone et al., 2016). Moreover, in up to 60% of STEMI patients, a reperfusion failure after PCI, or the "no-reflow" phenomenon is observed, significantly attenuating the benefits of the PCI. This observation and the fact that PCI is not readily available in every region of the world justifies also the pursuit of research on the treatment of definitive MI (Bouleti et al., 2015).

Global CVD burden has been steadily rising in an unprecedented manner in low- and middle-income countries, as it is estimated that 80% of all cardiovascular deaths now occur in these countries (Chandrashekhar et al., 2020). Additionally, the implementation of guideline-based treatments for AMI remains suboptimal due to multifactorial issues such as shortage of well-trained professionals, and financial, infrastructure, and geographical constraints (Mehta et al., 2018). More than one-half of the mortality in AMI occurs within the first hour of onset of the symptoms before the patient can reach the emergency services, hence the first hour represents the best opportunity to salvage myocardium by reperfusion. Nevertheless, the total ischemic time is often prolonged in low-middle income countries, if any treatment is provided. For example, it has been reported that the mean time delay from the onset of symptoms to presentation to the hospital was 180 minutes in Brazil and 360 minutes in India, as compared to 47 minutes in New York State (Baliga et al., 2014; Nascimento et al., 2019). Besides, it has been estimated that in Mexico, only 5 out of 10 patients with STEMI have access to reperfusion therapy (Baeza-Herrera et al., 2020).

1.2.3.4 Complications of Myocardial *Infarction*

Different complications can occur following MI, particularly when the treatment is delayed or ineffective. These complications, which represent an additional cause of morbidity and mortality, require timely and accurate diagnosis and treatment. Post-MI complications can be grouped into five categories: ischemic, mechanical, arrhythmic, embolic, and inflammatory (Table 2) (Stephens et al., 2019).

Complication	Manifestations
Ischemic	Angina, reinfarction, infarct extension.
Mechanical	Heart failure, cardiogenic shock, mitral valve regurgitation, aneurysms, cardiac rupture.
Arrhythmic	Tachyarrhythmia, bradycardia, intraventricular blocks.
Embolic	Central nervous system or peripheral embolization.
Inflammatory	Acute pericarditis.

Table 2. Categorization of post-MI complications

(Stephens et al., 2019).

1.2.4 Heart Failure

Heart failure (HF) is defined as a clinical syndrome caused by a structural and/or functional cardiac abnormality, resulting in reduced cardiac output and/ or high intracardiac pressures at rest or during stress. The prevalence of HF has increased due to a rise in cardiovascular risk factors and global population aging. Despite the current advances in HF treatments, this syndrome is still characterized by a poor prognosis, as HF patients have a reduced quality of life, may require repeated hospitalizations, tend to present additional health problems, and have a reduced life expectancy (Bhatt et al., 2017; Braunwald, 2015).

Mechanisms that lead to HF can have multiple origins, namely, IHD either caused by infarction or alteration of the coronary arteries circulation, hypertension, valvular disease, genetic mutations, alcohol/drug-induced heart disease, viral infections, and metabolic abnormalities (Lemieux et al., 2011; Ventura-Clapier et al., 2004). HF is generally associated with a wide spectrum of LV functional alterations,

ranging from patients with normal LV size and preserved EF to those with severe dilation and a reduced EF. EF is considered an important parameter in the classification of patients; the main terminology currently used to describe HF is based on the measurement of the EF. HF comprises a wide range of patients, from those with preserved EF, typically ≥50%; to those with reduced EF, considered as 40% or lower (Ponikowski et al., 2016). However, this relatively arbitrary classification, which was complexified by the introduction of a new category of in-between patients with a mildly reduced ejection fraction of 40-49% referred to as mid-range ejection fraction (mrEF) is challenged by some experts (Triposkiadis et al., 2019).
Large AMI which can affect as much as 30% of LV mass can result in adverse ventricular remodeling, an abnormal modification in the architecture of the ventricle, which is associated with dilation, increased volume, the formation of scar, rearrangements of the normal structure of the heart and underlying complex biological and molecular transformations (Bhatt et al., 2017; Braunwald, 2015; Konstam et al., 2011; Cokkinos et al., 2016).

1.2.4.1 Left Ventricle Remodeling

Adverse (LV) remodeling post-MI represents the structural basis for HF and comprised complex short- and long-term changes in LV size, shape, function, and cellular and molecular composition. Ventricular remodeling involves the dilatation of the ventricle, formation of scar, and geometrical changes in the global LV shape (from ellipsoid to more spherical) and is partly propelled by neurohormonal pathways. The underlying factors of this process and its progression to HF, are the extent of the initial infarction and the reparative process (Bhatt et al., 2017; Prabhu & Frangogiannis, 2016). LV remodeling (LVR) post-MI is triggered by an inflammatory response, in which various cell types and cytokines mediate, finally leading to degradation of the myocardial extracellular matrix and slippage of

muscle bundles in the infarct zone. This gives place to wall thinning, infarct expansion, increased wall stress, and ultimately to LVR remodeling.

1.2.4.2 Oxidative Stress in Heart Failure

Oxidative stress is an alteration between the production of ROS and the endogenous antioxidant defense mechanisms or redox state.

ROS are a group of molecules with at least one oxygen atom and one or more unpaired electrons. They are divided into radical or non-radical species. The radical species contain only one unpaired reactive electron in the outer orbit. Examples of radical species include superoxide ($O_2^{\cdot-}$), hydroxyl peroxyl, and alkoxyl radicals. The nonradical species contain two unpaired electrons, for example, hydrogen peroxide (H_2O_2), organic hydroperoxides, singlet molecular oxygen, hypochlorous acid, and hypobromous acid (Bevere et al., 2022).

In low concentrations, ROS play a vital function in cell homeostasis, since basal levels of ROS are necessary for various cellular functions, such as signal transduction pathways, defense against invading microorganisms, gene expression, and cellular growth or death (Senoner & Dichtl, 2019). The cell is capable of fighting against ROS through enzymatic compounds, such as superoxide dismutase, catalase, peroxiredoxin, and glutathione peroxidase. Likewise, non-enzymatic compounds can protect against ROS, for example, tocopherol, beta-carotene, ascorbate, glutathione (GSH, reduced form), and nicotinamide (NAM) (Senoner & Dichtl, 2019). However, exacerbated ROS production leads to cell damage and death. Particularly, increased ROS in the heart can lead to the development and progression of maladaptive ventricular remodeling and HF. Collectively, experimental and clinical studies have shown that increased generation of ROS is involved in the pathogenesis of HF (Hill & Singal, 1996; Mallat et al., 1998; Redout et al., 2007).

ROS impairs the contractile machinery of cardiomyocytes relevant in excitation-contraction coupling through protein modification, namely L-type calcium channels, sodium channels, potassium channels, and the Na^+/Ca^{2+} exchanger. ROS can also impair the activity of the SERCA pump. Furthermore, ROS can stimulate an energy deficit by altering the function of proteins involved in energy metabolism. ROS has a pro-fibrotic effect, by stimulating cardiac fibroblast proliferation and matrix metalloproteinases causing extracellular remodeling (van der Pol et al., 2019).

The predominant sources of ROS in the heart are, xanthine oxidoreductases (XOS), cytochrome P450 (CYP), NADPH oxidases (NOX), uncoupled nitric oxide synthases (NOSs), and lipoxygenases as well as organelles, like the peroxisome and endoplasmic reticulum, and the mitochondria contribute to intracellular ROS production; the latter is overall, considered as the main source of cellular ROS (Bevere et al., 2022; Nickel et al., 2014; Senoner & Dichtl, 2019). The primary sites of ROS formation in mitochondria are the flavin mononucleotide prosthetic group at Complex I and the ubisemiquinone bound to the Q_0 site at Complex III. The superoxide radical ($O_2^{\cdot -}$) is produced at both sites when the reduced forms of flavin mononucleotide or ubiquinone donate an electron to O_2 (Bertero & Maack, 2018a).

The rate of $O_2^{\cdot -}$ formation is increased if the respiratory chain is altered or when there is an excess of reduced NADH due to decreased ATP demand. Under physiological conditions, $O_2^{\cdot -}$ is rapidly converted to hydrogen peroxide (H_2O_2) by superoxide dismutase. H_2O_2 is then eliminated by glutathione peroxidase and peroxiredoxin, which are in turn regenerated by a cascade of enzymatic reactions terminally requiring reduced NADPH (nicotinamide adenine dinucleotide phosphate) (Bertero & Maack, 2018a).

1.3 CARDIAC METABOLISM

Cardiac metabolism encompasses all the biochemical pathways in cardiomyocytes aimed at the production of building blocks for cell maintenance, biosynthesis, and cellular growth. There is a close connection between cardiac metabolism and contractile function, as the normal fluctuations in contractility elicit changes in cardiac metabolism. The processes of excitation-contraction coupling use the majority of the ATP produced by the mitochondria to power the activity of the heart, being the myosin ATPase, SERCA, and the Na^+/K^+-ATPase the major energy consumers (Bertero & Maack, 2018b).

In the 1950s, Robert Olson proposed that myocardial substrate consumption can be divided into four different platforms (Figure 6). The first platform consists of the delivery and uptake of substrates by the cell. The second platform entails the cytosolic and mitochondrial pathways involved in the production of acetyl-CoA, primarily FAO and, glycolysis and pyruvate decarboxylation. The third platform encompasses the oxidation of acetyl-CoA to CO_2 and water in the tricarboxylic acid (TCA) cycle and the generation of the reducing equivalents, NADH and flavin adenine dinucleotide, hydroquinone form ($FADH_2$). The fourth platform includes the electron transport chain (ETC), in which electron transfer and the collapse of the proton gradient are coupled to oxidative phosphorylation (OXPHOS) of ADP to ATP (Olson, 1959; Taegtmeyeret al., 2016).

Large amounts of chemical energy in form of ATP are utilized by the heart to ensure constant pumping of blood under pressure through the circulation to provide sufficient O_2 supply and nutrients delivery to all organs of the body. The rate of energy utilization cannot exceed that of energy production, this requires an uninterrupted and great supply of ATP. The human heart produces and consumes approximately 6 kg of ATP daily (Ritterhoff & Tian, 2017) while maintaining a constant concentration of ~10 mmol/L in humans (Neubauer, 2009). The mitochon-

dria produce 90% of the cellular ATP and cytosolic concentration remains constant at 3–4 mM, this represents a hydrolysis rate of 50 g ATP per minute (Niemann & Rohrbach, 2016).

To meet high energetic demand, the heart depends on a wide variety of substrates for ATP production that are supplied through the coronary circulation. The principal cardiac substrates are triacylglycerols, long-chain fatty acids (LCFA), glucose, glycogen, lactate, pyruvate, ketone bodies (e. g. acetoacetate, and β-hydroxybutyrate), and amino acids, especially the long-branched amino acids leucine, isoleucine, and valine. The majority of the heart's energy requirements are obtained from fatty acids (FA) oxidation (FAO) (40-60%); while, carbohydrate metabolism generates the rest (20-40%) (Karwi et al., 2018). The human heart needs about 10% of the whole-body fuel consumption, as it consumes more than 20 g of carbohydrates and more than 30 g of FAs and triacylglycerols each day (Taegtmeyer, Young, et al., 2016). The heart is characterized by its metabolic flexibility, which is the capability to switch between the previously mentioned energy sources. This flexibility is thought to have been developed to protect cells with superior energy requirements from enhanced oxidative stress, to shunt glucose to side branches of glycolysis, to deliver energy faster, or to consume the most abundant fuel available (Vallerie & Bornfeldt, 2015). Additionally, this trait confers the heart the ability to adapt to hormonal status and a changing workload (Karwi et al., 2018).

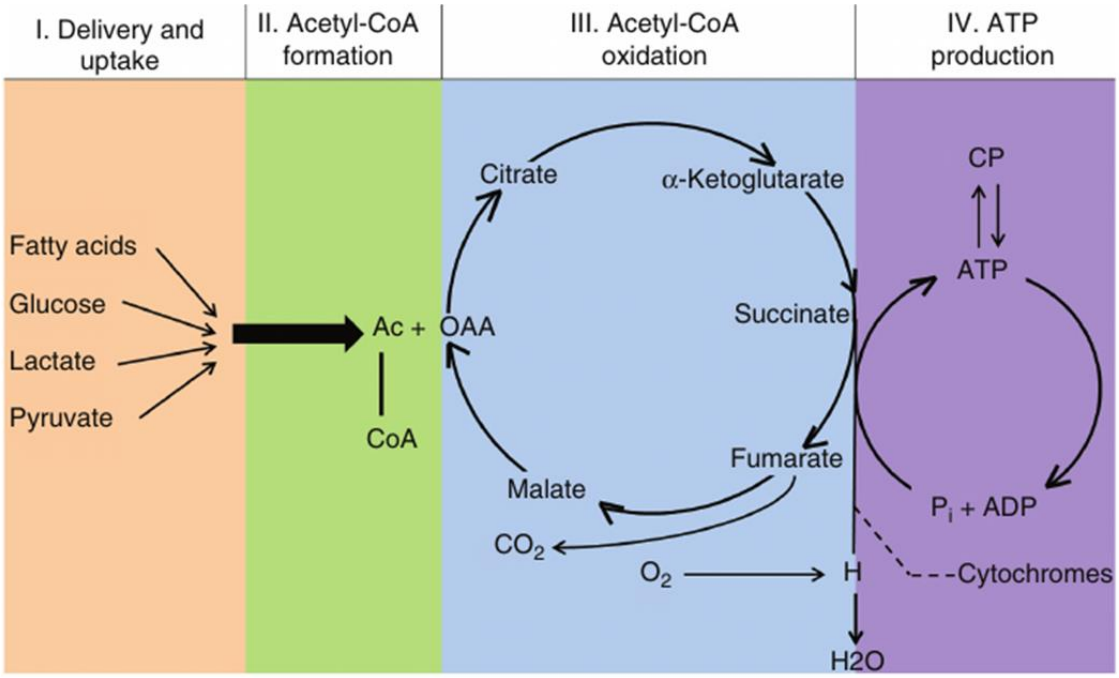

Figure 4. Metabolism of myocardial substrates

The metabolism of myocardial substrates is organized into four platforms delivery and uptake (I), acetyl-CoA formation (II), oxidation of Acetyl-CoA or smaller carbon units in the TCA cycle providing reducing equivalents for the respiratory chain (III), and ATP production (IV). ADP, adenosine diphosphate; ATP, adenosine triphosphate; Ac-CoA: acetyl-coenzyme A; CP: Phosphocreatine; OAA: Oxaloacetate (Taegtmeyer et al., 2016).

Mitochondria occupy nearly one-third of the adult cardiomyocyte volume, indicating the enhanced myocardial oxidative capacity. Under normoxic conditions, around 95% of ATP synthesis in the heart is derived from OXPHOS in the inner mitochondrial membrane, whilst the remaining 5% derives from glycolysis. Moreover, the phosphate bond of ATP is transferred by the mitochondrial creatine kinase (CK) to phosphocreatine (PCr), which then diffuses to the cytosol and provides the energy to regenerate cytosolic ATP through the myofibrillar CK isoform located near the sarcomere and other cellular ATPases such as the sarcoplasmic reticulum Ca^{2+} ATPase 2a (SERCA2A), where it catalyzes the reverse reaction: **PCr + ADP → Cr + ATP**. PCr is the major energy reserve in the myocardium, and ATP

production through the CK reaction is significantly faster than through OXPHOS (Weiss et al., 2005). The flux of the substrates through oxidative pathways is mainly determined by the catalytic activity of rate-limiting enzymes, and by the availability of the enzyme inside the cell. The catalytic activity can be regulated in a rather short timescale by various mechanisms, such as association or dissociation with regulatory proteins, allosteric effectors, and post-translational modifications, namely phosphorylation or acetylation. The availability of the enzymes is modulated by transcriptional and translational processes (Figure 7) (Bertero & Maack, 2018b).

.

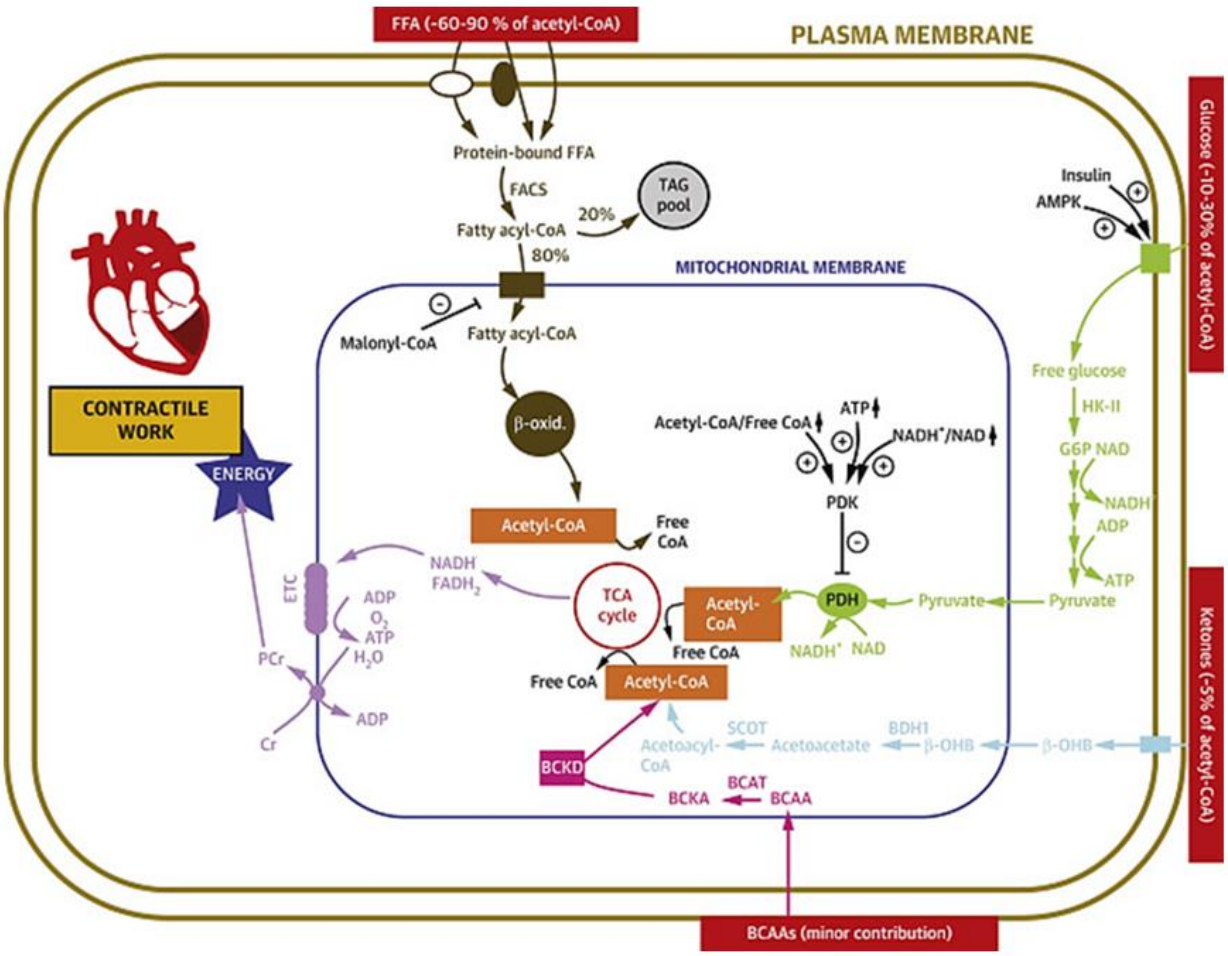

Figure 5. Energy metabolism in the heart

FAs (shown in brown) are the principal substrate for the heart (60-90% of acetyl-CoA), whereas carbohydrates (shown in green; ~30% of acetyl-CoA), ketones (shown in blue; ~5% of acetyl-CoA), and BCAA (shown in pink) play a lesser role. b-OHB, b-hydroxybutyrate; AMPK, adenosine monophosphate-activated protein kinase; ATP, adenosine triphosphate; BCAA, branched-chain amino acid; BCAT, branched-chain amino acid aminotransferase; BCKA, branched-chain ketoacid; BDH1, b-hydroxybutyrate dehydrogenase-1; CoA, coenzyme A; ETC, electron transport chain; FACS, fatty acyl-CoA synthetase; FFA, free fatty acids; G6P, glucose-6-phosphate; HK-II, hexokinase-II; PCr, phosphocreatine; PDH, pyruvate dehydrogenase; PDK, pyruvate dehydrogenase kinase; SCOT, succinyl-CoA:3-oxoacid CoA transferase; TAG, triglyceride (Honka et al., 2021).

1.3.1 The Randle Cycle

In general terms, the heart modifies its substrate utilization preference between its two major substrates: carbohydrates during the fed state and FAs during the fasted state. Under normal conditions, 50–70% of the acetyl-CoA of the heart comes from β-oxidation of FAs, whereas the remainder comes from the oxidation of pyruvate, which in turn is obtained from glycolysis and lactate oxidation. The glucose-FA cycle also known as the Randle cycle, refers to the interplay between FA and glucose metabolic pathways, which is biochemically regulated by feedback inhibition of metabolic intermediates that allows a fine-tuning of substrate supply and use. The Randle cycle describes the reciprocal crosstalk between FAO and glucose oxidation where increased synthesis of acetyl-CoA resulting from FAO decreases glucose oxidation, by inhibiting pyruvate dehydrogenase (PDH). In contrast, the enhanced production of acetyl-CoA inhibits FAO by inhibiting 3-keto-acyl CoA thiolase. In the cytoplasm, acetyl-CoA is a substrate for acetyl-CoA carboxylase 1 (ACC1), which generates malonyl-CoA, an inhibitor of CPT I, leading to decrease flux through FAO. The activity of AMP-activated protein kinase (AMPK) is a key determinant of ACC activity in the heart. In turn, AMPK/ is a serine/threonine kinase that responds to metabolic stresses that deplete cellular ATP, increase adenosine monophosphate (AMP), or increase the creatine/phosphocreatine (Cr/PCr) ratio. It is active in the heart with an important role in regulating FAO, as well as glucose uptake and glycolysis. Thus, AMPK acts as a sensor that increases FAO when energy demand is increased and decreases it when energy demand is low. It has also been speculated that malonyl-CoA dehydrogenase is a target of AMPK in skeletal muscle (El-Gharbawy & Vockley, 2017). Interestingly, this cycle also applies to lactate in the heart, as lactate inhibits the oxidation of both glucose and FAs (Hue & Taegtmeyer, 2009). Lactate is a major source of pyruvate formation under well-perfused conditions in vivo due to the predominant presence in the heart of the lactate dehydrogenase (LDH) 1 tetrameric complex (LDH-1) made of 4 subunits H (heart) whose reaction equilibrium is in favor

of lactate to pyruvate conversion, further generating nicotinamide adenine dinucleotide (NAD^+) reduction to reduced nicotinamide adenine dinucleotide (NADH) (as will be discussed later), at the opposite of other LDH isoenzymes complex that rather convert pyruvate to lactate and regenerate NAD^+ out of NADH for glycolysis to continue even in anaerobic condition, as in skeletal muscles. Under some conditions such as exercise, lactate can exceed glycolysis as a source of pyruvate (Stanley, 1991).

1.3.2 Glucose Metabolism

Glucose is considered the second most relevant substrate for cardiac energy metabolism in the adult heart. However, cardiac glucose consumption has a key role in the fetal development of the heart. The fetal heart is characterized by a high glucose delivery and a low level of O_2. During the neonatal period, the heart's consumption of glucose declines along with an increased dietary FA and O_2 supply (Piquereau & Ventura-Clapier, 2018; Wende et al., 2017). Glucose homeostasis in the heart is regulated by hemodynamic factors, neurohormonal factors, and O_2 availability. There are three energy-producing phases of glucose metabolism: glycolysis, the TCA cycle, and the respiratory chain or oxidative phosphorylation (OXPHOS) (Taegtmeyer, 2014).

Because of its polarity and large size, glucose cannot pass through the membrane of the cell by simple diffusion. Instead, glucose molecules enter the cells through glucose transporters.

Glucose utilization is begun mainly via glucose transporters, and glucose transport is the rate-limiting step in glycolytic flux in the heart. There are two classes of glucose transporters implicated in its homeostasis in the body, the facilitated transporters or uniporters (GLUTS) and the sodium-coupled active transporters or symporters (SGLTs) (Kashiwagi et al., 2015).

The regulation of the expression and the functional roles of the GLUT transporters in the heart has been investigated intensively through *in vitro* and *in vivo* models. However, less is understood regarding the role and function of SGLTs in the heart.

1.3.2.1 GLUT Transporters

The isoforms expressed in the heart of the GLUT transporters are GLUT1 and GLUT4. These are Na^+ and ATP independent transport systems. Extracellular glucose attaches to the transporter, which then changes its conformation, this allows the transport of glucose across the cell membrane via facilitated diffusion. Transcriptional regulation is one major mechanism that determines the expression and activity of GLUT in the heart. However, other isoforms have also been found in the heart, such as GLUT3, GLUT8, GLUT10, GLUT11, and GLUT12 with different expression levels (Ferrier, 2017; Schwarzer & Doenst, 2015; Shao & Tian, 2015). GLUT1 predominates during fetal and early postnatal life and is mainly localized in the sarcolemma under basal conditions. In contrast, GLUT4 is the major isoform present in differentiated cardiomyocytes and its expression is around four times higher than that of GLUT1. GLUT4 is mainly localized in the intracellular membrane compartments in unstimulated conditions and is translocated to the plasma membrane in response to stimuli such as workload, ischemia, catecholamines, contraction, and insulin (Chanda et al., 2016). Specifically, insulin and contraction are the two key stimuli that acutely regulate GLUT4 recruitment to the cell surfaces of the heart, skeletal muscle, independent of transcription or translation. However, these stimuli initiate different signaling mechanisms but both lead to increased GLUT4 translocation and glucose uptake (Chanda et al., 2016). Moreover, it has been shown that the activation of the AMPK system also promotes the translocation of GLUT4. Even though GLUT4 is the predominant isoform of glucose transporters in the myocardium, GLUT1 becomes more relevant during pathophysiological conditions in which GLUT4 is repressed, namely post-ischemic

reperfusion and HF post-MI (Rosenblatt-Velin et al., 2001; Tardy-Cantalupi et al., 1999).

1.3.2.2 SGLT Transporters

There are 12 members of the human SGLT (SLC5) gene family, which includes cotransporters for sugars, anions, vitamins, and short-chain FAs. The SGLTs belong to a structural class of membrane proteins from unrelated gene families of antiporters and Na^+ and H^+ symporters (Wright et al., 2011). All members of the SGLT family are 60 to 80 kDa proteins which contain from 580 to 718 amino acids. (Navale & Paranjape, 2016).

SGLT1 and 2 are integral membrane proteins that mediate the transport of glucose through the plasma membrane by active transport, which involves the co-transport of glucose molecules and sodium ions. The movement of a sodium ion across the plasma membrane into the cell is driven by a concentration gradient, generated by the sodium-potassium ATPase, and membrane potential (Scheepers et al., 2004).

The SGLT1 (*SLC5A1* gene) is a high-affinity, low-capacity sodium-glucose symporter and is mostly expressed in the intestine, kidney and, heart. In contrast, the SGLT2 (SLC5A2 gene) is a low-affinity, high-capacity sodium-glucose symporter (Scheepers et al., 2004).

Studies have found high levels of SGLT1 mRNA and/or protein in the heart, particularly during ischemia, hypertrophy, and diabetes. all of which were evaluated from whole heart samples in the chronic phase (Yoshii et al., 2019). Interestingly, SGLT inhibitors, a class of antihyperglycemic drugs that were first developed to treat diabetes mellitus type 2, have revolutionized the management of patients with HF. Clinical trials have revealed that SGLT2 inhibitors, such as empagliflozin and dapagliflozin) may improve outcomes in patients with HF, as seen by reduced

mortality and adverse cardiovascular events (Fitchett et al., 2020; McMurray et al., 2019). Still, their mechanisms of action are poorly understood.

1.3.2.3 Glycolysis

Glycolysis is the pathway that takes place in the cytosol, during which G6-P and NAD^+ are converted to pyruvate and NADH, respectively, and yields two ATP per molecule of glucose. Glycolysis is a focal point of carbohydrate metabolism since essentially all sugars, whether they are obtained from the diet or catabolic reactions, can be converted to glucose. Cytosolic NADH must be transferred into the mitochondrial matrix to enter the electron transport chain (ETC), and NAD^+ must be regenerated in the cytosol to maintain glycolysis and lactate conversion to pyruvate.

The inner mitochondrial membrane is impermeable to NADH (Purvis & Lowenstein, 1961). However, NADH shuttle pathways such as the malate-aspartate (M-A) shuttle, the α-glycerophosphate shuttle, the malate-citrate, and fatty acid shuttles mediate the transport of NADH into the mitochondria, being the M-A shuttle the main pathway in the heart (Lu et al., 2008). In anaerobic conditions such as ischemia or if there has been a sudden energy demand, pyruvate can be reduced to lactate by LDH and NADH is oxidized to NAD^+, allowing glycolysis to proceed. The conversion of glucose to pyruvate occurs in two phases. The first phase corresponds to the first five reactions in which there is energy investment to synthesize the phosphorylated forms of the intermediates at the expense of ATP consumption (Figure 9). The second phase called "pay-off" or energy-generation phase corresponds to the subsequent reactions that ultimately yield a net production of two molecules of ATP per glucose molecule through substrate-level phosphorylation, together with the production of 2 molecules of pyruvate, and 2 molecules of NADH (Dashty, 2013; Ferrier, 2017). NADH-reducing equivalents produced in the cytoplasm through glycolysis are transferred to the mitochondria

by shuttling mechanisms such as the malate-aspartate shuttle, in which NADH in the cytosol is oxidized to NAD^+, and NAD^+ in mitochondria is reduced to NADH. Alternatively, NADH is oxidized back to NAD^+ in the cytoplasm via LDH (Yang & Sauve, 2016).

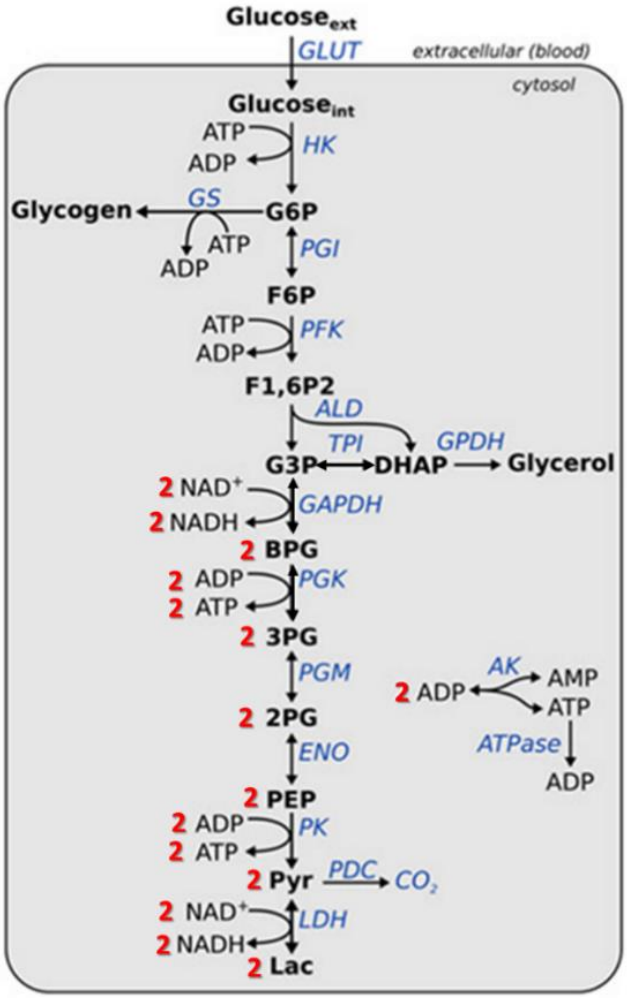

Figure 6. The glycolysis pathway

A series of enzymatic reactions of glycolysis converts glucose to pyruvate, which may be catabolized by the TCA cycle or reduced to lactate. GLUT indicates glucose transporter; HK, hexokinase; G6P, glucose 6-phosphate; GS, glycogen synthase; PGI, phosphoglucose; F6P, fructose 6-phosphate; PFK, phosphofructokinase 1; F1,6P2, fructose 1,6-bisphosphate; ALD, aldolase; TPI, triosephosphate isomerase; G3P, glyceraldehyde 3-phosphate; DHAP, dihydroxyacetone phosphate; GAPDH, glyceraldehyde-3-phosphate dehydrogenase; BPG, 1,3-bisphosphoglycerate; GPDH, glycerol-3-phosphate dehydrogenase; PGK, phosphoglycerate kinase; 3PG, 3-phosphoglycerate; PGM, phosphoglycerate mutase; 2PG, 2-phosphoglycerate; ENO, enolase; PEP, phosphoenolpyruvate; PK, pyruvate kinase; Pyr, pyruvate; PDC, pyruvate dehydrogenase complex; LDH, lactate dehydrogenase; Lac, lactate; AK, adenylate kinase (modified from Karlstaedt et al., 2020).

1.3.2.4 Pyruvate Decarboxylation

Pyruvate decarboxylation is the reaction that links glycolysis with the TCA cycle. Once pyruvate is formed it passes from the cytosol into the mitochondria through the mitochondrial pyruvate carrier (MCP1/2) (Figure 10) (Werner et al., 2016). There, pyruvate is decarboxylated by the pyruvate dehydrogenase complex (PDC). PDC is a multi-enzyme complex located in the mitochondrial matrix that plays a vital role in aerobic energy metabolism. PDC is composed of three catalytic components: Pyruvate dehydrogenase (PDH/E1), dihydrolipoamide acetyltransferase (E2), and dihydrolipoamide dehydrogenase (E3).

PDC also requires five different coenzymes: CoA, NAD^+, FAD^+, lipoic acid, and thiamine pyrophosphate (Sun et al., 2015). In this process, two pyruvic acids of the glycolysis pathway are consumed to produce two molecules of acetyl-CoA, two molecules of NADH, and two molecules of CO_2 per molecule of glucose. PDC can control the consumption and storage of fuels to achieve metabolic flexibility in response to the environment and nutrient availability (Figure 10). PDH can be inactivated by PDH kinases 1-4 (PDK1-4) isozymes which phosphorylate specific serine residues within the α subunit.

The activity of PDKs can be regulated by different metabolites as well as transcription factors under various conditions. They are stimulated by NADH and Acetyl-CoA and are inhibited by pyruvate. Three isoforms are expressed in the heart, PDK1, PDK2, and PDK4 (Rardin et al., 2009). Notably, PDK4 is highly expressed in the heart and its expression is significantly induced in the heart and skeletal muscle upon several metabolic stimuli, including fasting and a high-fat diet (Crewe et al., 2013; Spriet et al., 2004; Wu et al., 1998). The PDK4 gene is induced by the forkhead transcription factor FoxO1, which in turn is repressed by insulin, and peroxisome proliferator-activated receptor (PPAR)-α, which is activated by FAs (Zhao et al., 2008). Moreover, the reactivation of PDH is achieved by the action of pyruvate dehydrogenase phosphatase (PDP). Two isoforms of this enzyme have been found, PDP1 and PDP2 (Rardin et al., 2009). PDP1 is Ca^{2+}-sensitive is highly

expressed in the rat heart and is recognized as an important regulator of the activity of PDC. Its sensitivity to Ca^{2+} leads to the activation of the PDC in response to conditions that increase the mitochondrial concentrations of this cation. PDP2 is a Ca^{2+}-insensitive isoform and is regulated by starvation in the heart (Huang et al., 2003).

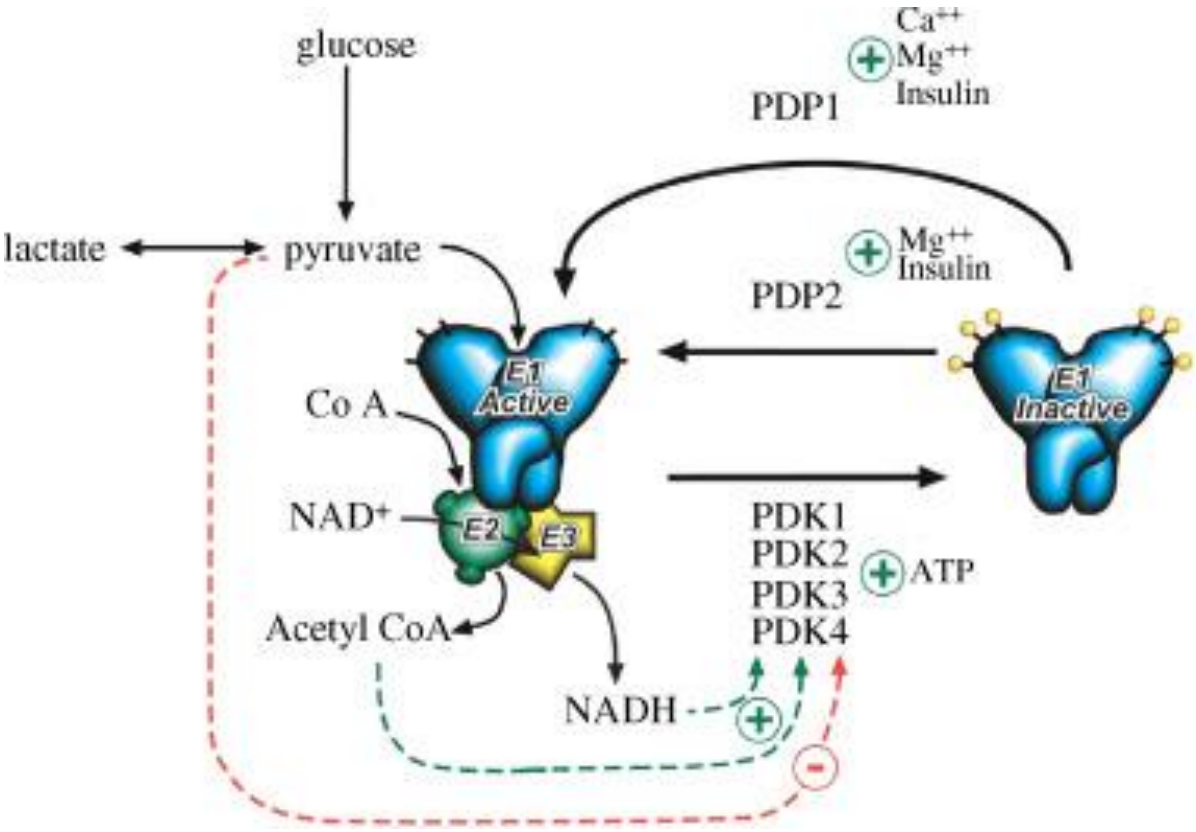

Figure 7. The activity of PDC

Interconversion of active (unphosphorylated) and inactive (phosphorylated) E1- alpha subunit (PDH) is catalyzed by PDP1-2 and PDK1-4, respectively (the regulators of these enzymes are indicated with "+" or "– "). E1 is represented in blue, and the three serine sites per E1-alpha subunit are shown as black lines with the addition of yellow spheres when phosphorylated. E2 is shown in green and E3 is shown in yellow (Maj et al., 2006).

1.3.2.5 The Pentose Phosphate Pathway

Once glucose molecules are taken up by muscle cells and transported into the cytosol, glucose may be first phosphorylated to glucose 6-phosphate (G6-P) by hexokinase or converted to sorbitol by the polyol pathway. G6-P is a branch-point for several pathways, including glycolysis and two alternate pathways, the pentose phosphate pathway (PPP), and the hexosamine biosynthetic pathway (Tran & Wang, 2019) (Figure 8).

The PPP allows for an alternative fate of glycolytic intermediates and has been detected in the cytosol (Kolwicz & Tian, 2011). There are two branches in the PPP, the oxidative and the nonoxidative. The oxidative PPP generates NADPH and ribulose 5-phosphate, and the nonoxidative branch metabolizes ribulose 5-phosphate to 5-carbon sugars for nucleotide biosynthesis or generation of intermediates for glycolysis (i.e., glyceraldehyde 3-phosphate and fructose 6-phosphate). The reactions of the nonoxidative branch are reversible, which may produce ribulose 5-phosphate from glycolytic intermediates (Tran & Wang, 2019). Also, the oxidative PPP supplies cytosolic NADPH, which maintains reduced glutathione (GSH) levels. In contrast, NADPH contributes to cytosolic ROS production by the activation of NOX and NOS. Consequently, the PPP may play a dual role in redox balance regulation (Jain et al., 2003).

Although this pathway is present in all cells, it is believed that its contribution is not highly relevant in the normal heart. It has been shown in early studies that an up-regulation of the PPP is present during cardiac hypertrophy (Zimmer et al., 1980). Moreover, it has been suggested that excessive NADPH derived from the oxidative PPP promotes HF (Gupte et al., 2006).

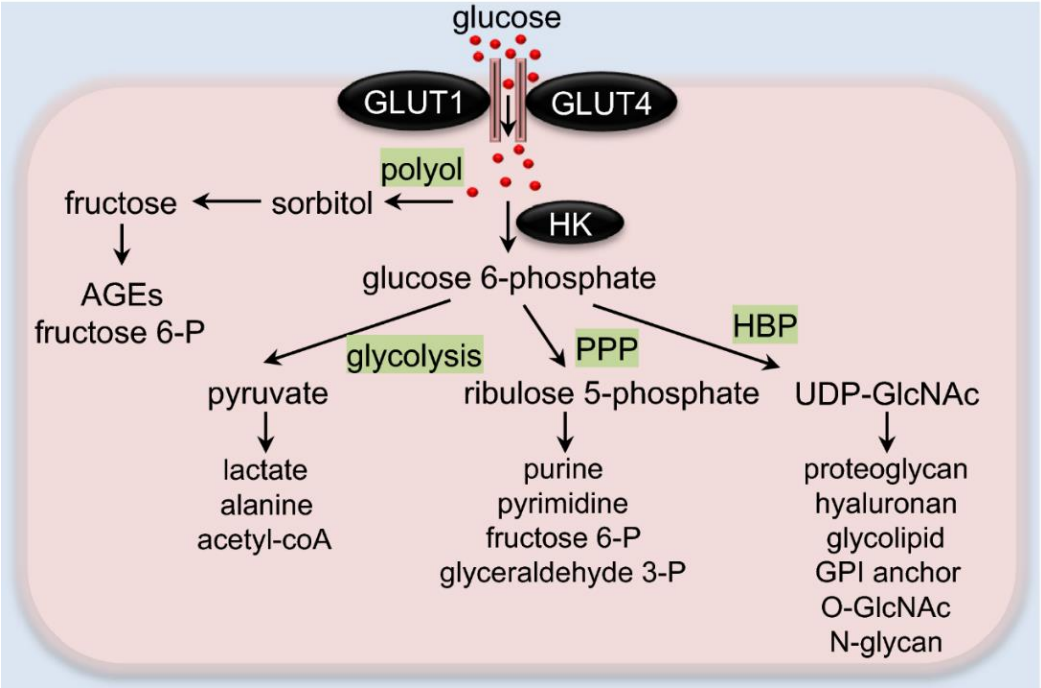

Figure 8. Glucose metabolism pathways in the heart

In cardiomyocytes, glucose is transported through glucose transporters GLUT1 or GLUT4. Polyol pathway-derived sorbitol and fructose may be converted to advanced glycation end-products (AGES) or fructose 6-P for glycolytic use. Intracellular glucose can be phosphorylated to glucose 6-phosphate by hexokinase (HK). Glucose 6-phosphate can be utilized by multiple pathways, such as glycolysis, pentose phosphate pathway (PPP), and hexosamine biosynthetic pathway (HBP) (Tran & Wang, 2019).

1.3.3 Fatty Acids Metabolism

The FAs used by the heart are carried in the bloodstream bound to albumin as free, non-esterified FAs or as FAs released from triacylglycerol (TAG) contained in chylomicrons of very-low-density lipoproteins (VLDL). Both sources contribute substantially to FA supply to the cardiomyocytes. Normally, the circulating free FA (FFA) concentration range is between 0.2 and 0.6 mM (Stanley et al., 2005), however, these levels can increase up to 2mM during MI (Lopaschuk et al., 1994). Chylomicron TAG is another source of FAs that competes with FFAs bound to albumin, yet, most of the FAs used by the heart that derive from TAG are originated from chylomicrons (Lopaschuk et al., 2010). Long-chain FAs (LCFAs)

transport across a biological membrane is facilitated and regulated by specific membrane-associated proteins, such as peripheral membrane FA-binding protein (FABPpm), a family of six FA transport proteins (FATP1-6), and CD36 (Gimeno et al., 2003; Schwarzer & Doenst, 2015).

Furthermore, chylomicron TAG must be assimilated into the myocardium through lipoprotein lipase (LPL), an endothelium-expressed enzyme that regulates the transport of TAG-derived FAs into the cardiomyocytes across the endothelium. A significant part of circulating FFAs are present as TAG in lipoproteins, hence the hydrolysis of this TAG by LPL is determinant for FA uptake and β-oxidation by the heart (Lee & Goldberg, 2007). Once FAs have entered the cell, they are either stored in the cell as triglycerides or oxidized to generate energy in the form of ATP when necessary. The major long-chain FAs (16-22 carbons) that will undergo oxidation are activated by the Acyl-coenzyme A synthetases (ACS). These include members of the long-chain acyl-CoA synthetases (ACSL) and very long-chain acyl-CoA synthetases (ACSVL)/FA transport protein (FATP) subfamilies that catalyze a two-step reaction: the formation of an intermediate fatty acyl-AMP with the release of pyrophosphate, and the formation of a fatty acyl-CoA with the release of AMP (Ellis et al., 2010; Mashek et al., 2007).

Following this activation step, 70–90% of the FAs go through immediate oxidation. The remainder is stored in the intracellular triglyceride pool (Lopaschuk et al., 1994). ACSL1, one of 5 independent ACSL isoforms, is specifically required for FA oxidation in highly oxidative tissues like the heart (Ellis et al., 2011).

FAs must be transported into the mitochondria so they can be oxidized. Short-chain FAs and ketone bodies can enter the mitochondria by diffusion. However, most FAs are long-chained and require a specific transport system, the carnitine-palmitoyl transferase system. This is achieved by a carnitine-mediated translocation, as there are no transporters for the CoA esters of FAs in the inner mitochondrial membrane. This process is catalyzed by the carnitine palmitoyl transferase-I (CPT1), which is localized in the outer membrane of the mitochondria and is a

rate-limiting enzyme of mitochondrial β-oxidation by controlling the entry of long-chain FA (LCFA) into the mitochondria (Kerner & Hoppel, 2000).

Then the carnitine esters are transported across the inner membrane and converted back to CoA esters by CPT-II. Then, the CoA esters can enter the β-oxidation pathway in the mitochondrial matrix (Jogl et al., 2004). CPT1 exists as two distinct isoforms, L-CPT (*a* isoform) and M-CPT (*b* isoform), and both isoforms are co-expressed in the heart muscle. In adult heart muscle, M-CPT1 is the predominant isoform. However, high levels of L-CPT1 have been found in the hypertrophied heart (Lewandowski et al., 2013). In turn, CPT2 is characterized by a widespread expression (Martín et al., 2000). CPT1 is inhibited by malonyl-CoA, which binds to CPT1 on the cytosolic side of the enzyme (Zammit et al., 1997) (Figure 11). Hence, malonyl-CoA is an important regulator of FAO in the heart as it decreases the uptake of FAs into the mitochondria. A decrease in malonyl-CoA boosts FA uptake and oxidation (Abu-Elheiga et al., 2001). Malonyl-CoA is synthesized from the carboxylation of acetyl-CoA through ACC, which in turn is inhibited by phosphorylation through AMPK (Jäger et al., 2007). There are two isoforms of ACC in the heart, α, and β, being ACCβ the predominant isoform. The regulation of ACC is under phosphorylation/dephosphorylation control, with AMPK having a major role in its regulation in the heart (Ussher & Lopaschuk, 2008).

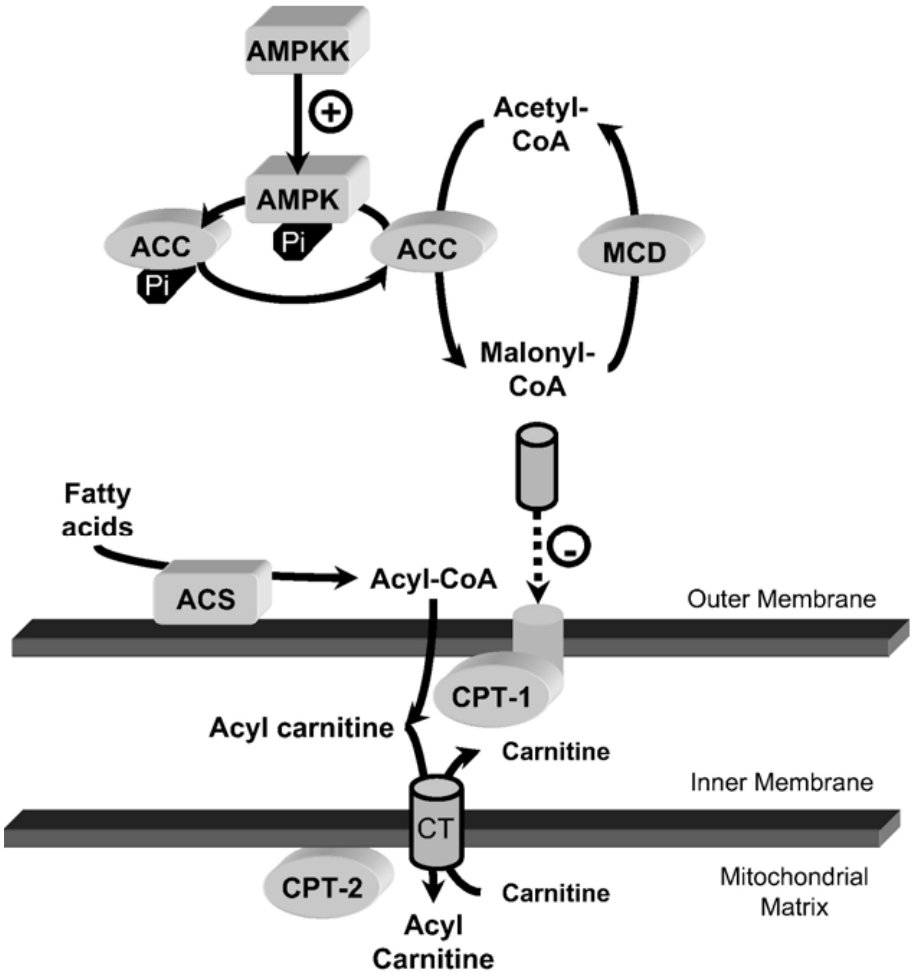

Figure 9. Regulation of malonyl-CoA

Enzymatic pathways involved in the regulation of malonyl-CoA control of cardiac fatty acid oxidation. ACC, acetyl-CoA carboxylase: ACS, acyl-CoA synthetase: AMPK, AMP-activated protein kinase: AMPKK, AMP-activated protein kinase kinase: CPT-1/2, carnitine palmitoyltransferase: MCD, malonyl-CoA decarboxylase (Folmes & Lopaschuk, 2007).

1.3.4 β-oxidation of Fatty Acids

Once inside the mitochondrial matrix, acyl-CoA enters β-oxidation directly, this process repetitively cleaves off two-carbon acetyl-CoA units, producing NADH and $FADH_2$ (Figure 12). The β-oxidation process requires four reactions, with specific enzymes for each step, and for each reaction, there are specific enzymes for long, medium, and short-chain length fatty intermediates (Clarke, 2013; Stanley

et al., 2005; Werner et al., 2016). First, acyl-CoA dehydrogenase catalyzes the oxidation at the β-carbon of the FA, this happens with a reduction of FAD to $FADH_2$ to produce Δ2-trans-enoyl-CoA. Then $FADH_2$ transfers its electrons to ubiquinone in the electron transport chain. The second step is catalyzed by enoyl-CoA reductase. The Δ2-trans-enoyl double bond is hydrated to create a 3-hydroxyl group. After, 3-Hydroxyacyl–CoA dehydrogenase oxidizes the 3-hydroxyl group with reduction of NAD^+ to NADH which produces a β-keto group. Finally, β-Ketothiolase cleaves acetyl-CoA at the β-keto group, and CoA is attached to the shortened acyl chain to return to the β-oxidation cycle. Acetyl-CoA will remain in the matrix as a substrate for the TCA cycle for further oxidation. The NADH, $FADH_2$, and acetyl-CoA produced from β-oxidation create a net of 129 moles of ATP for each palmitate oxidized (Pelley, 2007b).

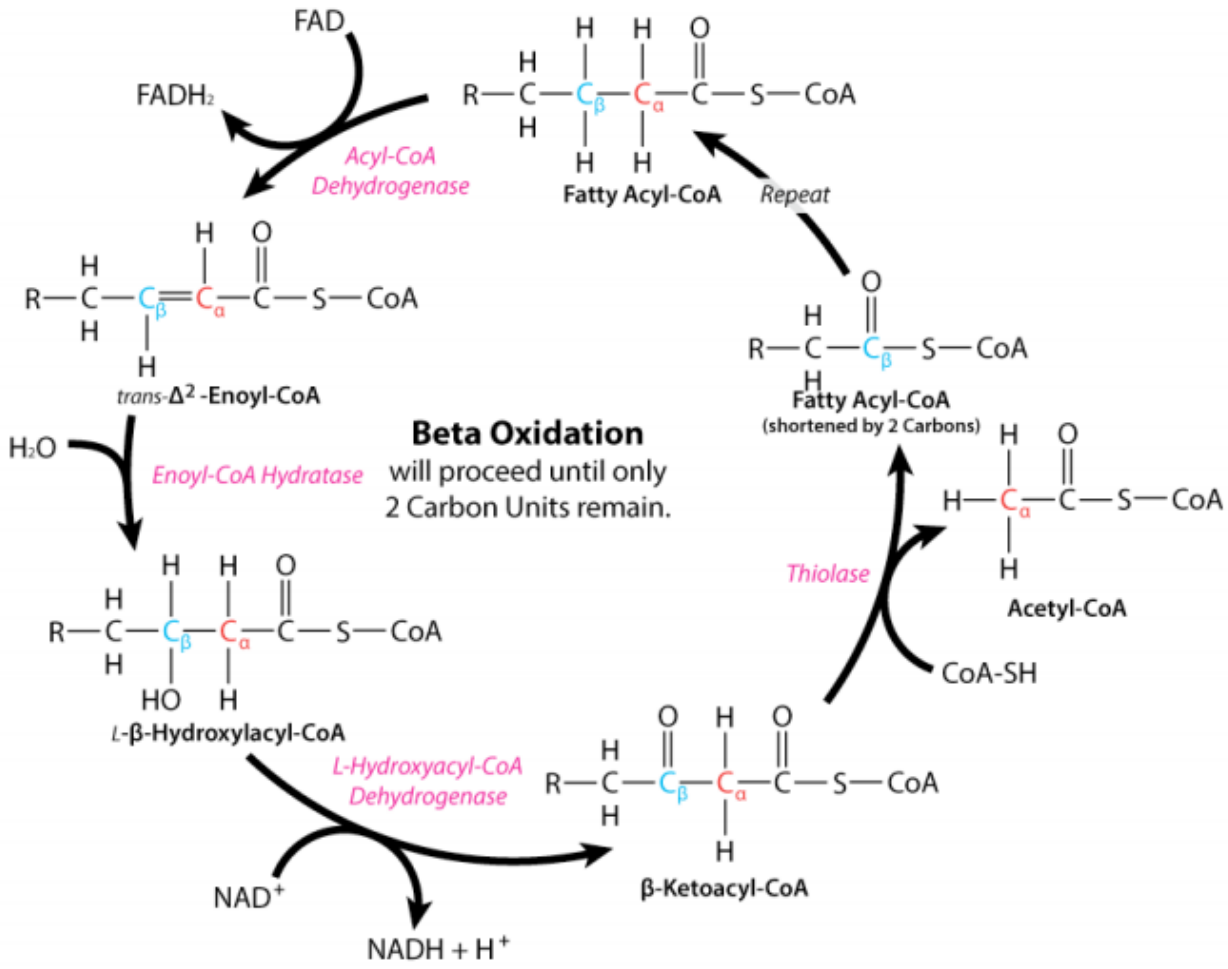

Figure 10. Scheme of β-oxidation of FAs

(Alabduladhem & Bordoni, 2021).

1.3.5 Regulation of Fatty Acid Metabolism

PPARα is a lipid-activated nuclear receptor that has been shown to regulate basal and FA-induced transcription of FAO enzyme genes, such as medium-chain acyl-CoA dehydrogenase and muscle carnitine palmitoyltransferase I *(M-CPT1)*. PPARα binds to target DNA elements as a heterodimeric partner with the retinoid X receptor. The most relevant endogenous ligands for the PPARs are LCFAa and their metabolites (Finck, 2007). The isoform PPARα is highly expressed in cardiomyocytes and regulates the expression of key components of uptake, esterification, and oxidation of FA via transcriptional activation of genes encoding important proteins in the pathway. Moreover, It has been shown that PPARα attenuates cardiac remodeling after pressure overload (Smeets et al., 2008). PPARs recruit transcriptional coactivators that are necessary to initiate target gene transcription whenever engaged by ligand. The best-characterized coactivator of PPARα in the heart is the cardiac-enriched PPARγ coactivator-1α (PGC1α). PGC1α is a coactivator that interacts with several members of the nuclear receptor superfamily. PGC1α acts via PPARα and other transcription factors in the heart, to couple metabolic requirements to the expression of genes involved in the control of energy metabolism (Finck, 2007). Mitochondrial biogenesis and respiration are stimulated by PGC1α through the downstream induction of NRF1 and NRF2 gene expression. PGC1α is considered a master regulator of mitochondria biogenesis and is enriched in tissue with high oxidative activity, like the heart (Ventura-Clapier et al., 2008). PGC1α levels correlate with cardiac and skeletal muscle oxidative capacity, suggesting that it plays a major role in setting mitochondrial content (Garnier et al., 2003).

1.3.6 Ketone Bodies Metabolism

Substrates such as ketone bodies enter the cell through facilitated diffusion. The heart expresses the monocarboxylate transporter 1 (MCT1), which facilitates the trans-sarcolemmal bidirectional movement of lactate and ketone bodies

(Halestrap, 2013). The two major enzymes involved in ketogenesis are mitochondrial hydroxymethyl glutaryl CoA synthase 2 (HMGCS2) and hydroxymethyl glutaryl CoA lyase (HL) (Fukao et al., 2004). Ketogenesis takes place in the liver, generating the three ketone bodies: acetone, acetoacetate (AcAc), and β-hydroxybutyrate (βOHB), being βOHB the predominant one found in circulation. The plasma concentration of ketone bodies is usually at a low level; thus, they are generally a minor substrate for the heart. However, the concentration of ketone bodies can increase during conditions such as starvation, ketogenic regime, prolonged exercise, and poorly controlled diabetes becoming an important substrate for the myocardium (Avogaro et al., 1990; Lopaschuk et al., 2020; Stanley et al., 2005).

Studies had shown that elevated plasma ketone bodies inhibit the uptake and oxidation of glucose and FA (Stanley et al., 2003; Sultan, 1992), with an inhibitory effect probably mediated through product inhibition on PDH (Stanley et al., 2005). In contrast, a recent study showed that increasing the contribution of ketone oxidation to the TCA cycle activity with high concentrations of βOHB, did not result in a decrease in the contribution of glucose oxidation or FA oxidation to TCA cycle activity (Ho et al., 2020). It has also been reported that ketones bodies, for example, βOHB, can become the major fuel of the healthy and failing heart (Ho et al., 2020; Murashige et al., 2020).

1.3.7 The Tricarboxylic Acid Cycle

The TCA cycle, also known as the citric acid cycle or the Krebs cycle is a hub in metabolism, as it constitutes a common pathway for the ultimate catabolism of carbohydrates and fats. The fuel for the cycle is acetyl-CoA, which has a key role in sugar and fat metabolism. It is comprised of eight enzymes, all of which are in the mitochondrial matrix, except for the succinate dehydrogenase, which is linked to the respiratory chain on the inner mitochondrial membrane and constitutes

the complex 2 of the ETC. Regulation of the TCA cycle occurs at three distinct points that include the three following enzymes: citrate synthase, isocitrate dehydrogenase, and α-ketoglutarate dehydrogenase. It also replenishes precursors for the storage form of fuels, such as amino acids and cholesterol (Alabduladhem & Bordoni, 2021).

The TCA cycle starts with Acetyl-CoA being combined with oxaloacetate by the enzyme citrate synthase to produce the 6-carbon molecule citrate. In the second step, the enzyme aconitase converts citrate into its isomer, isocitrate. Then, further enzymatic oxidation and decarboxylation of isocitrate convert into the five-carbon α-ketoglutarate by isocitrate dehydrogenase. Afterward, a four-carbon succinyl-CoA molecule is formed by α-ketoglutarate dehydrogenase, releasing two molecules of CO_2, and producing two NADH molecules. Next, succinyl-CoA synthetase converts succinyl-CoA converts into succinate. During this step, GTP is generated, which can ultimately be transformed into ATP. Succinate is oxidized by succinate dehydrogenase to produce fumarate. This step also generates 2 $FADH_2$ molecules. Subsequently, fumarate is converted into malate by the enzyme fumarase. Finally, one turn of the TCA cycle is completed by the formation of oxaloacetate and NADH after the oxidation of malate by malate dehydrogenase (Figure 13) (Martínez-Reyes & Chandel, 2020).

The series of sequential reactions during the TCA cycle forms reduced species, NADH and $FADH_2$, yielding three NADH and one $FADH_2$ per acetyl-CoA molecule. NADH and $FADH_2$ then enter the respiratory chain where O_2 is integrated as the final electron acceptor and ATP and H_2O are produced (Clarke, 2013).

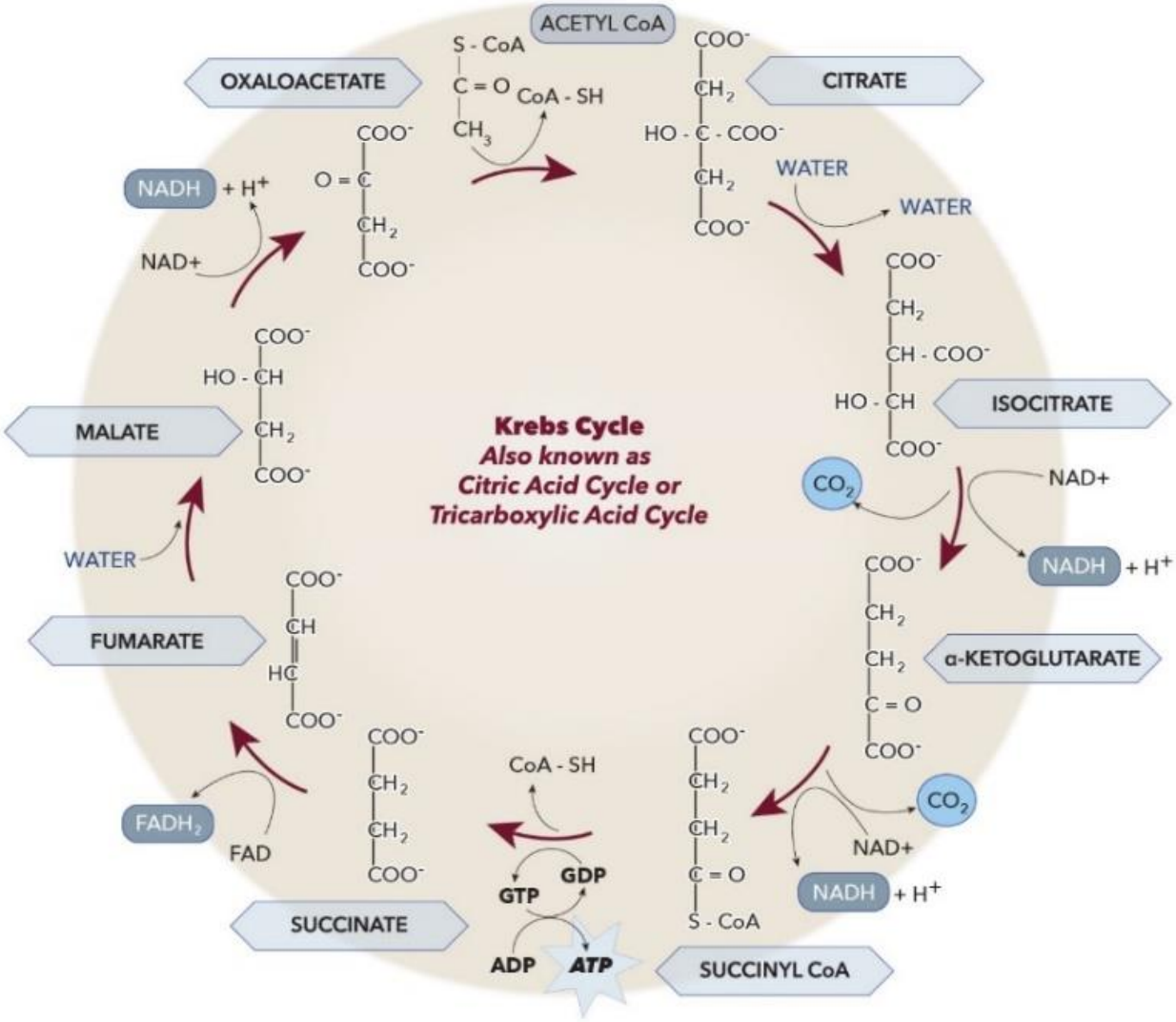

Figure 11. The TCA cycle

(Alabduladhem & Bordoni, 2021).

1.3.8 The Electron Transport Chain

The electron transport chain (ETC) can be considered the last phase in energy metabolism. In this final process, the electron carriers NADH and $FADH_2$ donate their electrons gained from the oxidation of energy substrates and TCA intermediates, to the ETC, and as the electrons pass along the chain of specialized electron acceptor and donor molecules, that fall to successively lower energy states. At this point, the reducing equivalents NADH and $FADH_2$, deliver their electrons to be passed on to Complex (C) I and CII, respectively that will then be conveyed to CIII and CIV. The successive redox reactions that drive electron transport provide the energy for the ETC to pump protons (at CI, CII, and CIV as detailed below) from the mitochondrial matrix to the intermembrane space, where a proton gradient is created. At the CIV, the endpoint of the ETC, tetravalent reduction ($4e^-$) of molecular O_2, produces 2 molecules of water. The enzyme complexes of the ETC and oxidative phosphorylation (ATP synthesis) are embedded in the inner mitochondrial membrane (Figure 14) (Alberts et al., 2002).

CI, also known as NADH–Q or NADH dehydrogenase, is a multi-subunit complex that transfers electrons from NADH in the mitochondrial matrix to coenzyme Q through its coenzyme, flavin mononucleotide (FMN). CII is the succinate dehydrogenase or succinate–Q reductase, a multi-subunit complex that gives electrons from a riboflavin coenzyme, $FADH_2$, to coenzyme Q. This complex comprises 4 enzymes that have FAD as a prosthetic group: Succinate dehydrogenase, from the TCA cycle; glycerol-3-phosphate dehydrogenase, and fatty acyl–CoA dehydrogenase, from the first step in β-oxidation. Coenzyme Q (ubiquinone) receives electrons from $FMNH_2$ in complex I and $FADH_2$ in CII and carries them through the inner mitochondrial membrane to cytochrome c reductase (CIII).

CIII or cytochrome c reductase is a multi-subunit complex that receives electrons from coenzyme Q and donates them to cytochrome c. CIII is formed by cyto-

chrome b and cytochrome c1. Cytochrome c is a water-soluble protein that diffuses along the surface of the inner membrane facing the intermembrane space to give electrons from CIII to CIV.

CIV or cytochrome oxidase is a multi-subunit protein that transfers electrons from cytochrome c to O_2. It is composed of two protein components, cytochromes and a3, and a copper component. One molecule of water is produced for each molecule of NADH or $FADH_2$ oxidized in the ETC.

Throughout this process of redox reactions, enough protons are pumped into the intermembrane space by CI, CIII, and CIV to preserve a 10:1 concentration gradient between the intermembrane space and the matrix. Finally, the ATP-synthase (CV) (F_1F_0-ATP synthase) uses the free energy stored as transmembrane electrochemical gradient or proton motive force, to drive the synthesis of ATP at the site of the F_0 rotor subunit. The ATP synthase is a large multi-subunit enzyme complex comprised of up to 20 distinct subunits or polypeptides that are in some cases present in multiple copies. The ATP synthase is attached to the inner membrane of the mitochondria with several subunits being water-soluble whilst others are integral membrane proteins. The ATP synthase is a reversible molecular motor comprised of two distinguishable components, a proton turbine (within F_0) and a molecular machine (F_1) that uses rotational energy to form ATP from ADP and phosphate. F_0, the proton turbine is driven by the flow of protons down a potential gradient across the mitochondrial membrane created by the ETC. The rotor of the turbine is within the F_1, its rotation drives the synthesis of ATP. The ATP synthase acts to transform the energy of oxidation reactions of the ETC to the phosphorylation of ADP. The number of ATP molecules made per number of atoms of oxygen reduced in the ETC (P/O ratio) is a measure of the coupling of ATP synthase with the ETC. The P/O ratio depends on several variables, comprising the membrane integrity, site of the electron transport chain where the electrons are accepted, and the integrity of the ATP synthase (Kulish et al., 2016; Xu et al., 2015). The consensus values for mammalian mitochondria are 2.5 and 1.5 for electrons

entering NADH dehydrogenase and succinate dehydrogenase, respectively (Hinkle, 2005). This enzymatic complex can also hydrolyze ATP to eject the protons out of the mitochondria to reestablish the proton motive force (Moyes & Le Moine, 2011). The ETC is coupled to ATP synthesis, which confers a regulatory impact on the flow of electrons. ETC activity and O_2 consumption rise with increased energy needs, i.e. whenever ADP levels increase (Pelley, 2007).

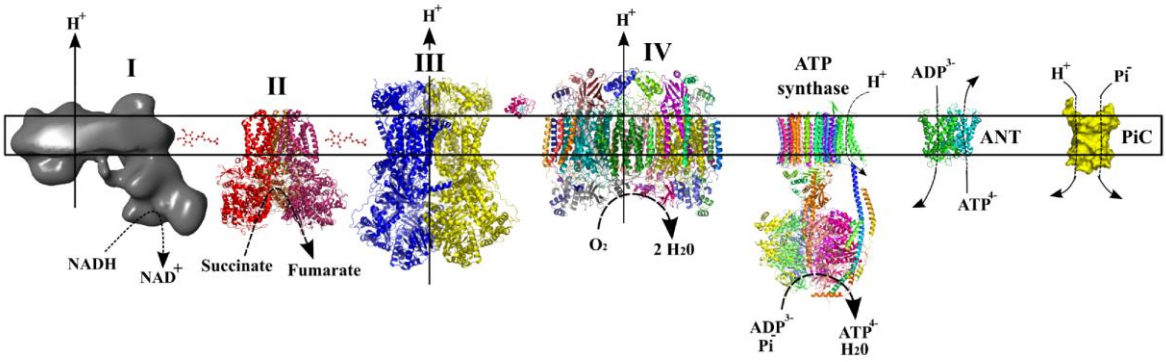

Figure 12. Schematic representation of the ETC complexes

(Mourier & Larsson, 2011).

1.3.9 Alterations of Energy Metabolism in Heart Failure

The progression of HF is characterized by a shift of the energy metabolic pathways, from predominant FA utilization to the O_2-sparing carbohydrate metabolism. Studies demonstrate that FAO is unaffected or slightly increased in the early stages of HF (Chandler et al., 2004). However, there is a down-regulation in FAO enzyme expression and a decrease in FA utilization in advanced or end-stage decompensated HF (Stanley et al., 2005); additionally, lipid storage and carnitine transport are down-regulated in the heart of patients with severe HF (Bedi et al., 2016). The decrease in FAO could be explained partially by the suppression of PPARα and PGC1α signaling. In animal models and patients with HF, the activity of PPARα and PGC1α is downregulated. As previously mentioned, PGC1α regulates mitochondrial biogenesis and is under the control of metabolic intermediates derived from lipid metabolism, which indicates another possible mechanism

linking FA buildup to altered mitochondrial function (Figure 15) (Bertero & Maack, 2018b). In contrast, there is an increase in glucose uptake and glycolysis during the early stages of HF. The failing heart is also characterized by an increase in glucose uptake and glycolytic rates, although this is not associated with an increase in glucose oxidation. This increase in glucose metabolism might be a result of modifications in the regulation of carbohydrate consumption pathways secondary to FAO suppression and/or upregulation of the anaplerotic pathway (TCA cycle) (Pound et al., 2009; Sorokina et al., 2007). In addition to these findings, it has been observed that HF leads to a switch in gene expression that resembles the expression pattern of the developing heart, this process is known as "cardiac fetal reprogramming." This HF hallmark might be an adaptive response to manage adverse remodeling in the heart (Birkenfeld et al., 2019).

Additionally, mitochondrial dysfunctions such as deficient creatin-kinase mediated energy transfer systems decreased FA β-oxidation and decreased mitochondrial OXPHOS capacities; and increased production of reactive O_2 species (ROS) play a major role in the development of HF. Typical outcomes of metabolic perturbations in HF are the decline of PCr/ATP ratio, the ATP/ADP ratio, and the reduction of total ATP concentration. Beyond the cardiac tissue, the malfunction of the heart impedes O_2 and substrates from being delivered to the periphery, therefore metabolic products are not adequately cleaned up, leading to a state of overall energy deficiency in the whole organism (Ventura-Clapier et al., 2011). Furthermore, it has been demonstrated that chronic HF results in alterations in mitochondrial function and decreased oxidative capacity in skeletal muscles (De Sousa et al., 2000; Mettauer et al., 2001). Current pharmacological treatments of HF mainly focus on reducing the workload of the cardiac pump, notably, the β-blockers that slow down heart rate and the angiotensin-converting enzyme inhibitors or angiotensin receptor blockers that lower blood pressure. However, while indirectly sparing energy consumption for the cardiac pump, these pharmacological

strategies do not address the perturbation of the heart's bioenergetics induced by HF (Diguet et al., 2018; Ventura-Clapier et al., 2011). Hence, the stimulation of cardiac metabolism represents a promising treatment of the failing heart. Remarkably, it has been observed that patients with chronic HF have elevated levels of ketone bodies in the blood (Lommi et al., 1997; Lommi et al., 1996). Furthermore, it has recently been demonstrated that acute infusion of βOHB to patients with HF with reduced EF can improve LV function (Nielsen et al., 2019). The oxidation of ketones produces more ATP per mole of O_2 compared to FAs, and ketone extraction by the cardiac muscle is very high. This shift in substrate preference is thought to represent a compensatory mechanism during HF (Honka et al., 2021). Also, a deficient branched chained amino acids (BCAA) catabolism has been observed in stressed hearts. In a mouse model of impaired BCAA catabolism, BCAA accumulation in cardiomyocytes inhibits PDH activity, and glucose oxidation, and increases infarct size after ischemia (Li et al., 2017).

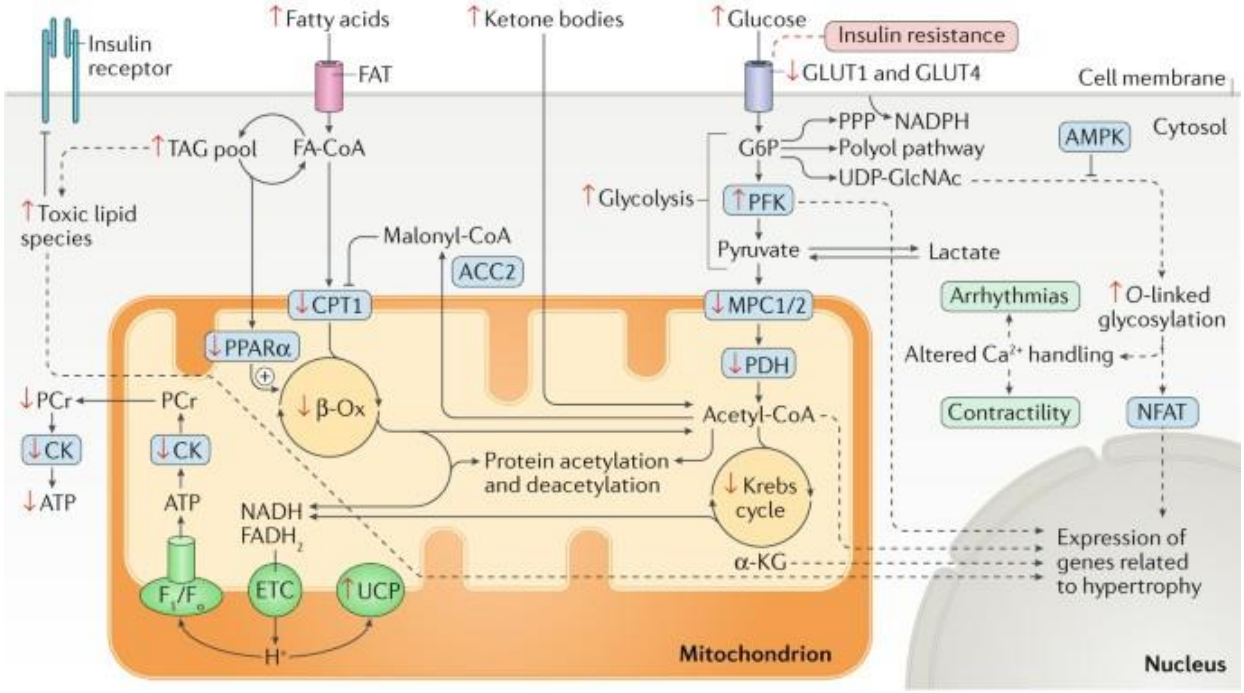

Figure 13. Metabolic and transcriptional remodeling in HF

In the failing heart, the glucose consumption to produce ATP is increased, however, this is not matched by an increase in pyruvate oxidation in the mitochondria. Ketone bodies might become an important energy substrate in the failing heart. Even though there is a decrease in FAO, this is not met by a decrease in FA uptake, causing a buildup of toxic lipid intermediates. Also, there is an impairment of the shuttling of high-energy phosphates via the creatine shuttle is impaired in HF. Numerous metabolic intermediates can impede metabolic enzymatic functions by genetic regulation, post-translational modifications of proteins, or by serving as substrates for chromatin-modifying enzymes. Red arrows show changes in HF. Dashed lines link metabolic intermediates to the regulation of gene expression. α- KG, α- ketoglutarate; ACC2, acetyl- CoA carboxylase 2; AMPK , 5'AMP-activated protein kinase; β- Ox, β- oxidation; CK, creatine kinase; CPT1, carnitine *O*- palmitoyltransferase 1; ETC, electron transport chain; F1/Fo, F1/Fo ATP synthase; FA- CoA , fatty acyl- CoA ester ; FAT, fatty acid translocase (also known as CD36); GLUT1, glucose transporter type 1 (SLC2A1); GLUT4, glucose transporter type 4 (SLC2A4); G6P, glucose 6-phosphate; MPC, mitochondrial pyruvate carrier; NFAT, nuclear factor of activated T cells; PCr, phosphocreatine; PDH, pyruvate dehydrogenase; PFK, ATP- dependent 6-phosphofructokinase; PPARα, peroxisome proliferator-activated receptor-α; PPP, pentose phosphate pathway; TAG, triacylglycerol; UCP, mitochondrial uncoupling protein; UDP- GlcNAc, uridine diphosphate- β-*N*- acetylglucosamine (Bertero & Maack, 2018b).

1.4 THE NICOTINAMIDE ADENINE DINUCLEOTIDE COENZYME

Nicotinamide adenine dinucleotide (NAD) has received abundant attention in research since its initial discovery in 1906, by Arthur Harden and William Young then named as *cozymase*, the first cofactor ever described. They observed that it could promote the fermentation reaction in yeast. In 1923, Hans von Euler-Chelpin purified the *cozymase* from yeast extracts and determined its chemical composition; later, also described the dinucleotide character of NAD: adenosine monophosphate (AMP) and nicotinamide mononucleotide (NMN). During the 1930s Otto Warburg detected the capability of NAD to transfer hydrogen from one molecule to another in yeast extracts. The pathways that produce NAD were further elucidated by the works of Arthur Kornberg during the 1940s and Preiss and Handler during the 1950s. Parallel to these findings, the role of NAD in metabolism was being revealed by many other scientific working groups, as well as descriptions of its roles in glycolysis, TCA cycle, and OXPHOS (Berger et al., 2004; Yang & Sauve, 2016).

The prominence of the metabolism of NAD in health and disease arose in 1937 from the discoveries of Elvehjem and colleagues; the group found that a heat-stable dietary factor then known as *"pellagra preventing factor"* cured both canine black tongue and human pellagra. This breakthrough provided the first evidence of the therapeutic roles of NAD^+ precursors as it was determined that this factor was niacin, a form of vitamin B3. Pellagra is a diet-related disease caused by the deficiency of vitamin B3 that reached epidemic proportions in different parts of the world a few centuries ago. Besides, a high mortality rate was observed in severe cases due to the depletion of NAD^+. Even though pellagra has virtually disappeared as a global health problem, decreased cellular NAD^+ occurs under many other pathological conditions namely aging, neurodegenerative diseases, cancer, and CVD (Xiao et al., 2018). NAD came back into the limelight a few decades ago,

as it was found that it also served as a substrate for a major class of deacetylase proteins known as Sirtuins (Rine & Herskowitz, 1987).

As an oxidoreductase cofactor in the regulations of the cellular redox state and energy metabolism, NAD^+ is crucial for a wide variety of enzymatic reactions that are tightly regulated. Additionally, it has been demonstrated in recent times that NAD^+ is also is a vital factor in the maintenance of several other biological processes through NAD^+-consuming signaling pathways (Houtkooper et al., 2010; Katsyuba & Auwerx, 2017). It is now evident that pathways involved in the synthesis and consumption of NAD^+ are essential targets for the development and treatment of several diseases related to altered metabolism. Hence, proper regulation of these metabolic and signaling processes depends on preserving NAD^+ levels.

NAD^+ is composed of two nucleotides joined through their phosphate groups by a phosphoanhydride bond. One nucleotide comprises an adenine nucleobase and the other, nicotinamide (Figure 16). NAD exists in two forms: an oxidized and reduced form, abbreviated as NAD^+ and NADH, respectively. The former undergoes a reversible reduction of the nicotinamide ring by accepting a hydride ion (: H^+), the equivalent of a proton and two electrons, and NADH is formed. A separate substrate molecule is oxidized (dehydrogenation), by donating two hydrogen atoms. The second proton removed the substrate is released to the aqueous solvent. The half-reactions for these nucleotide cofactors are $\mathbf{NAD^+ + 2e^- + 2H^+ \rightarrow NADH + H^+}$. The reduction of NAD^+ to NADH converts the benzenoid ring of the nicotinamide moiety, with a fixed positive charge on the ring nitrogen, to the quinonoid form, with no charge on the nitrogen (Nelson & Cox, 2017). The nicotinamide portion of NAD^+ is the site of redox reactions, and its reduced form, NADH, is a major energy transfer intermediary in various metabolic pathways, and notably at the CI of the ETC as mentioned above (Verdin, 2015).

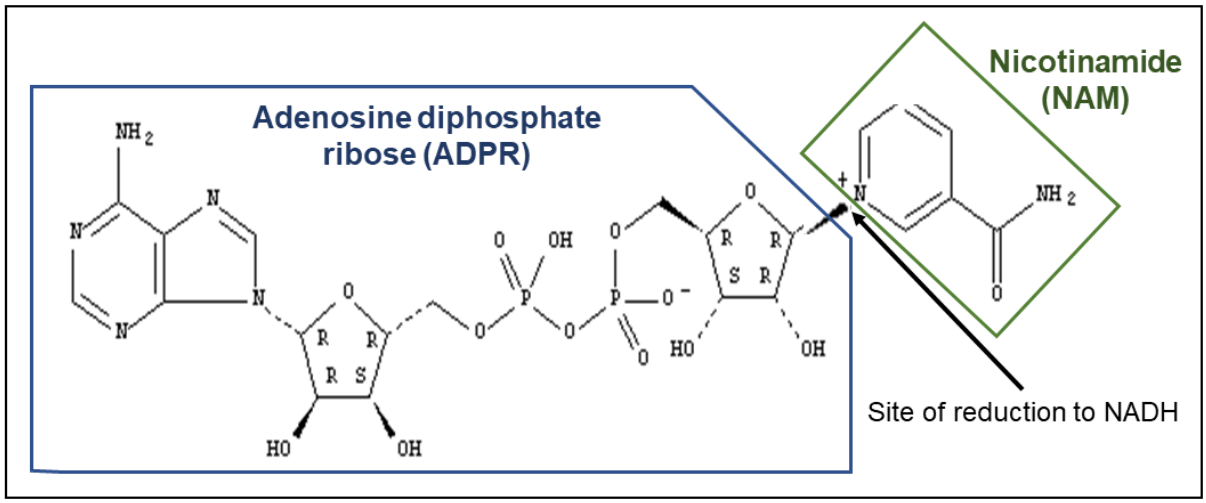

Figure 14. The NAD molecule

The formula of NAD^+ illustrates the molecule's site of reduction where redox reactions occur. The adenosine diphosphate ribose (ADPR) (blue box) and nicotinamide moieties (green box) are also depicted.

1.4.1 Roles of NAD^+ in Energy Metabolism as a Coenzyme

The essential role of NAD as a redox cofactor in energy metabolism-related pathways (as previously covered in detail) has been extensively investigated for decades. The enzymes using NAD^+ in hydride transfer, dehydrogenases, and oxidoreductases, catalyze the reduction of NAD^+ into NADH. Jointly, the NAD^+/NADH redox couple is involved in reactions that require the transfer of electrons from one molecule to another, such as glycolysis, pyruvate-to-lactate, and pyruvate-to-acetyl-CoA interconversions, FA β-oxidation, the TCA cycle, and OXPHOS (Okabe et al., 2019). In this type of reaction, there is no net production or consumption of NAD^+ or NADH. The coenzymes work catalytically and are frequently recycled without a net variation in the total amount of NAD^+ and NADH (Katsyuba & Auwerx, 2017). In the glycolytic pathway, glyceraldehyde 3-phosphate dehydrogenase transforms NADH from NAD^+ followed by pyruvate dehydrogenase complex which also converts NADH from NAD^+. NADH produced in the cytosol is transported into the mitochondrial matrix so it can enter the ETC, and cytosolic

NAD^+ must be renewed to sustain the glycolytic flux and lactate conversion to pyruvate. Since the inner mitochondrial membrane is impermeable to NADH (Purvis & Lowenstein, 1961), it must be carried across the mitochondrial membrane through reducing equivalent shuttles, namely, the malate-aspartate (M-A) shuttle the α-glycerophosphate shuttle, the malate-citrate and FA shuttles (Lu et al., 2008). In the heart, the reducing equivalents of cytosolic NADH are shuttled into the mitochondria mainly by the M-A shuttle (Safer, 1975), providing flux rates of NADH into the mitochondria that are 10-fold or greater than those of NADH delivery through the α-glycerophosphate shuttle (Scholz & Koppenhafer, 1995). The M-A shuttle consists of a transport-transamination-redox cycle in both cytosolic and mitochondrial domains (Figure 17). There are two antiporter proteins situated in the mitochondrial inner membrane, the glutamate-aspartate transporter, and the malate-α-ketoglutarate transporter. In the glutamate-aspartate transporter, the outflow of aspartate from the mitochondria is followed by the entry of glutamate and proton into the mitochondria. The interchange of malate and α-ketoglutarate through the malate-α-ketoglutarate transporter is driven by the concentration gradients of its substrates and therefore is bidirectional (Lu et al., 2008). These transporters are linked by biochemical reactions between the metabolites on both sides. The transporters enable the transfer of equal molar equivalents of metabolites across the membrane in opposite direction, and the direction of the transport is controlled by the concentration gradient of the metabolites. In one cycle, oxaloacetate is converted to malate in the cytosol, which gives place to oxidation of NADH to NAD^+ by malate dehydrogenase. Malate is then shuttled to the mitochondrial matrix and by the action of malate dehydrogenase, is used to regenerate NADH from NAD^+ in the matrix, this generates oxaloacetate. Oxaloacetate is converted to aspartate by the aspartate aminotransferase, which also generates α-ketoglutarate. Both oxaloacetate and α-ketoglutarate exit the mitochondrial matrix. In the cytosol, aspartate reacts with α-ketoglutarate and is shuttled in exchange of malate to provide glutamate and oxaloacetate, maintaining

the cycle. Ultimately, this process shifts electrons from NADH and regenerating NAD^+ in the cytosol to generate NADH in the matrix (Korla et al., 2015).

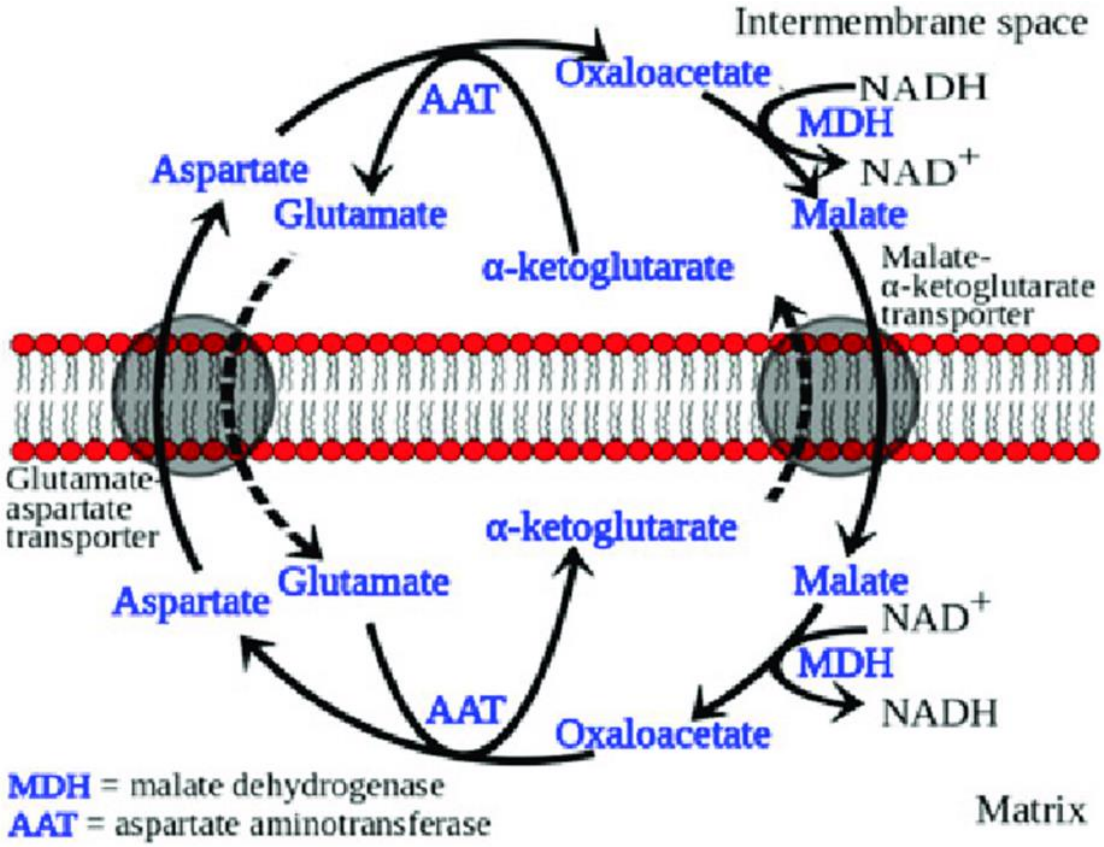

Figure 15. Representation of the M-A shuttle

The shuttle consists of two transporters, aspartate–glutamate antiport transporter and malate–α-ketoglutarate antiport transporter, which transfer reducing equivalents between the mitochondrial intermembrane space and the mitochondrial matrix (Korla et al., 2015).

Inside the mitochondria, the pyruvate dehydrogenase complex also produces NADH from NAD^+. The TCA cycle produces 3 molecules of NADH, attributed to the enzymes isocitrate dehydrogenase, α-ketoglutarate dehydrogenase, and malate dehydrogenase. Additionally, one molecule of $FADH_2$ is also produced, which makes NADH the main electron donor of the ETC. FA β-oxidation is also a substantial source of NADH, as NAD^+ is used as a cofactor by 3-hydroxy acyl CoA dehydrogenase (Barycki et al., 1999). Moreover, the oxidation of ketone bodies also generates NADH through the enzyme β-hydroxybutyrate dehydrogenase (Lopaschuk et al., 2020).

Role of NADP, the phosphorylated form of NAD

NAD^+ is also a precursor for NAD phosphate (NADP) and its reduced form (NADPH). Around 10% of cellular NAD^+ can be phosphorylated by NAD^+ kinases into $NADP^+$, which can be dephosphorylated to NAD^+ by $NADP^+$ phosphatases (Kawai & Murata, 2008). Furthermore, $NADP^+$ can receive electrons from NADH to generate NADPH by the mitochondrial enzyme NAD(P) transhydrogenase (NNT) (Ying, 2008). NADPH is essential for reductive biosynthetic reactions of cholesterol and palmitate and the oxidative reactions catalyzed by NADPH oxidases, nitric oxide synthase, and cytochrome P-450. NADPH also delivers the primary reducing power for the thioredoxin and glutathione systems to remove ROS (Xie et al., 2020) (Figure 18).

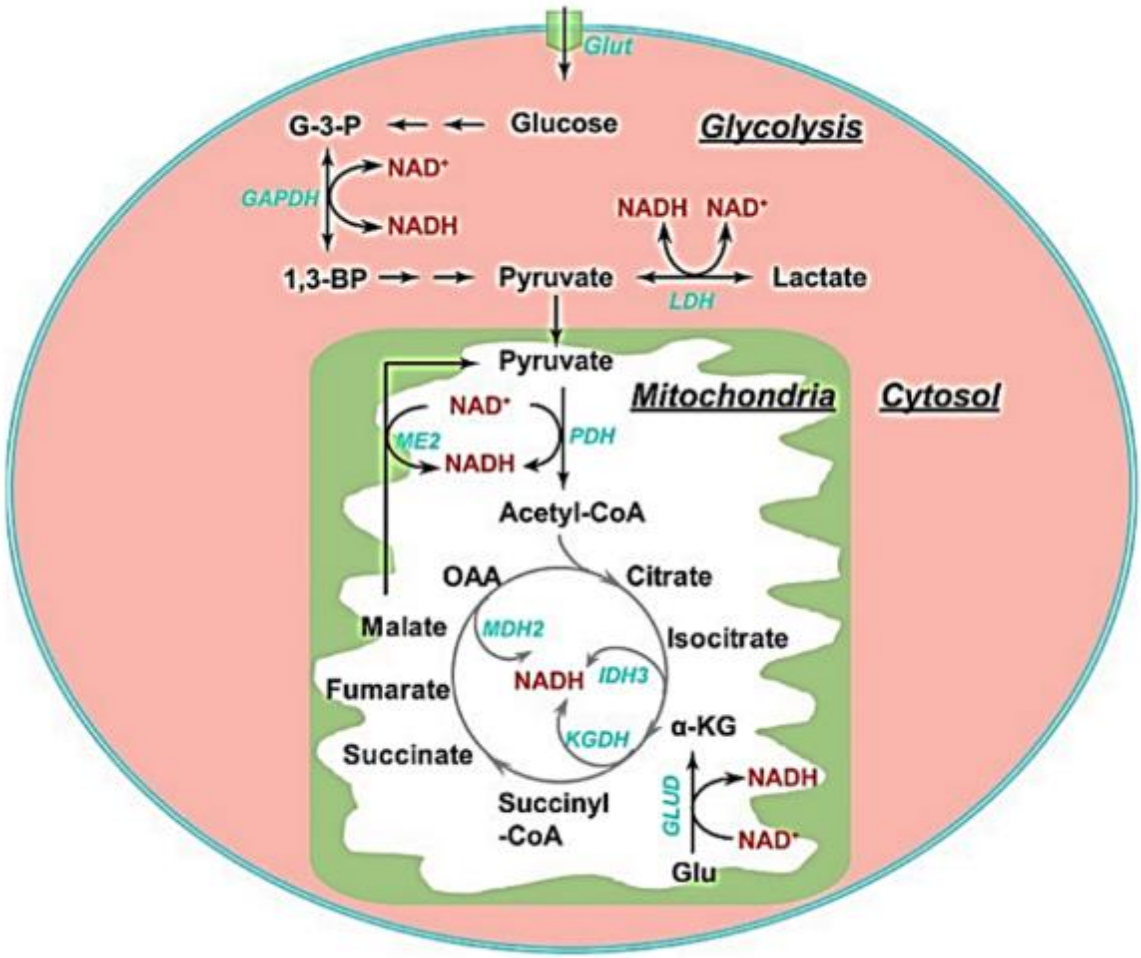

Figure 16. Metabolic sources of NAD(H)

In the cytosol, interconversion of NAD^+ and NADH is mediated by the glycolytic enzymes GAPDH and LDH. In the mitochondrial matrix, PDH, ME2, GLUD, and TCA cycle enzymes (IDH3, KGDH, and MDH2) contribute to NAD(H) production. G3P, glyceraldehyde-3-phosphate; GAPDH, glyceraldehyde phosphate dehydrogenase; Glu, glutamate; GLUD, glutamate dehydrogenases; Glut, glucose transporters; GPDH, glycerol-3-phosphate dehydrogenase; IDH, isocitrate dehydrogenase; KGDH, α-ketoglutarate dehydrogenase; LDH, lactate dehydrogenase; MDH, malate dehydrogenase; ME, malic enzyme; OAA, oxaloacetate; PDH, pyruvate dehydrogenase (Xiao et al., 2018).

1.4.2 NAD^+ Metabolism

Different NAD^+ biosynthetic pathways have been discovered in mammalian cells, which rely on these pathways to maintain a high turnover and to prevent its depletion. NAD^+ is synthesized from extracellular precursors that are provided by the diet, these precursors include the bases, nicotinamide (NAM) and nicotinic acid (NA), and the nucleosides nicotinamide riboside (NR) and nicotinic acid riboside (NAR); all of which are collectively referred to as vitamin B3 (Bogan & Brenner, 2008a) (Figure 19). NA and NR are found in the basic diet, NA is produced by plants and algae, whereas NR is found in milk (Trammell et al., 2016). The amino acid tryptophan is also another NAD^+ precursor. A regular diet provides additional NAD^+, NADH, NADP, and NADPH, which are considered nutritional niacin equivalents as well (Bogan & Brenner, 2008). There are three major pathways from which NAD^+ is synthesized in mammals: the *de novo* pathway, the Preiss-Handler pathway, and the salvage pathway. Additionally, NAD^+ serves as a substrate for signaling enzymes implicated in post-translational protein modifications, such as sirtuins and poly(ADP–ribose) polymerases (PARPs), or the production by the ectoenzyme CD38 of cyclic ADP–ribose (cADPR), a calcium-mobilizing messenger (Ziegler & Nikiforov, 2020). The cleavage of NAD^+ by these signaling enzymes leads to the generation of NAM as a by-product, thus providing an intracellular source of vitamin B3, in addition to the fact that NAM is also the main form of vitamin B3 that can be absorbed from animal-based food (Braidy et al., 2019).

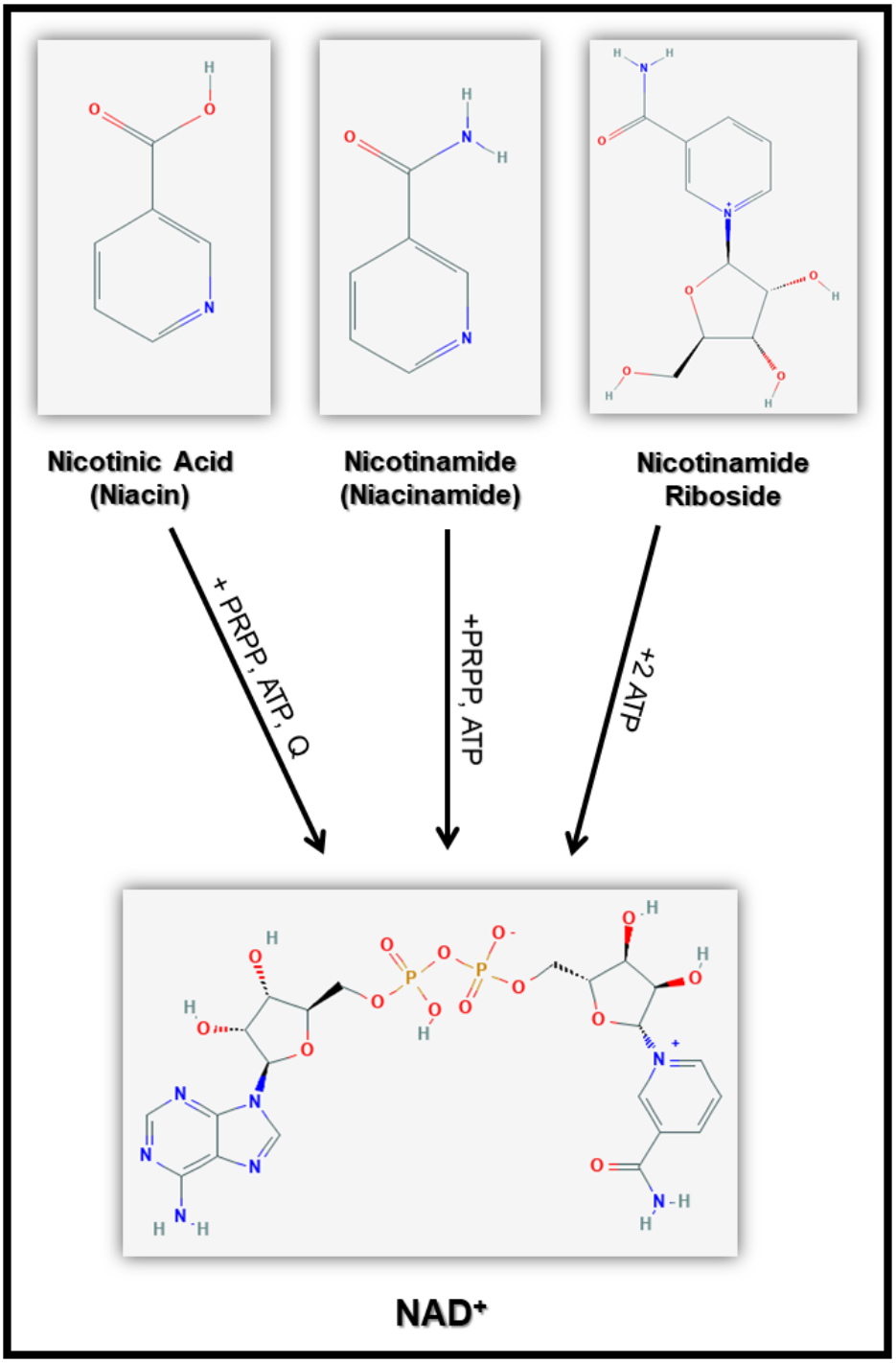

Figure 17. NAD+ precursors

Nicotinic acid, nicotinamide, and nicotinamide riboside are vitamin B3 molecules that are dietary precursors of nicotinamide adenine dinucleotide (NAD^+). Cofactors for the synthesis of NAD^+ from the respective precursor are indicated: ATP; PRPP, 5-phosphoribosyl-ribose-1-pyrophosphate; Q, glutamate**.**

De novo Pathway

The essential amino acid L-Tryptophan (trp) is the *de novo* precursor of NAD^+ by the kynurenine pathway in all vertebrates and almost all eukaryotes that have been investigated (Belenky et al., 2007). In humans, it occurs primarily in the liver (Bender & Olufunwa, 1988) and the biosynthetic at which trp is converted to NAD^+ appears to be independent of the presence of NAM and activity of the salvage pathways (Fukuwatari & Shibata, 2007).

The first and rate-limiting step in this pathway consists of the conversion of tryptophan to N-formyl kynurenine by either indoleamine 2,3-dioxygenase 1 (IDO-1) or IDO-2, or tryptophan 2,3-dioxygenase (TDO) (Cantó et al., 2015) (Figure 20). In mammals, TDO is the main enzyme that contributes to NAD^+ biosynthesis, it is found primarily in the liver and is induced by tryptophan or corticosteroids (Salter & Pogson, 1985). IDO-1 is found mostly extra-hepatically and can be found in several tissues such as the lung, small intestine, and placenta (Yamazaki et al., 1985). It is expressed at low levels under basal conditions and upregulated by certain cytokines, notably interferon-gamma, and inflammatory stimuli such as lipopolysaccharides and amyloid peptides (Chen & Guillemin, 2009). The second isoform of IDO, IDO-2, is expressed in various tissues and responds to immune stimulation differently than IDO-1 (Larkin et al., 2016) and shows distinctive behavior in terms of substrate specificity and affinity than that of IDO-1 (Pantouris et al., 2014).

Four subsequent enzymatic conversions transform N-formyl kynurenine to 2-amino-3-carboxymuconate semialdehyde (ACMS), which can undergo spontaneous cyclization producing quinolinic acid, which also serves as NAD^+ precursor. Instead, ACMS can enzymatically be converted to α-amino-β-muconate-ε-semialdehyde by ACMS decarboxylase, which leads to complete oxidation to CO_2 and water by the glutarate pathway and the TCA cycle, or to the production of picolinic acid by a spontaneous reaction (Cantó et al., 2015). This might clarify why tryptophan is not the main NAD^+ precursor in vivo, as it will only be redirected to

NAD^+ synthesis when its quantity surpasses the enzymatic capacity of ACMS decarboxylase (ACMSD) (Ikeda et al., 1965). Afterward, quinolinic acid is condensed with phosphoribosyl pyrophosphate (PRPP) to form nicotinic acid mononucleotide (NAMN) and inorganic pyrophosphate (PPi) and CO_2. This step is catalyzed by the enzyme quinolinate phosphoribosyl-transferase (QPRT) which is a major enzyme in the synthesis of NAD^+ through this pathway (Badawy, 2017; Houtkooper et al., 2010). QPRT is mainly localized in the liver, kidney, and endocrine tissues (Shibata et al., 1986; *The Human Protein Atlas*, n.d.). NAMN is converted to NA adenine dinucleotide (NAAD) by the enzyme NAM mononucleotide adenylyltransferase (NMNAT), of which three isoforms have been recognized in humans (Jayaram et al., 2011). Human NMNAT1 is localized in the nucleus, whereas NMNAT2 is found in the Golgi apparatus and cytoplasm, and NMNAT3 in the mitochondria (Berger et al., 2005). Moreover, NMNAT1 is ubiquitously expressed, however, it has been shown that its major sites of expression are skeletal muscle, heart, liver, and kidney (Emanuelli et al., 2001). It has been reported that human NMNAT1 interacts specifically with poly(ADP-ribose) polymerase (PARP) (Schweiger et al., 2001). NMNAT2 is expressed mainly in the nervous system, and its expression levels are considerably lower than those of NMNAT1 (Raffaelli et al., 2002). NMNAT3 is mostly expressed in the lung and spleen, tissues in which the other isoforms are lowly expressed. The diverse subcellular localization of the NMNAT isoforms indicates the existence of distinct NAD pools that are synthesized separately.

The final step in the *de novo* pathways consists of the glutamine and ATP-dependent amidation of NAAD by the enzyme NAD synthase (NADS) using glutamine as a donor (Hara et al., 2003). Mammalian NADS activity rate varies among tissues, with high levels in the brain and kidney, intermediate levels in the heart, and very low activity in skeletal muscle (Mori et al., 2014).

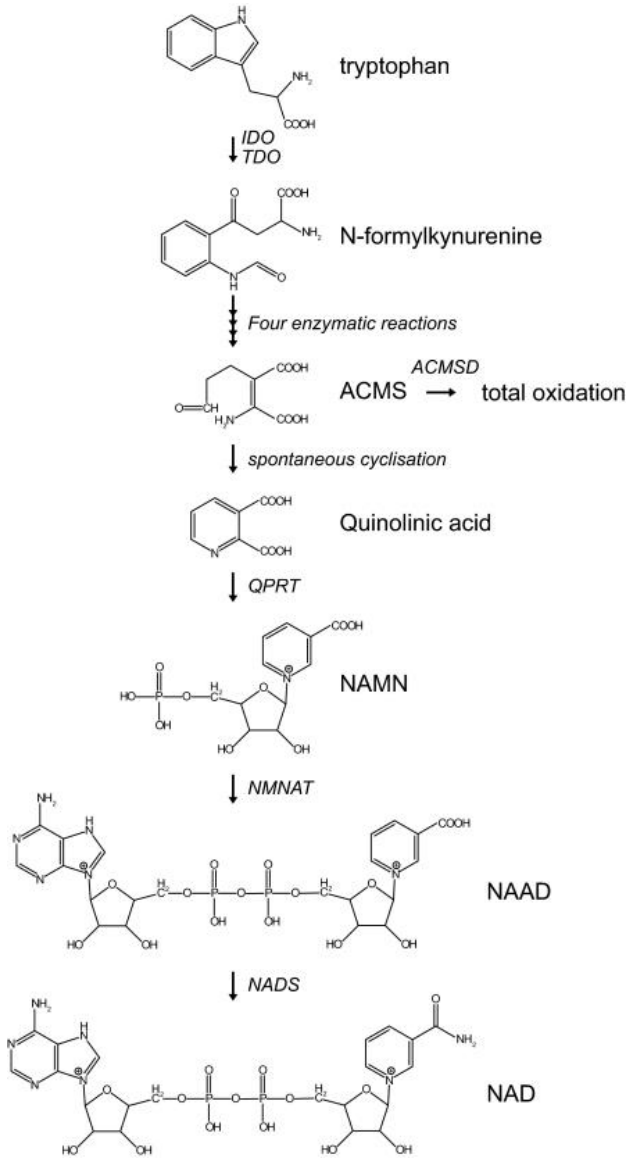

Figure 18. De novo NAD+ biosynthesis from tryptophan

This pathway starts with the conversion of tryptophan to N-formylkynurenine catalyzed by either IDO or TDO. N-Formylkynurenine is then transformed in four individual steps to the unstable ACMS, which can undergo either enzymatic conversion directed to total oxidation or nonenzymatic cyclization to quinolinic acid. Then, the formation of NAMN is catalyzed by the enzyme QPRT. NAMN is converted to NAAD by the enzyme NMNAT. The final step in the biosynthesis of NAD^+ is the amidation of NAAD by the NAD synthase enzyme (Houtkooper et al., 2010).

The Preiss-Handler Pathway

NAD^+ is synthesized from NA via the Preiss-Handler pathway which encompasses three individual metabolic conversions (Figure 21) (Preiss & Handler, 1958). First, NA is transformed into nicotinic acid mononucleotide (NAMN) by the enzyme nicotinic acid phosphoribosyltransferase (NAPRT) using phosphoribosyl pyrophosphate (PRPP) as a cosubstrate. NAMN is then converted to nicotinic acid adenine dinucleotide (NAAD) by the enzyme NMNAT (nicotinamide mononucleotide adenylyltransferase), consuming ATP (Kirkland & Meyer-Ficca, 2018). Both human NMNAT1 and 2 isoforms recognize NMN and NAMN substrates equally well (Zhang et al., 2003). Once NAAD is synthesized, NAD^+ synthesis is the same as the *de novo* pathway (previously covered in detail).

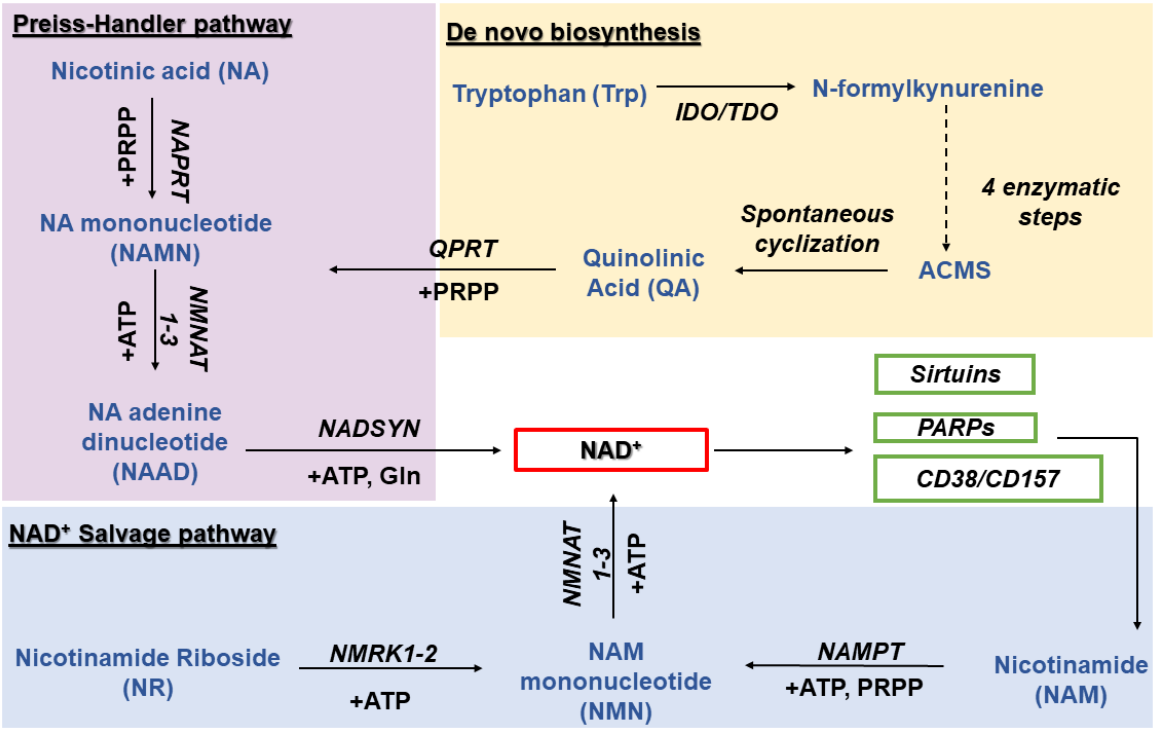

Figure 19. Overview of NAD biosynthetic pathways

(Adapted from Cantó et al., 2015).

1.4.3 The Salvage Pathway

1.4.3.1 NAMPT Pathway

The salvage pathway starts from pre-formed pyridine moieties, NAM, and NR (Figure 21). The nicotinamide phosphoribosyltransferase (NAMPT) name indicates the role of this pathway in the re-utilization of NAM moieties released by ADP-ribosylases and NAD glycohydrolases, which is why NAM is the most common NAD^+ precursor in mammals (Revollo et al., 2004). The enzyme NAMPT carries out the first step, synthesizing NMN and inorganic PPi by condensing NAM and PRPP. The salvage through NAMPT is a key recycling mechanism of NAD^+ since NAM is a product of sirtuins (SIRT), PARP, and CD38-mediated NAD^+ signaling. In a second step, NMN is transformed into NAD by nicotinamide mononucleotide adenylyltransferases 1-3 as in the de novo pathway (NMNAT 1-3) (Romacho et al., 2013). Remarkably, NAMPT is the rate-limiting enzyme in the synthesis of NAD^+ and has a vital role in normal physiological conditions. The activity of NAMPT is considered a key regulator of downstream NAD-consuming enzymes, e.g. sirtuins (Revollo et al., 2004). It is highly conserved from prokaryotes to eukaryotes, and it is expressed in virtually all organs, tissues, and cells examined which indicates pleiotropic effects and suggests a crucial role in cellular metabolism (Garten et al., 2015).

NAMPT is found in both intracellularly (mainly in cytoplasm and nucleus), and extracellular spaces. Intracellular NAMPT is mainly implicated in NAD^+ biosynthesis, while extracellular NAMPT is secreted by several cell types, including cardiomyocytes and beta cells (Pillai et al., 2013; Revollo et al., 2007). Interestingly, it has been shown that the gene that encodes NAMPT is regulated by the circadian locomotor output cycles protein kaput (CLOCK)–aryl hydrocarbon receptor translocator-like protein 1 (BMAL1) core clock machinery, which is responsible for circadian rhythmicity and leads to a circadian oscillation of NAD^+ levels *in vivo*. The NAMPT-mediated NAD^+ biosynthesis comprises a feedback loop in which NAD^+

functions as a metabolic oscillator and regulates the core clock machinery through SIRT1 (Ramsey et al., 2009). Moreover, in the context of the heart's health and disease, it has been demonstrated that NAMPT plays a critical role in energy status and survival in cardiomyocytes as it regulates NAD^+ and ATP contents. Preventing downregulation of NAMPT inhibits myocardial injury in response to ischemia and reperfusion (Hsu et al., 2009). Additionally, NAMPT preserves cardiac function and metabolism in the failing heart, whereas its overexpression is detrimental during pressure-overload, probably due to excessive activation of SIRT1, suppression of mitochondrial function, and upregulation of proinflammatory mechanisms (Byun et al., 2019). Our group has previously demonstrated a drop in NAMPT expression in human failing hearts and a model of dilated cardiomyopathy (DCM), SRF^{hKO} mice treated with phenylephrine, as compared to healthy hearts and controls, respectively (Diguet et al., 2018). Consistently, it was demonstrated that *Nampt* gene expression progressively decreased due to aging, both in Nmrk2 *knockouts* (KO) and control mice (Tannous et al., 2021).

1.4.3.2 NMRK Pathway

The NMRK pathway comprises the phosphorylation of NR by the enzyme NR kinases 1/2 (NMRK 1/2) to form NMN, which then serves as a substrate for NAD^+ synthesis via NMNAT adenylyl transfer, as discussed previously (Figure 21, bottom left). The energetic cost of synthesizing NAD^+ through the NMRK pathway involves the consumption of 2 ATP equivalents, whereas via the NAMPT pathway 4 ATP molecules are required (Diguet et al., 2018).

The NMRK appears to be highly conserved among species, namely, yeast and humans (Belenky et al., 2007; Bieganowski & Brenner, 2004). Two isoforms of the NMRKs have been found, NMRK1 with ubiquitous expression and NMRK2 mostly detected in heart and skeletal muscle (Bieganowski & Brenner, 2004; Diguet et al., 2018; Fletcher et al., 2017). It has been demonstrated that NMRKs are rate-limiting

enzymes for NR-mediated NAD^+ synthesis. NMRK2 levels are normally undetectable in other organs different than muscle, however, under normal conditions, it tends to be more abundant in skeletal muscle as compared to cardiac muscle. In contrast, high levels of NMRK2 have been identified in human post-MI hearts (~75 fold) as compared to healthy hearts (Ahmad et al., 2020). Additionally, NMRK2 has been detected as a top upregulated protein in HF and DCM mouse models (Ahmad et al., 2020; Diguet et al., 2018; Tannous et al., 2021). A recent study from Ahmad and colleagues demonstrated, in a model of *Nmrk2 KO* mice, that the deficiency of NMRK2 leads to a fast progression of HF after ischemia characterized by an enhanced LV chamber dilatation, cardiac dysfunction, and large fibrotic scar formation. Furthermore, the gain of NMRK2 function diminished cardiac cell death after hypoxia/re-oxygenation. Remarkably, it was also found that NMRK2 regulates p38α activation after ischemia. These findings indicate the relevancy of NMRK2 in the pathogenesis of ischemic heart disease.

Recent work in our group shed some light regarding the involvement of NMRK2 in the progression of DCM and aging employing a model of *Nmrk2 KO* mice. The mice were viable yet progressively developed cardiac dysfunction which worsened with age and presented eccentric cardiac remodeling linked to an alteration in laminin deposition in the extracellular matrix. Interestingly, it was demonstrated that NMRK enzymes are not essential for NAD^+ maintenance in young healthy adults. However, the expression of *Nmrk1* in the heart strongly declined with aging (24 months) whilst the expression of *Nmrk2* remained stable. It has been shown that the NMRK pathway is redundant in terms of NAD^+ production, as NAMPT seems to be the main pathway from which NAD^+ is obtained in the healthy young heart. Myocardial NAD^+ pools were not modified in *Nmrk2 KO* mice at 6 weeks, neither at baseline nor after transverse aortic constriction (TAC). However, NAD^+ drastically decreased at 24 weeks in Nmrk2 *KO* mice. This shows that NMRK2 becomes more relevant in terms of NAD^+ biosynthesis in the aged myocardium (Tannous et al., 2021).

1.4.4 NAD^+ Subcellular Compartmentalization

There are two principal subcellular NAD^+ pools in mammalian cells, the nucleo-cytoplasmic NAD^+ pool, and the mitochondrial NAD^+ pool. Furthermore, NAD^+ pools are subdivided into reduced (NADH), phosphorylated (NADP), and reduced, phosphorylated (NADPH) pools, in addition to the NAD^+ pool. Each one of them is located in membrane-bound compartments and is bound to proteins, except for free NAD^+ (Belenky et al., 2007).

The total concentration of NAD^+ plus NADH in most tissues is about 10^{-5} M. In numerous tissues, the ratio of NAD^+ to NADH is high, favoring hydride transfer from a substrate to NAD^+ to form NADH. Free NAD^+/NADH ratio varies between 60 to 700 in eukaryotic cells, although the estimated mitochondrial NAD^+/NADH ratios are possibly maintained at 7-10 (Veech et al., 1972; Williamson et al., 1967). The feedback of NADH into metabolism determines the rate of catabolism and energy production (Yang & Sauve, 2016). The enzymes involved in NAD^+ biosynthesis and consumption are localized in distinct subcellular compartments (Table 3). While the awareness of the compartmentalization of NAD^+ synthesis and consumption has existed for some time, however, it is not fully understood due to technical constraints. It has been reported that cardiomyocytes have a total cellular NAD^+ concentration of 5.63 ± 1.32 nmol/mg protein (Alano et al., 2007), with nearly all of it localized in the mitochondrial (~80%) (Alano et al., 2007; Di Lisa et al., 2001). Cardiomyocytes may be exceptionally rich in mitochondrial NAD^+, as compared to other cell types, due to their large requirements of non-glucose substrates. It has only recently been possible to corroborate with more precision the existence of individual subcellular pools of NAD^+ in the mitochondria, nucleus, and cytoplasm through fluorescence biosensors (Cambronne et al., 2016; Sallin et al., 2018; VanLinden et al., 2015). Employing an organelle-targeted NAD^+ biosensor it was determined that the concentration of free NAD^+ in (HEK) 293T cell line

is 92–122 µM in the cytoplasm, 87–136 µM in the nucleus, and 191–275 µM in the mitochondria (Cambronne et al., 2016). Similar to these results free intracellular NAD^+ in U2OS cells was found to be around 70–120 µM (Sallin et al., 2018).

Enzyme	Activity	Pathway(s)	Subcellular localization
QPRT (Quinolinate phosphoribosyl transferase)	Catalyzes the formation of nicotinic acid mononucleotide (NAMN) from quinolinic acid (QA).	***De novo* pathway**	Cytosol
NADS (NAD^+ synthetase)	Catalyzes the amidation of nicotinic acid adenine dinucleotide (NAAD), leading to the production of NAD^+.	***De novo* pathway**	Cytosol
NAPRT (Nicotinic acid phosphoribosyltransferase)	Catalyzes the formation of NAMN from nicotinic acid (NA); rate-limiting step.	**Preiss-Handler pathway**	Cytosol, nucleus
NAMPT (Nicotinamide phosphoribosyltransferase)	Catalyzes the production of nicotinamide mononucleotide (NMN) from NA; rate-limiting step.	**Salvage pathway (NMN)**	Cytosol, nucleus
NMRK (Nicotinamide riboside kinase), 2 isoforms	Catalyzes the production of NMN from nicotinamide riboside (NR); rate-limiting step.	**Salvage pathway (NR)**	Cytosol, mitochondria
NMNAT (Nicotinamide mononucleotide adenylyltransferase), 3 isoforms	Catalyzes the formation of NAAD from NAMN, or of NAD^+ from NMN.	***De novo* and salvage pathways**	NMNAT1: nucleus NMNAT2: Golgi apparatus NMNAT3: mitochondria

Table 3. Summary key enzymes for NAD+ biosynthesis.

1.4.5 Cellular Entrances of NAD^+ and NAD^+ Precursors

It has been demonstrated that mammalian cells require the conversion of extracellular NMN to NR for cellular uptake, hence the overlapping metabolic effects that have been observed with both substrates (Ratajczak et al., 2016).

It has been proposed that the ectonucleotidase CD73 converts extracellular NMN to NR as a precursor for intracellular NAD^+ biosynthesis in human cells (Grozio et al., 2013). NMN might be synthesized by an extracellular form of NAMPT (eNAMPT) although this concept has been challenged by the fact that this would require the other NAMPT substrate, PRPP to be also present in the extracellular compartment as well as ATP, required for an autophosphorylation step of NAMPT. As these phosphate compounds are unstable in the extracellular compartment and NMN is poorly detected in blood plasma, the enzymatic activity of eNAMPT remains to be formally demonstrated and could occur only in very localized and transient conditions, for instance when cell death has occurred, and phosphate compounds are released in the extracellular medium.

On the other hand, eNAMPT has originally been described as the visfatin adipokine which is associated with metabolic disorders, such as overweight/obesity, type 2 diabetes mellitus, metabolic syndrome, different types of cancers, and CVD, and could act through unidentified cellular receptors (Carbone et al., 2017). It has also been proposed that NAD^+ could be released from cells through connexin 43 hemichannels (Cx43) (Kulikova et al., 2019).

Intriguingly, the source of mitochondrial NAD^+ remains a matter of debate in the field. It remains incompletely understood how NAD^+ and its precursors, NAM, NMN, NR, NA, and NAR, pass through the mitochondrial membrane. A subcellular study of the localization of NAD^+ biosynthetic enzymes and precursors indicated that NMN is the mitochondrial precursor for NAD^+generation (Nikiforov et al., 2015). In contrast, recent studies indicated that NAD^+ might be directly imported into mitochondria from the cytosol by the newly discovered SLC2A51/MCART1 mitochondrial transporter (Davila et al., 2018; Kory et al., 2020). A study showed

that the expression of SLC25A51 determines mitochondrial NAD⁺ levels and uptake capacity in mammalian cells and complements yeast lacking their known mitochondrial NAD⁺ transporters (Luongo et al., 2020). However, it is important to note that these findings have yet to be confirmed on animal models.

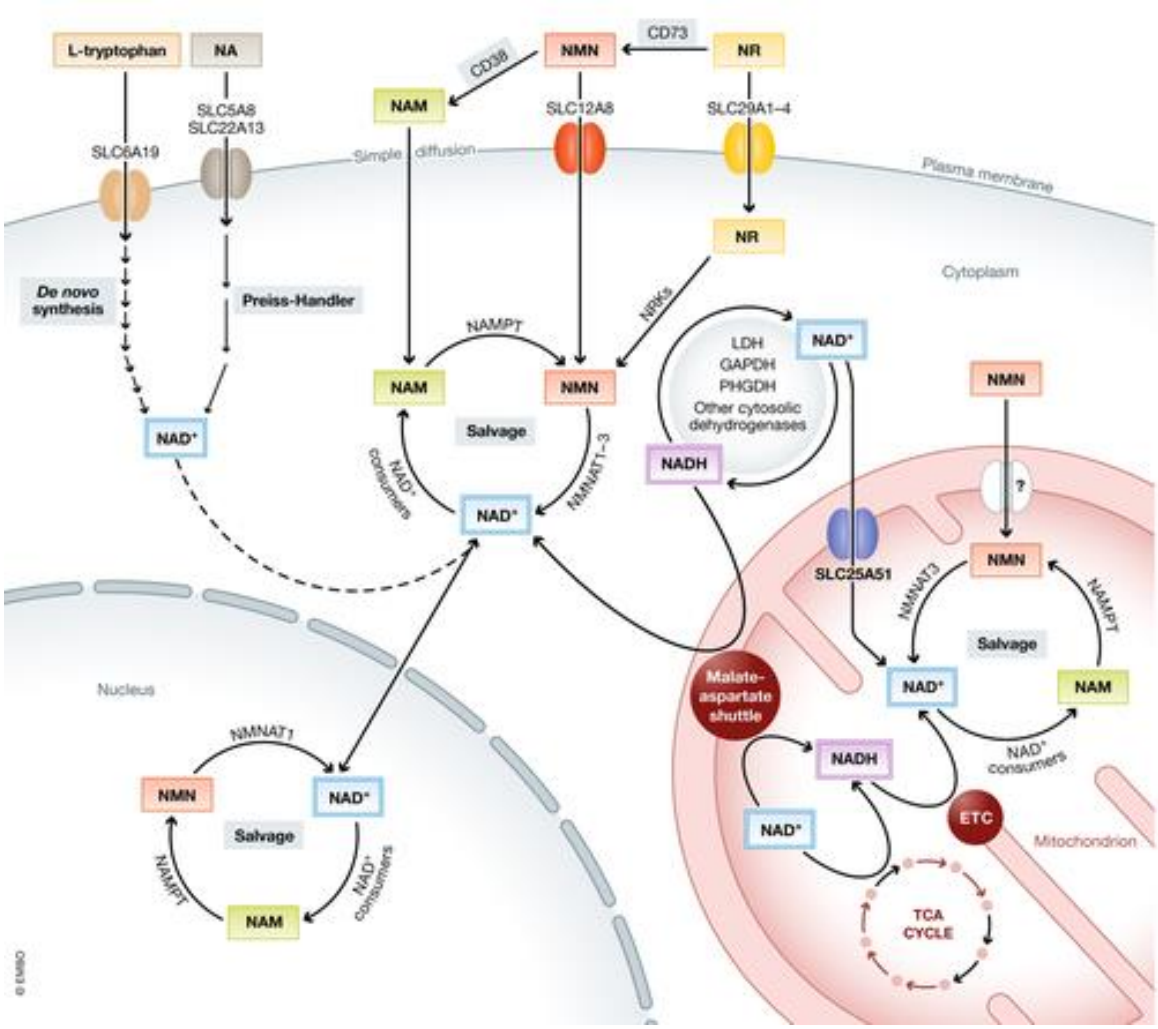

Figure 20. Intracellular NAD(H) pools

Various pathways and redox systems are participating in the maintenance of cellular NAD(H) homeostasis. The NAD⁺ precursors trp, NA, NAM, NMN, NR are transported into the cell via specific transporters or simple diffusion and incorporated into the cytosolic or nuclear NAD⁺ pools. Via the reactions cytosolic dehydrogenases or the M-A shuttle, NAD⁺ and NADH can then be interconverted to keep the cytosolic and nuclear NAD⁺: NADH ratios. In the mitochondria, the M-A shuttle acts in combination with the TCA cycle, ETC to preserve the redox balance. The mitochondrial NAD(H) pool is maintained by salvage pathways and active NAD⁺ transport through the newly discovered transporter SLC25A51 (Zapata-Pérez et al., 2021).

1.4.6 NAD^+-Consuming Enzymes

NAD^+ is a substrate for enzymes regulating energy metabolism (Sirtuins), response to oxidative stress (Sirtuins and PARPs), and $Ca2^+$ signaling (CD38). All these signaling enzymes cleave the oxidized NAD^+ into nicotinamide (NAM) and ADP-ribose moieties. The remaining ADP-ribose moiety is transferred onto acceptor molecules, these reactions are key constituents of intracellular signaling networks that control vital processes (Berger et al., 2005).

Sirtuins

Sirtuins are a family of class III NAD^+-dependent deacetylases that remove acetyl and other acyl groups from protein lysine residues and use ADP-ribose (ADPR) as the acetyl group acceptor. Deacetylation occurs when the modified lysine side chain is coupled to the cleavage of the glycosidic bonds in NAD^+, which leads to the creation of the deacetylated lysine, acetylated ADPR, and NAM as by-products (Braidy et al., 2019). This family of proteins has been found in prokaryotes and eukaryotes and is highly conserved among species (Imai et al., 2000). The fact that sirtuins require NAD^+ implies that they can act as sensors of a cell's metabolic state (Fulco et al., 2003; Haigis and Guarente, 2006). Sirtuins can transmit modifications in metabolism to chromatin through the deacetylation of histones and other proteins.

Two main functions are associated with sirtuins, metabolism and chromatin regulation. A third role is a stress response and is extensively found in eukaryotes (Vaquero, 2009). Sirtuins modulate the adaptation to altered cellular energetic status, specifically in the activation of oxidative metabolism and stress response in mitochondria in response to energy stress through the stimulation of mitochondrial biogenesis and OXPHOS-related genes. Sirtuins are distributed in the nucleus (e.g. SIRT1, SIRT6, and SIRT7), the cytoplasm (e.g., SIRT2), and mitochon-

dria (e.g. SIRT3-5) (Xie et al., 2020). They are implicated in the regulation of nuclear events and are regarded as master switches of metabolism, DNA repair, stress response, chromatin remodeling, and circadian rhythm (Mehmel et al., 2020). SIRT1 to 7 cleave NAD into NAM and ADPR moieties to carry out post-translational modifications on proteins. In one type of reaction, sirtuins remove the acetyl group (SIRT1, SIRT2, SIRT3, SIRT6, SIRT7), succinyl group (SIRT5), or lipids (SIRT6, SIRT7) that have been covalently linked to lysine residues on proteins, modifying the charge and activity. In that case, ADPR is used as the acceptor of the removed group. In addition, SIRT4, SIRT6, and SIRT7 carry out mono-ADP-ribosylation, this ADPR moiety is transferred to arginine residues (Mericskay, 2016).

SIRT1, the most studied sirtuin is localized in the nucleus and cytosol and along with its histone deacetylation function, is also a transcription factors modulator, namely p53, nuclear factor κ-light-chain-enhancer of activated B cells (NFκB), forkhead box (FOXOs), and PGC1α, and DNA repair proteins, such as PARP1. SIRT3, 4, and 5 are localized in the mitochondria and have roles in oxidative stress and lipid metabolism (Kane & Sinclair, 2018). Particularly, SIRT3 and SIRT5 enhance the activity of enzymes involved in the TCA cycle and OXPHOS (Mericskay, 2016). SIRT6 and 7 are localized in the nucleus with roles in gene expression and DNA repair (Kane & Sinclair, 2018). SIRT1-mediated deacetylation of the PGC1α transcription factor stimulates its activity which translates to increased mitochondrial biogenesis, in skeletal muscle (Lagouge et al., 2006). In the heart, mild overexpression of Sirt1 confers antiaging and stress-resistance effects, whilst higher levels of Sirt1 induce cardiomyopathy, possibly via the induction of mitochondrial dysfunction *in vivo* (Alcendor et al., 2007). Interestingly, SIRT3 is implicated in mitochondrial energy metabolism, as it regulates the enzymatic activity of key enzymes of OXPHOS through deacetylation. SIRT3 modifies and activates long-chain acyl-CoA dehydrogenase (LCAD), which is the key enzyme of FAO, to promote FA metabolism (Sun et al., 2018). SIRT3 overexpression protects the heart

from pressure overload stress in transgenic mice (Sundaresan et al., 2009). Moreover, the downregulation of SIRT2 protects against I/R injury. SIRT6 decreases cardiac hypertrophy, and SIRT7 regulates apoptosis and stress responses in the heart (Matsushima & Sadoshima, 2015).

PARP1

NAD^+ is also used as an ADPR donor by a great family of enzymes known as ADP-ribosyl transferases (ARTD1-18), also known as the poly(ADP-ribose) polymerase (PARPs 1 to 16) and ARTC (1-5) (Hottiger et al., 2010). In particular, PARP1 is a major NAD^+ consumer and it is the most abundant of the 18 different PARP isoforms and accounts for more than 90% of the catalytic activity of PARP in the nucleus (Henning et al., 2018). PARP-1 is widely known as a DNA damage sensor induced by excess ROS, which binds to both single and double-stranded DNA breaks. Upon binding to damaged DNA, PARP-1 creates homodimers and catalyzes the cleavage of NAD^+ into nicotinamide and ADP-ribose moieties to form long branches of ADP-ribose polymers on glutamic acid residues of many target proteins, such as histones and PARP-1, to recruit DNA repair enzymes (Mericskay, 2016; Pacher & Szabó, 2007). PARP1 is involved in the regulation of energy metabolism, as it regulates many cellular processes by enzymatic activity via protein-protein interactions. Several of these processes lead to the destabilization of mitochondrial membrane systems and impairment of mitochondrial function that eventually can result in cell death (Vida et al., 2017). PARP-1 interacts with a large number of nuclear receptors and transcription factors regulating mitochondrial and lipid oxidation genes, such as PPARγ, FOXO1, and ER, among others (Bai & Cantó, 2012). Overall, several reports indicate that PARP-1 has a key role in many CVD, namely I/R injury, MI, and HF and that PARP-1 inhibition confers protective effects against the progression of HF post-MI (Halmosi et al., 2016). It has been demonstrated that PARP1 has a hypertrophic effect mediated by BRD4 (Li et al.,

2021), and its overactivation could deplete the cellular NAD^+ pool and alter SIRT1, leading to hyperacetylation of pro-apoptotic factors such as p53 (Pillai et al., 2005). Its overactivation has also been linked to necrotic cell death, by NAD^+ and thereby ATP depletion (Halmosi et al., 2001). PARP inhibition or genetic deletion has had beneficial effects in animal models of MI (Wang et al., 2018). Thus, inhibitors of PARP-1 hold great promise in the treatment of heart disease.

CD38

Cyclic ADP-ribose cyclases 38 (CD38) is a multifunctional enzyme that acts on NAD^+ to form the cyclic compounds $NAADP^+$, ADPR, and cADPR, which play important roles in Ca^{2+} signaling and immune function (Czura & Czura, 2006). CD38 plays a vital role in regulating Ca^{2+} signaling pathways, NAD^+ metabolism, and immunity (Zuo et al., 2020). CD38 expression was first observed on thymocytes and T lymphocytes. Nowadays, CD38 is considered virtually ubiquitous. The great majority of CD38 has a type II membrane orientation, with the catalytic site facing the outside of the cell (Chini et al., 2018; Czura & Czura, 2006). Notably, CD38 also degrades circulating NAD^+ precursors, NMN, and NR (Camacho-Pereira et al., 2016; Grozio et al., 2013) to be incorporated inside the cells. Remarkably, CD38 has a key role in the regulation of NAD-dependent processes in several cellular compartments, such as the activity of the nuclear and mitochondrial sirtuins (Camacho-Pereira et al., 2016). Thus, the potential role of CD38 as a sirtuin regulator is of major pharmacological relevance. It has been demonstrated that CD38 deficiency protects the heart from I/R injury *in vitro* and *in vivo*, the protection is mostly linked with suppressing ROS generation and overloading of intracellular Ca^{2+} in myocardial cells by the activation of the SIRT1/FOXOs signaling pathway (Guan et al., 2016). CD38 also plays an essential role in cardiac hypertrophy, via inhibition of SIRT3 expression and activation of the Ca^{2+}-NFAT signaling pathway (Guan et al., 2017). Interestingly, it was shown that CD38 activation is a critical

mechanism contributing to the pathogenesis of I/R injury. CD38 activation causes post-ischemic depletion of NAD(P)(H) within the heart, with severe depletion in the endothelium, resulting in endothelial dysfunction and myocardial injury (Boslett et al., 2018).

1.4.7 NAD^+ Perturbation in Heart Failure

It is known that myocardial NAD^+ levels are drastically decreased after MI. A study showed that 30 minutes of ischemia in isolated rat hearts led to a 30% decrease in NAD^+ in isolated mitochondria or at the whole tissue level. The cause of NAD attrition was not identified in this study but attributed to an unidentified NAD glycohydrolase located in the mitochondrial intermembrane space (Di Lisa et al., 2001) Furthermore, it has been demonstrated that NAD^+ has a protective effect against ischemia. In a study by Zhang and colleagues, exogenous NAD^+ administration before ischemia (intravenous 10-20 mg/kg) reduced the infarct size and improved cardiac function. Troponin I levels were decreased, as well as apoptotic signaling (Zhang et al., 2016). Hsu and colleagues showed that the expression of *Nampt* in the heart was drastically decreased by ischemia and ischemia/reperfusion (I/R) (Hsu et al., 2009). Furthermore, they showed that *Nampt* deletion worsens myocardial injury in response to myocardial ischemia and reperfusion while *Nampt* overexpression is cardioprotective. The upregulation of *Nampt* increased NAD^+ and ATP levels. The existence of different pathways for NAD^+ synthesis raised the question of which precursor represents the best option to boost NAD^+ levels during HF. A recent study from our workgroup in a model of inducible cardiac-specific Serum response factor (SRF) knockout (SRF^{hKO}) mice that develop non-ischemic DCM, demonstrated that NAD content was reduced by 30% after 15 days of SRF inactivation in the heart and the enzyme NMRK2 was upregulated (Diguet et al., 2018). In contrast, the enzyme NAMPT was downregulated. To restore NAD levels, SRF^{hKO} mice were supplemented with dietary NR (400 mg/kg

daily), this prevented LV remodeling and the drop in EF as compared to *SRF*^{hKO} mice on a maintenance diet. Supplementation with the precursor NAM did not preserve NAD levels in the heart. These findings lead us to hypothesize that dietary NR supplementation could be beneficial in a context of MI-induced HF, especially because NAMPT that uses the alternative precursor NAM is repressed in the mouse model of MI (Hsu et al., 2009) while preliminary exploration of public gene expression datasets suggest that *Nmrk2* gene expression is stable or even up-regulated after MI.

1.4.8 NR Supplementation

The great involvement of NAD^+ in all the processes previously described indicates a huge potential for the employment of NAD^+ precursors as treatments for a wide range of diseases. Nevertheless, there are several options in terms of precursors, and it is still needed to find the ideal precursor, the dosage for each specific condition, and the best delivery method. Recently, the precursor NR has come into the limelight as a promising therapy for a wide variety of conditions and diseases. A significant body of work produced during the past decade showed the potential of this molecule. NR is the third discovered NAD^+ precursor and is already available as a nutraceutical. It has been reported that NAD^+ levels can be increased upon NR supplementation in yeast (Belenky et al., 2007; Bieganowski & Brenner, 2004) and a wide range of mammalian cell lines and mouse liver (Cantó et al., 2012b; Yang et al., 2007). Remarkably, NR oral supplementation has been shown to increase NAD^+ levels in various tissues, along with enhanced SIRT activity (Belenky et al., 2007; Bieganowski & Brenner, 2004) and improved mitochondrial function (Cantó et al., 2012). NR is currently considered a favorable precursor since it has not been linked to severe side effects or flushing, like other NAD^+ precursors (Martens et al., 2018). Particularly, NR chloride has been given GRAS

status (Generally Recognized as Safe) which further proves its beneficial use as a nutraceutical therapy.

The precursors NR and MNM are converted to NAM in the liver upon oral supplementation, nonetheless intravenous delivery allows both precursors to reach other tissues intact (Liu et al., 2018). In line with these results, increased mouse liver NAD^+ levels were observed upon oral administration of the precursors NR, NAM, and NA, in the same order as mentioned. Likewise, oral NR consumption by healthy human subjects boosted NAD^+ levels in peripheral blood mononuclear cells. Single doses of 100, 300, and 1,000 mg of NR produce dose-dependent increases in the blood NAD^+ metabolome in humans (Trammell et al., 2016). As of recently, it has been reported on 62 clinical trials during the last few years, for several diseases such as acute kidney injury, psoriasis, Parkinson's disease, and hypertension. In the context of DCM, in a genetic mouse model induced by the deletion of serum response factor in the heart (SRF^{hKO}), our group has demonstrated that oral supplementation of NR significantly reduced LV contractile dysfunction and dilation. Stabilization of the myocardial NAD^+/NADH ratio and an increase in citrate synthase (CS) and ATP-citrate lyase (ACL) activities in the heart were observed. Additionally, it was observed *in vitro* that another beneficial effect of NR is the increase of glycolysis in cardiomyocytes. Interestingly, it was also demonstrated that NR supplementation increased acetylation of nuclear proteins such as FOXO1 and p53, which could probably be due to an increase in acetyl-CoA generation (Diguet et al., 2018).

1.5 NOVEL APPROACHES FOR BIOMARKER DISCOVERY

A biologic marker or biomarker is defined as a characteristic that is objectively measured and evaluated as an indicator of normal biologic processes, pathogenic processes, or pharmacologic responses to a therapeutic intervention. This defini-

tion can be derived from molecular, histologic, radiographic, or physiologic characteristics. Several subtypes of biomarkers have been delineated according to their applications (Califf, 2018). Nowadays, available biomarkers for diagnosis or prognostic were mostly developed through physiologic studies that explore well-known pathways. On the other hand, new technologies make feasible a systematic and unbiased classification of variation in proteins and metabolites that are related to diseases or exposure to treatments. Modern technologies have a great potential to increase the range of biomarkers applicable to the cardiovascular field, nuclear magnetic resonance (NMR), gas and liquid chromatography (GC and LC), mass spectrometry (MS), and bioinformatics. Metabolomics can offer a better interpretation of the full complexity of a pathological condition, as metabolites can give a glimpse of the cellular state. Moreover, it can also provide evidence concerning the response to stressors, nutrition, or consumption of other compounds. Through metabolomics, it is possible to obtain the snapshot of smaller biochemical compounds, for instance, amino acids, lipids, sugars, nucleotides, and other types of intermediary metabolites (Zipes & Libby, 2018). Recent studies on the physiological distribution in mammalian tissues of the NAD-related metabolites have been solidly increasing as a result of the advancement of analytical detection methods (Yamada et al., 2006). Even more evidence concerning the role of some of them, notably NMN and NR, has emerged (Cantó et al., 2012; Mori et al., 2014). Particularly, the cardiac metabolome may be regarded as the most informative proxy for the mechanistic biochemistry of healthy and diseased hearts (Raghow, 2016).

2 OBJECTIVES

Regardless of the vast knowledge about the pathophysiology of HF, the existing therapies are restricted to the reduction of heart rate, inhibition of neuroendocrine activation, and reduction of myocardial O_2 consumption. However, there is still a need for targeting the deficient cardiac metabolism linked to HF which contributes to the evolution of the disease. NAD^+ is a central molecule to metabolism, classically known as a coenzyme involved in redox reactions of energy metabolism, and the principal donor of electrons in OXPHOS. In addition, NAD^+ is also a substrate for enzymes PARPs, sirtuins, and CD38 that are implicated in mediating gene expression, genomic stability, inflammation, resistance to stress, and calcium signaling. Collectively, these three families of enzymes control key biological cellular processes, making NAD^+ homeostasis critical for proper cellular functioning as the depletion and metabolism alterations of NAD^+ are common factors in a wide variety of diseases, for example, CVD. Consequently, developing strategies to re-establish NAD^+ homeostasis as a strategy to treat CVD, including LVR post-MI, has gained relevance in recent years to treat these pathologies. In the context of NAD^+ biosynthesis, it has been demonstrated, both in different experimental models and hearts of human patients with DCM, that the NMRK2 pathway is significantly up-regulated, whereas the NAMPT pathway is severely down-regulated. Furthermore, previous studies in our group have demonstrated the implication of the NMRK2 pathway in basal and cardiac stress conditions led us to focus on this pathway. Hence, we hypothesized that stimulating the cost-effective NMRK2 pathway through dietary NR supplementation would be beneficial in the context of LVR post-MI, both functionally and metabolically.

Thus, our primary objective was to evaluate the effect of dietary supplementation with the NAD^+ precursor, NR, in an *in vivo* MI rat model in a medium time frame

(up to 16 weeks). This project is divided into two parts: (**1**) Evaluation of the cardioprotective effect of NR to assess the progression of LVR. For this purpose, first, we evaluated cardiac function structural remodeling of the LV through echocardiography. Furthermore, we assessed cardiac injury and cardiac stress markers to further validate our *in vivo* model of MI. Afterward, we studied the mitochondrial function and energy signaling mediators in the LV. And lastly, we investigated the effect of NR supplementation in the expression of enzymes implicated in the NAD^+ salvage pathway, NAMPT, and NMRK2. (**2**) For the second part of the project, we aimed to assess the impact of oral NR supplementation in the myocardial and circulation metabolome. For this objective, we implemented several biostatistical methods, notably exploratory analysis, to thoroughly examine the differences between the data obtained from LC/MS.

3 MATERIALS AND METHODS

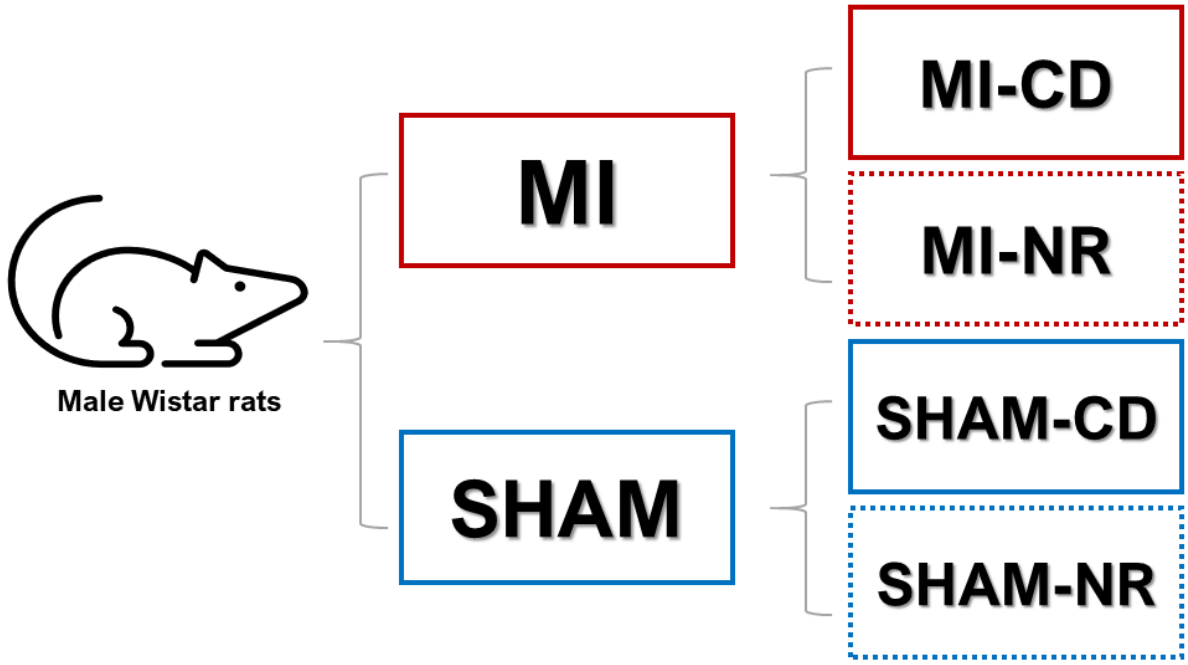

Figure 21. Experimental groups

Male Wistar rats were randomly assigned to either MI group, that underwent ligation of left anterior descending (LAD) coronary artery or Sham group (mock surgery). In turn, MI and Sham rats were assigned to either CD group (fed with standard diet) or NR group (fed with NR-enriched diet) 30 minutes after surgery.

3.1 EXPERIMENTAL MODEL OF MYOCARDIAL INFARCTION

The Institutional Review Board Statement: Animal research was conducted according to the guidelines of the Declaration of Helsinki, conformed to the Directive 2010/63/EU of the European Parliament, and approved (agreement APAFIS# 12519-2017112318499166v4, October 16th, 2018) by the national Ethics Committee #26 of the French Ministry of Research. Animals were housed under standard conditions with free access to food and water. Male Wistar rats weighing

around 250 g of around 42 to 49 days old were randomly selected to either undergo a MI or sham surgery. Surgery was always performed during the morning. Anesthesia was induced by intraperitoneal injection of ketamine (100 mg/kg) and xylazine (10 mg/kg) in a volume of 0.1 ml/100 g and temperature during surgery was maintained at 37°C using a heating pad. A left thoracotomy was performed and then the heart was exteriorized. The left coronary artery was ligated with a 6-0 suture. In sham-operated animals, only the needle was passed. The heart was placed back into the chest cavity and closed. Animals were kept under a heating lamp until awakening. The infarction was produced through the permanent ligation of the left anterior descending (LAD) coronary artery downstream of the bifurcation with the left circumflex artery that irrigates the LV posterior lateral and posterior wall. Hence, the area at risk in this model is mostly the left ventricle anterior wall (LVAW) and to some extent the anterior part of the interventricular septum. As a control, rats underwent a sham surgery in which the needle passed underneath the LAD coronary artery without ligation.

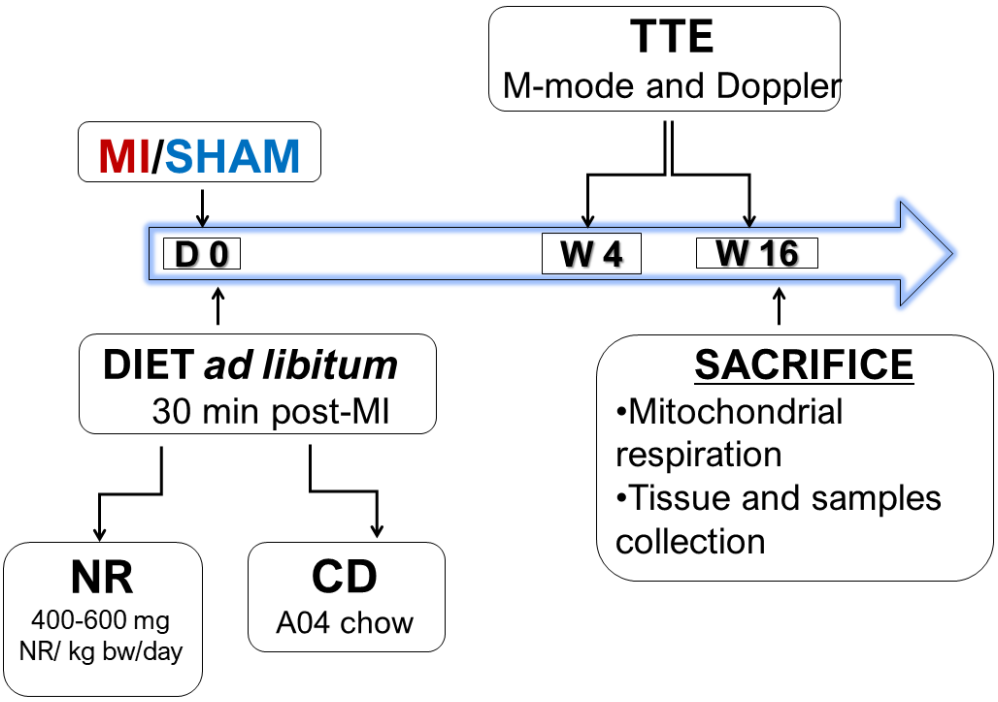

Figure 22. Experimental design

3.2 DIETARY NR ADMINISTRATION

Rats were randomly assigned to the NR group (NR supplementation) or CD group (A04 standard rodent chow, SAFE scientific diets). The NR-supplemented diet was specially prepared for this protocol by the manufacturers (SAFE) with NR chloride (Niagen, ChromaDex) that we provided. The content of NR chloride was 6.96 g per kilogram of standard chow, which represents an average range dose of 400-600 mg NR/ kg body weight/day. NR-supplemented chow was stored at 4° degrees to avoid fast degradation of NR and was renewed every day. The administration of the diet supplemented with NR started immediately after the awakening of anesthesia (~30 minutes after surgery). Blood samples from the jugular vein were collected 24 hours after surgery for further cardiac Troponin I (cTnI) quantification.

3.3 FOLLOW-UP TRANSTHORACIC ECHOCARDIOGRAPHY

The transthoracic echocardiographic (TTE) measurements were performed 4 weeks and 16 weeks after surgery for the first part of the study. The anesthetic induction was carried out in an induction chamber. The anesthesia was induced with 3% isofluorane for ~5 minutes. Throughout the TTE exploration, the rats were maintained under light sedation (1.8%-1.5% isofluorane), and the body temperature was monitored by a rectal temperature probe and controlled (37-37.5°C) with a heating system. The measurements of the LV dimensions (M-mode) and the myocardial velocities (tissue Doppler Imaging) were performed with a 12 MHz transducer (VividE9, GE Healthcare). The room where the TTEs were performed was maintained at 20-25°C. Two-dimensional (2D) echocardiography was used to visualize the LV in short and long-axis views. Thicknesses of LV anterior and posterior walls at end-diastole and systole and LV dimensions at diastole and systole were measured by M-mode echocardiography. LV fractional shortening, LV volumes at end-diastole and systole, and LVEF% were calculated by EchoPAC software (GE Healthcare). The A wave deriving from atrial contraction could not be detected in every rat, as high heart rates along with anatomical impediments can make it difficult to delineate the part of the signal corresponding to A wave.

3.4 SACRIFICE

Animals were sacrificed within the 16th-week post-surgery under anesthesia induced with intraperitoneal of pentobarbital**.** Tissue samples were snap-frozen in liquid nitrogen and stored at -80°C until further assays.

3.5 *IN SITU* QUANTIFICATION OF MITOCHONDRIAL RESPIRATION

The evaluation of mitochondrial respiration in isolated cardiac permeabilized fibers was performed reproducing as previously reported (Kuznetsov et al., 2008;

Sanchez et al., 2001). The animal was sacrificed, and tissues were rapidly obtained. Cardiac fibers were carefully excised and dissected, removing fat and connective tissue. Thin fiber bundles (100-200 μM of diameter) were excised from ventricular and white gastrocnemius under microscopes in ice-cold solution S. Then, the fibers were incubated in solution S containing 50 ug/ml of saponin for 30 minutes while shaking gently. Saponin is a soft detergent that allows the selective permeabilization of the sarcolemma by solubilizing cholesterol, which is abundant in the plasma membranes but not on mitochondrial and nuclear membranes. The permeabilized fibers were transferred into solution S without saponin while mixing gently for 10 minutes to wash out saponin and ATP. All the procedures were carried out at 4°C. Afterward, fibers were transferred to oxygraph chambers the O_2 consumption was measured employing Clark electrodes in oxygraph chambers (Oxygen Model 928, Strathkelvin Instruments, U.K.) containing 0.4 to 0.7 mg dry weight of fibers in 3 ml of solution R at 22°C with continuous stirring. The solubility of O_2 was considered as 267 nmol of O_2/ml. After the measurements, the fibers were carefully recovered, dried in a speed vacuum, and weighed. Respiration was expressed as μmol O_2 min/g of dry weight.

Solution	Composition
Solution S	10 mM EGTA, 2.77 mM $CaCO_3$, 70 mM KOH, 20 mM imidazole, 1 mM free Mg^{2+}, 20 mM taurine, 0.5 mM dithiotreitol, 5.7 mM MgATP, 15 mM phosphocreatine, 50 mM potassium methanesulfonate, pH 7.1.
Solution R	10 mM EGTA, 2.77 mM $CaCO_3$, 110 mM KOH, 10 mM NaOH, 3 mM K_2HPO_4, 20 mM imidazole, 1 mM free Mg^{2+}, 20 mM taurine, 0.5 ml DTT, 10 mM glutamate, 4 mM malate, 100 mM CH_3KO_3S, BSA 2 mg/ml, pH 7.1.

The rates of O_2 consumption of saponin-permeabilized cardiac muscle fibers were measured in a respirometer (RC650, Strathkelvin) equipped with Clarke electrodes which allow measuring changes in O_2 concentration inside the chambers after the successive addition of the compounds. First, the initial rate of respiration in the absence of fibers was recorded. The initial rate reflects the O_2 consumption by the membrane of the chamber. Next, with the addition of the permeabilized fibers, the basal respiration rate was recorded, this corresponds to the O_2 basal consumption of the fibers. Afterward, specific activators and inhibitors of each complex of the respiratory chain were added successively (Protocol 1), as well as different substrates of the respiratory chain complexes (Protocol 2), 2 to 3 minutes in between each compound.

3.5.1 Protocol 1: Mitochondrial Respiratory Complexes

Glutamate (10 mM) and malate (4 mM), were utilized to feed electrons to the Complex I of the ETC. Both enter the mitochondrial matrix via the M-A shuttle and generate NADH, which in turn the addition of ADP at 0.1 mM, a substrate for ATP synthase, was used to stimulate respiration at a submaximal rate. Afterward, mitochondrial-creatine kinase was stimulated with the addition of creatine (30 mM). The addition of creatine stimulates the transfer of phosphate from ATP to phospho-creatine by mitochondrial-creatine kinase, restoring locally ADP to be used

by the ATP synthase, indicating the extent of functional coupling of the mitochondrial-creatine kinase. Then, ADP was used at saturating concentration (2mM) to reach maximal mitochondrial respiration and to assess OXPHOS capacity (state 3). Subsequently, pyruvate (1mM) was incorporated to further fuel NADH-linked respiration (Complex I) by the pyruvate dehydrogenase. Oxidative decarboxylation of pyruvate is catalyzed by pyruvate dehydrogenase and yields acetyl-CoA and NADH. After, succinate (15 mM) was utilized to induce complex-II supported respiration allowing to measure the sum of Complex I and II activities. Complex I was then blocked by the inhibitor, amytal (2mM) to measure Complex-II supported respiration alone. Finally, TMPD (tetramethyl-phenylenediamine) and ascorbate (0.5 mM each) were used to activate complex IV as TMPD is a direct donor of electrons to cytochrome C.

3.5.2 Protocol 2: Mitochondrial Substrate Utilization and FAO

First, malate (4 mM) and ADP (2 mM) were added to the chamber. Malate is a substrate for malate dehydrogenase in the TCA cycle to produce oxaloacetate. Additionally, malate will stimulate the generation of NADH in the mitochondria (as previously mentioned). ADP was added at a saturating concentration, is a phosphate acceptor. After, glycerol-3-phosphate (4 mM) was used to provide electrons to complex II, as it is oxidized by the mitochondrial glycerol-3-phosphate dehydrogenase. After this point, either palmitoyl-CoA plus carnitine or octanoate were added. Palmitoyl-CoA (0.1 mM) and carnitine (2 mM) were added to evaluate FAO. Palmitoyl-CoA is a LCFA that requires the transporter CPT1 to be sent into the mitochondria and carnitine is required for this process. Alternatively, octanoate (0.1 mM) is a medium-chain FA that passes freely into the mitochondrial matrix, as it does not require the carnitine-palmitoyl-transferases system and activates β-oxidation. After entering the mitochondria, octanoate and palmitoyl-

carnitine provide NADH, H^+, and $FADH_2$. These molecules are oxidized by complex I and electro-transferring-flavoprotein dehydrogenase in the presence of malate. After, pyruvate (1mM), was added to fuel the electron flow to complex I. Glutamate (10 mM) and succinate (15 mM), were used to fuel complex I and II-linked respiration, respectively. The addition of both allows reaching maximal respiration if ADP is present. Afterward, complex I was blocked by amytal (2 mM) to measure complex-II linked respiration. TMPD and ascorbate (0.5 mM each) were employed to donate electrons to cytochrome C and subsequently stimulate Complex IV.

3.6 Real-Time Quantitative Polymerase Chain Reaction (RT qPCR)

We conducted mRNA expression analysis to detect gene expression variations among the experimental groups. With this technique, it is possible to detect, amplify, and quantify complementary cDNA, synthesized by reverse transcription (RT), which corresponds to messenger RNA of interest. The general steps are as follows: RNA isolation and quality control check, cDNA synthesis, qPCR and data acquisition, and data analysis.

3.6.1 RNA Isolation

The RNA isolation was conducted by the Trizol reagent method (Gibco BRL). Briefly, frozen LV samples (~20 mg) were homogenized (Precellys, Bertin technologies) in 1 ml of Trizol. Then, 0.2 ml of chloroform (per ml of Trizol) were added and samples were centrifugated at 4°C (10000 G, 15 minutes) to obtain two phases, an aqueous phase at the top (RNA) and a lower phase at the bottom (proteins), separated by an interface (DNA). The aqueous phase was recovered and mixed with 0.5 ml isopropanol, to be stored overnight at -20°C to precipitate the RNA. Afterward, RNA pellets were obtained by centrifugation (4°C, 12000 G, 15 minutes). The RNA pellets were washed twice with 75% ethanol to remove

isopropanol and Trizol reagent. The pellets were dried at room temperature and then put back into solution (15-20 µl of RNAase/Dnase-free water). Samples were stored at -80 °C. The RNA concentration was measured by a Nanodrop spectrophotometer (Thermofisher). The purity of the RNA (vs DNA) is estimated by the OD 260/280 ratio, a ratio of 1.8 to 2.0 is generally accepted as pure for RNA, a ratio lower than 1.5 indicates contamination by proteins or aromatic compounds, on the contrary, a ratio greater than 2 shows contamination by genomic DNA. The OD 260/230 ratio was used to test for the presence of trizol in the samples', expected values are 2 to 2.2.

3.6.2 Reverse Transcription

The purified mRNAs were transformed into complementary double-stranded DNA (cDNA) by reverse transcription using the iScript Reverse Transcriptase kit (BioRad, 1708840). Following the manufacturer's protocol, 1 µg of mRNA was transcribed into cDNA in 20 µL of the mix, for 20 minutes at 46°C.

3.6.3 Real-Time Quantitative PCR (RT-qPCR)

The cDNAs were quantified by qPCR, which involves replication of a target cDNA sequence overtime throughout the amplification cycles. This technique is based on the endpoint PCR, however, the amplification of the cDNA sequence of interest is observed through the polymerization cycles using a DNA intercalator that emits green fluorescence (SYBR Green) as it is being incorporated between the bases of double-stranded DNA. The reactions were done on 384 well-plates in a volume of 7.5 µL per reaction, containing 450 ng of cDNA, 0.5 µM of each primer, and 3.5 µL of SsoAdvanced Supermix (Biorad), which includes SYBR Green, Taq Polymerase, and the oligonucleotides. The amplification was carried out using a thermal cycler coupled to a fluorescence detection system (CFX384, Biorad). The quantifi-

cation of the expression level of the genes of interest is based on its cycle threshold (Ct), which is the thermal cycle at which the fluorescent signal exceeds that of the background. Ct is inversely proportional to the quantity of target cDNA in the sample. The expression values of the target genes are relative to the expression levels of genes that are unchanged by the experimental conditions (reference genes). The data obtained were acquired and analyzed with the CFX Maestro software (Biorad). Gene expression was calculated as $R=2^{\Delta Ct}$ (Ref Ct – target Ct), using *Hprt* as a reference gene. Hprt was selected among a series of other reference genes as the most stable reference gene in the same range of Ct in our conditions.

3.7 WESTERN BLOT

Total proteins were extracted from LV samples by homogenization (Precellys, Bertin technologies) in 200 µl of RIPA lysis buffer (50 mM Tris, 150 mM NaCl, 1% Triton, 0.1% SDS, 1 mM EDTA, 1 mM DTT, 10 µM PJ34, 70 µM tannic acid) containing antiproteases, anti-phosphatases, and anti-deacetylases. The homogenates were centrifuged at 10,000 g for 15 min at 4°C the supernatant (proteins) was collected and stored at -80°C. The protein concentration was then determined by bicinchoninic acid (BCA) colorimetric assay (Pierce BCA Protein Assay Kit, ThermoFisher). This assay is based on the reduction of Cu^{2+} to Cu^{1+} by protein in an alkaline medium with the sensitive and selective colorimetric detection of the cuprous cation (Cu^{1+}) by BCA. An intense, purple-colored reaction product results from the chelation of two molecules of BCA with one cuprous ion. The microplate was read at 562 nm (VICTOR Nivo Multimode Microplate Reader, Perkin Elmer). A standard curve was developed employing a series of bovine serum albumin (BSA) standards (1000 µg/ml to 10 µg/ml) to determine the protein concentration in the samples. Then samples were prepared in LDS 4X Nu-PAGE Denaturing Buffer (Thermo Fischer Scientific) using 1 volume of buffer per 3 volumes of protein sample. The samples were denatured heating for 10 minutes at 70°C in

the presence of the surfactant sodium dodecyl sulfate (SDS), which also coats the proteins with a negative charge. 40 µg of protein per sample were loaded in pre-cast gels and separated by SDS-PAGE electrophoresis at a constant voltage (200 V) in Tris Glycine-SDS or Bis-Tris migration or MES running buffer (Tris-Glycine-SDS, Euromedex; NuPAGE™ MES, Invitrogen). The proteins are concentrated and then separated by their molecular weight. Afterward, the gels were transferred to a pre-assembled dry transfer stack (PVDF 0.2 µm, Iblot Transfer Stack, ThermoFisher) employing an iBlot 2 Dry Blotting System (ThermoFisher) following the manufacturers indications. The blots were stained with Ponceau red (Ponceau red 0.2%, acetic acid 5%) for 5 minutes to verify the transfer of the proteins. The blots were blocked in 5% milk in TBS-Tween (0.1%) for 2 hours at room temperature with constant shaking. The blot was then incubated with a primary antibody (0.1% TBS-Tween, 1% milk) overnight, at 4°C. The membrane was washed times with 0.1% TBS-Tween for 5 minutes to remove the primary antibody. Next, the blot was incubated with a secondary antibody for 1 hour at room temperature and with constant shaking. The secondary antibody which reacts against the primary antibody is conjugated to the enzyme horseradish peroxidase, this allows the detection in the presence of its substrate. The blot was incubated with a solution containing the peroxidase substrate (Pierce ECL western blotting substrate, Thermo Scientific) and the reaction was detected by a chemiluminescence detection system (iBright, Thermo Fisher Scientific). Finally, the detected bands corresponding to the proteins were quantified by ImageJ. The intensities of the bands corresponding to the proteins of interest were normalized with those of a reference protein (Actin or Vinculin). The data obtained are expressed as a ratio of these two intensities (protein of interest/reference protein).

Target protein of primary antibody	Supplier/Reference	Dilution
Nampt	Abcam/#ab24149	1:500
ACC (total)	Cell Signaling/3676	1:1000
Phosphorylated ACC	Cell Signaling/3661	1:1000
Nmrk2	Provided by Dr. Gareth Lavery	1:500
Vinculin	Sigma/ V9131	1:1000

3.8 CARDIAC TROPONIN I QUANTIFICATION

The Access AccuTnI+3 assay (Beckman Coulter) was employed to quantify cTnI levels in serum samples. It is based on the principle of a chemiluminescent sandwich immunoassay; it uses paramagnetic particles and anti cTnI antibodies for the highly sensitive determination of cTnI in serum using the UniCel DxI 800 Immunoassay System (Beckman Coulter). This was carried out in collaboration with Laboratoire d'Hormonologie-Ria-Immunoanalyse, Hôpitaux Universitaires Est-Parisien/INSERM UMR 1193, Faculty of Pharmacy, (Châtenay-Malabry, France).

3.9 METABOLOMICS

Metabolomics was carried out in collaboration with the Département Médicaments et Technologies pour la Santé (DMTS), MetaboHUB, F-91191 of Université Paris-Saclay.

3.9.1 Chemicals and Reagents

All analytical grade reference compounds were from Sigma (Saint Quentin Fallavier, France). The standard mixtures used for the external calibration of the MS instrument (Calmix-positive, for the positive ion mode, consisting of caffeine, L-methionyl-arginylphenylalanyl-alanine acetate, and Ultramark 1621, and Calmix-negative, for the negative ion mode, consisting of same mixture plus sodium dodecyl sulfate and sodium taurocholate) were from Thermo Fisher Scien-

tific (Courtaboeuf, France). Acetonitrile (ACN) was from SDS (Peypin, France), formic acid from Merck (Briare-le-Canal, France), methanol from VWR Chemicals (Fontenay-sous-Bois, France) and deionized water from Biosolve chemicals (Dieuse, France).

3.9.2 Metabolite Extraction

Tissue samples were resuspended in 170µL of ultrapure water and then sonicated 5 times for 10 s using a sonication probe (Vibra cell, Bioblock Scientific, Illkirich, France). At this step, 20µL of each sample were withdrawn for further determining the total protein concentration using the bicinchoninic acid method following manufacturer specifications (Pierce BCA Protein Assay Kit, Thermo Fisher Scientific, Courtaboeuf, France). A volume of 350µL of methanol containing internal standards at 3.75µg/mL (Dimetridazole, AMPA, MCPA, Dinoseb; Sigma-Aldrich, Saint-Quentin Fallavier, France) was added to the remaining 150µL of tissue lysate. Cell debris was then removed by centrifugation for 15 min at 4 °C and 20,000g. Supernatants) were collected and then left on ice for 90 minutes until complete protein precipitation. After a final centrifugation step at 20,000 g for 15 minutes at 4°C, supernatants were recovered and split into two equal aliquots for C18 and HILIC analyses. The resulting aliquots were then dried under a stream of nitrogen using a TurboVap instrument (Thermo Fisher Scientific, Courtaboeuf, France) and stored at −80 °C until analysis. Before LC-MS analysis, dried extracts were resuspended to reach a fixed protein concentration using variable volumes of H_2O/Acetonitrile (ACN) (95:5, v/v), containing 0.1% formic acid or 10 mM ammonium carbonate pH 10.5/ACN (40:60, v/v) for metabolite analysis using C18 and ZIC-pHILIC columns, respectively. After reconstitution, the tubes were vortexed and incubated in an ultrasonic bath for 5 minutes and then centrifuged at 20,000 g for 15 minutes at 4°C. A volume of 95µL of the supernatant was trans-

ferred into 0.2-mL vials. External standard solution (5 µL; the mixture of 9 authentic chemical standards covering the mass range of interest: 13C-glucose, 15N-aspartate, ethylmalonic acid, amiloride, prednisone, metformin, atropine sulfate, colchicine, imipramine) was added to all samples to check for consistency of analytical results in terms of signal and retention time stability throughout the experiments. In addition, a quality control (QC) sample was obtained by pooling 20 µL of each sample preparation. QC samples were injected every 5 samples to evaluate the signal variations of any metabolite.

3.9.3 Liquid Chromatography Coupled to High-Resolution Mass Spectrometry

The ultra-high-performance liquid chromatographic (UHPLC) separation was performed on a Hypersil GOLD C8 1.9 µm, 2.1 mm x 150 mm column (RP) at 30°C (Thermo Fisher Scientific, les Ulis, France), and HPLC chromatographic separations were performed on a Sequant ZICpHILIC 5 µm, 2.1 x 150 mm (HILIC) at 15°C (Merck, Darmstadt, Germany). All chromatographic systems were equipped with an online prefilter (Thermo Fisher Scientific, Courtaboeuf, France). Experimental settings for each LC-MS condition are described below. Mobile phases for RP columns were 100% water in A and 100% ACN in B, both containing 0.1% formic acid. Regarding HILIC, phase A consisted of an aqueous buffer of 10 mM ammonium carbonate in water adjusted to pH 10.5 with ammonium hydroxide, whereas pure ACN was used as solvent B. Chromatographic elutions were achieved under gradient conditions as follows: (i) RP-based system: the flow rate was set at 500 µL/min. The elution consisted of an isocratic step of 2 minutes at 5% phase B, followed by a linear gradient from 5 to 100% of phase B for the next 11 minutes. These proportions were kept constant for 12.5 min before returning to 5% B for 4.5 min. (ii) HILIC-based system: the flow rate was 200 µL/min. Elution started with an isocratic step of 2 min at 80% B, followed by a linear gradient from 80 to 40% of phase B from 2 to 12 min. The chromatographic system was then rinsed for 5

min at 0% B, and the run ended with an equilibration step of 15 min (80% B). LC-MS analyses were performed using a U3000 liquid chromatography system coupled to an Exactive mass spectrometer from Thermo Fisher Scientific. (Courtaboeuf, France) fitted with an electrospray source operated in the positive and negative ion modes. The software interface was Xcalibur (version 2.1) (Thermo Fisher Scientific, Courtaboeuf, France). The mass spectrometer was calibrated before each analysis in both ESI polarities using the manufacturer's predefined methods and recommended calibration mixture provided by the manufacturer (external calibration). The Exactive mass spectrometer was operated with capillary voltage at -3 kV in the negative ionization mode and 5 kV in the positive ionization mode and a capillary temperature set at 280°C. The sheath gas pressure and the auxiliary gas pressure were set, respectively, at 60 and 10 arbitrary units with nitrogen gas. The mass resolution power of the analyzer was 50,000 m/dm, full width at half maximum (FWHM) at m/z 200, for singly charged ions. The detection was achieved from m/z 85 to 1000 for RP conditions in the positive ionization mode and from m/z 50 to 1000 for HILIC conditions in the negative ionization mode.

3.9.4 Processing of Data

All raw data were manually inspected using the Qualbrowser module of Xcalibur version 2.1 (Thermo Fisher Scientific, Courtaboeuf, France). Raw files were first converted to mzXML format using MSConvert software. Automatic peak detection and integration were performed using the XCMS software package (W4M platform (https://galaxy.workflow4metabolomics.org), which returned a data matrix containing m/z and retention time values of features together with their concentrations expressed in arbitrary units (i.e., areas of chromatographic peaks). XCMS features were thereafter filtered according to the following criteria: (i) the correlation between dilution factors of QC samples and areas of chromatographic

peaks (filtered variables should exhibit coefficients of correlation above 0.7 to account for metabolites occurring at low concentrations and which are not detected anymore in the most diluted samples), (ii) repeatability (the coefficient of variations obtained for chromatographic peak areas of QC samples should be below 30%) and (iii) ratio of chromatographic peak area of biological to blank samples above a value of 3. Optionally, if necessary, chromatographic peak areas of each variable present in the XCMS peak lists were normalized using the LOESS algorithm to remove analytical drift induced by clogging of the ESI source observed during analytical runs.

3.9.5 Annotation

Features were annotated by matching their accurate measured masses ± 10 ppm with theoretical masses contained in biochemical and metabolomic databases by using an informatics tool developed in R language. The databases used were the Kyoto Encyclopedia of Genes and Genomes (KEGG), the Human Metabolome Database (HMDB), and METLIN. Features were also annotated by our spectral database according to accurately measured masses and chromatographic retention times. To be identified, ions had to match at least 2 orthogonal criteria (accurately measured mass, isotopic pattern, MS/MS spectrum, and retention time) to those of an authentic chemical standard analyzed under the same analytical conditions, as proposed by the Metabolomics Standards Initiative. KHM annotation was done using public databases (KEGG, METLIN, and HMDB), facilitating the annotation of unknown metabolites. However, it is not current and is only based on mz. SPI annotation was done using SPI intern databases and is based on a comparison of mz and retention time from experimental data to referent molecules from SPI Chimiotech. Compared to annotation by public databases, this system considers the fact that mz are not necessarily pseudomolecular ions, but can be isotopes,

adducts, or fragments. It also considers the different chromatographic systems used in the laboratory for retention times (HILIC, C18).

3.10 STATISTICAL ANALYSIS

Statistical analyses were performed using GraphPad Prism 7 software. Experimental groups were analyzed by 2-way ANOVA followed by multiple comparisons with Tukey's *post hoc* analysis. Values are presented as the mean ± standard error of the mean (SEM). We assessed the time to an adverse event by Kaplan-Meier survival curves and determining differences between groups by the log-rank test ($P>0.05$).

For the metabolomics section, data was generated on the LV tissue and plasma samples for a total of 42 rats. Metabolites with more than 40% missing values overall were removed. The remaining missing data were imputed using the k-nearest neighbor imputation approach through MetaboDiff (Mock et al., 2018), yielding for LV samples, n=1840 signals measured for HILIC and n=3416 signals measured for C18; for plasma samples, n=2207 signals measured for HILIC and n=3800 signals measured for C18. Two samples were identified as outliers using principal component analysis (PCA) scores plot and removed: one was confirmed to have had a high proportion of missing data (>10%, technical outlier) and the other had died before sacrifice (biological outlier). To reduce biases due to highly variable metabolites' range, raw metabolite concentrations were subjected to variance stabilizing normalization. PCA was performed on the normalized data for the 40 remaining rats, separately for plasma and LV tissue. Uniform Manifold Approximation and Projection (UMAP) dimensionality reduction was performed to summarize in two dimensions the information included in multiple PCs, helping their visualization, including 10, 20, or 40 principal yield similar results.

For differential quantification analyses, linear models were used to estimate the fold change (FC) of metabolites that differed between groups. An absolute value

of FC over 1.5 is considered biologically significant. For each pairwise comparison, we excluded metabolites with more than 40% missing values in the specific subset of samples. Furthermore, near-constant metabolites, with low interquartile range (IQR), which are non-informative variables, were also removed. The final number of metabolites considered for each comparison (with and without SPI annotations). Benjamini and Hochberg's method was used to compute false discovery rate (FDR) adjusted p-values. An FDR below 5% is considered statistically significant, below 10% is considered suggestive. These analyses are done using R 3.6.3. MetaboAnalyst 4.0 web-based tool (Chong et al., 2018) was used to determine the difference between groups, regarding diet and surgery effects on metabolites by the two 2-way ANOVA test, p-values were adjusted by the false discovery rate (FDR) method. Cutoff q-value (FDR adjusted p-value) was set at 0.05. Metabolites that showed surgery and diet effect were represented by hierarchical clustering heatmaps using the web-based tool ClustVis (https://biit.cs.ut.ee/clustvis/).

KEGG was used as the database for quantitative enrichment analysis (QEA) in pairwise comparisons (Sham CD and Sham NR groups, and MI CD and MI NR groups). QEA considers the presence/absence of metabolites and the importance measure (Q-statistic) calculated for each compound for enrichment analysis. Q can be interpreted as an aggregate of squared covariance between concentration changes and the phenotypes. Compounds with large variance have more influence on the Q-statistic than a compound with small variance.

4 RESULTS

Article

Nicotinamide riboside supplementation administrated after experimental myocardial infarction in rats results in a more favourable left ventricular remodeling and improved survival

Selma Lopez Vaquera[1], Pamela Mehana[2], Ahmed Karoui[1], Florence Castelli[3], Valérie Domergue[4], Mélanie Gressette[1], Bénédicte L. Tremblay[2], Jean-Christophe Grenier[2], Antoine Pilon[5], Jérôme Piquereau[1], Matthieu Ruiz[2], François Fenaille[3], Julie Hussin[2*], Mathias Mericskay[1*]

[1] Université Paris-Saclay, Inserm, UMR-S 1180, 92296, Châtenay-Malabry, France.

[2] Université de Montréal, Montreal Heart Institute, Faculté de médecine, Canada

[3] Université Paris-Saclay, Département Médicaments et Technologies pour la Santé (DMTS), MetaboHUB, F-9119, France

[4] Université-Paris-Saclay, IPSIT, US31 Inserm, UMS3679 CNRS, Châtenay-Malabry, France.

[5] Université Paris-Saclay, Inserm, UMR-S -1193, Team "Mécanismes moléculaires et cellulaires de réponse aux stress et cancérogènese, 92296, Châtenay-Malabry, France.

*Addresses for correspondence:

Dr Mathias Mericskay

UMR-S1180, INSERM

Université Paris-Saclay, Faculté de Pharmacie,

5 rue J-B Clément, 92296 Châtenay-Malabry, France

E-mail: mathias.mericskay@inserm.fr

Tel: (33-1) 46.83.53.25, Fax: (33-1) 46.83.54.75

Dr Julie Hussin

Computational Biomedicine Lab

Montreal Heart Institute, Université de Montréal
5000 Bélanger, Room S-1450.
Montréal, QC H1T 1C8, Canada
E-mail : Julie.Hussin@mhi-omics.org

Abstract

The NAD precursor, nicotinamide riboside (NR), holds great promise for restoring altered cardiac metabolism, which is a hallmark of heart failure (HF) after myocardial infarction (MI). We investigated the impact of orally supplemented NR on adverse LVR post-MI in a rat model. Male Wistar rats were either subjected to MI through permanent ligation of the left anterior descending coronary artery and were fed with NR-supplemented chow *ad libitum* (400-600 mg/kg) for 16 weeks. Echocardiography was conducted 4- and 16-weeks post-surgery. Mitochondrial respiration (cardiac fibers) assays, determination of relative gene and protein expression (LV), and LC-MS (plasma and LV) were performed. 16 weeks of oral NR improved survival probability and cardiac function in MI NR-fed group. NR boosted the expression of NAD^+ salvage pathway enzymes, namely, NAMPT and NMRK2 after MI. However, mitochondrial respiration parameters altered by MI were not restored through NR treatment. Interestingly, LV metabolomes were remarkably modified on NR-fed groups. These findings altogether suggest that *in vivo* NR is efficient to counteract the progression LVR after MI.

Introduction

Acute myocardial infarction (MI) is the most severe subtype ischemic heart disease and is defined pathologically as myocardial cell death caused by sustained ischemia. The mortality attributable to MI has been declining for the last decades thanks to critical advancements in prevention strategies and treatment (Anderson & Morrow, 2017; OECD, 2017). Heart failure (HF) is a post-MI complication characterized

by structural and/or functional cardiac abnormalities. The prevalence of HF has increased due to a rise in cardiovascular risk factors and global population aging. Despite the current advances in HF treatments, this syndrome is still characterized by a poor prognosis as patients may require frequent hospitalizations and have reduced life expectancy (Bhatt et al., 2017). It has been estimated that 64.3 million people are living with HF worldwide. In developed countries, the prevalence of detected HF is estimated at 1% to 2% of the adult population (Groenewegen et al., 2020).

Adverse left ventricular remodeling (LVR), an abnormal modification in the architecture of the ventricle, is associated with dilation, increased volume, rearrangements of the normal structure of the heart, and underlying complex biological and molecular perturbations (Cokkinos & Belogianneas, 2016). Most notably, alterations in mitochondrial homeostasis and metabolic remodeling represent an important pathophysiological process in adverse LVR linked to HF progression. During metabolic remodeling, changes in oxidative phosphorylation, high-energy phosphate metabolism, and substrate utilization occur. Even though the complex molecular mechanisms and signal transduction pathways regulating mitochondrial function and cardiac metabolism are partially identified nowadays, existing pharmacological strategies do not address the perturbation of the heart's bioenergetics induced by HF.

NAD^+ is a central molecule to metabolism, classically known as a coenzyme involved in redox reactions of energy metabolism and, is also a substrate for enzymes that participate in crucial processes in the development of cardiovascular pathologies, namely PARPs, Sirtuins, and CD38. In the healthy heart, the main substrate for NAD^+ synthesis is nicotinamide (NAM), through the successive actions of the enzymes nicotinamide phosphoribosyl transferase (NAMPT) and NMN adenylyl transferases (NMNAT1-3) implicated in the salvage pathway. Nicotinamide riboside is another precursor for NAD^+ and holds great promise for restoring altered cardiac metabolism due to LVR-post MI. NR is the substrate of the enzyme nicotinamide

riboside-kinase 2 (NMRK2). In the context of HF, the expression of NMRK2 is severely upregulated whereas NAMPT is downregulated (Diguet et al., 2018; Tannous et al., 2021; Vignier et al., 2018). We hypothesized that stimulating the NMRK2 pathway by dietary NR supplementation would be beneficial in the context of LVR post-MI. Thus, our primary aim was to evaluate the effect of dietary supplementation with the NAD^+ precursor, NR (400-600 mg/kg), in a rat model of MI for 16 weeks.

Material and Methods

Upon paper submission, the material and method section presently described above in the manuscript thesis will be summarized here and developed in the supplementary information section.

Results

NR impact on anatomical parameters and survival

Juvenile male rats (250 g, 42-49 days old) were subjected to either simulated (Sham) or MI surgery and were randomly divided immediately after recovery of anesthesia, between control diet (CD) and NR supplemented diet (NR). We assessed anatomical and survival parameters in the four experimental groups. We observed on average a 15% decline in body weight gain in NR-fed groups, both Sham and MI, as compared to CD-fed groups at the time of sacrifice (4 to 5 months after MI (Fig.1A). When we measured the tibial length and whole-body length (nose to tail) in a subset of animals, we could observe that body length was slightly less in NR groups than in CD groups (Table 1); suggesting that the decline in body weight is related to a reduction in postnatal growth. Both MI CD and MI NR groups showed a significantly increased heart weight (HW), HW to body weight, and HW to tibia length ratio (Fig. 1B, Table 1), and heart size was visibly increased at the macroscopic level (Fig. 1G); lungs weight to bodyweight/tibia length ratio (Fig. 1C

and table 1), and lungs wet weight to dry weight ratio (Fig. 1D, table 1) as compared to the Sham groups, which indicates the onset of HF. The weight of the kidneys nor kidney weight to bodyweight/ tibia length did not show a significant difference (Table 1). Interestingly, NR-fed animals tended to have lower heart weight to body weight ratios (Fig. 1B, table 1). Importantly, NR did not alter the life span in the Sham NR group compared to Sham CD, as there were no death events before sacrifice (data not shown; Sham MI vs Sham NR p=1). Both MI groups showed a significantly lower percent survival, as compared to the Sham groups, which were pooled for this analysis (Fig 1E). Remarkably, there was a significant difference when comparing the MI CD and MI NR groups' overall survival percentages, with a median survival of 172 days versus 212 days, respectively (p=0.0467).

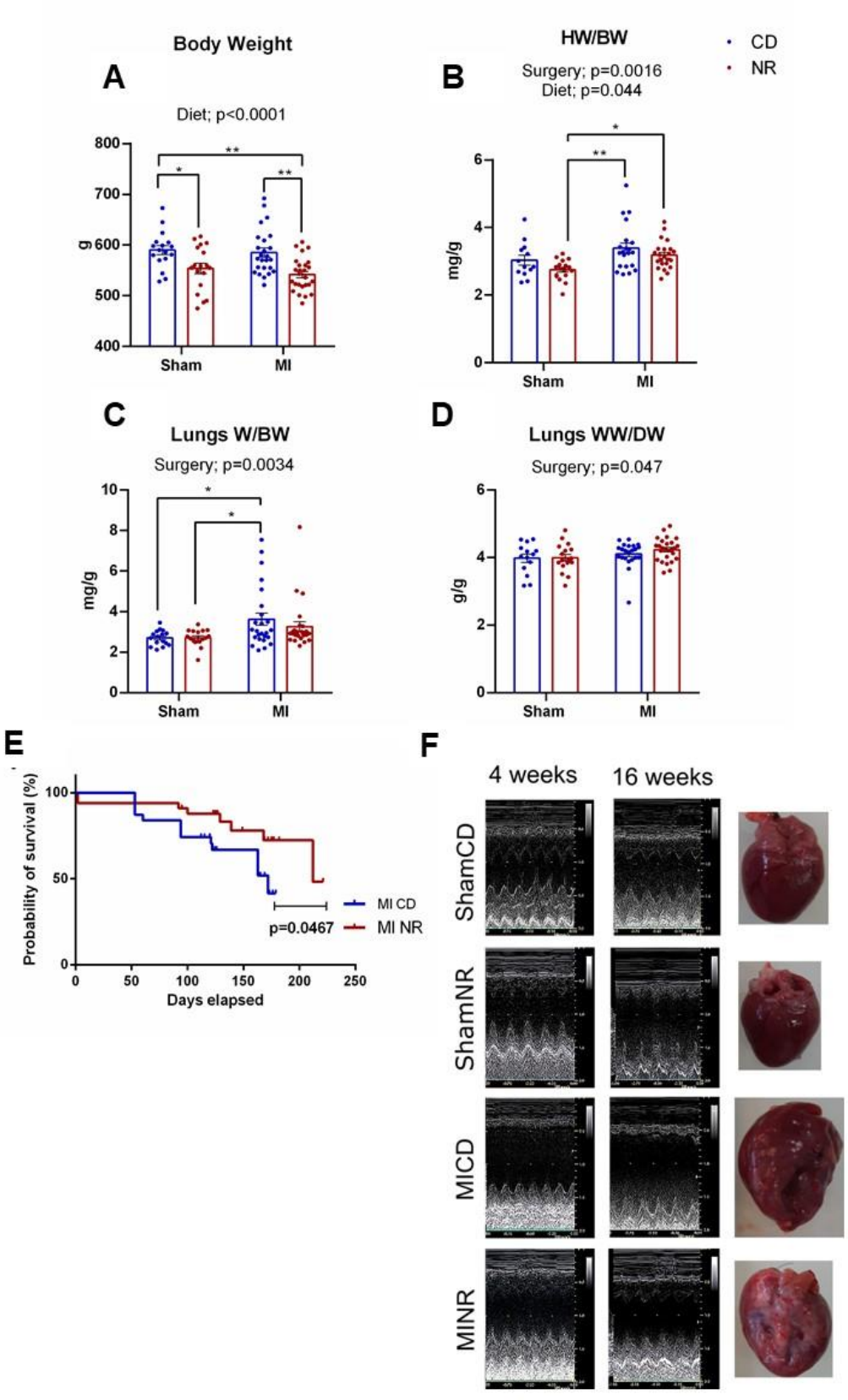

Figure 1. Anatomical parameters and survival after MI. Anatomical parameters were obtained at sacrifice. (**A**) Body weight; (**B**) heart weight normalized to body weight, (HW/BW); (**C)** lungs weight normalized to body weight, (lungs W/BW); (**D**) lungs wet weight normalized to lungs dry weight, (lungs WW/DW). Bars and error bars represent mean ± standard error of the mean (SEM). 2-Way ANOVA for independent samples was performed, followed by multiple comparisons with

Tukey's *posthoc* test: *, $p \leq 0.05$; **; $p \leq 0.01$. (**E**) Survival curve comparison between MI CD and MI NR groups. Sham, n=35; MI CD, n=31; MI NR n=33. Log-rank test was performed, $p \leq 0.05$. Marks on lines indicate censored events (**F**) Representative pictures of each group depicting gross examination of hearts after 16 weeks of NR-enriched diet or CD.

NR preserved cardiac function after MI

Because NR diet lowered body weight gain, all LV dimensions were normalized to body weight to evaluate whether LV chamber dimensions and wall thicknesses were altered independently of the variations in body weight.

During the first 4 weeks after surgery, rats that underwent MI whether under CD or NR diet developed a reduction in left ventricular anterior wall thickness at end-systole (LVAWs) (Fig. 2A, Table 2) and augmentation of left ventricular end-diastolic volume (LVEDV), end-systolic volume (LVESV) and stroke volume (SV) (Fig. 2D-E, Table 2). Mean LVEDV was larger MI CD than in MI NR group, with a difference of 0.4 ml (posthoc Tukey p-value <0.05 (Fig. 2D, Table 2). Left ventricular ejection fraction (EF) and fractional shortening (FS) showed a 20% reduction (Fig. 2G-H, Table 2). The ratio of wall thickness to the end-diastolic radius (h/r), which reflects myocardium adaptative remodeling in response to increased wall stress, was decreased in the MI groups, indicating a trend to eccentric remodeling. This reduction was seen in the MI CD group (Fig. 2I, Table 2, posthoc Tukey p-value < 0.001 vs Sham CD) but not in the MI NR group (interaction p value= 0.029, posthoc Tukey p-value > 0.05). In the MI groups, LV internal diameter at end-systole (LVIDs) and end-diastole (LVIDd) were significantly dilated, consistent with LVR past 4 weeks after MI (Table 2). In contrast, MI did not have a significant impact on LVPW. Additionally, tissue Doppler imaging revealed that both MI groups showed an increased A peak velocity, E/A ratio, and E wave deceleration slope (DS) and a reduced deceleration time (DT) (Fig. 4A-D, Table 3). The A wave could not be detected in every rat, as lower heart rates are required along with anatomical impediments that made it difficult to visualize the required region. Overall, NR supplementation had no relevant impact on any cardiac function parameter at this point of the study. After 16 weeks, the MI effect on LVAWs was still significant with and decreased thickness in the MI groups; nevertheless, NR had a beneficial effect on this parameter in the MI NR group, as the fast thinning of this LV region was less pronounced. Also, we

observed a slight increase in LVAWs thickness in the Sham NR group, which evidences a diet effect (Fig. 3A, table 2). As for LVID at end-diastole and end-systole, the MI effect prevailed in the MI groups which NR did not modify (Table 2). For LVPW thicknesses, there was a slight thickening effect of LVPW in NR-fed animals, which represents the remote myocardium unaffected by MI; there were no substantial variations among groups (Fig. 3B-C, table 2).

Notably, LVEDV and LVESV were almost completely rescued in the MI NR group compared to the MI CD groups, there was a significant difference between both MI groups in both parameters (Fig. 3D-E, table 2). NR markedly protected against the drastic reduction of LV EF and FS observed in the MI CD rats (Fig. 3G-H, Table 2). Tissue Doppler imaging revealed that the E peak velocity was markedly increased in the MI CD group, but not in the MI NR group (Fig. 4E, Table 3). For the A peak velocity, E/A ratio, DT and DS lost the MI effect was no longer observed at this point (Fig. 4F-G, table 4)’ The E/E' ratio was noticeably increased in MI CD compared to the other groups (Fig. 4H, table 3).

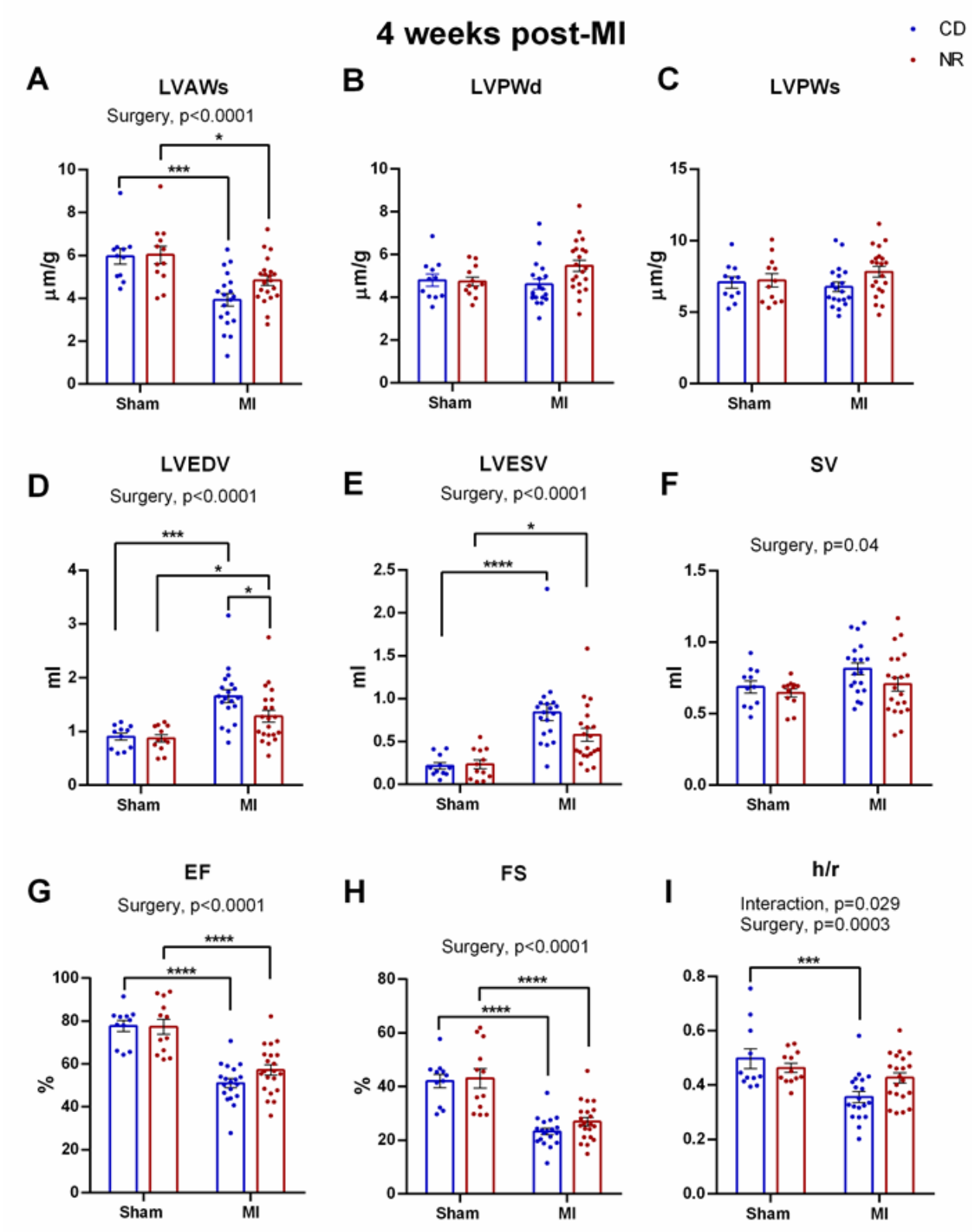

Figure 2. Echocardiographic parameters measured 4 weeks after MI. Abbreviations: (**A**) LVAWs, left ventricular anterior wall thickness at end-systole; (**B**) LVPWd, left ventricular posterior wall at end-diastole; (**C**) LVPWs, left ventricular posterior wall at end-systole; (**D**) LVEDV, left ventricular end-diastolic volume; € LVESV, left ventricular end-diastolic volume; (**F**) SV, stroke volume; (**G**) EF, ejection fraction; (**H**) FS, fractional shortening; (**I**) h/r thickness to radius. Bars and error bars repre-

sent mean ± standard error of the mean (SEM). 2-Way ANOVA for independent samples was performed, followed by multiple comparisons with Tukey's *posthoc* test: *, $p \leq 0.05$; **; $p \leq 0.01$; ***, $p \leq 0.001$; ****, $p \leq 0.0001$.

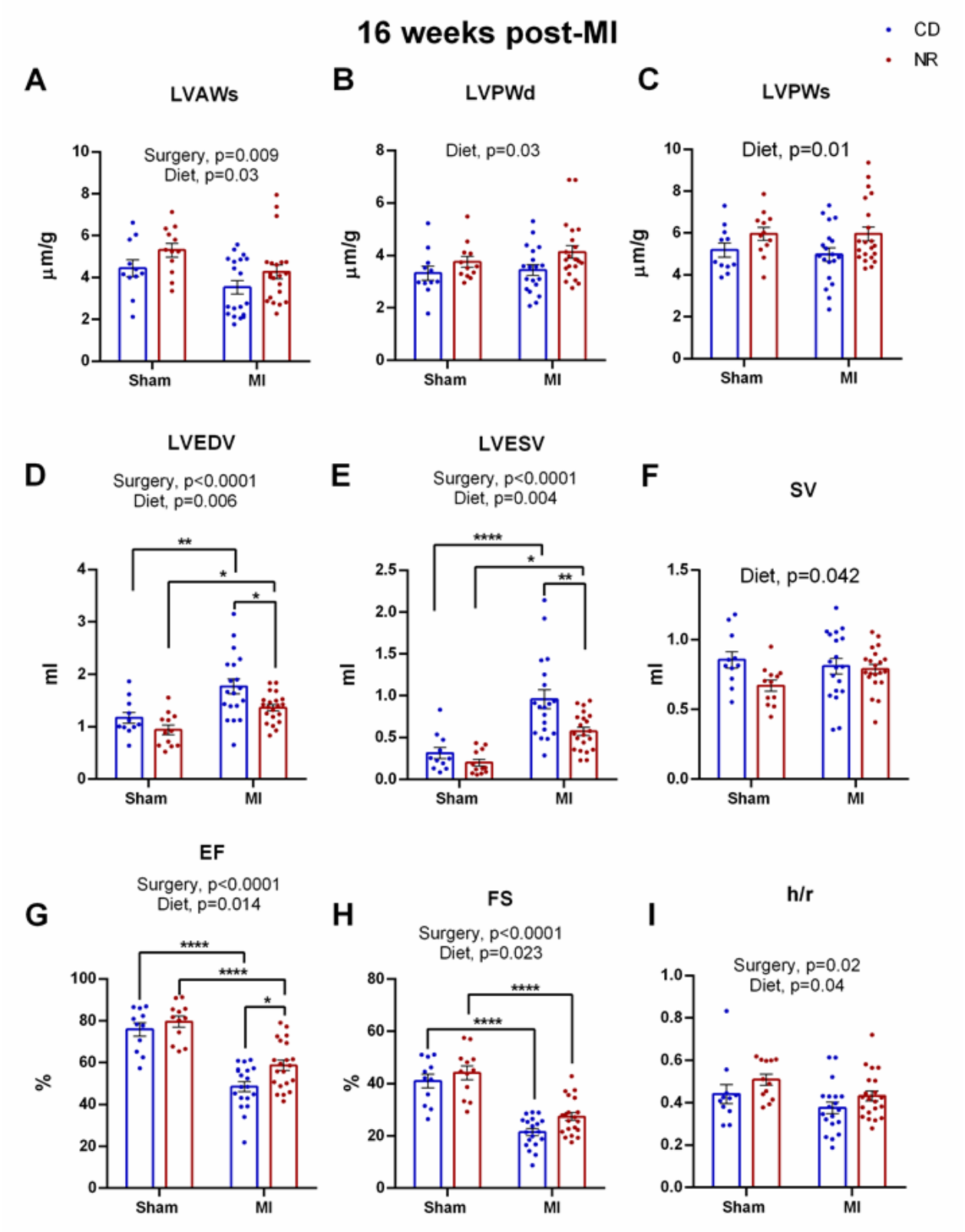

Figure 3. Echocardiographic parameters measured 16 weeks after MI. Abbreviations: (**A**) LVAWs, left ventricular anterior wall at end-systole; (**B**) LVPWd, left ventricular posterior wall at end-diastole; (**C**) LVPWs, left ventricular posterior wall at end-systole; (**D**) LVEDV, left ventricular end-diastolic volum€(**E**) LVESV, left ventricular end-diastolic volume; (**F**) SV, stroke volume; (**G**) EF, ejection fraction; (**H**) FS, fractional shortening; (**I**) h/r thickness to radius. Bars and error bars represent

the mean ± standard error of the mean (SEM). 2-Way ANOVA for independent samples was performed, followed by multiple comparisons with Tukey's *posthoc* test: *, $p \leq 0.05$; **; $p \leq 0.01$; ***, $p \leq 0.001$; ****, $p \leq 0.0001$.

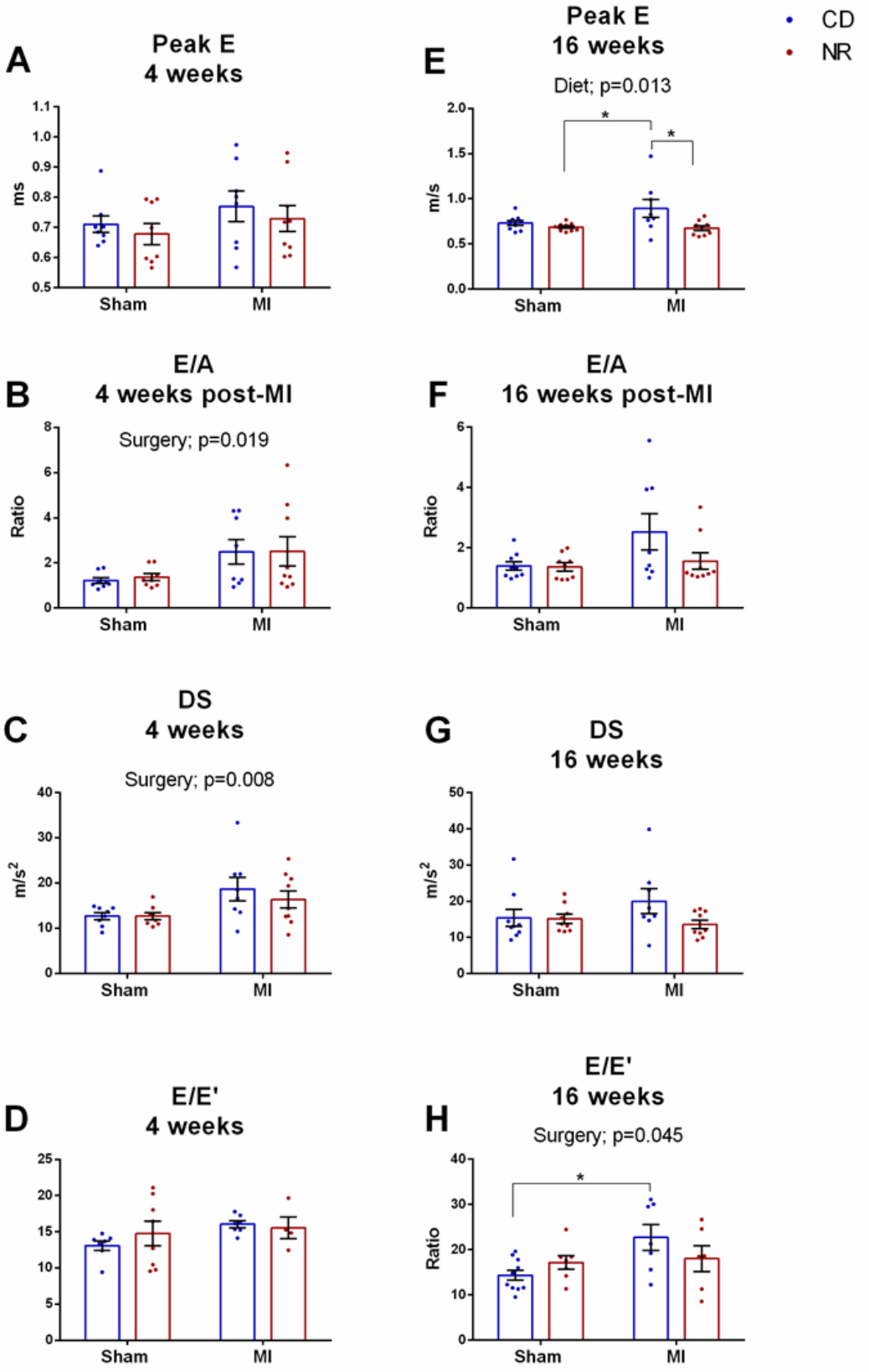

Figure 4. Doppler echocardiographic parameters. Abbreviations: early diastolic filling peak velocity, E peak at 4 weeks (A); ratio of early diastolic filling peak velocity to late diastolic peak velocity (A), E/A at 4 weeks (B); E deceleration slope, DS at 4 weeks (C); ratio of E peak velocity to early diastolic mitral annular peak velocity (E'), E/E' at 4 weeks (D); early diastolic filling peak velocity, E peak at 16 €ks (E); ratio of early diastolic filling peak velocity to late diastolic peak velocity (A), E/A

at 16 weeks (F); E deceleration slope, DS at 16 weeks (G); ratio of E peak velocity to early diastolic mitral annular peak velocity (E'), E/E' at 16 weeks (H). Bars and error bars represent mean ± standard error of the mean (SEM). 2-Way ANOVA for independent samples was performed, followed by multiple comparisons with Tukey's *posthoc* test: *, $p \leq 0.05$.

Cardiac injury and stress markers assessment

To further confirm that the rats included in the study presented AMI after surgery, cTnI serum levels were measured 24 hours after LAD ligation or Sham surgery. During this time point, this circulating biomarker reaches its peak value. As expected, serum cTnI increased drastically in animals that underwent a permanent LAD ligation as compared to Sham rats (Fig. 5A). Linear correlation was calculated for cTnI levels at 24 hours post-surgery versus LVEF % measured at 4 weeks post-MI (Fig. 5B). The variables were negatively correlated (R^2=0.6018). Based on this result, we estimated a cTnI cutoff value of 20.86 µg/L (depicted with dotted line) and decided to exclude MI rats that showed cTnI levels below this value (values outlined in black boxes). We examined the expression levels of mRNA of different genes linked to cardiac stress on LV samples; *Bnp* (Fig. 5C), *Ckm* (Fig. 5D), *Col1a1* (Fig. 5E), and *Serca2a* (Fig. 5F). *Bnp* was increased in the MI CD and MI NR groups. (Fig. 5C). We observed only a down-regulation trend of the *Ckm* mRNA level in the MI groups (Fig. 5D). The mRNA levels of *Col1a1* showed a noticeable upregulation on MI CD and MI NR groups, regardless of the diet (Fig. 5E). The *Serca2a* gene expression was, overall, downregulated by MI. On the other hand, NR increased the expression of *Serca2a,* as evidenced by a diet effect in the ANOVA (p=0.0001), particularly on the Sham NR rats and the MI NR rats (Fig. 5F).

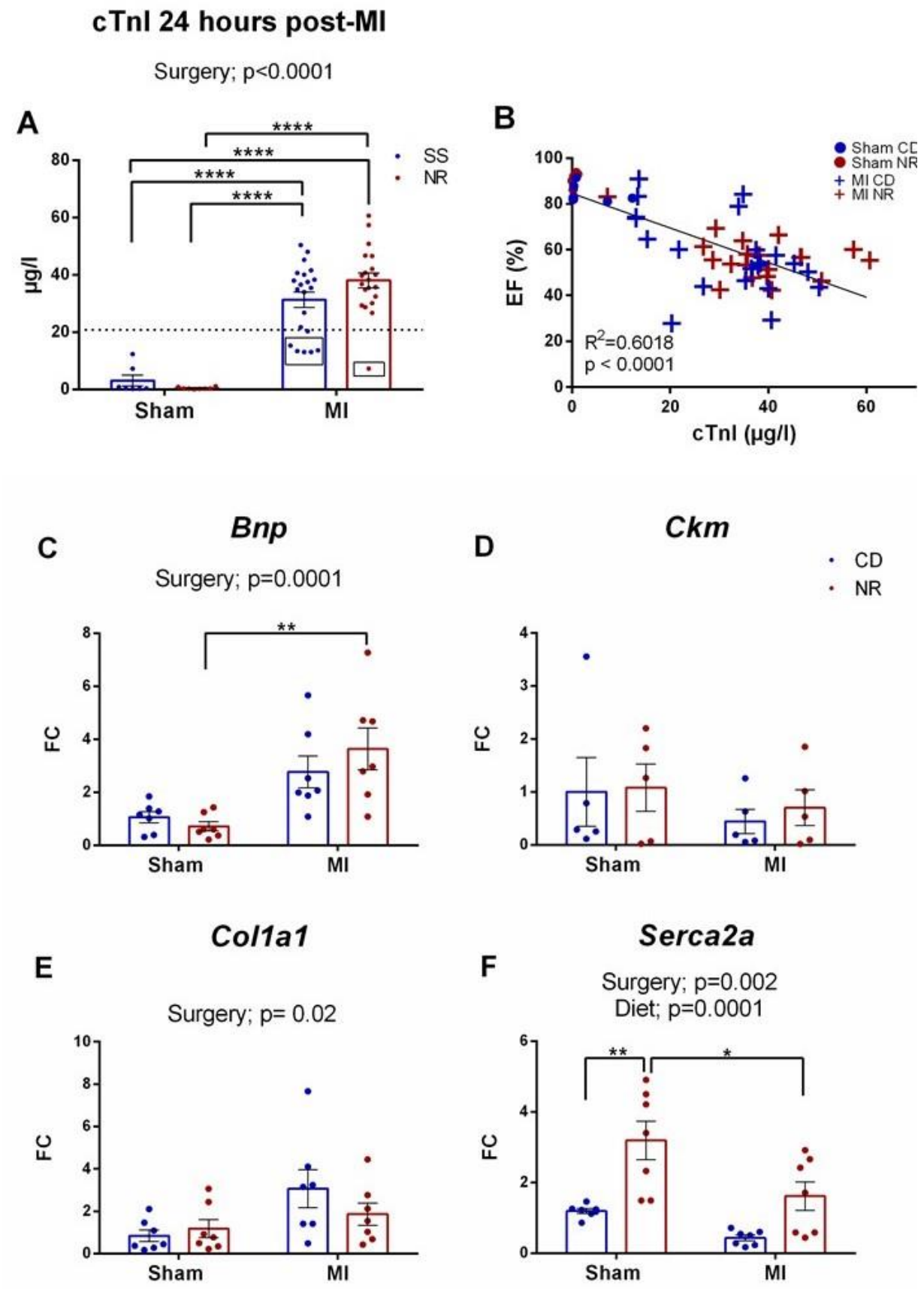

Figure 5. Assessment of cardiac injury and stress markers after MI. (**A**) Level of cardiac troponin I (cTnI) levels 24 hours after surgery (MI or Sham). SS: Saline solution. Bars and error bars represent mean ± standard error of the mean (SEM). 2-Way ANOVA for independent samples was performed,

followed by multiple comparisons with Tukey's *posthoc* test: ****, $p \leq 0.0001$. (**B**) Correlation between cTnI levels (µg/L) 24 hours after surgery and EF % 4 weeks after surgery. Pearson's correlation test was performed, a value of $p < 0.05$ was considered statistically significant. Gene expression of cardiac stress markers in the LV: *Bnp* (**C**), *Ckm* (**D**), *Col1a1* (**E**), and *Serca2a* (**F**). mRNA levels of target genes were normalized over *Hprt* and are expressed as fold change (FC) over the mean of the Sham CD group. Bars and error bars represent mean ± standard error of the mean (SEM). 2-Way ANOVA for independent samples was performed, followed by multiple comparisons with Tukey's *posthoc* test: *, $p \leq 0.05$; **, $p \leq 0.01$.

Mitochondrial function and energy signaling

To evaluate whether NR elicited an effect upon the mitochondrial respiratory chain function on LV, we carried out quantification of substrate-dependent O_2 consumption by the mitochondrial respiratory chain complexes using cardiac saponin-permeabilized LV fibers (Fig. 6A-D). For the first protocol (Fig. 6A), mitochondrial O_2 consumption in the presence of glutamate and malate only (leak respiration) was slightly yet significantly increased in the MI groups compared to the Sham groups, evidencing an MI effect. The stimulation of ATP-synthase at a submaximal concentration of ADP induced an increase of respiration in all groups, without significant differences among groups. The addition of creatine demonstrated that the functional coupling of mitochondrial creatine-kinase was significantly decreased in the MI groups. Furthermore, MI significantly decreased complex I, II, and IV-linked respiration. NR supplementation did not show a difference in complexes I, II, IV, or V-mediated oxidative phosphorylation nor in the maximal respiratory capacity (Fig. 6A-B). Substantial differences related to FAO among groups were not detected (Fig. 6C-D). As depicted in fig. 6E-F, we did not detect any substantial differences in the expression of *Pgc1α* nor *Sirt1* mRNA levels on LV. Protein levels of total acetyl-CoA carboxylase (ACC) and phosphorylated-ACC (p-ACC) were quantified from LV homogenates (Fig. 6G). MI rats had lower levels of pACC and pACC to total ACC ratio, even though there was no effect after NR administration either on Sham or MI animals. We did not find changes on total ACC relative levels of protein (Fig. 6H-J).

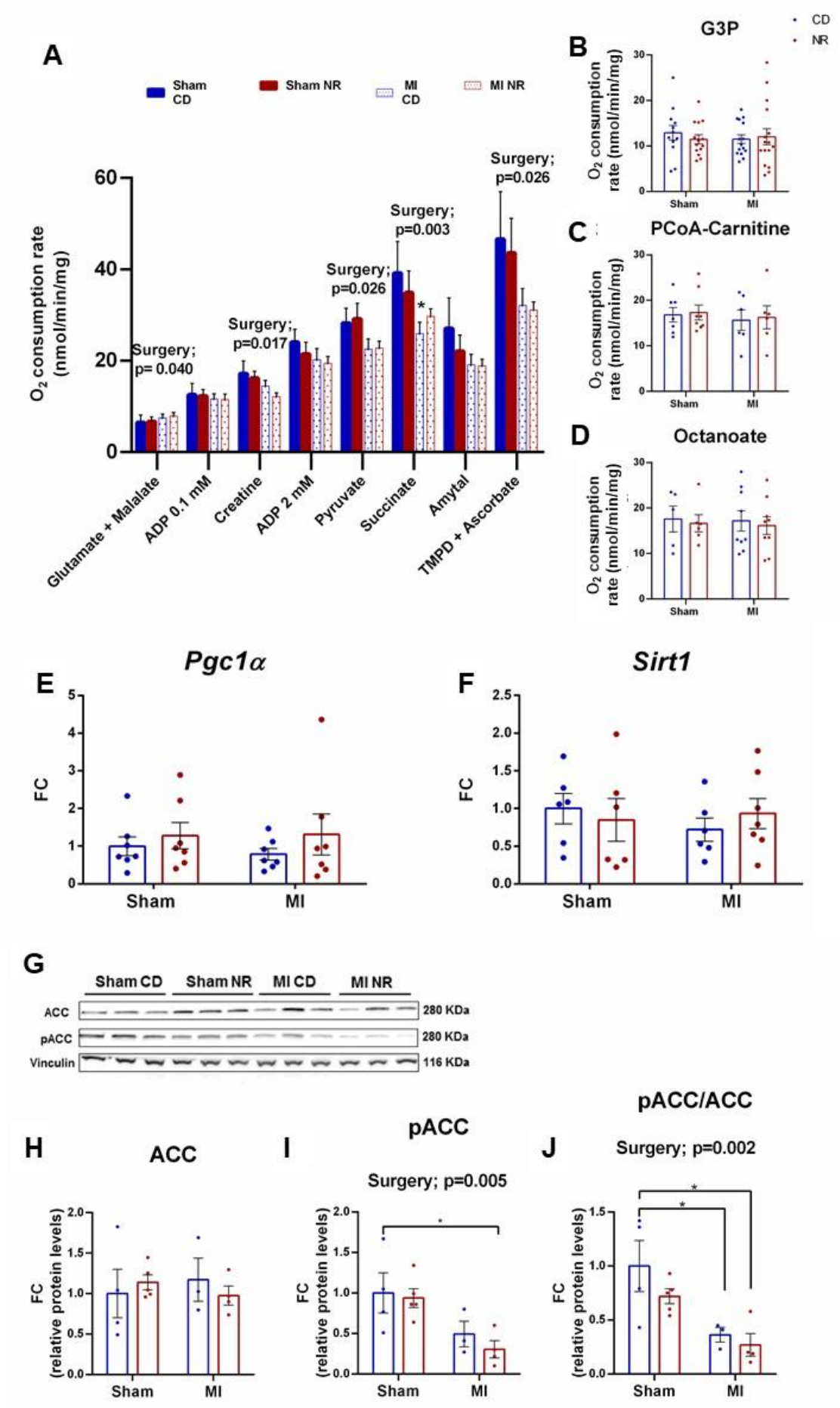
A
Sham CD
Sham NR
MI CD
MI NR
O2 consumption rate (nmol/min/mg)
Surgery; p= 0.040
Surgery; p=0.017
Surgery; p=0.026
Surgery; p=0.003
Surgery; p=0.026
Glutamate + Malalate
ADP 0.1 mM
Creatine
ADP 2 mM
Pyruvate
Succinate
Amytal
TMPD + Ascorbate
B
G3P
CD
NR
C
PCoA-Carnitine
D
Octanoate
Sham
MI
E
Pgc1α
FC
F
Sirt1
G
Sham CD
Sham NR
MI CD
MI NR
ACC
pACC
Vinculin
280 KDa
280 KDa
116 KDa
H
ACC
I
pACC
Surgery; p=0.005
J
pACC/ACC
Surgery; p=0.002
FC (relative protein levels)

Figure 6. Mitochondrial function and energy signaling. (**A-D**) Mitochondrial respiration of saponin-permeabilized remote myocardium fibers. (**A**) Measurement of substrate dependent O_2 consumption by the mitochondrial respiratory chain complexes upon subsequent addition of indicated TCA intermediates, activators, and inhibitors. Sham CD, n=9; Sham NR, n=12; MI CD, n=14; MI NR, n=14. (**B**) Mitochondrial O_2 consumption upon addition of G3P, glyceraldehyde-3-phosphate, (**C**) palmitoyl-CoA-carnitine, (**D**) octanoate. Bars and error bars represent mean ± standard error of the mean (SEM). 2-Way ANOVA for independent samples was performed, followed by multiple comparisons with Tukey's *posthoc* test. (**E-F**) Gene expression in LV samples of genes involved in energy metabolism: *Pgc1α* (**E**) and *Sirt1* (**F**). Levels were normalized over *Hprt*. (**G**) Representative immunoblots showing the protein expression of ACC and phosphorylated ACC (pACC). Vinculin was used as loading control. (**H-J**) Quantification of relative protein level for ACC (**H**) pACC (**I**) and pACC to ACC ratio (**J**). Levels are normalized over vinculin. Data are expressed as fold change (FC) over the mean of Sham CD group. Bars and error bars represent mean ± standard error of the mean (SEM). 2-Way ANOVA for independent samples was performed, followed by multiple comparisons with Tukey's *posthoc* test: *, $p \leq 0.05$; **, $p \leq 0.01$.

NAD$^+$ salvage pathway enzymes

NR supplementation elicited a significant up-regulating effect on *Nampt* and *Nmrk2* gene expression, particularly on MI NR rats (Fig. 7A and C). *Nampt* was drastically down-regulated on MI CD rats, by 50% (Fig. 7A), whereas *Nmrk2* levels were clearly up-regulated by MI irrespective of the diet. Neither MI nor NR supplementation altered *Nmrk1* gene expression (Fig. 7B). Consistent with mRNA levels, NAMPT protein levels dropped 50% in the MI CD group (*vs* Sham CD; Fig. 7D). Remarkably, this effect was milder in the MI NR group (Fig. 7D). Interestingly, NMRK2 protein levels were not consistent with those of mRNA, as NMRK2 dropped to 50% in MI CD rats (interaction effect), and an increase was observed in MI NR rats (not significant).

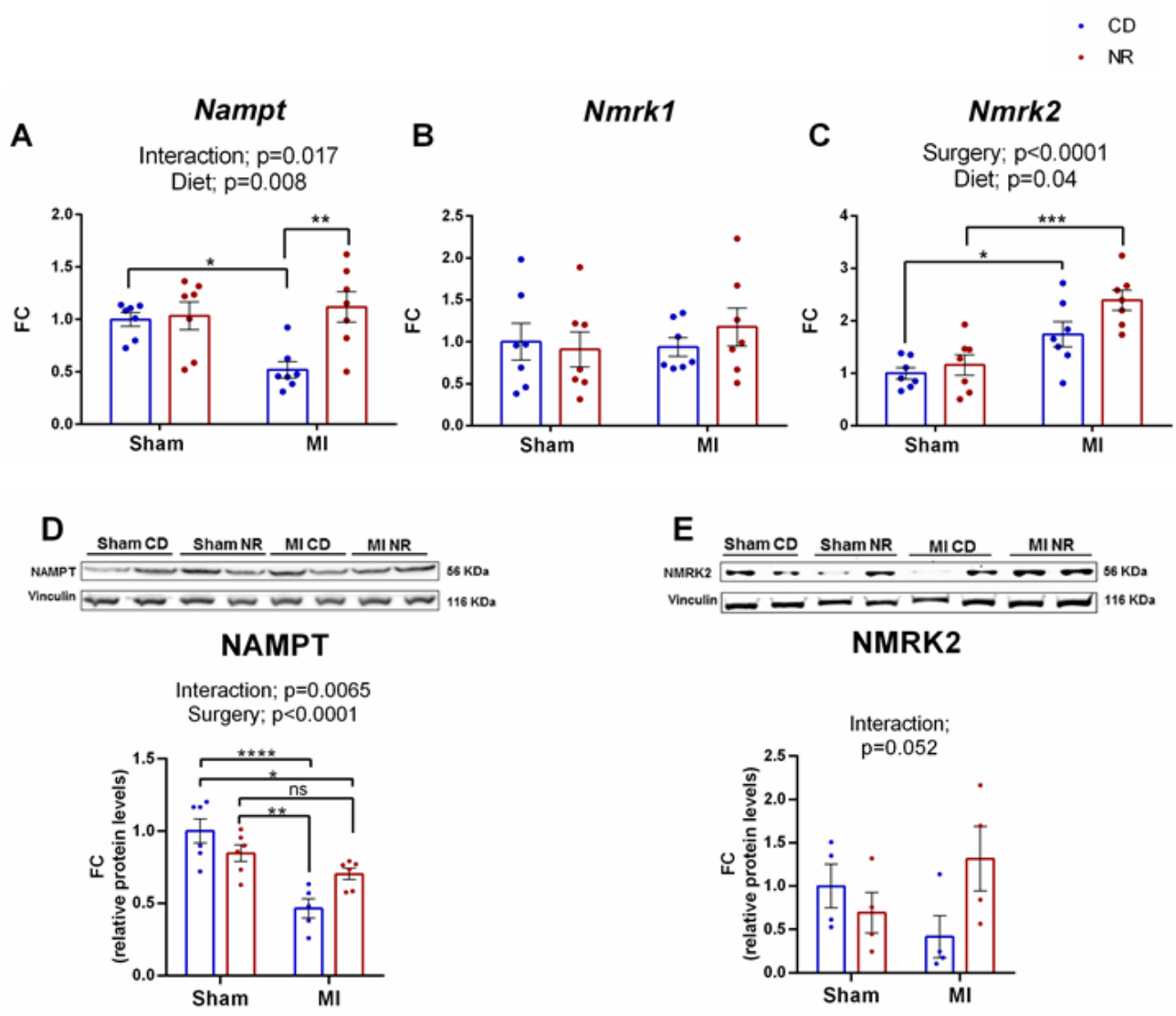

Figure 7. Effect of NR on NAD⁺ salvage pathway involved enzymes. Protein expression levels of the NAD⁺ salvage biosynthesis enzymes. Representative cropped blots and relative LV protein levels obtained by western blot of the enzymes NAMPT (**A**) and NMRK2 (**B**), respectively. Levels are normalized on vinculin as a loading control and are expressed in arbitrary units as fold change (FC) over the mean Sham CD group. Bars and error bars represent mean ± standard error of the mean (SEM). 2-Way ANOVA for independent samples was performed, followed by multiple comparisons with Tukey's *posthoc* test: *, $p \leq 0.05$, **; $p \leq 0.01$; ***, $p \leq 0.001$; ****, $p \leq 0.0001$; ns, not significant. mRNA gene expression of NAD⁺ salvage pathway enzymes: *Nampt* (**C**), *Nmrk1* (**D**) and *Nmrk2* (**E**)**.** Levels were normalized over *Hprt* and are expressed as fold change (FC) over the mean of the Sham CD group. Bars and error bars represent mean ± standard error of the mean (SEM). 2-Way ANOVA for independent samples was performed, followed by multiple comparisons with Tukey's *posthoc* test: *, $p \leq 0.05$; **; $p \leq 0.01$; ***.

NR impact in LV metabolome and specific metabolic pathways

We used untargeted metabolomics to interrogate metabolic pathways and identify potential novel biomarkers. Overall, 6007 unique peaks (metabolites) were detected in plasma (2207 by HILIC chromatography and 3800 peaks by C18 chromatography), and 5256 unique peaks in LV tissue (HILIC:1840; C18: 3416). Metabolites with less than 40% of values and near-constant metabolites, with low interquartile range (IQR), which are non-informative variables, were removed.

We used UMAP (Uniform Manifold Approximation and Projection) method for dimension reduction and visualization of the impact of surgery and diet on the whole metabolome. We observed a differential clustering of the NR- and CD-fed groups for the LV tissue metabolome (Figure 8A and B), this effect was even more obvious in the UMAP from C18 (Figure 8A). Showing that LV metabolic landscape distinctly discriminates according to the diet. For LV samples, within each diet group, we can also see a stratification according to Sham and MI groups.

In contrast, the separation of diet and surgery impact was not apparent in the plasma metabolome, as seen on the UMAPS for plasma (Figure 9A and B).

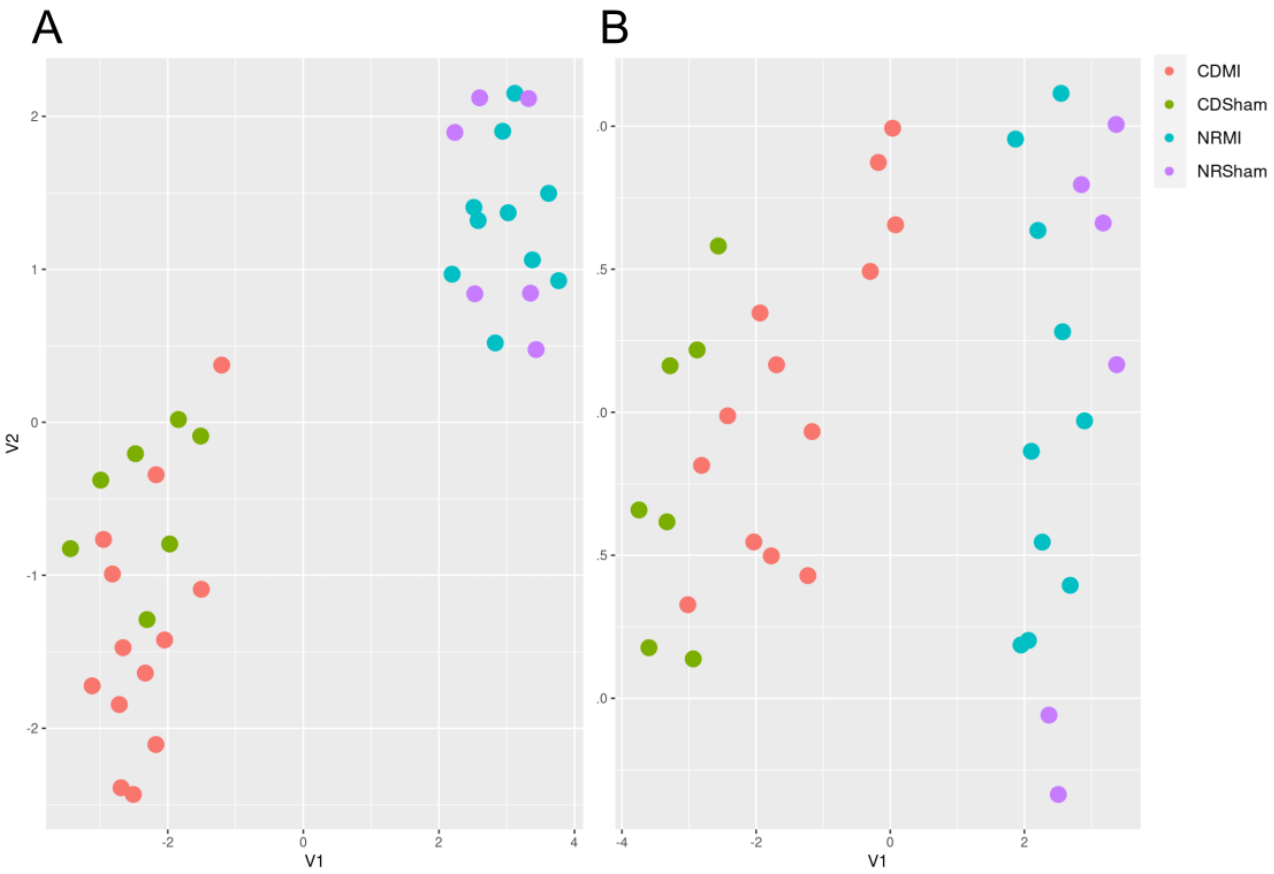

Figure 8. Uniform Manifold Approximation and Projection (UMAP) 2D visualization for LV samples fromC18 (**A**) and HILIC neg (**B**) chromatography. V1 represents dimension 1 and V2 represents dimension 2. Sham CD, n=7; Sham NR, n=6; MI CD, n=13; MI NR, n=10.

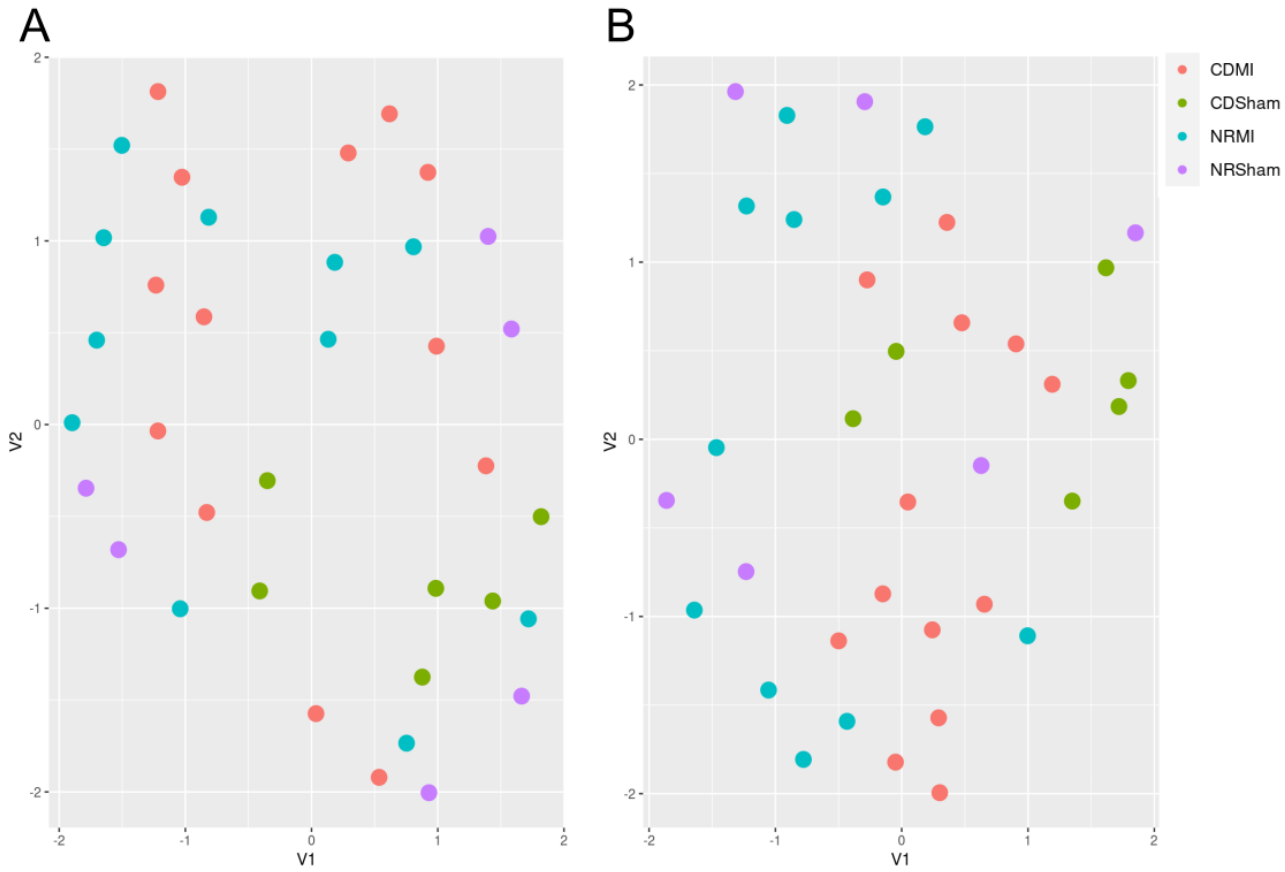

Figure 9. Uniform Manifold Approximation and Projection (UMAP) 2D visualization for plasma samples from C18 (**A**) and HILIC neg (**B**) chromatography. V1 represents dimension 1 and V2 represents dimension 2. Sham CD, n=7; Sham NR, n=6; MI CD, n=13; MI NR, n=10.

We performed pairwise differential quantification analysis of LV metabolome, comparing diet effects in Sham and MI groups separately (Figures 10 and 11). We observed an extreme myocardial metabolic signature of the NR diet in the MI group (Figure 11), with the levels of 70.90% (2142/3021) of measured metabolites differentially modulated between NR and CD diets (cut-off values adjusted p-value: FDR ⩽5%; -1.5 > FC > 1.5). In comparison, 41.22% (1240/3008) of myocardial metabolites were differentially modulated when comparing Sham CD and Sham NR groups (Figure 10), highlighting an attenuated diet signature in Sham-operated animals compared to MI, suggesting biological interactions between the NR diet and the disease state in the cardiac tissue metabolome.

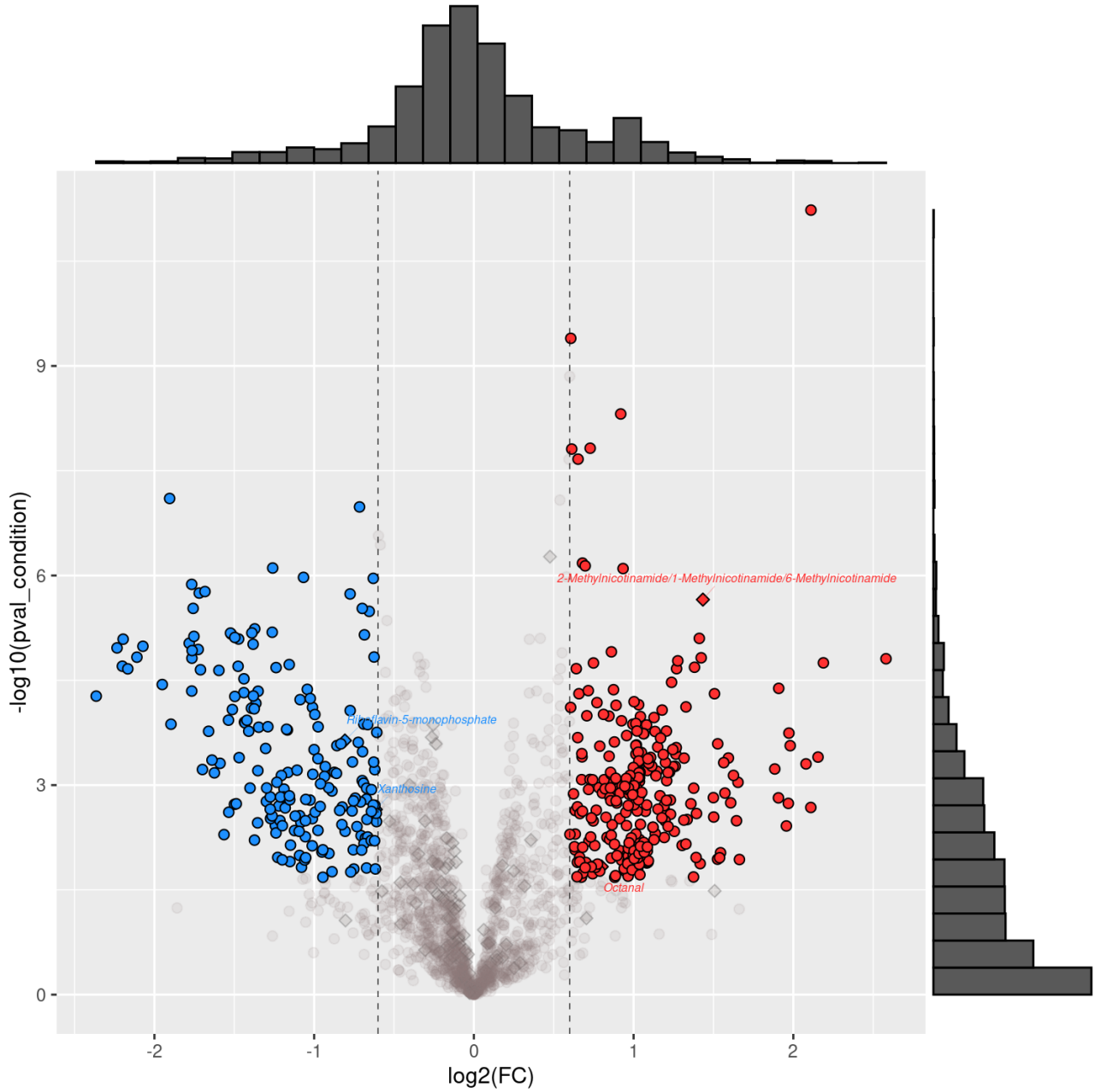

Figure 10. Diet effect in the Sham-operated groups on LV metabolites. Volcano plot for pairwise comparisons between Sham CD vs Sham NR groups, depicting diet effect in Sham groups in metabolites obtained from C18 liquid chromatography. Cut-off values (red and blue color codes): False discovery rate (FDR) adjusted p-value ⩽5%; -0.6 >log2 FC > 0.6. The log2 of the fold changes (FC) and -log10 of the raw p-values were calculated to display the differential metabolites. Down-regulated metabolites are shown in blue and up-regulated metabolites are shown in red..

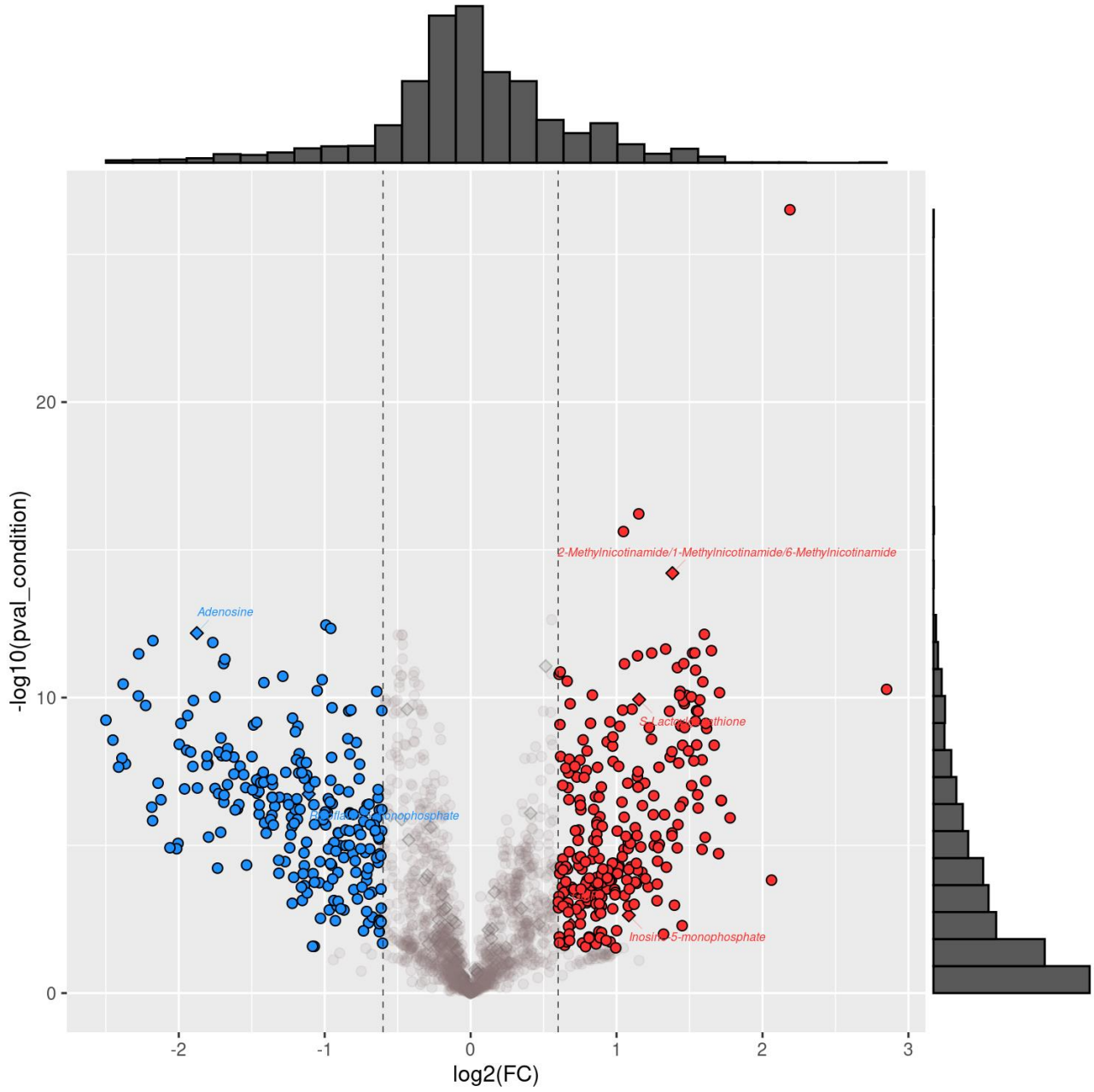

Figure 11. Diet effect in MI groups on LV metabolites. Volcano plot for pairwise comparisons between MI CD vs MI NR groups, depicting diet effect in MI groups in metabolites obtained from C18 liquid chromatography. Cut-off values (red and blue color codes): False discovery rate (FDR) adjusted p-value ⩽5%; -0.6 >log2 FC > 0.6. The log2 of the fold changes (FC) and -log10 of the raw p-values were calculated to display the differential metabolites. Down-regulated metabolites are shown in blue and up-regulated metabolites are shown in red.

We focused our analyses on the differential expression of annotated metabolites on the LV tissue. Metabolites with validated annotations amounted to 154 metabolites for HILIC and 105 metabolites in C18. There was close to 20% overlap between these two lists, i.e., identical metabolites detected by two chromatographic methods, C18 and HILIC neg. For those, we selected the peak values of the chromatography method providing the lowest p-value in the analysis of variance (ANOVA). We performed a 2-way ANOVA to detect the annotated metabolites that were significantly affected either by MI or NR supplementation (Figure 12 and 13). Out of these analyses, 29 metabolites were modulated by MI (Figure 12), whereas 105 metabolites were modified by NR consumption (Figure 13). Additionally, through KEGG QEA analysis (Figures 14 and 15), we performed pairwise comparisons using exclusively annotated and 2-way ANOVA significant metabolites (FDR set at 0.05). When comparing Sham CD vs Sham NR groups (Figure 14), we observed that the top 5 enriched pathways were arginine and proline metabolism, pentose phosphate pathway (PPP), nicotinate, and nicotinamide (NAM) metabolism, glutathione metabolism, and pentose and glucuronate interconversions. When comparing MI CD vs MI NR groups (Figure 15), the top 5 overly enriched pathways were arginine and proline metabolism, glutathione metabolism, purine metabolism (not enriched in the sham groups), alanine, aspartate and glutamate metabolism, nicotinate, and NAM metabolism.

We studied the levels of metabolites implicated in major metabolic pathways such as glycolysis, the TCA cycle, and the pentose phosphate pathway (PPP) (Figure 16). Regarding the glycolytic pathway, we observed that MI increased glucose 6-phosphate (G6-P) (Figure 16B). In the Sham group, NR showed lowered levels of dihydroxyacetone phosphate (DHAP), but this did not occur in the MI group suggesting that glycolysis is preserved in the context of MI (Figure 16B). Concerning the TCA cycle, NR-fed groups showed lower levels of citrate and fumarate (Figure 16C). Interestingly, NR had a striking effect on PPP metabolites (Fig 16D), as NR-fed groups

showed lower levels of ribulose 5-phosphate, D-ribose, sedoheptulose 7-phosphate, and d-erythrose compared to CD-fed groups. As for glutathione levels, we NR slightly increased levels of reduced glutathione (GSH) (Figure 17A) and, also significantly decreased oxidized glutathione (GSSG) (Figure 17B). Additionally, we determined the GSH to GSSG ratio, which is a measure of cellular oxidative stress, our results revealed an increased GSH:GSSG ratio in NR-fed groups (Figure 17C). Concerning NAD^+ related metabolites (Figure 18), NR-fed groups showed significantly lower cardiac levels of nicotinamide mononucleotide (NMN), the precursor for NAMPT (Figure 18A), and nicotinamide N-oxide, which is the product of nicotinamide (NAM) oxidation (Figure18B). However, NR did increase levels of methyl nicotinamide, a previously validated biomarker of NR treatment (Figure 18C) and cADPR, which is a product of NAD^+ breakdown by the NADase CD38 (Figure 18D). NR was not detectable in cardiac samples.

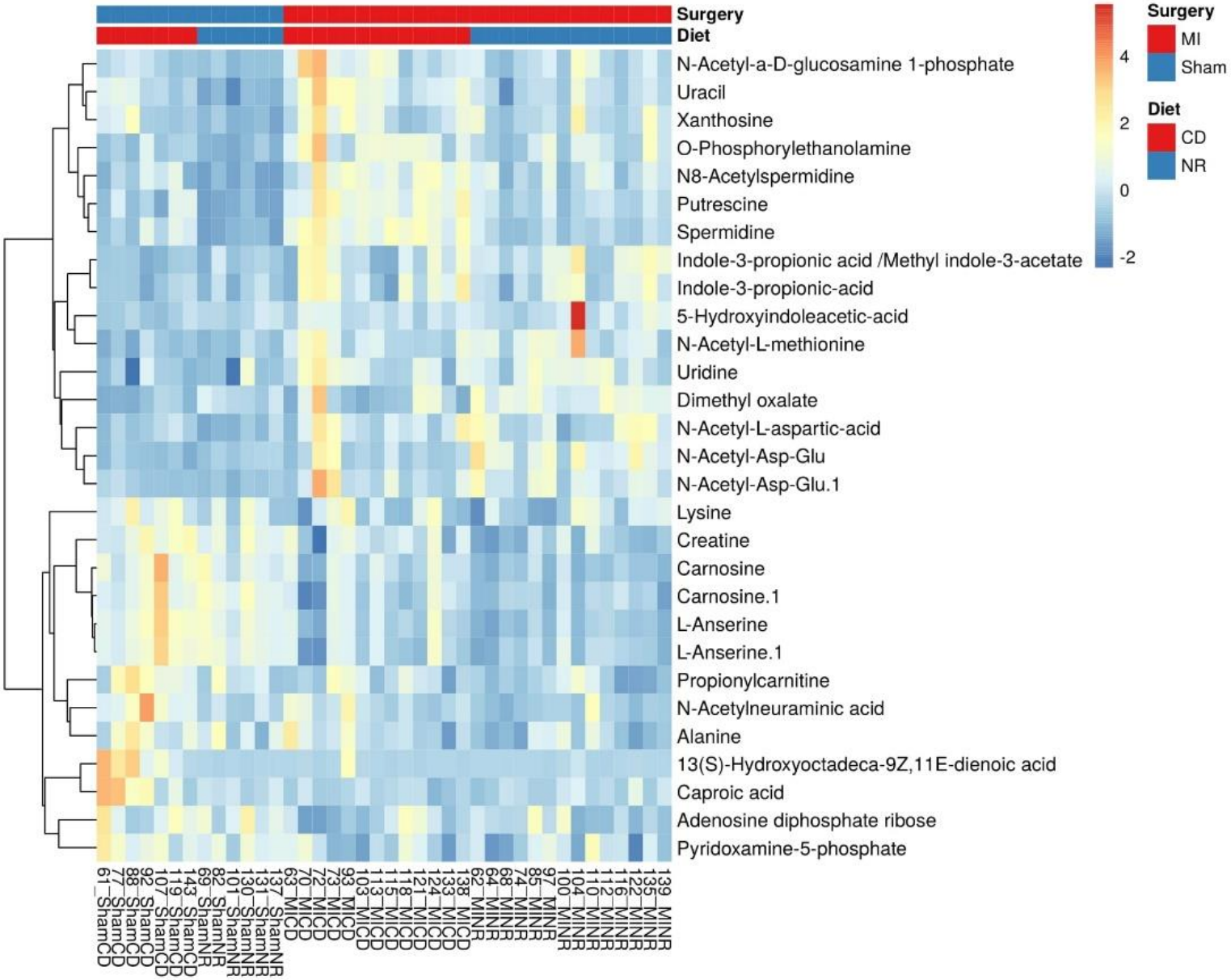

Figure 12. Hierarchical heat map showing 29 annotated metabolites modulated by MI. Unit variance scaling was applied to rows. Rows are clustered using correlation distance and average linkage. Sham CD, n= 7; Sham NR, n=6; MI CD, n=13; MI NR, n=14. For rows, clustering distance by correlation. No clustering distance was applied for columns. The most abundant metabolites are shown in red, least abundant metabolites are shown in blue. 2-way ANOVA was assessed to determine the surgery effect. FDR (p-adjusted) value was set at 0.05.

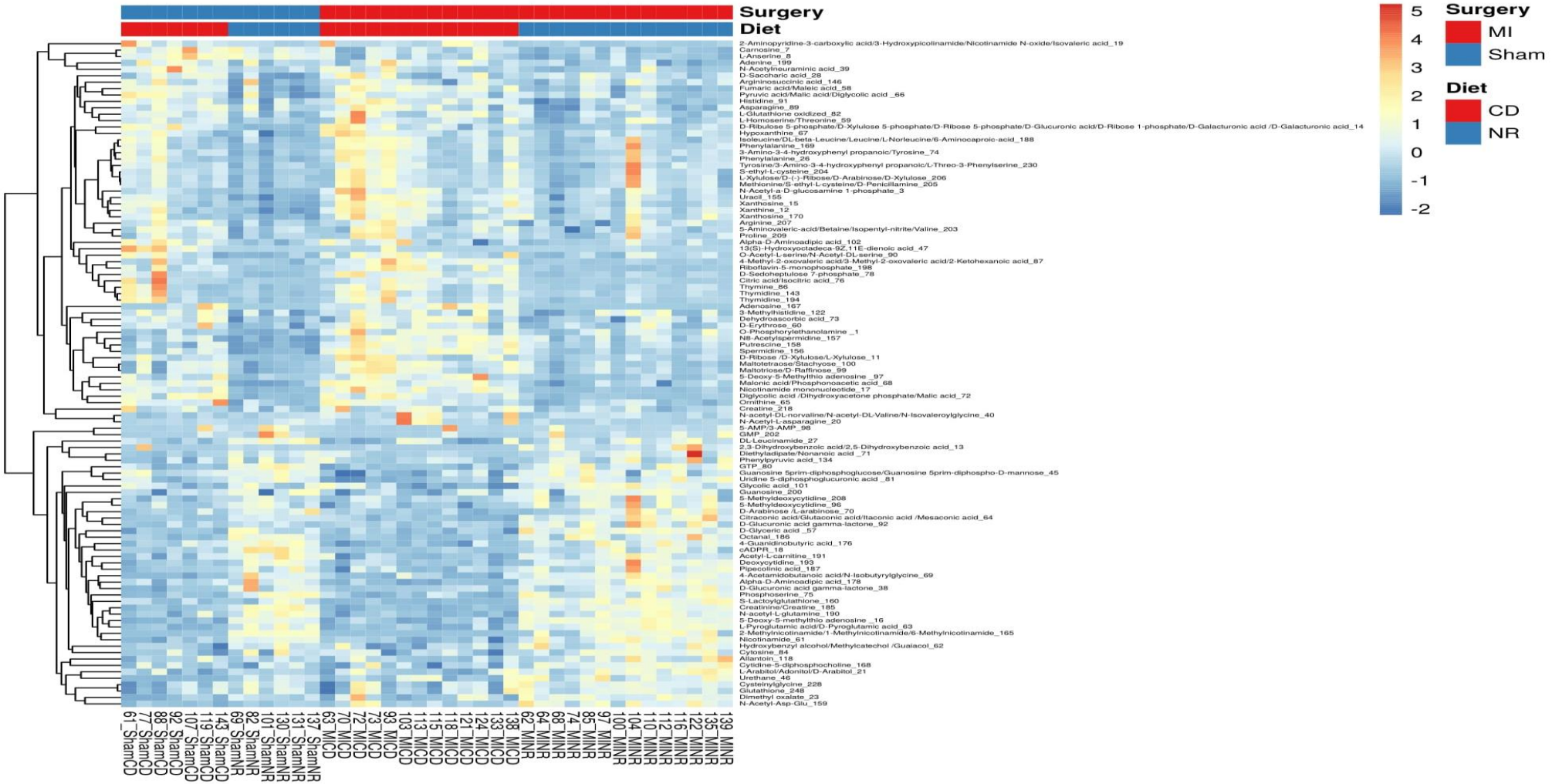

Figure 13. Hierarchical heat map showing 105 annotated metabolites modulated by NR. Unit variance scaling was applied to rows. Rows are clustered using correlation distance and average linkage. Sham CD, n= 7; Sham NR, n=6; MI CD, n=13; MI NR, n=14. For rows, clustering distance by correlation. No clustering distance was applied for columns. The most abundant metabolites are shown in red, least abundant metabolites are shown in blue. 2-way ANOVA was assessed to determine the surgery effect. FDR (p-adjusted) value was set at 0.05.

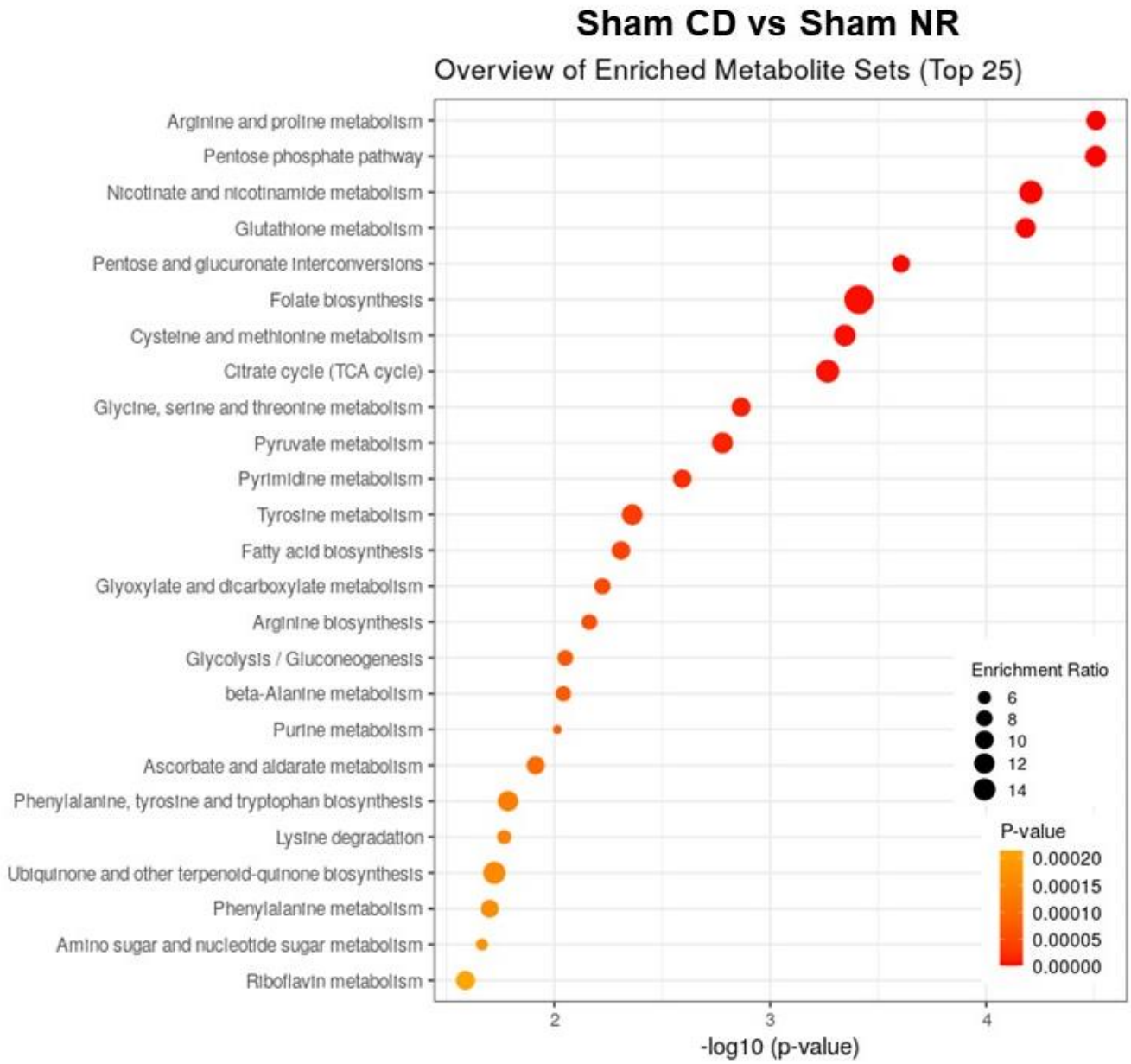

Figure 14. KEGG QEA analysis showing top 25 differentially modulated metabolic pathways by diet in Sham groups. Pairwise comparison between Sham CD vs Sham NR groups. Enrichment ratio is computed by hits/expected. Size of the node is determined by enrichment ratio, whereas the color is determined by p-values, lower p-values shown in red, higher p-values shown in yellow.

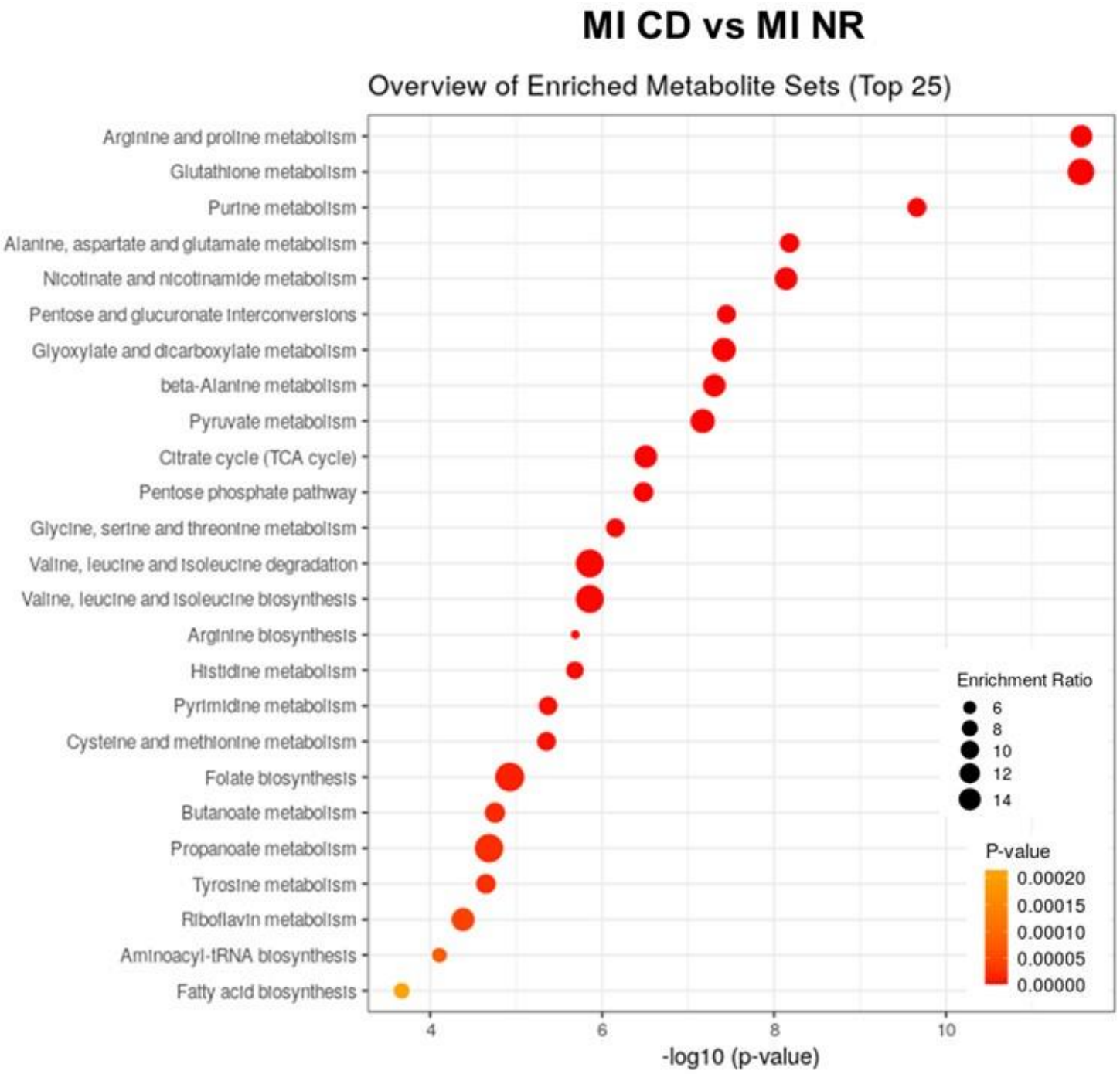

Figure 15. KEGG QEA analysis showing top 25 differentially modulated metabolic pathways diet in MI groups. Pairwise comparison between MI CD vs MI NR groups. Enrichment ratio is computed by hits/expected. Size of the node is determined by enrichment ratio, whereas the color is determined by p-values, lower p-values shown in red, higher p-values shown in yellow.

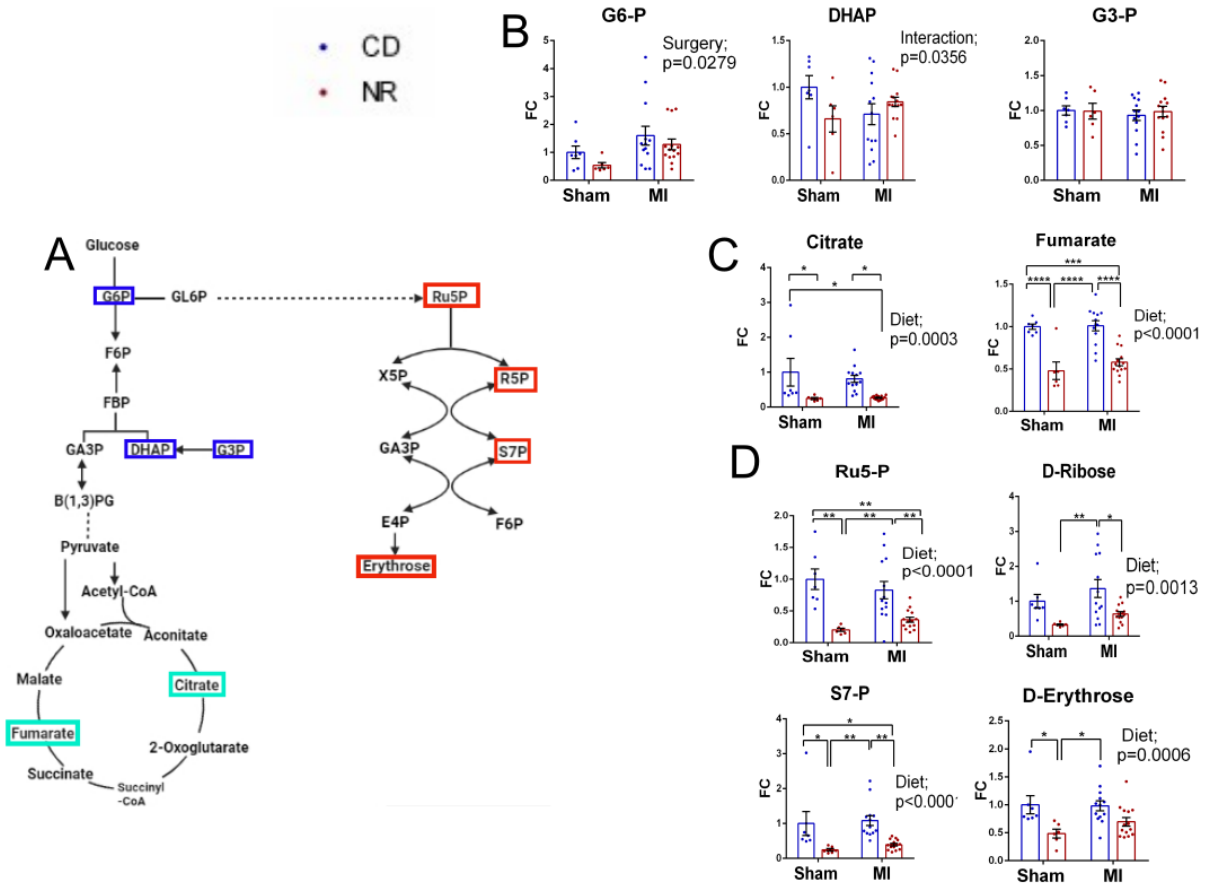

Figure 16. Specific metabolites implicated in major metabolic pathways (**A**) Schematic metabolic pathway depicting glycolysis (gly), TCA cycle, and PPP. Identified metabolites for each pathway are highlighted in blue (gly), green (TCA) and red (PPP). Levels of quantified metabolites that lay within glycolysis (**B**), the TCA cycle (**C**), and the PPP (**D**). Metabolites were quantified through LC/MS, values are shown as fold change (FC) over the mean of the Sham CD group. Bars and error bars represent mean ± standard error of the mean (SEM). CD-fed groups are shown in blue, NR-fed groups are shown in red. 2-Way ANOVA for independent samples was performed, followed by multiple comparisons with Tukey's *posthoc* test: *, $p \leq 0.05$; **; $p \leq 0.01$; ***, $p \leq 0.001$; ****, $p \leq 0.0001$. Abbreviations: DHAP, dihydroxyacetone phosphate; E4P, erythrose 4-phosphate; FBP, fructose 1,6-bisphosphate; F6P, fructose 6-phosphate; GA3P, glyceraldehyde 3-phosphate; G3P, glycerol 3-phosphate; G6P, glucose 6-phosphate; Ru5P, ribulose 5-phosphate; R5P, ribose 5-phosphate; S7P, sedoheptulose 7-phosphate; X5P, xylulose 5-phosphate.

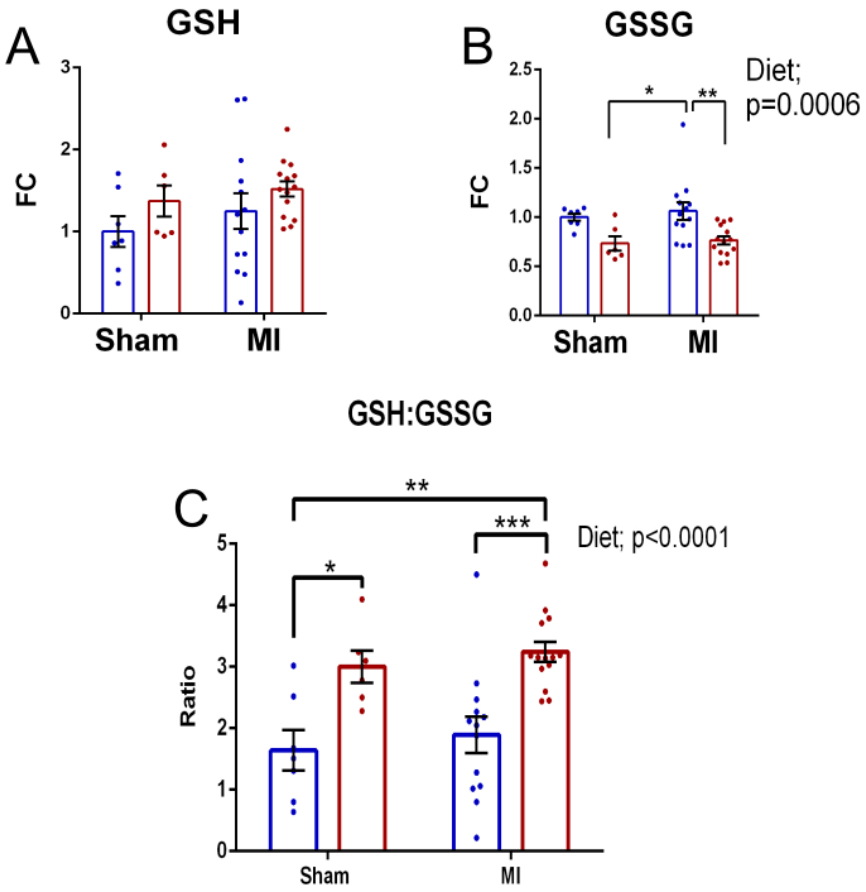

Figure 17. Quantification of reduced and oxidized forms of glutathione. Levels of GSH (**A**), GSSG (**B**), and the GSH to GSSG ratio. Metabolites were quantified through LC/MS, values are shown as fold change (FC) over the mean of the Sham CD group. Bars and error bars represent the mean ± standard error of the mean (SEM). CD-fed groups are shown in blue, NR-fed groups are shown in red. 2-Way ANOVA for independent samples was performed, followed by multiple comparisons with Tukey's posthoc test: *, $p \leq 0.05$; **; $p \leq 0.01$; ***, $p \leq 0.001$; ****, $p \leq 0.0001$. Abbreviations: GSH, reduced glutathione; GSSG, oxidized glutathione.

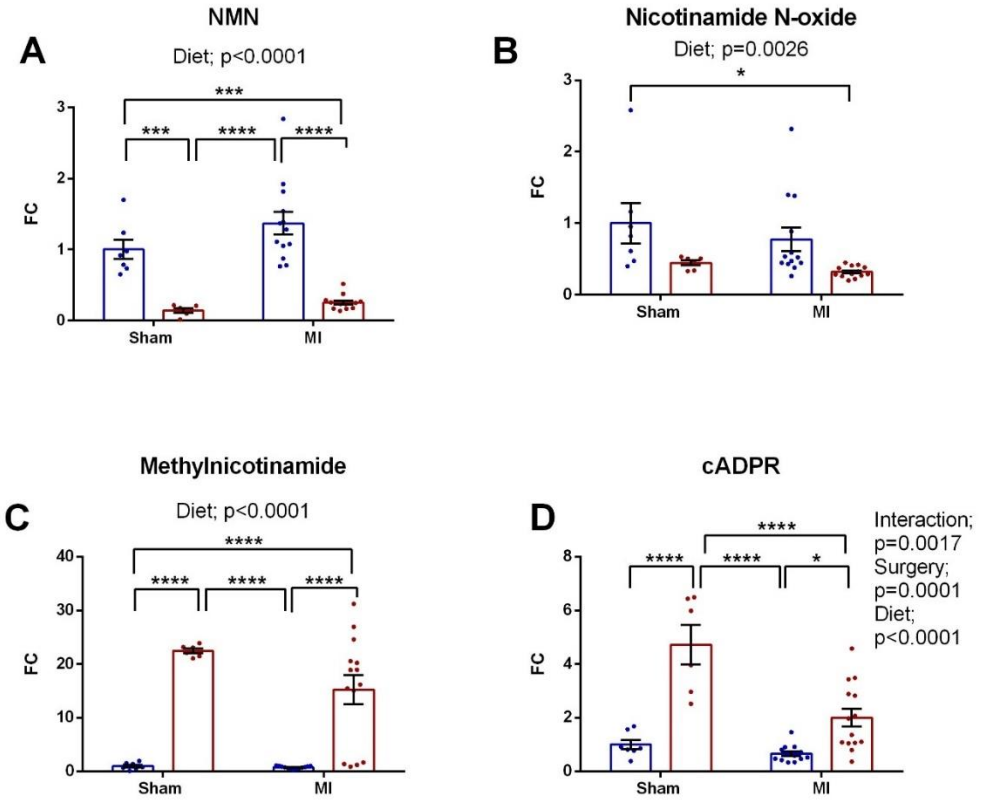

Figure 18. NAD⁺ related metabolites in LV. Metabolites were quantified through LC/MS, values are shown as fold change (FC) over the mean of the Sham CD group. Bars and error bars represent mean ± standard error of the mean (SEM). 2-Way ANOVA for independent samples was performed, followed by multiple comparisons with Tukey's *posthoc* test: *, $p \leq 0.05$; **; $p \leq 0.01$; ***, $p \leq 0.001$; ****, $p \leq 0.0001$. Abbreviations: NMN, nicotinamide mononucleotide; cADPR, cyclic adenosine di-phosphate ribose. CD-fed groups are shown in blue, NR-fed groups are shown in red.

Parameter	Sham CD	Sham NR	MI CD	MI NR	N	ANOVA
BW (g)	590.1 ± 8.962	553.9 ± 10.468 *****	585.3 ± 8.914	541.7 ± 28.539 ****, ##**	17, 18, 25, 26	**§§§§**
TL (cm)	4.6 ± 0.06	4.5 ± 0.053	4.6 ± 0.049	4.5 ± 0.051	7, 8, 17, 17	**ns**
BW/TL (g/cm)	129.2 ± 3.655	121.9 ± 3.864	127.6 ± 1.865	122.1 ± 10.573	7, 8, 17, 15	**§**
Body length (cm)	49 ± 0.472	47.3 ± 0.608	49.6 ± 0.715	48.1 ± 0.364	7, 8, 17, 17	**§**
HW (mg)	1790.1 ± 91.298	1512.9 ± 45.682	1977.2 ± 98.576 **$**	1715.5 ± 82.74	13, 17, 21, 25	**¶, §**
HW/BW (mg/g)	3.1 ± 0.172	2.7 ± 0.073	3.4 ± 0.151 **$$**	3.2 ± 0.229 **$**	13, 17, 21, 23	**¶¶, §**
HW/TL (mg/cm)	327.4 ± 7.58	306.7 ± 8.666	425.8 ± 20.592 ***, $$$**	384.9 14.71 **$**	5, 8, 14, 17	**¶¶¶¶**
Lungs W(mg)	1595.5 ± 110.59	1499.2 ± 100.369	2120.2 ± 183.126 **$**	1749.1 ± 121.153	16,17,25,28	**¶¶**
Lungs W/BW (mg/g)	2.7 ± 0.188	2.7 ± 0.182	3.6 ± 0.302 ***, $**	3.3 ± 0.278	16, 17, 25, 26	**¶¶**
Lungs W/TL (mg/cm)	326.8 ± 23.056	327.4 ± 50.946	466.4 ± 45.951	382.1 ± 24.389	7, 7, 17, 17	**¶**
Lungs DW (mg)	404.8 ± 33.643	378.3 ± 26.32	527.2 ± 69.367	395.3 ± 19.627	14, 17, 22, 26	**ns**
Lungs WW/DW (mg/mg)	4 ± 0.299	4 ± 0.247	4.1 ± 0.083	4.2 ± 0.067	14, 17, 22, 26	**¶**
Kidneys W (mg)	2586.2 ± 100.291	2442.3 ± 106.721	2585.1 ± 105.008	2419.1 ± 94.69	17, 18, 25, 28	**ns**
Kidneys W/BW (mg/g)	4.4 ± 0.167	4.4 ± 0.177	4.4 ± 0.16	4.6 ± 0.294	17, 18, 25, 26	**ns**
Kidneys W/TL (mg/cm)	504.9 ± 20.353	483.9 ± 29.225	566.4 ± 31.239	521.7 ± 32.051	7, 8, 17, 17	**ns**
Liver W (g)	16 ± 0.437	15.2 ± 0.511	16.5 ± 0.857	14.9 ± 0.412	17, 18, 25, 28	**§**
Liver W/BW (mg/g)	27.1 ± 0.589	27.4 ± 0.636	27.8 ± 0.774	27.8 ± 1.594	17, 18, 25, 26	**ns**
Liver W/TL (g/cm)	3.4 ± 0.136	3.1 ± 0.081	3.6 ± 0.162	3.3 ± 0.114	7, 8, 17, 17	**§**
EAT (g)	8.4 ± 1.753	7.8 ± 0.573	8.5 ± 0.906	8.5 ± 0.893	5, 8, 14, 14	**ns**
EAT/BW (mg/g)	14.4 ± 2.916	14.5 ± 1.054	15.1 ± 1.25	15.8 ± 1.015	5, 8, 15, 16	**ns**
EAT/TL (g/cm)	1.8 ± 0.38	1.8 ± 0.124	1.9 ± 0.165	1.8 ± 0.108	5, 8, 15, 15	**ns**

Table 1 Anatomical parameters measured at sacrifice. Abbreviations: BW, body weight; TL, tibia length; BW/TL, bodyweight normalized to tibia length; HW, heart weight; HW/BW, heart weight normalized to body weight; HW/TL, heart weight normalized to tibia length; lungs W, lungs wet weight; lungs W/BW, lungs wet weight normalized to body weight; lungs W/TL, lungs wet weight normalized to tibia length; lungs DW, lungs dry weight; lungs WW/DW, lungs wet weight normalized to dry weight; kidneys W, kidneys weight; kidneys W/BW, kidneys weight normalized to body weight; kidneys W/TL, kidneys weight to tibia length; liver W, liver weight; liver W/BW, liver weight to body weight; liver W/TL, liver weight to tibia length; EAT, epididymal adipose tissue; EAT/BW, epididymal adipose tissue weight normalized to body weight; EAT/TL, epididymal adipose tissue weight normalized to tibia length. 2-way ANOVA for independent samples was performed: ¶, $p \leq 0.05$; ¶¶, $p \leq 0.01$ and ¶¶¶¶, $p \leq 0.0001$ for surgery effect. §, $p \leq 0.05$ and §§§§, $p \leq 0.0001$ for diet effect. *Post-hoc* Tukey test for multiple

comparisons: *, $p \leq 0.05$ and **, $p \leq 0.01$ for comparisons *vs* Sham CD group. $, $p \leq 0.05$; $$, $p \leq 0.01$ and $$$, $p \leq 0.001$ for comparisons *vs* Sham NR group. #, $p \leq 0.001$ and ## ≤ 0.01 for MI CD *vs* MI NR groups comparisons; ns, not significant. Some measurements were not performed in all the samples, notably the TL.

	4 weeks					16 weeks				
N	**11**	**12**	**19**	**21**		**11**	**12**	**19**	**21**	
Parameter	**Sham CD**	**Sham NR**	**MI CD**	**MI NR**	**ANOVA**	**Sham CD**	**Sham NR**	**MI CD**	**MI NR**	**ANOVA**
LVAWd/BW (um/g)	3.3 ± 0.157	3.6 ± 0.225	2.8 ± 0.181 **$**	3.4 ± 0.183	**§**	2.6 ± 0.225	3 ± 0.177	2.5 ± 0.217	3.1 ± 0.243	**ns**
LVAWs/BW (um/g)	6 ± 0.365	6 ± 0.413	3.9 ± 0.298 *****, $$$**	4.8 ± 0.222 **$**	**¶¶¶¶**	4.4 ± 0.367	5 ± 0.342	3.4 ± 0.311 **$$**	4.2 ± 0.308	**¶¶, §**
LVAW systolic thickening (%)	267.1 ± 26.599	244.5 ± 34.121	116.7 ± 15.956 *****, $$**	145.5 ± 18.35 ****, $**	**¶¶¶¶**	184.9 ± 18.871	204.8 ± 18.21	93.1 ± 13.79 ****, $$$$**	117.5 ± 16.305 **$$**	**¶¶¶¶**
LVIDd/BW (um/g)	16.5 ± 0.494	18.1 ± 0.462	21.2 ± 0.677 *****, $**	21.3 ± 0.748 *****, $**	**¶¶¶¶**	13.8 ± 0.346	14.2 ± 0.376	16.4 ± 0.53 ****, $$**	16.5 ± 0.394 ****, $$**	**¶¶¶¶**
LVIDs/BW (um/g)	9.6 ± 0.54	10.3 ± 0.745	16.4 ± 0.707 ******, $$$$**	15.7 ± 0.77 ******, $$$$**	**¶¶¶¶**	8.4 ± 0.566	8.3 ± 0.58	13 ± 0.503 ******, $$$$**	12 ± 0.378 ******, $$$$**	**¶¶¶¶**
LVPWd/BW (um/g)	4.8 ± 0.286	4.7 ± 0.208	4.6 ± 0.241	5.5 ± 0.249	**ns**	3.3 ± 0.251	3.6 ± 0.165	3.4 ± 0.199	4 ± 0.222	**§**
LVPWs/BW (um/g)	7.1 ± 0.398	7.2 ± 0.459	6.8 ± 0.33	7.9 ± 0.354	**ns**	5.2 ± 0.303	5.8 ± 0.269	4.9 ± 0.313	5.7 ± 0.314	**§**
LVPW systolic thickening (%)	227.2 ± 13.607	247.4 ± 28.201	215.8 ± 17.023	240.6 ± 15.847	**ns**	187.7 ± 21.558	220.5 ± 18.45	148.6 ± 18.787	171 ± 15.858	**ns**
LVEDV (ml)	0.9 ± 0.066	0.9 ± 0.069	1.7 ± 0.119 *****, $$$$**	1.3 ± 0.109 **$, #**	**¶¶¶¶**	1.2 ± 0.098	1 ± 0.097	1.8 ± 0.136 ****, $$$$**	1.3 ± 0.063 **$, #**	**¶¶¶¶, §§**
LVESV (ml)	0.2 ± 0.036	0.2 ± 0.052	0.8 ± 0.096 ******, $$$$**	0.6 ± 0.072 ***, $**	**¶¶¶¶**	0.3 ± 0.064	0.3 ± 0.061	1 ± 0.107 ******, $$$$**	0.6 ± 0.045 **$, ##**	**¶¶¶¶, §§**
EF (%)	77.6 ± 2.608	77.3 ± 3.551	51 ± 2.09 ******, $$$$**	57.2 ± 2.324 ******, $$$$**	**¶¶¶¶**	74.7 ± 3.103	78.1 ± 2.549	47.9 ± 2.341 ******, $$$$**	58.3 ± 2.182 *****, $$$$**	**¶¶¶¶, §**
FS (%)	42 ± 2.506	43.1 ± 3.617	23.2 ± 1.246 ******, $$$$**	26.9 ± 1.49 ******, $$$$**	**¶¶¶¶**	39.8 ± 2.679	42.4 ± 2.695	21.1 ± 1.306 ******, $$$$**	27.1 ± 1.323 ******, $$$$**	**¶¶¶¶, §**
SV (ml)	0.7 ± 0.042	0.6 ± 0.029	0.8 ± 0.041	0.7 ± 0.049	**¶**	0.9 ± 0.055	0.7 ± 0.044	0.8 ± 0.054	0.8 ± 0.035	**§**
h/r	0.5 ± 0.036	0.5 ± 0.017	0.4 ± 0.021 *****, $$**	0.4 ± 0.019	**i, ¶¶¶**	0.4 ± 0.043	0.5 ± 0.027	0.4 ± 0.027 **$**	0.4 ± 0.022	**¶, §**
LVM index (mg/g)	2.1 ± 0.087	2.1 ± 0.115	2.7 ± 0.17	2.9 ± 0.279	**¶¶**	1.8 ± 0.289	1.8 ± 0.056	2.3 ± 0.165	2.4 ± 0.142	**¶¶**
CO (ml/min)	240 ± 15.624	225.2 ± 6.524	286.3 ± 16.591	257.1 ± 18.521	**¶**	281.2 ± 17.315	233.3 ± 14.048	270.6 ± 19.827	272.2 ± 10.407	**§**
CI (µL/min/g)	541.9 ± 39.257	562.9 ± 15.736	667.1 ± 41.256	652.2±46.523	**¶**	476 ± 27.072	438±22.655	478 ± 37.754	531.5 ± 23.272	**ns**
HR (bpm)	349.9 ± 8.674	353.1 ± 10.796	350.3 ± 6.102	354.3 ± 5.302	**ns**	329.6 ± 8.213	325.2±7.252	335.6 ± 9.311	347.5 ± 6.731	**ns**

Table 2. Trans-thoracic echocardiographic parameters obtained at 4 and 16 weeks after surgery. LVAWd/BW, left ventricular anterior wall thickness in diastole normalized to body weight; LVAWs/BW, left ventricular anterior wall thickness in systole normalized to body weight; LVAW systolic thickening, left ventricular anterior wall systolic thickening; LVIDd/BW, left ventricular internal diameter in diastole; LVIDs/BW, left ventricular internal diameter in systole; LVPWd/BW, left ventricular posterior wall thickness in diastole normalized to body weight; LVPWs/BW, left ventricular posterior wall thickness in systole normalized to body weight; LVPW systolic thickening, left ventricular posterior wall systolic thickening; LVEDV, left ventricular end-diastolic volume; LVESV, left ventricular end-systolic volume; EF, ejection fraction; FS, fractional shortening; SV, stroke volume; h/r, left ventricular wall thickness to radius ratio (at end-diastole); LVM index, left ventricular mass index; CO, cardiac output; CI, cardiac index; HR, heart rate. Data are presented as the mean ± standard deviation (SD). 2-way ANOVA for independent samples was performed: ¶, $p \leq 0.05$; ¶¶, $p \leq 0.01$; ¶¶¶, $p \leq 0.001$ and ¶¶¶¶, $p \leq 0.0001$ for surgery effect. §, $p \leq 0.05$ and §§, $p \leq 0.01$ for diet effect. *Post-hoc* Tukey test for multiple comparisons: *, $p \leq 0.05$; **, $p \leq 0.01$; ***, $p \leq 0.001$ and ****, $p \leq 0.0001$ for comparisons *vs* Sham CD group. $, $p \leq 0.05$; $$, $p \leq 0.01$; $$$, $p \leq 0.001$ and $$$$, $p \leq 0.0001$ for comparisons *vs* Sham NR group. #, $p \leq 0.001$ and ## ≤ 0.01 for MI CD *vs* MI NR groups comparisons; ns, not significant.

	4 weeks					16 weeks				
N	**7-8**	**7-8**	**7-8**	**3-9**		**9**	**7-9**	**7-8**	**6-9**	
Parameter	**Sham CD**	**Sham NR**	**MI CD**	**MI NR**	**ANOVA**	**Sham CD**	**Sham NR**	**MI CD**	**MI NR**	**ANOVA**
E peak (m/s)	0.7±0.03	0.7±0.036	0.8±0.051	0.7±0.043	Ns	0.7±0.028	0.7±0.015	0.9±0.101 **$**	0.7±0.027 **#**	§
A peak (m/s)	0.6±0.044	0.5±0.047	0.4±0.07	0.4±0.066	¶	0.6±0.05	0.5±0.053	0.4±0.071	0.5±0.057	ns
E/A	1.3±0.128	1.4±0.16	2.5±0.538	2.5±0.651	¶	1.4±0.141	1.4±0.137	2.5±0.606	1.6±0.276	ns
E' (cm/s)	5.6±0.34	5.2±0.469	4.9±0.267	4.1±0.466	Ns	5.6±0.498	4.1±0.467	4.1±0.328	4.5±1.024	ns
E/E'	12.9±0.71	14.3±1.87	16±0.474	15.6±1.504	Ns	13.7±1.082	17.2±1.552	22.7±2.862 *****	18±2.902	¶
DT (ms)	55.8±2.566	55.2±3.839	46.3±3.752	49.4±4.08	¶	53.9±4.207	50±2.838	50.6±3.639	52.1±2.944	ns
DS (m/s^2)	13.2±0.583	12.7±0.779	18.7±2.591	16.4±1.895	¶¶	15.4±2.355	15.1±1.236	20±3.401	13.6±1.162	ns

Table 3. Doppler echocardiographic parameters obtained at 4 and 16 weeks after surgery. Abbreviations: early diastolic filling peak velocity, E peak; late diastolic peak velocity, A peak; E/A ratio, E/A; early diastolic mitral annular velocity, E'; E peak to E' ratio, E/E'; deceleration time, DT; E deceleration slope, DS. Values are represented as the mean ± standard error of the mean (SEM). 2-way ANOVA for independent samples was performed: ¶, $p \leq 0.05$ and ¶¶, $p \leq 0.01$ for surgery effect, and §, $p \leq 0.05$ for diet effect. *Post-hoc* Tukey test for multiple comparisons: *, $p \leq 0.05$ for comparisons *vs* Sham CD group; $, $p \leq 0.05$ for comparisons *vs* Sham NR group; # ≤ 0.05 for comparisons between MI CD and MI NR group

	4 weeks					16 weeks				
N	**11**	**12**	**19**	**21**		**11**	**12**	**19**	**21**	
Parameter	**Sham CD**	**Sham NR**	**MI CD**	**MI NR**	**ANOVA**	**Sham CD**	**Sham NR**	**MI CD**	**MI NR**	**ANOVA**
LVAWd/BW (um/g)	3.3 ± 0.157	3.6 ± 0.225	2.8 ± 0.181 **$**	3.4 ± 0.183	**§**	2.6 ± 0.225	3 ± 0.177	2.5 ± 0.217	3.1 ± 0.243	**ns**
LVAWs/BW (um/g)	6 ± 0.365	6 ± 0.413	3.9 ± 0.298 *****, $$$**	4.8 ± 0.222 **$**	**¶¶¶¶**	4.4 ± 0.367	5 ± 0.342	3.4 ± 0.311 **$$**	4.2 ± 0.308	**¶¶, §**
LVAW systolic thickening (%)	267.1 ± 26.599	244.5 ± 34.121	116.7 ± 15.956 *****, $$**	145.5 ± 18.35 ****, $**	**¶¶¶¶**	184.9 ± 18.871	204.8 ± 18.21	93.1 ± 13.79 ****, $$$$**	117.5 ± 16.305 **$$**	**¶¶¶¶**
LVIDd/BW (um/g)	16.5 ± 0.494	18.1 ± 0.462	21.2 ± 0.677 *****, $**	21.3 ± 0.748 *****, $**	**¶¶¶¶**	13.8 ± 0.346	14.2 ± 0.376	16.4 ± 0.53 ****, $$**	16.5 ± 0.394 ****, $$**	**¶¶¶¶**
LVIDs/BW (um/g)	9.6 ± 0.54	10.3 ± 0.745	16.4 ± 0.707 ******, $$$$**	15.7 ± 0.77 ******, $$$$**	**¶¶¶¶**	8.4 ± 0.566	8.3 ± 0.58	13 ± 0.503 ******, $$$$**	12 ± 0.378 ******, $$$$**	**¶¶¶¶**
LVPWd/BW (um/g)	4.8 ± 0.286	4.7 ± 0.208	4.6 ± 0.241	5.5 ± 0.249	**Ns**	3.3 ± 0.251	3.6 ± 0.165	3.4 ± 0.199	4 ± 0.222	**§**
LVPWs/BW (um/g)	7.1 ± 0.398	7.2 ± 0.459	6.8 ± 0.33	7.9 ± 0.354	**Ns**	5.2 ± 0.303	5.8 ± 0.269	4.9 ± 0.313	5.7 ± 0.314	**§**
LVPW systolic thickening (%)	227.2 ± 13.607	247.4 ± 28.201	215.8 ± 17.023	240.6 ± 15.847	**Ns**	187.7 ± 21.558	220.5 ± 18.45	148.6 ± 18.787	171 ± 15.858	**ns**
LVEDV (ml)	0.9 ± 0.066	0.9 ± 0.069	1.7 ± 0.119 *****, $$$$**	1.3 ± 0.109 **$, #**	**¶¶¶¶**	1.2 ± 0.098	1 ± 0.097	1.8 ± 0.136 ****, $$$$**	1.3 ± 0.063 **$, #**	**¶¶¶¶, §§**
LVESV (ml)	0.2 ± 0.036	0.2 ± 0.052	0.8 ± 0.096 ******, $$$$**	0.6 ± 0.072 ***, $**	**¶¶¶¶**	0.3 ± 0.064	0.3 ± 0.061	1 ± 0.107 ******, $$$$**	0.6 ± 0.045 **$, ##**	**¶¶¶¶, §§**
EF (%)	77.6 ± 2.608	77.3 ± 3.551	51 ± 2.09 ******, $$$$**	57.2 ± 2.324 ******, $$$$**	**¶¶¶¶**	74.7 ± 3.103	78.1 ± 2.549	47.9 ± 2.341 ******, $$$$**	58.3 ± 2.182 *****, $$$$**	**¶¶¶¶, §**
FS (%)	42 ± 2.506	43.1 ± 3.617	23.2 ± 1.246 ******, $$$$**	26.9 ± 1.49 ******, $$$$**	**¶¶¶¶**	39.8 ± 2.679	42.4 ± 2.695	21.1 ± 1.306 ******, $$$$**	27.1 ± 1.323 ******, $$$$**	**¶¶¶¶, §**
SV (ml)	0.7 ± 0.042	0.6 ± 0.029	0.8 ± 0.041	0.7 ± 0.049	**¶**	0.9 ± 0.055	0.7 ± 0.044	0.8 ± 0.054	0.8 ± 0.035	**§**
h/r	0.5 ± 0.036	0.5 ± 0.017	0.4 ± 0.021 *****, $$**	0.4 ± 0.019	**i, ¶¶¶**	0.4 ± 0.043	0.5 ± 0.027	0.4 ± 0.027 **$**	0.4 ± 0.022	**¶, §**
LVM index (mg/g)	2.1 ± 0.087	2.1 ± 0.115	2.7 ± 0.17	2.9 ± 0.279	**¶¶**	1.8 ± 0.289	1.8 ± 0.056	2.3 ± 0.165	2.4 ± 0.142	**¶¶**
CO (ml/min)	240 ± 15.624	225.2 ± 6.524	286.3 ± 16.591	257.1 ± 18.521	**¶**	281.2 ± 17.315	233.3 ± 14.048	270.6 ± 19.827	272.2 ± 10.407	**§**
CI (µL/min/g)	541.9 ± 39.257	562.9 ± 15.736	667.1 ± 41.256	652.2±46.523	**¶**	476 ± 27.072	438±22.655	478 ± 37.754	531.5 ± 23.272	**ns**
HR (bpm)	349.9 ± 8.674	353.1 ± 10.796	350.3 ± 6.102	354.3 ± 5.302	**Ns**	329.6 ± 8.213	325.2±7.252	335.6 ± 9.311	347.5 ± 6.731	**ns**

Table 4. Trans-thoracic echocardiographic parameters obtained at 4 and 16 weeks after surgery. LVAWd/BW, left ventricular anterior wall thickness in diastole normalized to body weight; LVAWs/BW, left ventricular anterior wall thickness in systole normalized to body weight; LVAW systolic thickening, left ventricular anterior wall systolic thickening; LVIDd/BW, left ventricular internal diameter in diastole; LVIDs/BW, left ventricular internal diameter in systole; LVPWd/BW, left ventricular posterior wall thickness in diastole normalized to body weight; LVPWs/BW, left ventricular posterior wall thickness in systole normalized to body weight; LVPW systolic thickening, left ventricular posterior wall systolic thickening; LVEDV, left ventricular end-diastolic volume; LVESV, left ventricular end-systolic volume; EF, ejection fraction; FS, fractional shortening; SV, stroke volume; h/r, left ventricular wall thickness to radius ratio (at end-diastole); LVM index, left ventricular mass index; CO, cardiac output; CI, cardiac index; HR, heart rate. Data are presented as the mean ± standard deviation (SD). 2-way ANOVA for independent samples was performed: ¶, $p \leq 0.05$; ¶¶, $p \leq 0.01$; ¶¶¶, $p \leq 0.001$ and ¶¶¶¶, $p \leq 0.0001$ for surgery effect. §, $p \leq 0.05$ and §§, $p \leq 0.01$ for diet effect. Post-hoc Tukey test for multiple comparisons: *, $p \leq 0.05$; **, $p \leq 0.01$; ***, $p \leq 0.001$ and ****, $p \leq 0.0001$ for comparisons vs Sham CD group. $, $p \leq 0.05$; $$, $p \leq 0.01$; $$$, $p \leq 0.001$ and $$$$, $p \leq 0.0001$ for comparisons vs Sham NR group. #, $p \leq 0.001$ and ## ≤ 0.01 for MI CD vs MI NR groups comparisons; ns, not significant.

Discussion

NR impact on survival and cardiac function

We report that a 16-week dietary intervention with the NMRK1/2 substrate, NR, was efficient to counteract the progression of adverse LVR in a rat model of MI and resulted in an improvement of survival probability, a gold standard in clinical end-point trials. Notably, NR was effective to improve the probability of survival after MI, without modifying the life span of the Sham NR group. In agreement with this, several studies that have tested NR as a means to re-establish energetic/NAD^+ homeostasis have also found improvement in survival probability (Fang et al., 2016; Vannini et al., 2019; Vignier et al., 2018), however, the underlying mechanisms for these effects remain to be understood. In terms of cardiac function, NR preserved LVAW thickness at end-systole, the region of the heart that is the most impacted by the infarction. Interestingly, NR induced a slight increase in LVPW thickness (systolic and diastolic) and h/r ratio on Sham and MI rats, which suggests that it might stimulate compensatory hypertrophy in the remote myocardium that was not directly affected by the ischemic insult. A protective effect against the drop in LVEF and FS and an increase in LVESV/LVEDV was observed on MI NR-fed rats, although LV dilation was not modified by diet. Parallel findings in our group in a non-ischemic model of dilated cardiomyopathy (DCM) in mice (SRF^{hKO}) showed that the NR-supplemented diet prevented a severe drop in LVEF. These mice were also protected from LV dilation and thinning of the LV wall (Diguet et al. 2018). Similarly, NR-supplemented diet was tested for 9 weeks on a mouse model with $Lmna^{H222P/H222P}$ mutation that develops contractile dysfunction and cardiac remodeling. Heart size and LV dilation were reduced in $Lmna^{H222P/H222P}$ mice fed with NR, and LVEF and FS were improved (Vignier et al., 2018). Concerning diastolic function, at the end of the study, non-treated MI CD rats exhibited a significant rise of the E peak wave and lowered A wave (not significant), and an E/A > 2 might suggest a restrictive filling pattern. In contrast,

MI NR rats did not exhibit this pattern of restrictive filling, as the E peak rise was prevented, and the E/A ratio was lowered, from 2.5 at 4 weeks to 1.6 at 16 weeks (not significant). NR had no impact on this parameter in Sham-operated rats, which indicates that NR does not increase atrial pressure. In MI CD rats, the increased atrial blood inflow (E wave) could be caused by an increase in LV chamber compliance and reduced filling pressure because of the fibrous and thinned-out wall of the infarcted zones causes. Our results show that this could be reduced by NR probably due to improved contractility in the infarcted zone and an increased LV thickness (anterior and posterior walls), which helps maintain compliance.

Possible mechanisms linked to improved cardiac contractility after NR supplementation

We determined the mRNA level of *Serca2a*, an essential marker of cardiac as it mediates Ca^{2+} reuptake into the sarcoplasmic reticulum in cardiomyocytes. *Serca2a* expression was increased by NR, which could explain the improved cardiac contractility observed on MI NR-fed animals. Since it occurs at the transcript level, it may suggest that a transcriptional regulator of the *Serca2a* gene is activated. One transcriptional regulator candidate that we propose is the serum response factor (SRF). SRF is a transcription factor member of the MADS-box superfamily that regulates the activity of a wide range of genes. It binds as a homodimer to the DNA consensus sequence CC(A/T)6GG, referred to as a CArG box present in the promoter of CArG box-dependent genes. CArG boxes are essential for the expression of numerous cardiac genes, namely *Serca2a* (Baker et al., 1998). Moreover, we detected increased levels of cADPR upon NR-supplementation. cADPR is generated by the NADase CD38 and is known as a second messenger implicated in Ca^{2+} mobilization in the heart. It has been found that cADPR could activate SERCA by enhancing the sarcoplasmic reticulum Ca^{2+} load in skeletal

muscle (Park et al., 2018). Thus, these findings suggest increased NAD^+ availability and enhanced contractility caused by NR. Nevertheless, the direct association between the NR-mediated NAD^+ pathway and SERCA2A is still unknown. Indeed, this hypothesis will need further exploration.

In addition, SRF is also a major upstream regulator of the muscle creatine kinase isoform gene (*Ckm*) (Chang et al., 2001) and *Nmrk2* (Diguet et al., 2018). The downregulation of CKM is a hallmark of HF, it correlates with the degree of cardiac dysfunction and/or the outcome of HF, given its involvement in the maintenance of phospho-Creatine/ADP/ATP balance. We found a trend in down-regulation of *Ckm* mRNA that was most pronounced in non-treated MI rats, although differences were not significant. Moreover, it has been shown *in vitro* that *Ckm* depression alone induces *Nmrk2* expression (Diguet et al., 2018). Consistent with this, we observed an enhanced expression of *Nmrk2* in LV in both MI groups. Regardless, we also detected a poor relationship between mRNA and protein NRMK2 expression, as NRMK2 protein levels were particularly reduced in MI CD rats compared to MI NR rats. These findings may suggest that over time, NMRK2 expression decreases in non-treated MI rats, which represents a sign of HF worsening. Thus, NR could support the maintenance of NMRK2 protein levels in the MI NR group. NMRK2 has been recently recognized to play a critical role in HF progression following myocardial ischemia. In *Nmrk2* knockout mice, it was demonstrated that its deficiency stimulates post-MI scar expansion, rapid LV chamber dilation, cardiac dysfunction, and fibrosis possibly due to p38α activation (M. Ahmad et al., 2020). In line with this, in an *Nmrk2* knockout mice model, a study in our group showed that these mice developed a progressive DCM-like phenotype with aging, accompanied by LVR and a drop of LVEF, and a reduction of NAD^+ levels. Interestingly, it was observed that NMRK2 gains relevance regarding NAD^+ biosynthetic pathways over time (Tannous et al., 2021).

NR strikingly modified LV metabolome

An overall clustering between CD-fed groups and NR-fed groups was observed through the untargeted exploratory analysis of the cardiac metabolome. With a slightly less evident sub-clustering among Sham and MI groups. This effect was not observed in plasma samples, as there was no evident clustering. Which was more pronounced in the MI NR groups compared to the Sham NR group, as evidenced by the percentage of differentially modulated metabolites, detected through fold change pairwise comparisons (70.9% for MI NR vs 41.22% for Sham NR). Likewise, through 2-way ANOVA analysis using annotated metabolites, we detected 105 metabolites showing NR-effect, whereas MI only significantly modulated 29 metabolites. Altogether, these findings demonstrate that NR-supplementation for 16 weeks had a profound effect on cardiac metabolism, outnumbering the metabolites modified by MI.

Impact of NR in major metabolic pathways and NAD^+ metabolism

It has been consistently reported that NAD^+ and NAMPT levels are decreased in several cardiomyopathy mice models (Diguet et al., 2018; Vignier et al., 2018), the physiologically favored enzyme for the salvage of NAD^+. As expected, we observed that MI diminished the level of NAMPT protein and gene expression, and NR-diet rescued NAMPT levels on MI rats in the remote myocardium. A study on the effects of NAMPT inhibition with the small molecule FK866 demonstrated that NAMPT inhibition leads to the attenuation of glycolysis at the glyceraldehyde 3-phosphate dehydrogenase step, triggered by a reduction of $NAD^{+\cdot}$ Carbon labeling studies established that the carbon overflow into the PPP is mostly through its non-oxidative branch (Tan et al., 2013). In agreement with these findings, through LC-MS-based metabolomics from LV samples, we could detect that the PPP intermediates, namely sedoheptulose-7-phosphate, ribose, D-ribulose-5-phosphate, and D-erythrose were significantly reduced in the NR-fed groups.

Comparably, sedoheptulose-7-phosphate and fructose-6-phosphate levels were reduced in responder patients that underwent left ventricular assist device intervention relative to non-responders. This pattern could be consistent with increased non-oxidative pentose phosphate pathway flux in patients with HF with signs of myocardial recovery (Badolia et al., 2020). Regarding glycolysis and the TCA cycle, there was no evidence that NR improved the bioavailability of its intermediaries. Whereas glutathione metabolism was activated by NR, as in NR-fed groups we observed a trend in which the reduced and active form of glutathione (GSH) was increased (although not significant), conversely its oxidized form (GSSG) was significantly decreased. Notably, the increase of the GSH:GSSG ratio in NR-fed animals reveals that NR can effectively boost global antioxidant capacity as GSH is one the most important scavengers of reactive oxygen species (ROS), and its decrease has been linked to the development and progression of cardiovascular diseases (Chen et al., 2010; Damy et al., 2009). Our results might indicate an improved defense against oxidative stress characteristic of adverse LVR through NR supplementation.

Regarding NAD^+- related metabolism, NR induced increased cardiac levels of methyl nicotinamide, which has been previously reported and validated as a marker of NR treatment (Diguet et al., 2018).

NR impact on bodyweight

We detected an important reduction in body weight gain caused by NR supplementation, both in MI and Sham-operated rats. It has been previously described that NR stimulates resistance to weight gain and decreases fat mass body composition in mice fed a high-fat diet (Cantó et al., 2012) and that combined with the caloric restriction it can enhance bodyweight loss without altering muscle weight in obese rats (de Castro et al., 2021). Even though the processes underlying

this effect are not fully known, it was proposed that they may be related to increased NAD^+ levels, boosting the activities of SIRT1 and SIRT3, and basal oxidative metabolism. In addition, it was shown that NR at 400 mg/kg/day for 5 weeks induced a thermogenic response in adult lean mice associated with a reduction of visceral fat but a minor increase in whole-body O_2 consumption (Crisol et al., 2018). In contrast, very low doses of NR (5 to 10 mg/kg/day) to neonate lactating mice, only males were slightly but significantly heavier (6%) and had higher (20%) body fat content and fat/lean ratio without any change in length, showing that NR does not affect post-natal growth (Asnani-Kishnani et al., 2019). In this study, NR was given at a high dose to young adult male rats, that had not yet fully completed growth. We did not discover a significant difference in epididymal fat content to body weight ratio on NR-fed rats. The reduction in weight gain was partially due to the limitation of body growth as suggested by the body length measurements. Altogether, these observations indicate that a high dose of NR may overstimulate basal metabolism, as a form of energy-wasting, which might implicate an impairment for growth when the high NR administration is started before full development.

NR did not restore mitochondrial respiration nor energy signaling effectors

While MI altered mitochondrial respiration significantly in the remote myocardium as previously reported by many studies, we found no differences upon NR administration. It is important to note that testing mitochondrial function *in situ* using permeabilized cardiac fibers allows the characterization of functional mitochondria with preserved interactions with another organelle. However, this methodology requires removing the cytosol content and all its metabolites and soluble cytosolic enzymes. Therefore, this method does not allow for an evaluation of the ability of cardiac cells to uptake energy substrates at the interface between the

sarcolemma and the bloodstream. It would be interesting to assess whether NR could rescue the metabolic flexibility of the heart, by testing substrate utilization such as glucose and FA in live cells or organs. MI rats had lower levels of pACC and pACC to total ACC ratio, in agreement with the idea that AMPK is activated in this context, although there was no effect after NR administration either on Sham or MI animals. We did not find changes in total ACC relative levels of protein. Additionally, we observed a decrease in pACC and pACC to total ACC ratio levels on MI rats. This result indicates a probable increase in AMPK signaling in response to the energetic stress triggered by the higher contractile demand in the remote myocardium and a higher pACC/ACC ratio should increase FAO to provide more energy to the working remote myocardium. MI. These regulatory changes were not modified by the NR treatment. We need to further explore additional pathways such as those linked to autophagy, and notably, the mitochondrial unfolded response that has been described as activated by NR in other settings, notably the TAC model in mice (Smyrnias et al., 2019; Vannini et al., 2019; J. Zhang et al., 2019).

Acknowledgments

We thank Susana Gomez (UMR1180, University Paris-Saclay) for initiating and training S.L.V. for echocardiography, Florence Lefebvre (UMR1180, University Paris-Saclay) for help with blood samples harvesting, Bénédicte Tremblay (University of Montreal) for preliminary analyses of metabolomics data and Matthieu Ruiz (University of Montreal) for expert advises on metabolomics.

Conclusion

With our data, we can conclude that 16 weeks of oral NR supplementation were effective to counteract hallmarks of adverse LVR, namely, cardiac function, con-

sequently improving survival probability after MI. Interestingly, NR not only up-regulated NMRK2 as expected, but it also restored the downregulation of NAMPT, implying an improvement in terms of NAD^+ homeostasis. Moreover, NR stimulated NMRK2 expression, an effect that was maintained throughout 16 weeks on rats that underwent MI as compared to CD-fed rats, confirming previous findings that suggest that NMRK2 plays an important role during LVR.

Our results indicate that oral NR might ameliorate contractility after MI, however, there were no evident improvements related to energetic metabolism.

NR extensively modulated LV metabolome but not the circulation metabolome. Remarkably, NR modified two relevant pathways in terms of cardioprotection, PPP, and glutathione metabolism. The underlying molecular effectors and modulated pathways that are contributing to this cardioprotective effect remain to be unraveled.

Bibliography

Abu-Elheiga, L., Matzuk, M. M., Abo-Hashema, K. A., & Wakil, S. J. (2001). Continuous fatty acid oxidation and reduced fat storage in mice lacking acetyl-CoA carboxylase 2. *Science (New York, N.Y.)*, *291*(5513), 2613–2616. https://doi.org/10.1126/science.1056843

Ahmad, F., Tomar, D., Aryal A C, S., Elmoselhi, A. B., Thomas, M., Elrod, J. W., Tilley, D. G., & Force, T. (2020). Nicotinamide riboside kinase-2 alleviates ischemia-induced heart failure through P38 signaling. *Biochimica et Biophysica Acta (BBA) - Molecular Basis of Disease*, *1866*(3), 165609. https://doi.org/10.1016/j.bbadis.2019.165609

Ahmad, M., Wolberg, A., & Kahwaji, C. I. (2020). Biochemistry, Electron Transport Chain. In *StatPearls*. StatPearls Publishing. http://www.ncbi.nlm.nih.gov/books/NBK526105/

Alabduladhem, T., & Bordoni, B. (2021). Physiology, Krebs Cycle. *StatPearls*. https://www.statpearls.com/ArticleLibrary/viewarticle/23952

Alano, C. C., Tran, A., Tao, R., Ying, W., Karliner, J. S., & Swanson, R. A. (2007). Differences among cell types in NAD(+) compartmentalization: A comparison of neurons, astrocytes, and cardiac myocytes. *Journal of Neuroscience Research*, *85*(15), 3378–3385. https://doi.org/10.1002/jnr.21479

Alberts, B., Johnson, A., Lewis, J., Raff, M., Roberts, K., & Walter, P. (2002). The Mitochondrion. *Molecular Biology of the Cell. 4th Edition*. https://www.ncbi.nlm.nih.gov/books/NBK26894/

Alcendor, R. R., Gao, S., Zhai, P., Zablocki, D., Holle, E., Yu, X., Tian, B., Wagner, T., Vatner, S. F., & Sadoshima, J. (2007). Sirt1 Regulates Aging and Resistance to Oxidative Stress in the Heart. *Circulation Research*, *100*(10), 1512–1521. https://doi.org/10.1161/01.RES.0000267723.65696.4a

Anderson, J. L., & Morrow, D. A. (2017). Acute Myocardial Infarction. *New England Journal of Medicine*, *376*(21), 2053–2064. https://doi.org/10.1056/NEJMra1606915

Antman, E., Bassand, J.-P., Klein, W., Ohman, M., Lopez Sendon, J. L., Rydén, L., Simoons, M., & Tendera, M. (2000). Myocardial infarction redefined—a consensus document of The Joint European Society of Cardiology/American College of Cardiology committee for the redefinition of myocardial infarction: The Joint European Society of Cardiology/ American College of Cardiology Committee∗∗A list of contributors to this ESC/ACC Consensus Document is provided in Appendix B. *Journal of the American College of Cardiology*, *36*(3), 959–969. https://doi.org/10.1016/S0735-1097(00)00804-4

Asnani-Kishnani, M., Rodríguez, A. M., Serrano, A., Palou, A., Bonet, M. L., & Ribot, J. (2019). Neonatal Resveratrol and Nicotinamide Riboside Supplementations Sex-Dependently Affect Beige Transcriptional Programming of Preadipocytes in Mouse Adipose Tissue. *Frontiers in Physiology*, *10*, 83. https://doi.org/10.3389/fphys.2019.00083

Avogaro, A., Nosadini, R., Doria, A., Fioretto, P., Velussi, M., Vigorito, C., Sacca, L., Toffolo, G., Cobelli, C., Trevisan, R., & et, al. (1990). Myocardial metabolism in insulin-deficient diabetic humans without coronary artery disease. *American Journal of Physiology-Endocrinology and Metabolism*, *258*(4), E606–E618. https://doi.org/10.1152/ajpendo.1990.258.4.E606

Badawy, A. A.-B. (2017). Kynurenine Pathway of Tryptophan Metabolism: Regulatory and Functional Aspects. *International Journal of Tryptophan Research: IJTR*, *10*, 1178646917691938. https://doi.org/10.1177/1178646917691938

Badolia, R., Ramadurai, D. K. A., Abel, E. D., Ferrin, P., Taleb, I., Shankar, T. S., Krokidi, A. T., Navankasattusas, S., McKellar, S. H., Yin, M., Kfoury, A. G., Wever-Pinzon, O., Fang, J. C., Selzman, C. H., Chaudhuri, D., Rutter, J., & Drakos, S. G. (2020). The Role of Nonglycolytic Glucose Metabolism in Myocardial Recovery Upon Mechanical Unloading and Circulatory Support in Chronic Heart Failure. *Circulation*, *142*(3), 259–274. https://doi.org/10.1161/CIRCULATIONAHA.119.044452

Baeza-Herrera, L. A., Araiza-Garaygordobil, D., Gopar-Nieto, R., Raymundo-Martínez, G. I., Loáisiga-Sáenz, A., Villalobos-Flores, A., Martínez-Ramos, M., Torres-Araujo, L. V., Pohls-Vázquez, R., Luna-Herbert, A., Alonso-Vázquez, A. I., Delgado-Cruz, I. V., Cabello-López, A., Martínez-Amezcua, P., Arias-Mendoza, M. A., Baeza-Herrera, L. A., Araiza-Garaygordobil, D., Gopar-Nieto, R., Raymundo-Martínez, G. I., … Arias-Mendoza, M. A. (2020). Evaluation of pharmacoinvasive strategy versus percutaneous coronary intervention in patients with acute myocardial infarction with ST-segment elevation at the National Institute of Cardiology (PHASE-MX). *Archivos de Cardiología de México*, *90*(2), 137–141. https://doi.org/10.24875/acme.m20000107

Bai, P., & Cantó, C. (2012). The Role of PARP-1 and PARP-2 Enzymes in Metabolic Regulation and Disease. *Cell Metabolism*, *16*(3), 290–295. https://doi.org/10.1016/j.cmet.2012.06.016

Baker, D. L., Dave, V., Reed, T., Misra, S., & Periasamy, M. (1998). A novel E box/AT-rich element is required for muscle-specific expression of the sarcoplasmic reticulum

Ca2+-ATPase (SERCA2) gene. *Nucleic Acids Research*, *26*(4), 1092–1098. https://www.ncbi.nlm.nih.gov/pmc/articles/PMC147358/

Baliga, R. R., Bahl, V. K., Alexander, T., Mullasari, A., Manga, P., Dec, G. W., & Narula, J. (2014). Management of STEMI in low- and middle-income countries. *Global Heart*, *9*(4), 469–510. https://doi.org/10.1016/j.gheart.2014.11.001

Barycki, J. J., O'Brien, L. K., Bratt, J. M., Zhang, R., Sanishvili, R., Strauss, A. W., & Banaszak, L. J. (1999). Biochemical Characterization and Crystal Structure Determination of Human Heart Short Chain l-3-Hydroxyacyl-CoA Dehydrogenase Provide Insights into Catalytic Mechanism. *Biochemistry*, *38*(18), 5786–5798. https://doi.org/10.1021/bi9829027

Bedi, K. C., Snyder, N. W., Brandimarto, J., Aziz, M., Mesaros, C., Worth, A. J., Wang, L. L., Javaheri, A., Blair, I. A., Margulies, K. B., & Rame, J. E. (2016). Evidence for Intramyocardial Disruption of Lipid Metabolism and Increased Myocardial Ketone Utilization in Advanced Human Heart Failure. *Circulation*, *133*(8), 706–716. https://doi.org/10.1161/CIRCULATIONAHA.115.017545

Belenky, P., Bogan, K. L., & Brenner, C. (2007). NAD+ metabolism in health and disease. *Trends in Biochemical Sciences*, *32*(1), 12–19. https://doi.org/10.1016/j.tibs.2006.11.006

Bender, D. A., & Olufunwa, R. (1988). Utilization of tryptophan, nicotinamide and nicotinic acid as precursors for nicotinamide nucleotide synthesis in isolated rat liver cells. *The British Journal of Nutrition*, *59*(2), 279–287. https://doi.org/10.1079/bjn19880035

Berger, F., Lau, C., Dahlmann, M., & Ziegler, M. (2005). Subcellular compartmentation and differential catalytic properties of the three human nicotinamide mononucleotide

adenylyltransferase isoforms. *The Journal of Biological Chemistry*, *280*(43), 36334–36341. https://doi.org/10.1074/jbc.M508660200

Berger, F., Ramírez-Hernández, M. H., & Ziegler, M. (2004). The new life of a centenarian: Signalling functions of NAD(P). *Trends in Biochemical Sciences*, *29*(3), 111–118. https://doi.org/10.1016/j.tibs.2004.01.007

Bertero, E., & Maack, C. (2018a). Calcium Signaling and Reactive Oxygen Species in Mitochondria. *Circulation Research*, *122*(10), 1460–1478. https://doi.org/10.1161/CIRCRESAHA.118.310082

Bertero, E., & Maack, C. (2018b). Metabolic remodelling in heart failure. *Nature Reviews. Cardiology*, *15*(8), 457–470. https://doi.org/10.1038/s41569-018-0044-6

Betts, J. G., Desaix, P., Johnson, E. W., Johnson, J. E., Korol, O., Kruse, D., Poe, B., College, O., Wise, J., Womble, M. D., & Young, K. A. (2013). *Anatomy & Physiology*. OpenStax College, Rice University.

Bevere, M., Morabito, C., Mariggiò, M. A., & Guarnieri, S. (2022). The Oxidative Balance Orchestrates the Main Keystones of the Functional Activity of Cardiomyocytes. *Oxidative Medicine and Cellular Longevity*, *2022*, 7714542. https://doi.org/10.1155/2022/7714542

Bhatt, A. S., Ambrosy, A. P., & Velazquez, E. J. (2017). Adverse Remodeling and Reverse Remodeling After Myocardial Infarction. *Current Cardiology Reports*, *19*(8), 71. https://doi.org/10.1007/s11886-017-0876-4

Bieganowski, P., & Brenner, C. (2004). Discoveries of nicotinamide riboside as a nutrient and conserved NRK genes establish a Preiss-Handler independent route to NAD+ in fungi and humans. *Cell*, *117*(4), 495–502. https://doi.org/10.1016/s0092-8674(04)00416-7

Birkenfeld, A. L., Jordan, J., Dworak, M., Merkel, T., & Burnstock, G. (2019). Myocardial metabolism in heart failure: Purinergic signalling and other metabolic concepts. *Pharmacology & Therapeutics*, *194*, 132–144. https://doi.org/10.1016/j.pharmthera.2018.08.015

Bogan, K. L., & Brenner, C. (2008). Nicotinic acid, nicotinamide, and nicotinamide riboside: A molecular evaluation of NAD+ precursor vitamins in human nutrition. *Annual Review of Nutrition*, *28*, 115–130. https://doi.org/10.1146/annurev.nutr.28.061807.155443

Boslett, J., Helal, M., Chini, E., & Zweier, J. L. (2018). Genetic deletion of CD38 confers post-ischemic myocardial protection through preserved pyridine nucleotides. *Journal of Molecular and Cellular Cardiology*, *118*, 81–94. https://doi.org/10.1016/j.yjmcc.2018.02.015

Bouleti, C., Mewton, N., & Germain, S. (2015). The no-reflow phenomenon: State of the art. *Archives of Cardiovascular Diseases*, *108*(12), 661–674. https://doi.org/10.1016/j.acvd.2015.09.006

Braidy, N., Berg, J., Clement, J., Khorshidi, F., Poljak, A., Jayasena, T., Grant, R., & Sachdev, P. (2019). Role of Nicotinamide Adenine Dinucleotide and Related Precursors as Therapeutic Targets for Age-Related Degenerative Diseases: Rationale, Biochemistry, Pharmacokinetics, and Outcomes. *Antioxidants & Redox Signaling*, *30*(2), 251–294. https://doi.org/10.1089/ars.2017.7269

Braunwald, E. (2015). The war against heart failure: The Lancet lecture. *The Lancet*, *385*(9970), 812–824. https://doi.org/10.1016/S0140-6736(14)61889-4

Burke, A. P., & Virmani, R. (2007). Pathophysiology of Acute Myocardial Infarction. *Medical Clinics of North America*, *91*(4), 553–572. https://doi.org/10.1016/j.mcna.2007.03.005

Byun, J., Oka, S.-I., Imai, N., Huang, C.-Y., Ralda, G., Zhai, P., Ikeda, Y., Ikeda, S., & Sadoshima, J. (2019). Both gain and loss of Nampt function promote pressure overload-induced heart failure. *American Journal of Physiology. Heart and Circulatory Physiology*, *317*(4), H711–H725. https://doi.org/10.1152/ajpheart.00222.2019

Califf, R. M. (2018). Biomarker definitions and their applications. *Experimental Biology and Medicine*, *243*(3), 213–221. https://doi.org/10.1177/1535370217750088

Calvert, J. W. (2014). Ischemic Heart Disease and its Consequences. In *Cellular and Molecular Pathobiology of Cardiovascular Disease* (pp. 79–100). Elsevier. https://doi.org/10.1016/B978-0-12-405206-2.00005-3

Camacho-Pereira, J., Tarragó, M. G., Chini, C. C. S., Nin, V., Escande, C., Warner, G. M., Puranik, A. S., Schoon, R. A., Reid, J. M., Galina, A., & Chini, E. N. (2016). CD38 dictates age-related NAD decline and mitochondrial dysfunction through a SIRT3-dependent mechanism. *Cell Metabolism*, *23*(6), 1127–1139. https://doi.org/10.1016/j.cmet.2016.05.006

Cambronne, X. A., Stewart, M. L., Kim, D., Jones-Brunette, A. M., Morgan, R. K., Farrens, D. L., Cohen, M. S., & Goodman, R. H. (2016). Biosensor reveals multiple sources for mitochondrial NAD^+. *Science (New York, N.Y.)*, *352*(6292), 1474–1477. https://doi.org/10.1126/science.aad5168

Cantó, C., Houtkooper, R. H., Pirinen, E., Youn, D. Y., Oosterveer, M. H., Cen, Y., Fernandez-Marcos, P. J., Yamamoto, H., Andreux, P. A., Cettour-Rose, P., Gademann, K.,

Rinsch, C., Schoonjans, K., Sauve, A. A., & Auwerx, J. (2012). The NAD(+) precursor nicotinamide riboside enhances oxidative metabolism and protects against high-fat diet-induced obesity. *Cell Metabolism*, *15*(6), 838–847. https://doi.org/10.1016/j.cmet.2012.04.022

Cantó, C., Menzies, K., & Auwerx, J. (2015). NAD+ metabolism and the control of energy homeostasis—A balancing act between mitochondria and the nucleus. *Cell Metabolism*, *22*(1), 31–53. https://doi.org/10.1016/j.cmet.2015.05.023

Carbone, F., Liberale, L., Bonaventura, A., Vecchiè, A., Casula, M., Cea, M., Monacelli, F., Caffa, I., Bruzzone, S., Montecucco, F., & Nencioni, A. (2017). Regulation and Function of Extracellular Nicotinamide Phosphoribosyltransferase/Visfatin. In *Comprehensive Physiology* (pp. 603–621). American Cancer Society. https://doi.org/10.1002/cphy.c160029

Chanda, D., Luiken, J. J. F. P., & Glatz, J. F. C. (2016). Signaling pathways involved in cardiac energy metabolism. *FEBS Letters*, *590*(15), 2364–2374. https://doi.org/10.1002/1873-3468.12297

Chandler, M. P., Kerner, J., Huang, H., Vazquez, E., Reszko, A., Martini, W. Z., Hoppel, C. L., Imai, M., Rastogi, S., Sabbah, H. N., & Stanley, W. C. (2004). Moderate severity heart failure does not involve a downregulation of myocardial fatty acid oxidation. *American Journal of Physiology. Heart and Circulatory Physiology*, *287*(4), H1538-1543. https://doi.org/10.1152/ajpheart.00281.2004

Chandrashekhar, Y., Alexander, T., Mullasari, A., Kumbhani, D. J., Alam, S., Alexanderson, E., Bachani, D., Wilhelmus Badenhorst, J. C., Baliga, R., Bax, J. J., Bhatt, D. L., Bossone, E., Botelho, R., Chakraborthy, R. N., Chazal, R. A., Dhaliwal, R. S., Gamra, H.,

Harikrishnan, S. P., Jeilan, M., … Narula, J. (2020). Resource and Infrastructure-Appropriate Management of ST-Segment Elevation Myocardial Infarction in Low- and Middle-Income Countries. *Circulation*, *141*(24), 2004–2025. https://doi.org/10.1161/CIRCULATIONAHA.119.041297

Chang, P. S., Li, L., McAnally, J., & Olson, E. N. (2001). Muscle Specificity Encoded by Specific Serum Response Factor-binding Sites*. *Journal of Biological Chemistry*, *276*(20), 17206–17212. https://doi.org/10.1074/jbc.M010983200

Chen, C.-A., Wang, T.-Y., Varadharaj, S., Reyes, L. A., Hemann, C., Talukder, M. A. H., Chen, Y.-R., Druhan, L. J., & Zweier, J. L. (2010). S-glutathionylation uncouples eNOS and regulates its cellular and vascular function. *Nature*, *468*(7327), 1115–1118. https://doi.org/10.1038/nature09599

Chen, Y., & Guillemin, G. J. (2009). Kynurenine Pathway Metabolites in Humans: Disease and Healthy States. *International Journal of Tryptophan Research*, *2*, IJTR.S2097. https://doi.org/10.4137/IJTR.S2097

Chini, E. N., Chini, C. C. S., Netto, J. M. E., de Oliveira, G. C., & van Schooten, W. (2018). The Pharmacology of CD38/NADase: An emerging target for cancer and aging diseases. *Trends in Pharmacological Sciences*, *39*(4), 424–436. https://doi.org/10.1016/j.tips.2018.02.001

Chong, J., Soufan, O., Li, C., Caraus, I., Li, S., Bourque, G., Wishart, D. S., & Xia, J. (2018). MetaboAnalyst 4.0: Towards more transparent and integrative metabolomics analysis. *Nucleic Acids Research*, *46*(W1), W486–W494. https://doi.org/10.1093/nar/gky310

Clarke, K. G. (2013). Carbon metabolism. In *Bioprocess Engineering* (pp. 53–74). Elsevier. https://doi.org/10.1533/9781782421689.53

Cokkinos, D. V., & Belogianneas, C. (2016). Left Ventricular Remodelling: A Problem in Search of Solutions. *European Cardiology*, *11*(1), 29–35. https://doi.org/10.15420/ecr.2015:9:3

Crewe, C., Kinter, M., & Szweda, L. I. (2013). Rapid Inhibition of Pyruvate Dehydrogenase: An Initiating Event in High Dietary Fat-Induced Loss of Metabolic Flexibility in the Heart. *PLoS ONE*, *8*(10). https://doi.org/10.1371/journal.pone.0077280

Crisol, B. M., Veiga, C. B., Lenhare, L., Braga, R. R., Silva, V. R. R., da Silva, A. S. R., Cintra, D. E., Moura, L. P., Pauli, J. R., & Ropelle, E. R. (2018). Nicotinamide riboside induces a thermogenic response in lean mice. *Life Sciences*, *211*, 1–7. https://doi.org/10.1016/j.lfs.2018.09.015

Czura, A. W., & Czura, C. J. (2006). CD38 and CD157: Biological Observations to Clinical Therapeutic Targets. *Molecular Medicine*, *12*(11–12), 309–311. https://doi.org/10.2119/2007-00006.Czura

Damy, T., Kirsch, M., Khouzami, L., Caramelle, P., Le Corvoisier, P., Roudot-Thoraval, F., Dubois-Randé, J.-L., Hittinger, L., Pavoine, C., & Pecker, F. (2009). Glutathione Deficiency in Cardiac Patients Is Related to the Functional Status and Structural Cardiac Abnormalities. *PLoS ONE*, *4*(3), e4871. https://doi.org/10.1371/journal.pone.0004871

Dashty, M. (2013). A quick look at biochemistry: Carbohydrate metabolism. *Clinical Biochemistry*, *46*(15), 1339–1352. https://doi.org/10.1016/j.clinbiochem.2013.04.027

Davila, A., Liu, L., Chellappa, K., Redpath, P., Nakamaru-Ogiso, E., Paolella, L. M., Zhang, Z., Migaud, M. E., Rabinowitz, J. D., & Baur, J. A. (2018). Nicotinamide adenine dinucleotide is transported into mammalian mitochondria. *ELife*, *7*. https://doi.org/10.7554/eLife.33246

de Castro, J. M., Stein, D. J., Medeiros, H. R., de Oliveira, C., & Torres, I. L. S. (2021). Nicotinamide Riboside Neutralizes Hypothalamic Inflammation and Increases Weight Loss Without Altering Muscle Mass in Obese Rats Under Calorie Restriction: A Preliminary Investigation. *Frontiers in Nutrition*, *8*, 620. https://doi.org/10.3389/fnut.2021.648893

De Sousa, E., Veksler, V., Bigard, X., Mateo, P., & Ventura-Clapier, R. (2000). Heart Failure Affects Mitochondrial but Not Myofibrillar Intrinsic Properties of Skeletal Muscle. *Circulation*, *102*(15), 1847–1853. https://doi.org/10.1161/01.CIR.102.15.1847

Di Lisa, F., Menabò, R., Canton, M., Barile, M., & Bernardi, P. (2001). Opening of the Mitochondrial Permeability Transition Pore Causes Depletion of Mitochondrial and Cytosolic NAD $^{+}$ and Is a Causative Event in the Death of Myocytes in Postischemic Reperfusion of the Heart. *Journal of Biological Chemistry*, *276*(4), 2571–2575. https://doi.org/10.1074/jbc.M006825200

Di Stefano, R., Di Bello, V., Barsotti, M. C., Grigoratos, C., Armani, C., Dell'Omodarme, M., Carpi, A., & Balbarini, A. (2009). Inflammatory markers and cardiac function in acute coronary syndrome: Difference in ST-segment elevation myocardial infarction (STEMI) and in non-STEMI models. *Biomedicine & Pharmacotherapy*, *63*(10), 773–780. https://doi.org/10.1016/j.biopha.2009.06.004

Diguet, N., Trammell, S. A. J., Tannous, C., Deloux, R., Piquereau, J., Mougenot, N., Gouge, A., Gressette, M., Manoury, B., Blanc, J., Breton, M., Decaux, J.-F., Lavery, G. G., Baczkó, I., Zoll, J., Garnier, A., Li, Z., Brenner, C., & Mericskay, M. (2018). Nicotinamide Riboside Preserves Cardiac Function in a Mouse Model of Dilated Cardiomyopathy. *Circulation*, *137*(21), 2256–2273. https://doi.org/10.1161/CIRCULATIONAHA.116.026099

El-Gharbawy, A., & Vockley, J. (2017). Chapter 14—Nonmitochondrial Metabolic Cardioskeletal Myopathies. In J. L. Jefferies, B. C. Blaxall, J. Robbins, & J. A. Towbin (Eds.), *Cardioskeletal Myopathies in Children and Young Adults* (pp. 265–303). Academic Press. https://doi.org/10.1016/B978-0-12-800040-3.00014-5

Ellis, J. M., Frahm, J. L., Li, L. O., & Coleman, R. A. (2010). Acyl-coenzyme A synthetases in metabolic control. *Current Opinion in Lipidology*, *21*(3), 212–217. https://www.ncbi.nlm.nih.gov/pmc/articles/PMC4040134/

Ellis, J. M., Mentock, S. M., DePetrillo, M. A., Koves, T. R., Sen, S., Watkins, S. M., Muoio, D. M., Cline, G. W., Taegtmeyer, H., Shulman, G. I., Willis, M. S., & Coleman, R. A. (2011). Mouse Cardiac Acyl Coenzyme A Synthetase 1 Deficiency Impairs Fatty Acid Oxidation and Induces Cardiac Hypertrophy. *Molecular and Cellular Biology*, *31*(6), 1252–1262. https://doi.org/10.1128/MCB.01085-10

Emanuelli, M., Carnevali, F., Saccucci, F., Pierella, F., Amici, A., Raffaelli, N., & Magni, G. (2001). Molecular Cloning, Chromosomal Localization, Tissue mRNA Levels, Bacterial Expression, and Enzymatic Properties of Human NMN Adenylyltransferase. *Journal of Biological Chemistry*, *276*(1), 406–412. https://doi.org/10.1074/jbc.M008700200

Fang, E. F., Kassahun, H., Croteau, D. L., Scheibye-Knudsen, M., Marosi, K., Lu, H., Shamanna, R. A., Kalyanasundaram, S., Bollineni, R. C., Wilson, M. A., Iser, W. B., Wollman, B. N., Morevati, M., Li, J., Kerr, J. S., Lu, Q., Waltz, T. B., Tian, J., Sinclair, D. A., … Bohr, V. A. (2016). NAD+ replenishment improves lifespan and healthspan in Ataxia telangiectasia models via mitophagy and DNA repair. *Cell Metabolism*, *24*(4), 566–581. https://doi.org/10.1016/j.cmet.2016.09.004

Ferrier, D. (2017). *Lippincott Illustrated Reviews: Biochemistry*.

Finck, B. N. (2007). The PPAR regulatory system in cardiac physiology and disease. *Cardiovascular Research*, *73*(2), 269–277. https://doi.org/10.1016/j.cardiores.2006.08.023

Fitchett, D., Inzucchi, S. E., Wanner, C., Mattheus, M., George, J. T., Vedin, O., Zinman, B., & Johansen, O. E. (2020). Relationship between hypoglycaemia, cardiovascular outcomes, and empagliflozin treatment in the EMPA-REG OUTCOME® trial. *European Heart Journal*, *41*(2), 209–217. https://doi.org/10.1093/eurheartj/ehz621

Fletcher, R. S., Ratajczak, J., Doig, C. L., Oakey, L. A., Callingham, R., Da Silva Xavier, G., Garten, A., Elhassan, Y. S., Redpath, P., Migaud, M. E., Philp, A., Brenner, C., Canto, C., & Lavery, G. G. (2017). Nicotinamide riboside kinases display redundancy in mediating nicotinamide mononucleotide and nicotinamide riboside metabolism in skeletal muscle cells. *Molecular Metabolism*, *6*(8), 819–832. https://doi.org/10.1016/j.molmet.2017.05.011

Folmes, C. D. L., & Lopaschuk, G. (2007). Role of malonyl-CoA in heart disease and the hypothalamic control of obesity. *Undefined*. /paper/Role-of-malonyl-CoA-in-heart-disease-and-the-of-Folmes-Lopaschuk/5eefdd8a16d07f68cf25af97fcbc4fe73b72bc11

Fox, C. S., Pencina, M. J., Wilson, P. W. F., Paynter, N. P., Vasan, R. S., & D'Agostino, R. B. (2008). Lifetime Risk of Cardiovascular Disease Among Individuals With and Without Diabetes Stratified by Obesity Status in the Framingham Heart Study. *Diabetes Care*, *31*(8), 1582–1584. https://doi.org/10.2337/dc08-0025

Fukao, T., Lopaschuk, G. D., & Mitchell, G. A. (2004). Pathways and control of ketone body metabolism: On the fringe of lipid biochemistry. *Prostaglandins, Leukotrienes and Essential Fatty Acids*, *70*(3), 243–251. https://doi.org/10.1016/j.plefa.2003.11.001

Fukuwatari, T., & Shibata, K. (2007). Effect of nicotinamide administration on the tryptophan-nicotinamide pathway in humans. *International Journal for Vitamin and Nutrition Research. Internationale Zeitschrift Fur Vitamin- Und Ernahrungsforschung. Journal International De Vitaminologie Et De Nutrition*, *77*(4), 255–262. https://doi.org/10.1024/0300-9831.77.4.255

Garnier, A., Fortin, D., Deloménie, C., Momken, I., Veksler, V., & Ventura-Clapier, R. (2003). Depressed mitochondrial transcription factors and oxidative capacity in rat failing cardiac and skeletal muscles. *The Journal of Physiology*, *551*(Pt 2), 491–501. https://doi.org/10.1113/jphysiol.2003.045104

Garten, A., Schuster, S., Penke, M., Gorski, T., de Giorgis, T., & Kiess, W. (2015). Physiological and pathophysiological roles of NAMPT and NAD metabolism. *Nature Reviews. Endocrinology*, *11*(9), 535–546. https://doi.org/10.1038/nrendo.2015.117

Gimeno, R. E., Ortegon, A. M., Patel, S., Punreddy, S., Ge, P., Sun, Y., Lodish, H. F., & Stahl, A. (2003). Characterization of a Heart-specific Fatty Acid Transport Protein *. *Journal of Biological Chemistry*, *278*(18), 16039–16044. https://doi.org/10.1074/jbc.M211412200

Groenewegen, A., Rutten, F. H., Mosterd, A., & Hoes, A. W. (2020). Epidemiology of heart failure. *European Journal of Heart Failure*, *22*(8), 1342–1356. https://doi.org/10.1002/ejhf.1858

Grozio, A., Sociali, G., Sturla, L., Caffa, I., Soncini, D., Salis, A., Raffaelli, N., De Flora, A., Nencioni, A., & Bruzzone, S. (2013). CD73 Protein as a Source of Extracellular Precursors for Sustained NAD+ Biosynthesis in FK866-treated Tumor Cells. *The Journal of Biological Chemistry*, *288*(36), 25938–25949. https://doi.org/10.1074/jbc.M113.470435

Guan, X.-H., Hong, X., Zhao, N., Liu, X.-H., Xiao, Y.-F., Chen, T.-T., Deng, L.-B., Wang, X.-L., Wang, J.-B., Ji, G.-J., Fu, M., Deng, K.-Y., & Xin, H.-B. (2017). CD38 promotes angiotensin II-induced cardiac hypertrophy. *Journal of Cellular and Molecular Medicine*, *21*(8), 1492–1502. https://doi.org/10.1111/jcmm.13076

Guan, X.-H., Liu, X.-H., Hong, X., Zhao, N., Xiao, Y.-F., Wang, L.-F., Tang, L., Jiang, K., Qian, Y.-S., Deng, K.-Y., Ji, G., Fu, M., & Xin, H.-B. (2016). CD38 Deficiency Protects the Heart from Ischemia/Reperfusion Injury through Activating SIRT1/FOXOs-Mediated Antioxidative Stress Pathway. *Oxidative Medicine and Cellular Longevity*, *2016*, e7410257. https://doi.org/10.1155/2016/7410257

Gupte, S. A., Levine, R. J., Gupte, R. S., Young, M. E., Lionetti, V., Labinskyy, V., Floyd, B. C., Ojaimi, C., Bellomo, M., Wolin, M. S., & Recchia, F. A. (2006). Glucose-6-phosphate dehydrogenase-derived NADPH fuels superoxide production in the failing heart. *Journal of Molecular and Cellular Cardiology*, *41*(2), 340–349. https://doi.org/10.1016/j.yjmcc.2006.05.003

Halestrap, A. P. (2013). Monocarboxylic Acid Transport. In *Comprehensive Physiology* (pp. 1611–1643). American Cancer Society. https://doi.org/10.1002/cphy.c130008

Hall, J. E. (2015). *Guyton and Hall Textbook of Medical Physiology*.

Halmosi, R., Berente, Z., Osz, E., Toth, K., Literati-Nagy, P., & Sumegi, B. (2001). Effect of poly(ADP-ribose) polymerase inhibitors on the ischemia-reperfusion-induced oxidative cell damage and mitochondrial metabolism in Langendorff heart perfusion system. *Molecular Pharmacology*, *59*(6), 1497–1505. https://doi.org/10.1124/mol.59.6.1497

Halmosi, R., Deres, L., Gal, R., Eros, K., Sumegi, B., & Toth, K. (2016). PARP inhibition and postinfarction myocardial remodeling. *International Journal of Cardiology*, *217*, S52–S59. https://doi.org/10.1016/j.ijcard.2016.06.223

Hara, N., Yamada, K., Terashima, M., Osago, H., Shimoyama, M., & Tsuchiya, M. (2003). Molecular identification of human glutamine- and ammonia-dependent NAD synthetases. Carbon-nitrogen hydrolase domain confers glutamine dependency. *The Journal of Biological Chemistry*, *278*(13), 10914–10921. https://doi.org/10.1074/jbc.M209203200

Henning, R. J., Bourgeois, M., & Harbison, R. D. (2018). Poly(ADP-ribose) Polymerase (PARP) and PARP Inhibitors: Mechanisms of Action and Role in Cardiovascular Disorders. *Cardiovascular Toxicology*, *18*(6), 493–506. https://doi.org/10.1007/s12012-018-9462-2

Hill, M. F., & Singal, P. K. (1996). Antioxidant and oxidative stress changes during heart failure subsequent to myocardial infarction in rats. *The American Journal of Pathology*, *148*(1), 291–300. https://www.ncbi.nlm.nih.gov/pmc/articles/PMC1861605/

Hinkle, P. C. (2005). P/O ratios of mitochondrial oxidative phosphorylation. *Biochimica et Biophysica Acta (BBA) - Bioenergetics*, *1706*(1), 1–11. https://doi.org/10.1016/j.bbabio.2004.09.004

Ho, K. L., Karwi, Q. G., Wagg, C., Zhang, L., Vo, K., Altamimi, T., Uddin, G. M., Ussher, J. R., & Lopaschuk, G. D. (2020). Ketones can become the major fuel source for the heart but do not increase cardiac efficiency. *Cardiovascular Research*, *117*(4), 1178–1187. https://doi.org/10.1093/cvr/cvaa143

Honka, H., Solis-Herrera, C., Triplitt, C., Norton, L., Butler, J., & DeFronzo, R. A. (2021). Therapeutic Manipulation of Myocardial Metabolism. *Journal of the American College of Cardiology*, *77*(16), 2022–2039. https://doi.org/10.1016/j.jacc.2021.02.057

Hottiger, M. O., Hassa, P. O., Lüscher, B., Schüler, H., & Koch-Nolte, F. (2010). Toward a unified nomenclature for mammalian ADP-ribosyltransferases. *Trends in Biochemical Sciences*, *35*(4), 208–219. https://doi.org/10.1016/j.tibs.2009.12.003

Houtkooper, R. H., Cantó, C., Wanders, R. J., & Auwerx, J. (2010). The Secret Life of NAD+: An Old Metabolite Controlling New Metabolic Signaling Pathways. *Endocrine Reviews*, *31*(2), 194–223. https://doi.org/10.1210/er.2009-0026

Hsu, C.-P., Oka, S., Shao, D., Hariharan, N., & Sadoshima, J. (2009). Nicotinamide phosphoribosyltransferase regulates cell survival through NAD+ synthesis in cardiac myocytes. *Circulation Research*, *105*(5), 481–491. https://doi.org/10.1161/CIRCRESAHA.109.203703

Huang, B., Wu, P., Popov, K. M., & Harris, R. A. (2003). Starvation and Diabetes Reduce the Amount of Pyruvate Dehydrogenase Phosphatase in Rat Heart and Kidney. *Diabetes*, *52*(6), 1371–1376. https://www.ncbi.nlm.nih.gov/pmc/articles/PMC2147665/

Hue, L., & Taegtmeyer, H. (2009). The Randle cycle revisited: A new head for an old hat. *American Journal of Physiology - Endocrinology and Metabolism*, *297*(3), E578–E591. https://doi.org/10.1152/ajpendo.00093.2009

Imai, S., Armstrong, C. M., Kaeberlein, M., & Guarente, L. (2000). Transcriptional silencing and longevity protein Sir2 is an NAD-dependent histone deacetylase. *Nature*, *403*(6771), 795–800. https://doi.org/10.1038/35001622

Jäger, S., Handschin, C., St.-Pierre, J., & Spiegelman, B. M. (2007). AMP-activated protein kinase (AMPK) action in skeletal muscle via direct phosphorylation of PGC-1α. *Proceedings of the National Academy of Sciences*, *104*(29), 12017–12022. https://doi.org/10.1073/pnas.0705070104

Jain, M., Brenner, D. A., Cui, L., Lim, C. C., Wang, B., Pimentel, D. R., Koh, S., Sawyer, D. B., Leopold, J. A., Handy, D. E., Loscalzo, J., Apstein, C. S., & Liao, R. (2003). Glucose-6-Phosphate Dehydrogenase Modulates Cytosolic Redox Status and Contractile Phenotype in Adult Cardiomyocytes. *Circulation Research*, *93*(2), e9–e16. https://doi.org/10.1161/01.RES.0000083489.83704.76

Jayaram, H. N., Kusumanchi, P., & Yalowitz, J. A. (2011). NMNAT expression and its relation to NAD metabolism. *Current Medicinal Chemistry*, *18*(13), 1962–1972. https://doi.org/10.2174/092986711795590138

Jogl, G., Hsiao, Y.-S., & Tong, L. (2004). Structure and Function of Carnitine Acyltransferases. *Annals of the New York Academy of Sciences*, *1033*(1), 17–29. https://doi.org/10.1196/annals.1320.002

Kane, A. E., & Sinclair, D. A. (2018). Sirtuins and NAD+ in the Development and Treatment of Metabolic and Cardiovascular Diseases. *Circulation Research*, *123*(7), 868–885. https://doi.org/10.1161/CIRCRESAHA.118.312498

Karlstaedt, A., Khanna, R., Thangam, M., & Taegtmeyer, H. (2020). Glucose 6-Phosphate Accumulates via Phosphoglucose Isomerase Inhibition in Heart Muscle. *Circulation Research*, *126*(1), 60–74. https://doi.org/10.1161/CIRCRESAHA.119.315180

Karwi, Q. G., Uddin, G. M., Ho, K. L., & Lopaschuk, G. D. (2018). Loss of Metabolic Flexibility in the Failing Heart. *Frontiers in Cardiovascular Medicine*, *5*. https://doi.org/10.3389/fcvm.2018.00068

Kashiwagi, Y., Nagoshi, T., Yoshino, T., Tanaka, T. D., Ito, K., Harada, T., Takahashi, H., Ikegami, M., Anzawa, R., & Yoshimura, M. (2015). Expression of SGLT1 in Human Hearts and Impairment of Cardiac Glucose Uptake by Phlorizin during Ischemia-Reperfusion Injury in Mice. *PLoS ONE*, *10*(6), e0130605. https://doi.org/10.1371/journal.pone.0130605

Katsyuba, E., & Auwerx, J. (2017). Modulating NAD+ metabolism, from bench to bedside. *The EMBO Journal*, *36*(18), 2670–2683. https://doi.org/10.15252/embj.201797135

Katz, A. M. (2010). *Physiology of the Heart*. Lippincott Williams & Wilkins.

Kawai, S., & Murata, K. (2008). Structure and function of NAD kinase and NADP phosphatase: Key enzymes that regulate the intracellular balance of NAD(H) and NADP(H). *Bioscience, Biotechnology, and Biochemistry*, *72*(4), 919–930. https://doi.org/10.1271/bbb.70738

Kerner, J., & Hoppel, C. (2000). Fatty acid import into mitochondria. *Biochimica Et Biophysica Acta*, *1486*(1), 1–17. https://doi.org/10.1016/s1388-1981(00)00044-5

Khan, M. A., Hashim, M. J., Mustafa, H., Baniyas, M. Y., Al Suwaidi, S. K. B. M., AlKatheeri, R., Alblooshi, F. M. K., Almatrooshi, M. E. A. H., Alzaabi, M. E. H., Al Darmaki, R. S., & Lootah, S. N. A. H. (2020). Global Epidemiology of Ischemic Heart Disease: Results from the Global Burden of Disease Study. *Cureus*, *12*(7). https://doi.org/10.7759/cureus.9349

Kirkland, J. B., & Meyer-Ficca, M. L. (2018). Chapter Three—Niacin. In N. A. M. Eskin (Ed.), *Advances in Food and Nutrition Research* (Vol. 83, pp. 83–149). Academic Press. https://doi.org/10.1016/bs.afnr.2017.11.003

Kolwicz, S. C., & Tian, R. (2011). Glucose metabolism and cardiac hypertrophy. *Cardiovascular Research*, *90*(2), 194–201. https://doi.org/10.1093/cvr/cvr071

Konstam, M. A., Kramer, D. G., Patel, A. R., Maron, M. S., & Udelson, J. E. (2011). Left Ventricular Remodeling in Heart Failure. *JACC: Cardiovascular Imaging*, *4*(1), 98–108. https://doi.org/10.1016/j.jcmg.2010.10.008

Korla, K., Vadlakonda, L., & Mitra, C. K. (2015). Kinetic simulation of malate-aspartate and citrate-pyruvate shuttles in association with Krebs cycle. *Journal of Biomolecular Structure & Dynamics*, *33*(11), 2390–2403. https://doi.org/10.1080/07391102.2014.1003603

Kory, N., Uit de Bos, J., van der Rijt, S., Jankovic, N., Güra, M., Arp, N., Pena, I. A., Prakash, G., Chan, S. H., Kunchok, T., Lewis, C. A., & Sabatini, D. M. (2020). MCART1/SLC25A51 is required for mitochondrial NAD transport. *Science Advances*, *6*(43), eabe5310. https://doi.org/10.1126/sciadv.abe5310

Kulikova, V., Shabalin, K., Nerinovski, K., Yakimov, A., Svetlova, M., Solovjeva, L., Kropotov, A., Khodorkovskiy, M., Migaud, M. E., Ziegler, M., & Nikiforov, A. (2019). Degradation of Extracellular NAD+ Intermediates in Cultures of Human HEK293 Cells. *Metabolites*, *9*(12). https://doi.org/10.3390/metabo9120293

Kulish, O., Wright, A. D., & Terentjev, E. M. (2016). F1 rotary motor of ATP synthase is driven by the torsionally-asymmetric drive shaft. *Scientific Reports*, *6*(1), 28180. https://doi.org/10.1038/srep28180

Kuznetsov, A. V., Veksler, V., Gellerich, F. N., Saks, V., Margreiter, R., & Kunz, W. S. (2008). Analysis of mitochondrial function in situ in permeabilized muscle fibers, tissues and cells. *Nature Protocols*, *3*(6), 965–976. https://doi.org/10.1038/nprot.2008.61

Lagouge, M., Argmann, C., Gerhart-Hines, Z., Meziane, H., Lerin, C., Daussin, F., Messadeq, N., Milne, J., Lambert, P., Elliott, P., Geny, B., Laakso, M., Puigserver, P., & Auwerx,

J. (2006). Resveratrol Improves Mitochondrial Function and Protects against Metabolic Disease by Activating SIRT1 and PGC-1α. *Cell*, *127*(6), 1109–1122. https://doi.org/10.1016/j.cell.2006.11.013

Larkin, P. B., Sathyasaikumar, K. V., Notarangelo, F. M., Funakoshi, H., Nakamura, T., Schwarcz, R., & Muchowski, P. J. (2016). Tryptophan 2,3-Dioxygenfase and Indoleamine 2,3-Dioxygenase 1 Make Separate, Tissue-Specific Contributions to Basal and Inflammation-Induced Kynurenine Pathway Metabolism in Mice. *Biochimica et Biophysica Acta*, *1860*(11 Pt A), 2345–2354. https://doi.org/10.1016/j.bbagen.2016.07.002

Lee, J., & Goldberg, I. J. (2007). Lipoproteini lipase-derived fatty acids: Physiology and dysfunction. *Current Hypertension Reports*, *9*(6), 462–466. https://doi.org/10.1007/s11906-007-0085-4

Lemieux, H., Semsroth, S., Antretter, H., Höfer, D., & Gnaiger, E. (2011). Mitochondrial respiratory control and early defects of oxidative phosphorylation in the failing human heart. *The International Journal of Biochemistry & Cell Biology*, *43*(12), 1729–1738. https://doi.org/10.1016/j.biocel.2011.08.008

Lewandowski, E. D., Fischer, S. K., Fasano, M., Banke, N. H., Walker, L. A., Huqi, A., Wang, X., Lopaschuk, G. D., & O'Donnell, J. M. (2013). Acute L-CPT1 Overexpression Recapitulates Reduced Palmitate Oxidation of Cardiac Hypertrophy. *Circulation Research*, *112*(1), 57–65. https://doi.org/10.1161/CIRCRESAHA.112.274456

Li, T., Zhang, Z., Kolwicz, S. C., Abell, L., Roe, N. D., Kim, M., Zhou, B., Cao, Y., Ritterhoff, J., Gu, H., Raftery, D., Sun, H., & Tian, R. (2017). Defective Branched-Chain Amino

Acid Catabolism Disrupts Glucose Metabolism and Sensitizes the Heart to Ischemia-Reperfusion Injury. *Cell Metabolism*, *25*(2), 374–385. https://doi.org/10.1016/j.cmet.2016.11.005

Li, Z., Guo, Z., Lan, R., Cai, S., Lin, Z., Li, J., Wang, J., Li, Z., & Liu, P. (2021). The poly(ADP-ribosyl)ation of BRD4 mediated by PARP1 promoted pathological cardiac hypertrophy. *Acta Pharmaceutica Sinica B*, *11*(5), 1286–1299. https://doi.org/10.1016/j.apsb.2020.12.012

Liu, L., Su, X., Quinn, W. J., Hui, S., Krukenberg, K., Frederick, D. W., Redpath, P., Zhan, L., Chellappa, K., White, E., Migaud, M., Mitchison, T. J., Baur, J. A., & Rabinowitz, J. D. (2018). Quantitative Analysis of NAD Synthesis-Breakdown Fluxes. *Cell Metabolism*, *27*(5), 1067-1080.e5. https://doi.org/10.1016/j.cmet.2018.03.018

Lommi, J., Koskinen, P., Näveri, H., Härkönen, M., & Kupari, M. (1997). Heart failure ketosis. *Journal of Internal Medicine*, *242*(3), 231–238. https://doi.org/10.1046/j.1365-2796.1997.00187.x

Lommi, J., Kupari, M., Koskinen, P., Näveri, H., Leinonen, H., Pulkki, K., & Härkönen, M. (1996). Blood ketone bodies in congestive heart failure. *Journal of the American College of Cardiology*, *28*(3), 665–672. https://doi.org/10.1016/0735-1097(96)00214-8

Lopaschuk, G. D., Belke, D. D., Gamble, J., Itoi, T., & Schönekess, B. O. (1994). Regulation of fatty acid oxidation in the mammalian heart in health and disease. *Biochimica Et Biophysica Acta*, *1213*(3), 263–276. https://doi.org/10.1016/0005-2760(94)00082-4

Lopaschuk, G. D., Karwi, Q. G., Ho, K. L., Pherwani, S., & Ketema, E. B. (2020). Ketone metabolism in the failing heart. *Biochimica et Biophysica Acta (BBA) - Molecular and*

Cell Biology of Lipids, *1865*(12), 158813. https://doi.org/10.1016/j.bbalip.2020.158813

Lopaschuk, G. D., Ussher, J. R., Folmes, C. D. L., Jaswal, J. S., & Stanley, W. C. (2010). Myocardial Fatty Acid Metabolism in Health and Disease. *Physiological Reviews*, *90*(1), 207–258. https://doi.org/10.1152/physrev.00015.2009

Lu, M., Zhou, L., Stanley, W. C., Cabrera, M. E., Saidel, G. M., & Yu, X. (2008). Role of the Malate-Aspartate Shuttle on the Metabolic Response to Myocardial Ischemia. *Journal of Theoretical Biology*, *254*(2), 466–475. https://doi.org/10.1016/j.jtbi.2008.05.033

Luongo, T. S., Eller, J. M., Lu, M.-J., Niere, M., Raith, F., Perry, C., Bornstein, M. R., Oliphint, P., Wang, L., McReynolds, M. R., Migaud, M. E., Rabinowitz, J. D., Johnson, F. B., Johnsson, K., Ziegler, M., Cambronne, X. A., & Baur, J. A. (2020). SLC25A51 is a mammalian mitochondrial NAD+ transporter. *Nature*, *588*(7836), 174–179. https://doi.org/10.1038/s41586-020-2741-7

Maj, M. C., Cameron, J. M., & Robinson, B. H. (2006). Pyruvate dehydrogenase phosphatase deficiency: Orphan disease or an under-diagnosed condition? *Molecular and Cellular Endocrinology*, *249*(1–2), 1–9. https://doi.org/10.1016/j.mce.2006.02.003

Mallat, Z., Philip, I., Lebret, M., Chatel, D., Maclouf, J., & Tedgui, A. (1998). Elevated Levels of 8-iso-Prostaglandin F2α in Pericardial Fluid of Patients With Heart Failure. *Circulation*, *97*(16), 1536–1539. https://doi.org/10.1161/01.CIR.97.16.1536

Martens, C. R., Denman, B. A., Mazzo, M. R., Armstrong, M. L., Reisdorph, N., McQueen, M. B., Chonchol, M., & Seals, D. R. (2018). Chronic nicotinamide riboside supplementation is well-tolerated and elevates NAD+ in healthy middle-aged and older adults. *Nature Communications*, *9*. https://doi.org/10.1038/s41467-018-03421-7

Martín, M. A., Gómez, M. A., Guillén, F., Börnstein, B., Campos, Y., Rubio, J. C., de la Calzada, C. S., & Arenas, J. (2000). Myocardial carnitine and carnitine palmitoyltransferase deficiencies in patients with severe heart failure. *Biochimica Et Biophysica Acta*, *1502*(3), 330–336. https://doi.org/10.1016/s0925-4439(00)00061-2

Martínez-Reyes, I., & Chandel, N. S. (2020). Mitochondrial TCA cycle metabolites control physiology and disease. *Nature Communications*, *11*(1), 102. https://doi.org/10.1038/s41467-019-13668-3

Mashek, D. G., Li, L. O., & Coleman, R. A. (2007). Long-chain acyl-CoA synthetases and fatty acid channeling. *Future Lipidology*, *2*(4), 465–476. https://www.ncbi.nlm.nih.gov/pmc/articles/PMC2846691/

Matsushima, S., & Sadoshima, J. (2015). The role of sirtuins in cardiac disease. *American Journal of Physiology - Heart and Circulatory Physiology*, *309*(9), H1375–H1389. https://doi.org/10.1152/ajpheart.00053.2015

McMurray, J. J. V., Solomon, S. D., Inzucchi, S. E., Køber, L., Kosiborod, M. N., Martinez, F. A., Ponikowski, P., Sabatine, M. S., Anand, I. S., Bělohlávek, J., Böhm, M., Chiang, C.-E., Chopra, V. K., de Boer, R. A., Desai, A. S., Diez, M., Drozdz, J., Dukát, A., Ge, J., … DAPA-HF Trial Committees and Investigators. (2019). Dapagliflozin in Patients with Heart Failure and Reduced Ejection Fraction. *The New England Journal of Medicine*, *381*(21), 1995–2008. https://doi.org/10.1056/NEJMoa1911303

Mehmel, M., Jovanović, N., & Spitz, U. (2020). Nicotinamide Riboside—The Current State of Research and Therapeutic Uses. *Nutrients*, *12*(6). https://doi.org/10.3390/nu12061616

Mehta, S., Granger, C., Grines, C. L., Jacobs, A., Henry, T. D., Rokos, I., Lansky, A., Baumbach, A., Botelho, R., Ferre, A., Yepes, I., Salwan, R., Dalal, J., Makkar, J., Bhalla, N., Mishra,

S., Vijan, V., & Hiremath, S. (2018). Confronting system barriers for ST- elevation MI in low and middle income countries with a focus on India. *Indian Heart Journal*, *70*(1), 185–190. https://doi.org/10.1016/j.ihj.2017.06.020

Mericskay, M. (2016). Nicotinamide adenine dinucleotide homeostasis and signalling in heart disease: Pathophysiological implications and therapeutic potential. *Archives of Cardiovascular Diseases*, *109*(3), 207–215. https://doi.org/10.1016/j.acvd.2015.10.004

Mettauer, B., Zoll, J., Sanchez, H., Lampert, E., Ribera, F., Veksler, V., Bigard, X., Mateo, P., Epailly, E., Lonsdorfer, J., & Ventura-Clapier, R. (2001). Oxidative capacity of skeletal muscle in heart failure patients versus sedentary or active control subjects. *Journal of the American College of Cardiology*, *38*(4), 947–954. https://doi.org/10.1016/s0735-1097(01)01460-7

Mock, A., Warta, R., Dettling, S., Brors, B., Jäger, D., & Herold-Mende, C. (2018). MetaboDiff: An R package for differential metabolomic analysis. *Bioinformatics*, *34*(19), 3417–3418. https://doi.org/10.1093/bioinformatics/bty344

Mohrman, D. E., & Heller, L. J. (2018). *Cardiovascular Physiology, Ninth Edition*.

Mori, V., Amici, A., Mazzola, F., Stefano, M. D., Conforti, L., Magni, G., Ruggieri, S., Raffaelli, N., & Orsomando, G. (2014). Metabolic Profiling of Alternative NAD Biosynthetic Routes in Mouse Tissues. *PLOS ONE*, *9*(11), e113939. https://doi.org/10.1371/journal.pone.0113939

Mourier, A., & Larsson, N.-G. (2011). Tracing the Trail of Protons through Complex I of the Mitochondrial Respiratory Chain. *PLOS Biology*, *9*(8), e1001129. https://doi.org/10.1371/journal.pbio.1001129

Moyes, C. D., & Le Moine, C. M. R. (2011). TISSUE RESPIRATION | Mitochondrial Respiration. In *Encyclopedia of Fish Physiology* (pp. 959–965). Elsevier. https://doi.org/10.1016/B978-0-12-374553-8.00121-0

Mozaffarian, D., Benjamin, E. J., Go, A. S., Arnett, D. K., Blaha, M. J., Cushman, M., Das, S. R., de Ferranti, S., Després, J.-P., Fullerton, H. J., Howard, V. J., Huffman, M. D., Isasi, C. R., Jiménez, M. C., Judd, S. E., Kissela, B. M., Lichtman, J. H., Lisabeth, L. D., Liu, S., … Turner, M. B. (2015). *Heart Disease and Stroke Statistics—2016 Update*. *133*, 323. https://doi.org/DOI: 10.1161/CIR.0000000000000350

Murashige, D., Jang, C., Neinast, M., Edwards, J. J., Cowan, A., Hyman, M. C., Rabinowitz, J. D., Frankel, D. S., & Arany, Z. (2020). Comprehensive quantification of fuel use by the failing and nonfailing human heart. *Science*, *370*(6514), 364–368. https://doi.org/10.1126/science.abc8861

Nascimento, B. R., Brant, L. C. C., Marino, B. C. A., Passaglia, L. G., & Ribeiro, A. L. P. (2019). Implementing myocardial infarction systems of care in low/middle-income countries. *Heart*, *105*(1), 20–26. https://doi.org/10.1136/heartjnl-2018-313398

Navale, A. M., & Paranjape, A. N. (2016). Glucose transporters: Physiological and pathological roles. *Biophysical Reviews*, *8*(1), 5–9. https://doi.org/10.1007/s12551-015-0186-2

Nelson, D. L., & Cox, M. M. (2017). *Lehninger Principles of Biochemistry* (7th ed.). W.H. Freeman & Company.

Neubauer, S. (2009, October 9). *The Failing Heart—An Engine Out of Fuel* (world) [Review-article]. Http://Dx.Doi.Org/10.1056/NEJMra063052; Massachusetts Medical Society. https://doi.org/10.1056/NEJMra063052

Nickel, A., Kohlhaas, M., & Maack, C. (2014). Mitochondrial reactive oxygen species production and elimination. *Journal of Molecular and Cellular Cardiology*, *73*, 26–33. https://doi.org/10.1016/j.yjmcc.2014.03.011

Nielsen, R., Møller, N., Gormsen, L. C., Tolbod, L. P., Hansson, N. H., Sorensen, J., Harms, H. J., Frøkiær, J., Eiskjaer, H., Jespersen, N. R., Mellemkjaer, S., Lassen, T. R., Pryds, K., Bøtker, H. E., & Wiggers, H. (2019). Cardiovascular Effects of Treatment With the Ketone Body 3-Hydroxybutyrate in Chronic Heart Failure Patients. *Circulation*, *139*(18), 2129–2141. https://doi.org/10.1161/CIRCULATIONAHA.118.036459

Niemann, B., & Rohrbach, S. (2016). Chapter 3—Metabolically Relevant Cell Biology – Role of Intracellular Organelles for Cardiac Metabolism. In M. Schwarzer & T. Doenst (Eds.), *The Scientist's Guide to Cardiac Metabolism* (pp. 19–38). Academic Press. https://doi.org/10.1016/B978-0-12-802394-5.00003-0

Nikiforov, A., Kulikova, V., & Ziegler, M. (2015). The human NAD metabolome: Functions, metabolism and compartmentalization. *Critical Reviews in Biochemistry and Molecular Biology*, *50*(4), 284–297. https://doi.org/10.3109/10409238.2015.1028612

OECD. (2017). *Mortality following acute myocardial infarction (AMI)*. https://www.oecd-ilibrary.org/content/component/health_glance-2017-34-en

Okabe, K., Yaku, K., Tobe, K., & Nakagawa, T. (2019). Implications of altered NAD metabolism in metabolic disorders. *Journal of Biomedical Science*, *26*(1), 34. https://doi.org/10.1186/s12929-019-0527-8

Olson, R. E. (1959). Myocardial metabolism in congestive heart failure. *Journal of Chronic Diseases*, *9*(5), 442–464. https://doi.org/10.1016/0021-9681(59)90172-9

Olvera Lopez, E., Ballard, B. D., & Jan, A. (2020). Cardiovascular Disease. In *StatPearls*. StatPearls Publishing. http://www.ncbi.nlm.nih.gov/books/NBK535419/

Pacher, P., & Szabó, C. (2007). Role of Poly(ADP-ribose) polymerase 1 (PARP-1) in Cardiovascular Diseases: The Therapeutic Potential of PARP Inhibitors. *Cardiovascular Drug Reviews*, *25*(3), 235–260. https://doi.org/10.1111/j.1527-3466.2007.00018.x

Pantouris, G., Serys, M., Yuasa, H. J., Ball, H. J., & Mowat, C. G. (2014). Human indoleamine 2,3-dioxygenase-2 has substrate specificity and inhibition characteristics distinct from those of indoleamine 2,3-dioxygenase-1. *Amino Acids*, *46*(9), 2155–2163. https://doi.org/10.1007/s00726-014-1766-3

Park, D.-R., Nam, T.-S., Kim, Y.-W., Lee, S.-H., & Kim, U.-H. (2018). CD38-cADPR-SERCA Signaling Axis Determines Skeletal Muscle Contractile Force in Response to β-Adrenergic Stimulation. *Cellular Physiology and Biochemistry: International Journal of Experimental Cellular Physiology, Biochemistry, and Pharmacology*, *46*(5), 2017–2030. https://doi.org/10.1159/000489441

Pell, V. R., Chouchani, E. T., Frezza, C., Murphy, M. P., & Krieg, T. (2016). Succinate metabolism: A new therapeutic target for myocardial reperfusion injury. *Cardiovascular Research*, *111*(2), 134–141. https://doi.org/10.1093/cvr/cvw100

Pelley, J. W. (2007a). 7—Citric Acid Cycle, Electron Transport Chain, and Oxidative Phosphorylation. In J. W. Pelley (Ed.), *Elsevier's Integrated Biochemistry* (pp. 55–63). Mosby. https://doi.org/10.1016/B978-0-323-03410-4.50013-4

Pelley, J. W. (2007b). 10—Fatty Acid and Triglyceride Metabolism. In J. W. Pelley (Ed.), *Elsevier's Integrated Biochemistry* (pp. 79–85). Mosby. https://doi.org/10.1016/B978-0-323-03410-4.50016-X

Phibbs, B. (2007). *The Human Heart: A Basic Guide to Heart Disease*.

Pillai, J. B., Isbatan, A., Imai, S., & Gupta, M. P. (2005). Poly(ADP-ribose) Polymerase-1-dependent Cardiac Myocyte Cell Death during Heart Failure Is Mediated by NAD+

Depletion and Reduced Sir2α Deacetylase Activity*. *Journal of Biological Chemistry*, *280*(52), 43121–43130. https://doi.org/10.1074/jbc.M506162200

Pillai, V. B., Sundaresan, N. R., Kim, G., Samant, S., Moreno-Vinasco, L., Garcia, J. G. N., & Gupta, M. P. (2013). Nampt secreted from cardiomyocytes promotes development of cardiac hypertrophy and adverse ventricular remodeling. *American Journal of Physiology - Heart and Circulatory Physiology*, *304*(3), H415–H426. https://doi.org/10.1152/ajpheart.00468.2012

Piquereau, J., & Ventura-Clapier, R. (2018). Maturation of Cardiac Energy Metabolism During Perinatal Development. *Frontiers in Physiology*, *9*. https://doi.org/10.3389/fphys.2018.00959

Ponikowski, P., Voors, A. A., Anker, S. D., Bueno, H., Cleland, J. G. F., Coats, A. J. S., Falk, V., González-Juanatey, J. R., Harjola, V.-P., Jankowska, E. A., Jessup, M., Linde, C., Nihoyannopoulos, P., Parissis, J. T., Pieske, B., Riley, J. P., Rosano, G. M. C., Ruilope, L. M., Ruschitzka, F., … Document Reviewers. (2016). 2016 ESC Guidelines for the diagnosis and treatment of acute and chronic heart failure: The Task Force for the diagnosis and treatment of acute and chronic heart failure of the European Society of Cardiology (ESC). Developed with the special contribution of the Heart Failure Association (HFA) of the ESC. *European Journal of Heart Failure*, *18*(8), 891–975. https://doi.org/10.1002/ejhf.592

Pound, K. M., Sorokina, N., Ballal, K., Berkich, D. A., Fasano, M., Lanoue, K. F., Taegtmeyer, H., O'Donnell, J. M., & Lewandowski, E. D. (2009). Substrate-enzyme competition attenuates upregulated anaplerotic flux through malic enzyme in hypertrophied

rat heart and restores triacylglyceride content: Attenuating upregulated anaplerosis in hypertrophy. *Circulation Research*, *104*(6), 805–812. https://doi.org/10.1161/CIRCRESAHA.108.189951

Prabhu, S. D., & Frangogiannis, N. G. (2016). The Biological Basis for Cardiac Repair After Myocardial Infarction: From Inflammation to Fibrosis. *Circulation Research*, *119*(1), 91–112. https://doi.org/10.1161/CIRCRESAHA.116.303577

Preiss, J., & Handler, P. (1958). Biosynthesis of diphosphopyridine nucleotide. I. Identification of intermediates. *The Journal of Biological Chemistry*, *233*(2), 488–492.

Purvis, J. L., & Lowenstein, J. M. (1961). The relation between intra- and extramitochondrial pyridine nucleotides. *The Journal of Biological Chemistry*, *236*, 2794–2803.

Raffaelli, N., Sorci, L., Amici, A., Emanuelli, M., Mazzola, F., & Magni, G. (2002). Identification of a novel human nicotinamide mononucleotide adenylyltransferase. *Biochemical and Biophysical Research Communications*, *297*(4), 835–840. https://doi.org/10.1016/S0006-291X(02)02285-4

Raghow, R. (2016). An 'Omics' Perspective on Cardiomyopathies and Heart Failure. *Trends in Molecular Medicine*, *22*(9), 813–827. https://doi.org/10.1016/j.molmed.2016.07.007

Ramsey, K. M., Yoshino, J., Brace, C. S., Abrassart, D., Kobayashi, Y., Marcheva, B., Hong, H.-K., Chong, J. L., Buhr, E. D., Lee, C., Takahashi, J. S., Imai, S.-I., & Bass, J. (2009). Circadian clock feedback cycle through NAMPT-mediated NAD+ biosynthesis. *Science (New York, N.Y.)*, *324*(5927), 651–654. https://doi.org/10.1126/science.1171641

Rardin, M. J., Wiley, S. E., Naviaux, R. K., Murphy, A. N., & Dixon, J. E. (2009). Monitoring phosphorylation of the pyruvate dehydrogenase complex. *Analytical Biochemistry*, *389*(2), 157–164. https://doi.org/10.1016/j.ab.2009.03.040

Ratajczak, J., Joffraud, M., Trammell, S. A. J., Ras, R., Canela, N., Boutant, M., Kulkarni, S. S., Rodrigues, M., Redpath, P., Migaud, M. E., Auwerx, J., Yanes, O., Brenner, C., & Cantó, C. (2016). NRK1 controls nicotinamide mononucleotide and nicotinamide riboside metabolism in mammalian cells. *Nature Communications*, *7*. https://doi.org/10.1038/ncomms13103

Redout, E. M., Wagner, M. J., Zuidwijk, M. J., Boer, C., Musters, R. J. P., van Hardeveld, C., Paulus, W. J., & Simonides, W. S. (2007). Right-ventricular failure is associated with increased mitochondrial complex II activity and production of reactive oxygen species. *Cardiovascular Research*, *75*(4), 770–781. https://doi.org/10.1016/j.cardiores.2007.05.012

Reed, G. W., Rossi, J. E., & Cannon, C. P. (2017). Acute myocardial infarction. *The Lancet*, *389*(10065), 197–210. https://doi.org/10.1016/S0140-6736(16)30677-8

Reimer, K. A., & Jennings, R. B. (1979). The "wavefront phenomenon" of myocardial ischemic cell death. II. Transmural progression of necrosis within the framework of ischemic bed size (myocardium at risk) and collateral flow. *Laboratory Investigation; a Journal of Technical Methods and Pathology*, *40*(6), 633–644.

Reimer K A, Lowe J E, Rasmussen M M, & Jennings R B. (1977). The wavefront phenomenon of ischemic cell death. 1. Myocardial infarct size vs duration of coronary occlusion in dogs. *Circulation*, *56*(5), 786–794. https://doi.org/10.1161/01.CIR.56.5.786

Rentrop, K. P., & Feit, F. (2015). Reperfusion therapy for acute myocardial infarction: Concepts and controversies from inception to acceptance. *American Heart Journal*, *170*(5), 971–980. https://doi.org/10.1016/j.ahj.2015.08.005

Revollo, J. R., Grimm, A. A., & Imai, S. (2004). The NAD Biosynthesis Pathway Mediated by Nicotinamide Phosphoribosyltransferase Regulates Sir2 Activity in Mammalian Cells *. *Journal of Biological Chemistry*, *279*(49), 50754–50763. https://doi.org/10.1074/jbc.M408388200

Revollo, J. R., Körner, A., Mills, K. F., Satoh, A., Wang, T., Garten, A., Dasgupta, B., Sasaki, Y., Wolberger, C., Townsend, R. R., Milbrandt, J., Kiess, W., & Imai, S. (2007). Nampt/PBEF/visfatin regulates insulin secretion in β cells as a systemic NAD biosynthetic enzyme. *Cell Metabolism*, *6*(5), 363–375. https://doi.org/10.1016/j.cmet.2007.09.003

Rine, J., & Herskowitz, I. (1987). Four Genes Responsible for a Position Effect on Expression From HML and HMR in Saccharomyces cerevisiae. *Genetics*, *116*(1), 9–22. https://www.genetics.org/content/116/1/9

Ritterhoff, J., & Tian, R. (2017). Metabolism in cardiomyopathy: Every substrate matters. *Cardiovascular Research*, *113*(4), 411–421. https://doi.org/10.1093/cvr/cvx017

Romacho, T., Sánchez-Ferrer, C. F., & Peiró, C. (2013). Visfatin/Nampt: An Adipokine with Cardiovascular Impact. *Mediators of Inflammation*, *2013*, e946427. https://doi.org/10.1155/2013/946427

Rosenblatt-Velin, N., Montessuit, C., Papageorgiou, I., Terrand, J., & Lerch, R. (2001). Postinfarction heart failure in rats is associated with upregulation of GLUT-1 and downregulation of genes of fatty acid metabolism. *Cardiovascular Research*, *52*(3), 407–416. https://doi.org/10.1016/S0008-6363(01)00393-5

Safer, B. (1975). The Metabolic Significance of the Malate-Aspartate Cycle in Heart. *Circulation Research*, *37*(5), 527–533. https://doi.org/10.1161/01.res.37.5.527

Saleh, M., & Ambrose, J. A. (2018). Understanding myocardial infarction. *F1000Research*, *7*. https://doi.org/10.12688/f1000research.15096.1

Sallin, O., Reymond, L., Gondrand, C., Raith, F., Koch, B., & Johnsson, K. (2018). Semisynthetic biosensors for mapping cellular concentrations of nicotinamide adenine dinucleotides. *ELife*, *7*, e32638. https://doi.org/10.7554/eLife.32638

Salter, M., & Pogson, C. I. (1985). The role of tryptophan 2,3-dioxygenase in the hormonal control of tryptophan metabolism in isolated rat liver cells. Effects of glucocorticoids and experimental diabetes. *Biochemical Journal*, *229*(2), 499–504. https://www.ncbi.nlm.nih.gov/pmc/articles/PMC1145083/

Sanchez, H., Zoll, J., Bigard, X., Veksler, V., Mettauer, B., Lampert, E., Lonsdorfer, J., & Ventura-Clapier, R. (2001). Effect of cyclosporin A and its vehicle on cardiac and skeletal muscle mitochondria: Relationship to efficacy of the respiratory chain. *British Journal of Pharmacology*, *133*(6), 781–788. https://doi.org/10.1038/sj.bjp.0704129

Scheepers, A., Joost, H., & Schurmann, A. (2004). The glucose transporter families SGLT and GLUT: Molecular basis of normal and aberrant function. *Journal of Parenteral and Enteral Nutrition*, *28*(5), 364–371. https://doi.org/10.1177/0148607104028005364

Scholz, T. D., & Koppenhafer, S. L. (1995). Reducing equivalent shuttles in developing porcine myocardium: Enhanced capacity in the newborn heart. *Pediatric Research*, *38*(2), 221–227. https://doi.org/10.1203/00006450-199508000-00015

Schwarzer, M., & Doenst, T. (2015). *The Scientist's Guide to Cardiac Metabolism* (1st ed.). Academic Press. https://www.elsevier.com/books/the-scientists-guide-to-cardiac-metabolism/schwarzer/978-0-12-802394-5

Schweiger, M., Hennig, K., Lerner, F., Niere, M., Hirsch-Kauffmann, M., Specht, T., Weise, C., Oei, S. L., & Ziegler, M. (2001). Characterization of recombinant human nicotinamide mononucleotide adenylyl transferase (NMNAT), a nuclear enzyme essential for NAD synthesis. *FEBS Letters*, *492*(1–2), 95–100. https://doi.org/10.1016/s0014-5793(01)02180-9

Senoner, T., & Dichtl, W. (2019). Oxidative Stress in Cardiovascular Diseases: Still a Therapeutic Target? *Nutrients*, *11*(9), E2090. https://doi.org/10.3390/nu11092090

Shao, D., & Tian, R. (2015). Glucose Transporters in Cardiac Metabolism and Hypertrophy. *Comprehensive Physiology*, *6*(1), 331–351. https://doi.org/10.1002/cphy.c150016

Sharma, S., Jackson, P. G., & Makan, J. (2004). Cardiac troponins. *Journal of Clinical Pathology*, *57*(10), 1025–1026. https://doi.org/10.1136/jcp.2003.015420

Shibata, K., Hayakawa, T., & Iwai, K. (1986). Tissue Distribution of the Enzymes Concerned with the Biosynthesis of NAD in Rats. *Agricultural and Biological Chemistry*, *50*(12), 3037–3041. https://doi.org/10.1080/00021369.1986.10867882

Smeets, P. J. H., Teunissen, B. E. J., Willemsen, P. H. M., van Nieuwenhoven, F. A., Brouns, A. E., Janssen, B. J. A., Cleutjens, J. P. M., Staels, B., van der Vusse, G. J., & van Bilsen, M. (2008). Cardiac hypertrophy is enhanced in PPAR alpha-/- mice in response to chronic pressure overload. *Cardiovascular Research*, *78*(1), 79–89. https://doi.org/10.1093/cvr/cvn001

Smyrnias, I., Gray, S. P., Okonko, D. O., Sawyer, G., Zoccarato, A., Catibog, N., López, B., González, A., Ravassa, S., Díez, J., & Shah, A. M. (2019). Cardioprotective Effect of

the Mitochondrial Unfolded Protein Response During Chronic Pressure Overload. *Journal of the American College of Cardiology*, *73*(14), 1795–1806. https://doi.org/10.1016/j.jacc.2018.12.087

Sorokina, N., O'Donnell, J. M., McKinney, R. D., Pound, K. M., Woldegiorgis, G., LaNoue, K. F., Ballal, K., Taegtmeyer, H., Buttrick, P. M., & Lewandowski, E. D. (2007). Recruitment of Compensatory Pathways to Sustain Oxidative Flux With Reduced Carnitine Palmitoyltransferase I Activity Characterizes Inefficiency in Energy Metabolism in Hypertrophied Hearts. *Circulation*, *115*(15), 2033–2041. https://doi.org/10.1161/CIRCULATIONAHA.106.668665

Spriet, L. L., Tunstall, R. J., Watt, M. J., Mehan, K. A., Hargreaves, M., & Cameron-Smith, D. (2004). Pyruvate dehydrogenase activation and kinase expression in human skeletal muscle during fasting. *Journal of Applied Physiology*, *96*(6), 2082–2087. https://doi.org/10.1152/japplphysiol.01318.2003

Stanley, W. C. (1991). Myocardial lactate metabolism during exercise. *Medicine & Science in Sports & Exercise*, *23*(8), 920–924. https://journals.lww.com/acsm-msse/Abstract/1991/08000/Myocardial_lactate_metabolism_during_exercise.6.aspx

Stanley, W. C., Meadows, S. R., Kivilo, K. M., Roth, B. A., & Lopaschuk, G. D. (2003). Beta-Hydroxybutyrate inhibits myocardial fatty acid oxidation in vivo independent of changes in malonyl-CoA content. *American Journal of Physiology. Heart and Circulatory Physiology*, *285*(4), H1626-1631. https://doi.org/10.1152/ajpheart.00332.2003

Stanley, W. C., Recchia, F. A., & Lopaschuk, G. D. (2005). Myocardial Substrate Metabolism in the Normal and Failing Heart. *Physiological Reviews*, *85*(3), 1093–1129. https://doi.org/10.1152/physrev.00006.2004

Stephens, N. R., Restrepo, C. S., Saboo, S. S., & Baxi, A. J. (2019). Overview of complications of acute and chronic myocardial infarctions: Revisiting pathogenesis and cross-sectional imaging. *Postgraduate Medical Journal*, *95*(1126), 439–450. https://doi.org/10.1136/postgradmedj-2018-136279

Stone, G. W., Selker, H. P., Thiele, H., Patel, M. R., Udelson, J. E., Ohman, E. M., Maehara, A., Eitel, I., Granger, C. B., Jenkins, P. L., Nichols, M., & Ben-Yehuda, O. (2016). Relationship Between Infarct Size and Outcomes Following Primary PCI: Patient-Level Analysis From 10 Randomized Trials. *Journal of the American College of Cardiology*, *67*(14), 1674–1683. https://doi.org/10.1016/j.jacc.2016.01.069

Sultan, A. M. (1992). Effects of diabetes and insulin on ketone bodies metabolism in heart. *Molecular and Cellular Biochemistry*, *110*(1), 17–23. https://doi.org/10.1007/BF02385001

Sun, W., Liu, C., Chen, Q., Liu, N., Yan, Y., & Liu, B. (2018). SIRT3: A New Regulator of Cardiovascular Diseases. *Oxidative Medicine and Cellular Longevity*, *2018*, e7293861. https://doi.org/10.1155/2018/7293861

Sun, W., Liu, Q., Leng, J., Zheng, Y., & Li, J. (2015). The role of Pyruvate Dehydrogenase Complex in cardiovascular diseases. *Life Sciences*, *121*, 97–103. https://doi.org/10.1016/j.lfs.2014.11.030

Sundaresan, N. R., Gupta, M., Kim, G., Rajamohan, S. B., Isbatan, A., & Gupta, M. P. (2009). Sirt3 blocks the cardiac hypertrophic response by augmenting Foxo3a-dependent antioxidant defense mechanisms in mice. *The Journal of Clinical Investigation*, *119*(9), 2758–2771. https://doi.org/10.1172/JCI39162

Taegtmeyer, H. (2014). A Primer on Carbohydrate Metabolism in the Heart. In G. D. Lopaschuk & N. S. Dhalla (Eds.), *Cardiac Energy Metabolism in Health and Disease* (pp. 3–14). Springer. https://doi.org/10.1007/978-1-4939-1227-8_1

Taegtmeyer, H., Lam, T., & Davogustto, G. (2016). Cardiac Metabolism in Perspective. *Comprehensive Physiology*, *6*(4), 1675–1699. https://doi.org/10.1002/cphy.c150056

Taegtmeyer, H., Young, M. E., Lopaschuk, G. D., Abel, E. D., Brunengraber, H., Darley-Usmar, V., Des Rosiers, C., Gerszten, R., Glatz, J. F., Griffin, J. L., Gropler, R. J., Holzhuetter, H.-G., Kizer, J. R., Lewandowski, E. D., Malloy, C. R., Neubauer, S., Peterson, L. R., Portman, M. A., Recchia, F. A., … Wang, T. J. (2016). Assessing Cardiac Metabolism: A Scientific Statement From the American Heart Association. *Circulation Research*, *118*(10), 1659–1701. https://doi.org/10.1161/RES.0000000000000097

Tan, B., Young, D. A., Lu, Z.-H., Wang, T., Meier, T. I., Shepard, R. L., Roth, K., Zhai, Y., Huss, K., Kuo, M.-S., Gillig, J., Parthasarathy, S., Burkholder, T. P., Smith, M. C., Geeganage, S., & Zhao, G. (2013). Pharmacological Inhibition of Nicotinamide Phosphoribosyltransferase (NAMPT), an Enzyme Essential for NAD+ Biosynthesis, in Human Cancer Cells: METABOLIC BASIS AND POTENTIAL CLINICAL IMPLICATIONS *. *Journal of Biological Chemistry*, *288*(5), 3500–3511. https://doi.org/10.1074/jbc.M112.394510

Tannous, C., Deloux, R., Karoui, A., Mougenot, N., Burkin, D., Blanc, J., Coletti, D., Lavery, G., Li, Z., & Mericskay, M. (2021). NMRK2 Gene Is Upregulated in Dilated Cardiomyopathy and Required for Cardiac Function and NAD Levels during Aging. *International Journal of Molecular Sciences*, *22*(7). https://doi.org/10.3390/ijms22073534

Tardy-Cantalupi, I., Montessuit, C., Papageorgiou, I., Remondino-Müller, A., Assimacopoulos-Jeannet, F., Morel, D. R., & Lerch, R. (1999). Effect of Transient Ischemia on the Expression of Glucose Transporters GLUT-1 and GLUT-4 in Rat Myocardium. *Journal of Molecular and Cellular Cardiology*, *31*(5), 1143–1155. https://doi.org/10.1006/jmcc.1999.0952

The Global Burden of Disease: 2019 update. (2019). http://ghdx.healthdata.org/gbd-results-tool

The Human Protein Atlas. (n.d.). Tissue Expression of QPRT. Retrieved March 23, 2021, from https://www.proteinatlas.org/ENSG00000103485-QPRT/tissue

Thygesen, K., Alpert, J. S., Jaffe, A. S., Chaitman, B. R., Bax, J. J., Morrow, D. A., White, H. D., & Executive Group on behalf of the Joint European Society of Cardiology (ESC)/American College of Cardiology (ACC)/American Heart Association (AHA)/World Heart Federation (WHF) Task Force for the Universal Definition of Myocardial Infarction. (2018). Fourth Universal Definition of Myocardial Infarction (2018). *Journal of the American College of Cardiology*, *72*(18), 2231–2264. https://doi.org/10.1016/j.jacc.2018.08.1038

Thygesen, K., Alpert, J. S., Jaffe, A. S., Chaitman, B. R., Bax, J. J., Morrow, D. A., White, H. D., Group, E. S. D., Thygesen, K., Alpert, J. S., Jaffe, A. S., Chaitman, B. R., Bax, J. J., Morrow, D. A., White, H. D., Mickley, H., Crea, F., Van de Werf, F., Bucciarelli-Ducci, C., … Corbett, S. (2019). Fourth universal definition of myocardial infarction (2018). *European Heart Journal*, *40*(3), 237–269. https://doi.org/10.1093/eurheartj/ehy462

Thygesen, K., Alpert, J. S., White, H. D., Joint ESC/ACCF/AHA/WHF Task Force for the Redefinition of Myocardial Infarction, Jaffe, A. S., Apple, F. S., Galvani, M., Katus, H.

A., Newby, L. K., Ravkilde, J., Chaitman, B., Clemmensen, P. M., Dellborg, M., Hod, H., Porela, P., Underwood, R., Bax, J. J., Beller, G. A., Bonow, R., … Al-Attar, N. (2007). Universal definition of myocardial infarction. *Circulation*, *116*(22), 2634–2653. https://doi.org/10.1161/CIRCULATIONAHA.107.187397

Trammell, S. A. J., Schmidt, M. S., Weidemann, B. J., Redpath, P., Jaksch, F., Dellinger, R. W., Li, Z., Abel, E. D., Migaud, M. E., & Brenner, C. (2016). Nicotinamide riboside is uniquely and orally bioavailable in mice and humans. *Nature Communications*, *7*. https://doi.org/10.1038/ncomms12948

Trammell, S. A., Yu, L., Redpath, P., Migaud, M. E., & Brenner, C. (2016). Nicotinamide Riboside Is a Major NAD+ Precursor Vitamin in Cow Milk. *The Journal of Nutrition*, *146*(5), 957–963. https://doi.org/10.3945/jn.116.230078

Tran, D. H., & Wang, Z. V. (2019). Glucose Metabolism in Cardiac Hypertrophy and Heart Failure. *Journal of the American Heart Association*, *8*(12), e012673. https://doi.org/10.1161/JAHA.119.012673

Triposkiadis, F., Butler, J., Abboud, F. M., Armstrong, P. W., Adamopoulos, S., Atherton, J. J., Backs, J., Bauersachs, J., Burkhoff, D., Bonow, R. O., Chopra, V. K., de Boer, R. A., de Windt, L., Hamdani, N., Hasenfuss, G., Heymans, S., Hulot, J.-S., Konstam, M., Lee, R. T., … De Keulenaer, G. W. (2019). The continuous heart failure spectrum: Moving beyond an ejection fraction classification. *European Heart Journal*, *40*(26), 2155–2163. https://doi.org/10.1093/eurheartj/ehz158

Ussher, J. R., & Lopaschuk, G. D. (2008). The malonyl CoA axis as a potential target for treating ischaemic heart disease. *Cardiovascular Research*, *79*(2), 259–268. https://doi.org/10.1093/cvr/cvn130

V Cokkinos, D., Biomedical Research Foundation Academy of Athens, Onassis Cardiac Surgery Centre, Athens, Greece, Belogianneas, C., & Biomedical Research Foundation Academy of Athens, Onassis Cardiac Surgery Centre, Athens, Greece. (2016). Left Ventricular Remodelling: A Problem in Search of Solutions. *European Cardiology Review*, *11*(1), 29. https://doi.org/10.15420/ecr.2015:9:3

Vallerie, S. N., & Bornfeldt, K. E. (2015). Metabolic Flexibility and Dysfunction in Cardiovascular Cells. *Arteriosclerosis, Thrombosis, and Vascular Biology*, *35*(9), e37–e42. https://doi.org/10.1161/ATVBAHA.115.306226

van der Pol, A., van Gilst, W. H., Voors, A. A., & van der Meer, P. (2019). Treating oxidative stress in heart failure: Past, present and future. *European Journal of Heart Failure*, *21*(4), 425–435. https://doi.org/10.1002/ejhf.1320

VanLinden, M. R., Dölle, C., Pettersen, I. K. N., Kulikova, V. A., Niere, M., Agrimi, G., Dyrstad, S. E., Palmieri, F., Nikiforov, A. A., Tronstad, K. J., & Ziegler, M. (2015). Subcellular Distribution of NAD+ between Cytosol and Mitochondria Determines the Metabolic Profile of Human Cells. *The Journal of Biological Chemistry*, *290*(46), 27644–27659. https://doi.org/10.1074/jbc.M115.654129

Vannini, N., Campos, V., Girotra, M., Trachsel, V., Rojas-Sutterlin, S., Tratwal, J., Ragusa, S., Stefanidis, E., Ryu, D., Rainer, P. Y., Nikitin, G., Giger, S., Li, T. Y., Semilietof, A., Oggier, A., Yersin, Y., Tauzin, L., Pirinen, E., Cheng, W.-C., … Naveiras, O. (2019). The NAD-Booster Nicotinamide Riboside Potently Stimulates Hematopoiesis through Increased Mitochondrial Clearance. *Cell Stem Cell*, *24*(3), 405-418.e7. https://doi.org/10.1016/j.stem.2019.02.012

Vaquero, A. (2009). The conserved role of sirtuins in chromatin regulation. *The International Journal of Developmental Biology*, *53*(2–3), 303–322. https://doi.org/10.1387/ijdb.082675av

Veech, R. L., Guynn, R., & Veloso, D. (1972). The time-course of the effects of ethanol on the redox and phosphorylation states of rat liver. *The Biochemical Journal*, *127*(2), 387–397. https://doi.org/10.1042/bj1270387

Ventura-Clapier, R., Garnier, A., & Veksler, V. (2004). Energy metabolism in heart failure. *The Journal of Physiology*, *555*(Pt 1), 1–13. https://doi.org/10.1113/jphysiol.2003.055095

Ventura-Clapier, R., Garnier, A., & Veksler, V. (2008). Transcriptional control of mitochondrial biogenesis: The central role of PGC-1α. *Cardiovascular Research*, *79*(2), 208–217. https://doi.org/10.1093/cvr/cvn098

Ventura-Clapier, R., Garnier, A., Veksler, V., & Joubert, F. (2011). Bioenergetics of the failing heart. *Biochimica et Biophysica Acta (BBA) - Molecular Cell Research*, *1813*(7), 1360–1372. https://doi.org/10.1016/j.bbamcr.2010.09.006

Verdin, E. (2015). NAD+ in aging, metabolism, and neurodegeneration. *Science*, *350*(6265), 1208–1213. https://doi.org/10.1126/science.aac4854

Vida, A., Márton, J., Mikó, E., & Bai, P. (2017). Metabolic roles of poly(ADP-ribose) polymerases. *Seminars in Cell & Developmental Biology*, *63*, 135–143. https://doi.org/10.1016/j.semcdb.2016.12.009

Vignier, N., Chatzifrangkeskou, M., Morales Rodriguez, B., Mericskay, M., Mougenot, N., Wahbi, K., Bonne, G., & Muchir, A. (2018). Rescue of biosynthesis of nicotinamide adenine dinucleotide protects the heart in cardiomyopathy caused by lamin A/C

gene mutation. *Human Molecular Genetics*, *27*(22), 3870–3880. https://doi.org/10.1093/hmg/ddy278

Wang, C., Xu, W., Zhang, Y., Zhang, F., & Huang, K. (2018). PARP1 promote autophagy in cardiomyocytes via modulating FoxO3a transcription. *Cell Death & Disease*, *9*(11), 1–15. https://doi.org/10.1038/s41419-018-1108-6

Weiss, R. G., Gerstenblith, G., & Bottomley, P. A. (2005). ATP flux through creatine kinase in the normal, stressed, and failing human heart. *Proceedings of the National Academy of Sciences*, *102*(3), 808–813. https://doi.org/10.1073/pnas.0408962102

Wende, A. R., Brahma, M. K., McGinnis, G. R., & Young, M. E. (2017). Metabolic Origins of Heart Failure. *JACC: Basic to Translational Science*, *2*(3), 297–310. https://doi.org/10.1016/j.jacbts.2016.11.009

Werner, C., Doenst, T., & Schwarzer, M. (2016). Chapter 4—Metabolic Pathways and Cycles. In M. Schwarzer & T. Doenst (Eds.), *The Scientist's Guide to Cardiac Metabolism* (pp. 39–55). Academic Press. https://doi.org/10.1016/B978-0-12-802394-5.00004-2

Williamson, D. H., Lund, P., & Krebs, H. A. (1967). The redox state of free nicotinamide-adenine dinucleotide in the cytoplasm and mitochondria of rat liver. *Biochemical Journal*, *103*(2), 514–527. https://www.ncbi.nlm.nih.gov/pmc/articles/PMC1270436/

World Health Organization. (2017, May 17). *Cardiovascular diseases (CVDs)*. Fact Sheets. https://www.who.int/news-room/fact-sheets/detail/cardiovascular-diseases-(cvds)

Wright, E. M., Loo, D. D. F., & Hirayama, B. A. (2011). Biology of human sodium glucose transporters. *Physiological Reviews*, *91*(2), 733–794. https://doi.org/10.1152/physrev.00055.2009

WU, P., SATO, J., ZHAO, Y., JASKIEWICZ, J., POPOV, M. K., & HARRIS, A. R. (1998). Starvation and diabetes increase the amount of pyruvate dehydrogenase kinase isoenzyme 4 in rat heart. *Biochemical Journal*, *329*(1), 197–201. https://doi.org/10.1042/bj3290197

Xiao, W., Wang, R.-S., Handy, D. E., & Loscalzo, J. (2018). NAD(H) and NADP(H) Redox Couples and Cellular Energy Metabolism. *Antioxidants & Redox Signaling*, *28*(3), 251–272. https://doi.org/10.1089/ars.2017.7216

Xie, N., Zhang, L., Gao, W., Huang, C., Huber, P. E., Zhou, X., Li, C., Shen, G., & Zou, B. (2020). NAD + metabolism: Pathophysiologic mechanisms and therapeutic potential. *Signal Transduction and Targeted Therapy*, *5*(1), 1–37. https://doi.org/10.1038/s41392-020-00311-7

Xu, T., Pagadala, V., & Mueller, D. M. (2015). Understanding structure, function, and mutations in the mitochondrial ATP synthase. *Microbial Cell*, *2*(4), 105–125. https://doi.org/10.15698/mic2015.04.197

Yamada, K., Hara, N., Shibata, T., Osago, H., & Tsuchiya, M. (2006). The simultaneous measurement of nicotinamide adenine dinucleotide and related compounds by liquid chromatography/electrospray ionization tandem mass spectrometry. *Analytical Biochemistry*, *352*(2), 282–285. https://doi.org/10.1016/j.ab.2006.02.017

Yamazaki, F., Kuroiwa, T., Takikawa, O., & Kido, R. (1985). Human indolylamine 2,3-dioxygenase. Its tissue distribution, and characterization of the placental enzyme. *Biochemical Journal*, *230*(3), 635–638. https://doi.org/10.1042/bj2300635

Yang, T., Chan, N. Y.-K., & Sauve, A. A. (2007). Syntheses of nicotinamide riboside and derivatives: Effective agents for increasing nicotinamide adenine dinucleotide concentrations in mammalian cells. *Journal of Medicinal Chemistry*, *50*(26), 6458–6461. https://doi.org/10.1021/jm701001c

Yang, Y., & Sauve, A. A. (2016). NAD+ metabolism: Bioenergetics, signaling and manipulation for therapy. *Biochimica et Biophysica Acta*, *1864*(12), 1787–1800. https://doi.org/10.1016/j.bbapap.2016.06.014

Ying, W. (2008). NAD+/NADH and NADP+/NADPH in cellular functions and cell death: Regulation and biological consequences. *Antioxidants & Redox Signaling*, *10*(2), 179–206. https://doi.org/10.1089/ars.2007.1672

Yoshii, A., Nagoshi, T., Kashiwagi, Y., Kimura, H., Tanaka, Y., Oi, Y., Ito, K., Yoshino, T., Tanaka, T. D., & Yoshimura, M. (2019). Cardiac ischemia–reperfusion injury under insulin-resistant conditions: SGLT1 but not SGLT2 plays a compensatory protective role in diet-induced obesity. *Cardiovascular Diabetology*, *18*(1), 85. https://doi.org/10.1186/s12933-019-0889-y

Yusuf, S., Hawken, S., Ôunpuu, S., Dans, T., Avezum, A., Lanas, F., McQueen, M., Budaj, A., Pais, P., Varigos, J., & Lisheng, L. (2004). Effect of potentially modifiable risk factors associated with myocardial infarction in 52 countries (the INTERHEART study): Case-control study. *The Lancet*, *364*(9438), 937–952. https://doi.org/10.1016/S0140-6736(04)17018-9

Zammit, V. A., Fraser, F., & Orstorphine, C. G. (1997). Regulation of mitochondrial outer-membrane carnitine palmitoyltransferase (CPT I): Role of membrane-topology. *Advances in Enzyme Regulation*, *37*, 295–317. https://doi.org/10.1016/s0065-2571(96)00015-5

Zapata-Pérez, R., Wanders, R. J. A., van Karnebeek, C. D. M., & Houtkooper, R. H. (2021). NAD+ homeostasis in human health and disease. *EMBO Molecular Medicine*, *13*(7), e13943. https://doi.org/10.15252/emmm.202113943

Zhang, J., Tao, J., Ling, Y., Li, F., Zhu, X., Xu, L., Wang, M., Zhang, S., McCall, C. E., & Liu, T. F. (2019). Switch of NAD Salvage to de novo Biosynthesis Sustains SIRT1-RelB-Dependent Inflammatory Tolerance. *Frontiers in Immunology*, *10*. https://doi.org/10.3389/fimmu.2019.02358

Zhang, X., Kurnasov, O. V., Karthikeyan, S., Grishin, N. V., Osterman, A. L., & Zhang, H. (2003). Structural characterization of a human cytosolic NMN/NaMN adenylyltransferase and implication in human NAD biosynthesis. *The Journal of Biological Chemistry*, *278*(15), 13503–13511. https://doi.org/10.1074/jbc.M300073200

Zhang, Y., Wang, B., Fu, X., Guan, S., Han, W., Zhang, J., Gan, Q., Fang, W., Ying, W., & Qu, X. (2016). Exogenous NAD+ administration significantly protects against myocardial ischemia/reperfusion injury in rat model. *American Journal of Translational Research*, *8*(8), 3342–3350.

Zhao, G., Jeoung, N. H., Burgess, S. C., Rosaaen-Stowe, K. A., Inagaki, T., Latif, S., Shelton, J. M., McAnally, J., Bassel-Duby, R., Harris, R. A., Richardson, J. A., & Kliewer, S. A. (2008). Overexpression of pyruvate dehydrogenase kinase 4 in heart perturbs metabolism and exacerbates calcineurin-induced cardiomyopathy. *American Journal of Physiology-Heart and Circulatory Physiology*, *294*(2), H936–H943. https://doi.org/10.1152/ajpheart.00870.2007

Ziegler, M., & Nikiforov, A. A. (2020). NAD on the rise again. *Nature Metabolism*, *2*(4), 291–292. https://doi.org/10.1038/s42255-020-0197-6

Zimmer, H. G., Ibel, H., & Steinkopff, G. (1980). Studies on the hexose monophosphate shunt in the myocardium during development of hypertrophy. *Advances in Myocardiology*, *1*, 487–492.

Zipes, D. P., & Libby, P. (2018). *Braunwald's Heart Disease: A Textbook of Cardiovascular Medicine, 2-Volume Set* (R. O. Bonow, D. L. Mann, & G. F. Tomaselli, Eds.).

Zuo, W., Liu, N., Zeng, Y., Liu, Y., Li, B., Wu, K., Xiao, Y., & Liu, Q. (2020). CD38: A Potential Therapeutic Target in Cardiovascular Disease. *Cardiovascular Drugs and Therapy*. https://doi.org/10.1007/s10557-020-07007-8